

GEOCHEMISTRY OF INKPOT SPRING, SULPHUR CREEK-SEVENMILE HOLE AREA,
YELLOWSTONE CALDERA, WYOMING

By

ALLEN K. ANDERSEN

A thesis submitted in partial fulfillment of
the requirements for the degree of

MASTER OF SCIENCE IN GEOLOGY

WASHINGTON STATE UNIVERSITY
School of Earth and Environmental Sciences

MAY 2010

To the Faculty of Washington State University:

The members of the Committee appointed to examine the thesis of ALLEN K. ANDERSEN find it satisfactory and recommend that it be accepted.

Peter B. Larson, Ph.D., Chair

David R. Cole, Ph.D.

Franklin F. Foit, Jr., Ph.D.

ACKNOWLEDGEMENT

This project would not have been possible without the assistance of numerous people and institutions. I am grateful to many people for their advice and generous support toward my master's program and it is with pleasure that I now express my debt of gratitude.

Thanks to my advisor and committee member, Peter B. Larson, for his guidance, numerous helpful discussions, and high expectations, and to my thesis committee, Dr. David R. Cole and Dr. Franklin F. Foit, for their valuable discussions and direction. A special thanks to Dave Cole and the Oak Ridge National Laboratory for allowing me to use the Portable Ambient Air Analyzer.

I thank the Washington State University GeoAnalytical Laboratory, and especially Charles Knaack for his help in compiling geochemical data using a variety of instruments. Special thanks to Anita L. Fallen and the University of Idaho Pedology Laboratory, Dr. Zachary D. Sharp and the University of New Mexico, Department of Earth and Planetary Sciences' Stable Isotope Laboratory, and Stephen Dent and the WSU Department of Civil and Environmental Engineering for help with water chemistry analyses.

I thank Christie Hendrix and the National Park Service for enabling me to do research in Yellowstone National Park. I would also like to acknowledge the Yellowstone crew: Allie Phillips, Jennifer Manion, Chad Pritchard, Brian Pauley, David John, Mike Cosca, Todd Feeley, and all others who provided help and support in the field during July and August 2007 and 2008.

I would also like to thank Newmont Mining Corporation for their internship opportunity during the summers of 2008 and 2009, and the training and helpful career advice I received during that time.

Support for this project was provided by the Society of Economic Geologists' Hugh E. McKinstry Student Research Grant and the WSU School of Earth and Environmental Science's Charles D. Campbell Endowment, Joseph W. Mills Endowment, James W. Crosby Memorial Scholarship, and A to Z Award.

GEOCHEMISTRY OF INKPOT SPRING, SULPHUR CREEK-SEVENMILE HOLE AREA,
YELLOWSTONE CALDERA, WYOMING

Abstract

by Allen K. Andersen, M.S.
Washington State University
May 2010

Chair: Peter B. Larson

The Yellowstone hydrothermal system consists primarily of meteoric water circulating to deep levels within and just outside of the Yellowstone caldera. Inkpot Spring is a small group of bubbling pools located just outside the hypothesized northern margin of the Yellowstone Caldera. Here the Yellowstone hydrothermal system is vapor-dominated. Inkpot Spring fluids have previously been classified as acid-sulfate waters. This study presents evidence for multiple water types contributing to surface fluids at Inkpot Spring. The complex chemistry of fluids at Inkpot Spring can be attributed to mixing of multiple water types, boiling, and water-rock interaction. The geologic setting of Inkpot Spring is situated so that fluids may react with several lithologies during their ascension to the surface. High concentrations of mercury, boron, ammonia, and volatile light hydrocarbons at Inkpot Spring suggest that petroleum is flushed from Paleozoic or Mesozoic sediments by hot water and then distilled at high temperatures. The fluids probably also react with basaltic-andesites of the Eocene Absaroka volcanics, contributing high levels of iron, calcium, and magnesium, and producing a fluid supersaturated with pyrite. Pebbles recovered from Inkpot Spring pools exhibit coatings of layered pyrite bands, indicating

multiple episodes of pyrite precipitation from the fluids. Although considered to be acid-sulfate waters, many of the pools at Inkpot Spring are near neutral. Excess ammonia combines with sulfuric acid, produced from oxidation of hydrogen sulfide, to produce ammonium sulfate and neutralize the fluids. Other possible factors controlling the amount of sulfuric acid and pH are oxidation of sulfur or sulfide, disproportionation of SO₂ in vapor, and sulfuric acid production from sulfur-consuming bacteria (*sulfolobus*) in native sulfur deposits of buried solfataras from previous hydrothermal activity. An examination of fluid-mineral equilibria in Inkpot Spring fluids and suspended sediment has revealed several minerals at or near equilibrium with the fluids including kaolinite, alunite, opal, montmorillonite (beidellite), and pyrophyllite. This is consistent with an advanced argillic alteration mineral assemblage observed in the Grand Canyon of the Yellowstone River consisting of an association with quartz (opal) + kaolinite ± alunite ± dickite.

TABLE OF CONTENTS

ACKNOWLEDGEMENTS	iii
ABSTRACT	v
LIST OF FIGURES	x
LIST OF TABLES	xiii
CHAPTER	
1. INTRODUCTION	1
2. GEOLOGIC SETTING	4
3. HYDROTHERMAL BACKGROUND	12
4. METHODS AND PROCEDURES	19
4.1 Field Methods	19
4.2 Analytical Procedures	24
5. RESULTS	27
5.1 Stable Isotope Ratios	27
5.2 Water Chemistry	32
5.3 Geothermometry and Evidence of Mixing	37
6. FLUID-MINERAL EQUILIBRIA	46
6.1 Solubility-Activity Relationships	46
6.2 Redox Disequilibrium	47
6.3 Activity-Mineral Stability Diagrams	49
7. SUSPENDED SEDIMENT AND PARTICULATES	59

8. MERCURY	71
8.1 Comparisons to other Hg-depositing Geothermal Systems	71
8.2 Mercury Transport Mechanisms	80
9. ORGANIC AND INORGANIC GAS GEOCHEMISTRY.....	83
10. DISCUSSION	86
10.1 Overview.....	86
10.2 Stable Isotope Ratios, Boiling, and Mixing	87
10.3 Variable pH Conditions	88
10.4 Redox Conditions	89
10.5 Subsurface Temperature and Silica Concentrations	89
10.6 Fluid-Mineral Equilibria.....	90
10.7 Sediments.....	91
10.8 Gas Geochemistry.....	91
11. CONCLUSIONS.....	92
REFERENCES	97
APPENDIX	
A. PHOTOGRAPHS, COORDINATES, PH, AND TEMPERATURE AT INKPOT.....	105
B. PREVIOUS DATA FROM WASHBURN-INKPOT SPRINGS	118
C. 2008 INKPOT SPRING WATER CHEMISTRY DATA	124
D. ACTIVITY DIAGRAMS WITH INKPOT SPRING FLUIDS	130

E. GEOCHEMICAL DATA FROM INKPOT SPRING SEDIMENT	147
F. MERCURY DATA FROM INKPOT SPRING FLUIDS AND SEDIMENTS	151
G. PREVIOUS ORGANIC AND INORGANIC WASHBURN-INKPOT GAS DATA	153
H. 2008 INKPOT SPRING ORGANIC AND INORGANIC GAS GEOCHEMISTRY	155
I. EXPLANATION OF SYMBOLS AND ABBREVIATIONS	158

LIST OF FIGURES

Figure 1. Map of Yellowstone Hydrothermal Features	3
Figure 2a. Geologic Map of Sulphur Creek-Sevenmile Hole Area	8
Figure 2b. Description of Geologic Map Units	9
Figure 3. Topographic Map of Sulphur Creek-Sevenmile Hole Area	13
Figure 4. Google Earth Aerial Image of Washburn and Inkpot Hot Springs	14
Figure 5. General Model for Vapor-Dominated Geothermal Systems	15
Figure 6. Conditions in a Vapor-Dominated Geothermal System	17
Figure 7. Water Sampling Procedure	20
Figure 8. Gas Measurement Procedure	23
Figure 9. δD vs $\delta^{18}O$ of Fluids at Inkpot Spring Compared with Other YNP Thermal Areas	30
Figure 10. Trilinear Piper Diagram with Inkpot Spring Fluid Compositions	33
Figure 11. Ammonia vs Sulfate Control on pH	35
Figure 12. Silica versus Enthalpy for Inkpot Spring Thermal Waters	42
Figure 13. Silica versus Total Carbonate for Inkpot Spring Thermal Waters	44
Figure 14. Fluids on Stability of Al-silicates in the System $Na_2O-K_2O-Al_2O_3-H_2O$ at $225^{\circ}C$	51
Figure 15. Fluids on Stability of Al-silicates in the System $Al_2O_3-K_2O-SiO_2-H_2O$ at $225^{\circ}C$	52
Figure 16. Fluids on Stability of Al-silicates in the System $CaO-Al_2O_3-K_2O-H_2O$ at $225^{\circ}C$	54
Figure 17. Inkpot Spring Fluids Relative to Quartz and Amorphous Silica Solubility	56
Figure 18. Fluids on Stability of Sulfate Minerals as a Function of pH and Ba^{2+}/K^{+} at $100^{\circ}C$	57
Figure 19. Photograph of Devil's Ink Pot in 1935 from Allen and Day (1935)	60
Figure 20a. Photo of Pools and Altered Ground at Inkpot Spring/Devil's Ink Pot in 1935	61
Figure 20b. Photo of Pools and Altered Ground at Inkpot Spring in 2008	61

Figure 21a. Photo of Largest Pool (IKP06) and Altered Ground at Inkpot Spring in 2001	62
Figure 21b. Photo of Largest Pool (IKP06) and Altered Ground at Inkpot Spring in 2008.....	62
Figure 22a. Photograph of Pool IKP11 with Standing Water at 11:00 AM in August 2008.....	63
Figure 22b. Photograph of Pool IKP11 with Water Drained at 1:30 PM in August 2008	63
Figure 22c. Photograph of Pyrite Coated Pebbles Revealed at the Bottom of Pool IKP11	63
Figure 22d. Photograph of Large Pyrite Coated Cobble Discovered in Pool IKP11	63
Figure 23a. Backscattered Electron Image of Precipitated Layers of Pyrite on Pebble	64
Figure 23b. Backscattered Electron Image Barite within Precipitated Pyrite Coating.....	64
Figure 24. Scanning Electron Micrographs of Suspended Sediment & Particulates.....	68
Figure 25. Backscattered Electron Image of Fine Sulfide-bearing Suspended Sediment	69
Figure 26. Photographs of Native Sulfur Deposits in Fumaroles at Inkpot Spring	76
Figure 27. Backscattered Electron Image of Sub-micron-sized Cinnabar Grains	79
Figure 28. Log Oxygen Fugacity vs pH Stability Diagram for the System: Hg-Fe-S-H ₂ O-O	82
Figure 29. Hypothesized Cross Section of Hydrothermal System at Inkpot Spring	96
Figure 30. Schematic Drawing of Inkpot Pool Distribution.....	106
Figure D-1. Stability of Al-silicates in the System Na ₂ O-K ₂ O-Al ₂ O ₃ -H ₂ O at 100°C	131
Figure D-2. Stability of Al-silicates in the System Na ₂ O-K ₂ O-Al ₂ O ₃ -H ₂ O at 150°C	132
Figure D-3. Stability of Al-silicates in the System Na ₂ O-K ₂ O-Al ₂ O ₃ -H ₂ O at 225°C	133
Figure D-4. Stability of Al-silicates in the System Na ₂ O-K ₂ O-Al ₂ O ₃ -H ₂ O at 250°C	134
Figure D-5. Stability of Al-silicates in the System CaO-Al ₂ O ₃ -K ₂ O-H ₂ O at 100°C.....	135
Figure D-6. Stability of Al-silicates in the System CaO-Al ₂ O ₃ -K ₂ O-H ₂ O at 150°C.....	136
Figure D-7. Stability of Al-silicates in the System CaO-Al ₂ O ₃ -K ₂ O-H ₂ O at 225°C.....	137
Figure D-8. Stability of Al-silicates in the System CaO-Al ₂ O ₃ -K ₂ O-H ₂ O at 250°C.....	138

Figure D-9. Stability of Al-silicates in the System $\text{Al}_2\text{O}_3\text{-K}_2\text{O-SiO}_2\text{-H}_2\text{O}$ at 100°C	139
Figure D-10. Stability of Al-silicates in the System $\text{Al}_2\text{O}_3\text{-K}_2\text{O-SiO}_2\text{-H}_2\text{O}$ at 150°C	140
Figure D-11. Stability of Al-silicates in the System $\text{Al}_2\text{O}_3\text{-K}_2\text{O-SiO}_2\text{-H}_2\text{O}$ at 225°C	141
Figure D-12. Stability of Al-silicates in the System $\text{Al}_2\text{O}_3\text{-K}_2\text{O-SiO}_2\text{-H}_2\text{O}$ at 250°C	142
Figure D-13. Stability of Sulfate Minerals as a Function of pH and $\text{Ba}^{2+}/\text{K}^+$ at 100°C	143
Figure D-14. Stability of Sulfate Minerals as a Function of pH and $\text{Ba}^{2+}/\text{K}^+$ at 150°C	144
Figure D-15. Stability of Sulfate Minerals as a Function of pH and $\text{Ba}^{2+}/\text{K}^+$ at 225°C	145
Figure D-16. Stability of Sulfate Minerals as a Function of pH and $\text{Ba}^{2+}/\text{K}^+$ at 250°C	146

LIST OF TABLES

Table 1. Container Preparation & Stabilization, Filtration, & Analytical Methods	21
Table 2a. Fluid Reservoir Temperature Estimates from Chemical Geothermometers	39
Table 2b. Chemical Geothermometers used to Calculate Fluid Reservoir Temperatures	40
Table 3. Average Silica Geothermometer Temperatures of Yellowstone Geyser Basins	43
Table 4a. Saturation Indices (log Q/K) of Inkpot Fluids Considering Eh = -0.165	48
Table 4b. Saturation Indices (log Q/K) of Inkpot Fluids Considering Eh = +0.165	48
Table 5. Minerals Identified in Inkpot Spring Sediment Using XRD	65
Table 6. Comparison of Waters Associated with Hg-depositing Systems and Inkpot Fluids	72
Table 7. Mercury and Boron Abundances in Different Geologic Environments	74

1. INTRODUCTION

The epithermal environment formed in the magmatically-driven hydrothermal system of the Yellowstone caldera at Yellowstone National Park (YNP) is a modern analog to extinct systems that have produced significant precious and base metal mineralization around the world. Yellowstone gives a unique glimpse into a geologically young and active hydrothermal system driven by deeply circulating, convective meteoric water heated by a relatively shallow magmatic source. Studies of many epithermal systems have classified them into two broad groups based on alteration and gangue mineralogy, metal contents, and sulfide mineral assemblages (Simmons et al., 2005). The two alteration mineral assemblages are controlled by fluid chemistry. Acid-sulfate fluids with low pH produce a diagnostic alteration assemblage which usually includes quartz + alunite ± pyrophyllite ± dickite ± kaolinite, while alkaline-chloride fluids, with neutral to slightly alkaline pH, produce an assemblage that often includes quartz ± calcite ± adularia ± illite as characteristic phases (Simmons et al., 2005). The acid-sulfate fluids have low total solute concentrations, are more oxidized, have low pH, and high dissolved SO_4^{-2} concentrations. The alkaline-chloride fluids are neutral to slightly alkaline, have higher salinities, and tend to have higher discharge rates. Both types of fluids are found in active Yellowstone hot springs.

The western part of the park is dominated by hot-water systems in which fluid pressure and the maximum temperature increase gradually with depth and closely follow the hydrostatic boiling curve (Fournier, 1989). The surface manifestations of these systems appear as high temperature hot springs and geysers with alkaline-chloride fluids and high discharge rates. Vapor-dominated systems in which fluid pressures remain nearly constant throughout a significant depth are more common in the eastern part of the caldera (Fournier, 1989). In vapor-dominated systems steam, H_2S , CO_2 , and other gases are transported through large fractures

while liquid water fills the adjacent pore space (White, 1971; Fournier, 1989). Vapor-dominated systems produce acid-sulfate fluids. None of the aforementioned characteristics are restricted to one part of the Yellowstone hydrothermal system and variable mixtures exist between the two fluid type end members, where the degree of fluid evolution may be controlled by boiling and water/rock interaction, among other processes.

Many of Yellowstone's hot spring basins lie along the hypothesized position of the main-ring fracture zone of the 0.64 Ma caldera, a potential focus of upflow for hydrothermal fluids. Similar relationships between hydrothermal fluids and structures along caldera ring zones have been observed at the active system associated with the Valles Caldera, New Mexico (Goff and Gardner, 1994). The hydrothermal flow model for the 23 Ma Lake City Caldera, Colorado, proposed by Larson and Taylor (1986; 1987) also shows similarities to the shallow portion of the Yellowstone hydrothermal system.

Inkpot Spring is part of a vapor-dominated system located near the junction of the Yellowstone River and the 0.64 Ma caldera margin (Fig. 1). This spring is part of the more widely recognized Washburn Hot Springs, a larger group of mudpots and hot springs only ~150 meters away. Eight separate pools of water at Inkpot Spring were analyzed for major and trace element concentrations and oxygen and hydrogen isotope ratios along with in situ measurements of temperature and pH. Major and trace element analyses were also performed on hot spring sediment immediately surrounding the pool as well as suspended sediment and particulates. These analyses were performed to evaluate why the thermal fluids at Inkpot Spring have variable pH and to give some insight into subsurface water/rock interaction. The geologic setting of this spring implies that the fluids may be reacting with multiple rock types in the subsurface.

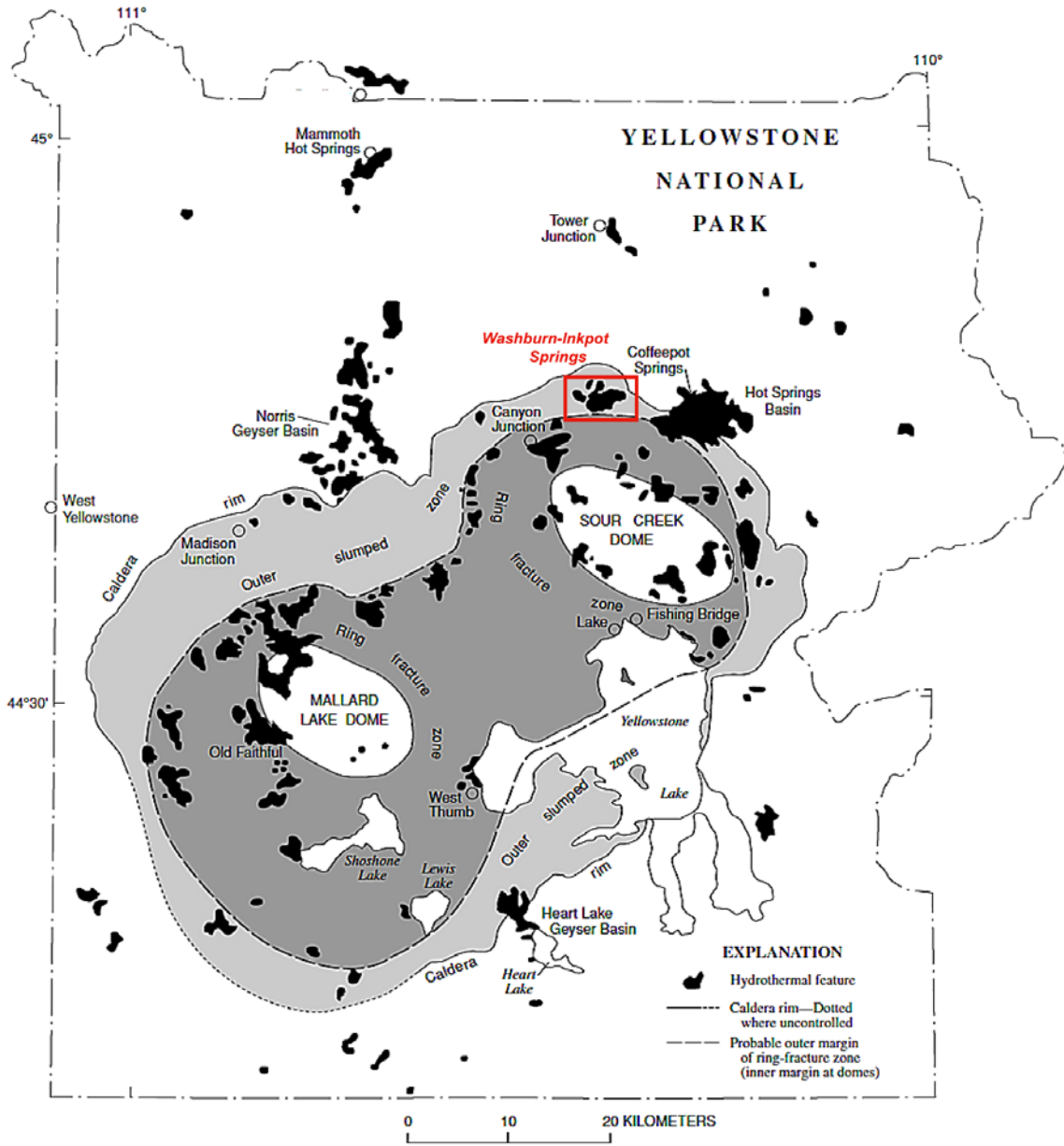


Figure 1. Hydrothermal features throughout the Yellowstone Plateau region (modified from Christiansen, 2001). Major hydrothermal areas are structurally controlled and many lie along the main-ring fracture zone of the Yellowstone caldera, including Washburn and Inkpot Hot Springs.

The purpose of this study is to determine the controls of variable pH conditions at Inkpot Spring, and if the fluid chemistry matches the composition predicted by the hydrothermal mineral assemblages exposed in the Grand Canyon of the Yellowstone River. Activity diagrams are used to show the relationship between the modern fluids at Inkpot Spring and the $\geq 147,000$ year old alteration in the nearby canyon walls (Larson et al., 2009, Phillips et al., 2007). This study also investigates different fluid sources that may contribute to the Inkpot Spring fluids, boiling and mixing processes that may affect fluid chemistry, subsurface conditions (reservoir temperature), and what produces the unique “ink” color of the pools. Stable isotope ratios are utilized to investigate the effects of boiling and mixing on the system. Determination of the different rocks with which fluids are likely reacting during ascension is another objective of this research.

2. GEOLOGIC SETTING

The Yellowstone Plateau Volcanic Field (YPVF) covers an area of 6500 km² in the middle Rocky Mountains of northwest Wyoming (Christiansen, 2001). Major eruptions have occurred in the last 2.1 million years, producing large volumes of ash-flow tuff and caldera collapse. Much of YPVF now covers the western Absaroka Range, a calc-alkaline to shoshonitic volcanic province comprised of eroded composite volcanoes active between 54 and 38 million years ago. Washburn volcano, located near the hypothesized northeast margin of the Yellowstone caldera ring-fault, is the largest calc-alkaline eruptive center in the Absaroka Volcanic Province (AVP) and largest Eocene volcanic center in YNP (Feeley et al., 2002). Magmatism at the volcano commenced as early as 55 Ma and continued until at least 52 Ma, based on ⁴⁰Ar/³⁹Ar age determinations by M.A. Cosca in Feeley et al. (2002). These ages

coincide with a period of crustal extension in the northwestern USA following the latest phases of Laramide foreland thrusting (Love et al., 1975; Feeley et al., 2002; Feeley and Cosca, 2003). The eroded remnants of Washburn volcano in the southwest Washburn Range include three major peaks; Mt. Washburn and Hedges and Dunraven Peaks. The Lamar River Formation, the eastern member of the Washburn Group, is a thick unit consisting of laharic breccias and discontinuous andesite lava flows (Smedes and Prostka, 1972; Feeley et al., 2002). It is the most laterally extensive unit with the Washburn volcano as its primary source area. The Sepulcher Formation of the Washburn Group and Langford Formation of the Thorofare Creek Group are also exposed in the southwest Washburn Range. The southwest Washburn Range consists of olivine + pyroxene basaltic andesite and amphibole-bearing dacite lava flows and dikes (Feeley et al., 2002) Dikes, stratigraphically higher lava flows, and the Sulphur Creek Stock to the east and northeast on Mt. Washburn are comprised of olivine + pyroxene basaltic andesites and pyroxene \pm amphibole andesites (Feeley et al., 2002).

The voluminous ignimbrite units of the YPVF cover much of the western Absaroka Range. They were produced by three major eruptions that accompanied caldera collapse. These units are the Huckleberry Ridge Tuff at 2.1 Ma, Mesa Falls Tuff at 1.3 Ma, and the Lava Creek Tuff at 0.64 Ma. Resurgent doming began within the caldera after the third volcanic cycle collapse. Domical uplift of the two subsided cauldron blocks produced the Sour Creek and Mallard Creek domes (Fig. 1) (Christiansen, 2001). The Sour Creek dome is located in the northeastern lobe of the caldera with the axis trending northwest toward the Solfatara fault system just outside the caldera (Love, 1961; Christiansen, 2001). The Mallard Lake dome is located in the southwestern lobe of the caldera with a northwest –trending graben system along its long axis. Based on K-Ar dating of overlying rhyolite flows, the present Mallard Lake dome

is much younger than the Sour Creek dome, although early contemporaneous doming in both caldron blocks may have occurred (Christiansen, 2001). The Mallard lake flow which was uplifted by the Mallard Lake dome is dated at 151 ± 4 ka, while an average age of 161 ± 1 ka was established for several younger flows that postdate the dome, indicating formation of the dome at about 160,000 years ago (Christiansen, 2001). Uplift of the Sour Creek dome began after caldera collapse (~ 640 ka), and the Canyon flow which onlaps the dome was dated at 484 ± 15 ka (Gansecki et al., 1996), thus constraining the timing of uplift (Christiansen, 2001). Geodetic measurements of the Yellowstone caldera from 1923 to present have revealed multiple episodes of caldera uplift and subsidence, suggesting the volcano continues to be in the later stages of a resurgent cauldron cycle (Christiansen, 2001; Chang et al., 2007; Puskas et al., 2007). Average rates of uplift and subsidence are ~ 1 to 2 cm/year centered at the two domes (Chang et al., 2007). Numerous post-collapse rhyolites, the Pleistocene Plateau Rhyolites of Christiansen (2001), fill the Yellowstone caldera and overlie and lap onto the resurgent domes.

Pervasively hydrothermally altered post-resurgent rhyolites are exposed in the Grand Canyon of the Yellowstone River between the northern caldera rim and Sour Creek dome to the south (Christiansen and Blank, 1975; Prostka et al., 1975; Christiansen, 2001). These rhyolitic lava flows and tuffs, the Upper Basin Member of the Plateau Rhyolites, are high-silica, vitrophyric deposits containing quartz, sanidine, and plagioclase with minor clinopyroxene, magnetite, and locally fayalite (Christiansen, 1975, 2001; Christiansen and Blank, 1975; Prostka et al., 1975; Hildreth et al., 1991). From youngest to oldest the units of the Upper Basin Member are the Dunraven Road Flow, the Canyon Flow, the Tuff of Sulfur Creek, and the Tuff of Uncle Tom's Trail which has limited exposure. The Dunraven Road Flow and Canyon Flow are rhyolitic lava flows, while the Tuff of Sulphur Creek is a bedded fallout tuff, and the Tuff of

Uncle Tom's Trail is a non-welded lithic-vitric ash-flow tuff (Christiansen, 2001). $^{40}\text{Ar}/^{39}\text{Ar}$ ages of the Tuff of Sulfur Creek, the Canyon Flow, and Dunraven Road Flow are 0.479 ± 0.010 , 0.484 ± 0.015 , and 0.486 ± 0.042 Ma, respectively (Gansecki et al., 1996). These units have very low magmatic $\delta^{18}\text{O}$ values (Friedman et al., 1974; Hildreth et al., 1984, 1991; Bindeman and Valley, 2000, 2001; Bindeman et al., 2001).

The three main units of the Upper Basin Member may be present near Inkpot Spring (Fig. 2a and 2b). The Tuff of Sulfur Creek is the closest mapped Yellowstone unit to Inkpot Spring but much of this unit has been covered by Quaternary detrital deposits in the numerous drainages around the spring. Where exposed in the area around Sevenmile Hole and Sulfur Creek, the rocks of the Canyon Flow and Tuff of Sulfur Creek are pervasively altered. Alteration is apparent from Sevenmile Hole along the Yellowstone River, in Sulfur Creek (an elevation of ~2050m), and across the hypothesized caldera margin to areas of active hydrothermal alteration at Inkpot and Washburn Hot Springs (an elevation of ~2475m). Alteration is sporadic and minor throughout the Absaroka volcanics exposed at Washburn volcano, but also occurs in localized zones near the caldera margin.

Inkpot and Washburn Hot Springs are located just outside the Yellowstone caldera ring fault where it truncates Washburn volcano. The southern flank of the Washburn volcano foundered during caldera collapse exposing the interior of the volcano. Several of the Washburn feeder dikes shown in Figure 2a are exposed in Sulfur Creek. The closest mapped unit to Inkpot and Washburn Hot Springs is the Sulphur Creek Stock, a shallow, fine-grained biotite tonalite intrusion related to the Washburn volcano (Fig. 2a and 2b) (Feeley et al., 2002). Andesitic lava flows and volcanoclastic rocks of the Lamar River and Sepulcher Mountain Formations (Washburn Group) make up a majority of the volcano and likely underlie the surficial

SURFICIAL DEPOSITS (HOLOCENE & PLEISTOCENE)	
Qa	Alluvium & glaciafluvial deposits - Unconsolidated coarse to fine-grained moderately well-sorted & well bedded stream channel, overbank, & fan deposits, glacial outwash, & stream-laid ice-contact deposits
Qg	Glacial deposits - Till, generally lacking distinct morainal form
Qhs	Siliceous hot-spring deposits - Generally white to light-gray siliceous sinter in mounds or sheets around active or extinct hot springs
PLATEAU RHYOLITE (PLEISTOCENE)	
Qpud	Dunraven Road flow - rhyolitic lava flow with well-preserved flow-breccia base & pumiceous glassy top
Qpus	Tuff of Sulphur Creek - Air-fall tuff, well-bedded and well-sorted. Agglutinated and resembles welded ash-flow tuff. Generally devitrified, gray to brown; basal zone is glassy, forming black vitrophyre where densely agglutinated, yellowish-brown where friable
LAVA CREEK TUFF (PLEISTOCENE)	
Qylb	Member B - Gray, brown, or pinkish-gray ash-flow tuff. Devitrified throughout; generally densely welded except for partially welded vapor-phase zones
HUCKLEBERRY RIDGE TUFF (PLEISTOCENE)	
Qyha	Member A - Brown, devitrified densely welded ash-flow tuff; black vitrophyre & gray microspherulitic zone at base
LANGFORD FORMATION (EOCENE)	
Tla	Alluvial facies - Light-gray to medium-gray well-sorted, massively bedded alluvial facies volcanic breccia and conglomerate consisting of andesite clasts in a light-medium gray ash-rich matrix
LAMAR RIVER FORMATION (EOCENE)	
Tlrd	Sulphur Creek stock - Medium- to dark-gray, fine- to medium grained diorite containing biotite, hornblende, and pyroxene
Tlri	Bodies of intrusive breccia and dikes associated with the Sulphur Creek stock - dikes of pyroxene andesite & hornblende pyroxene andesite
Tlrv	Vent facies - Medium- to dark-gray & brown laharic breccias, autoclastic flow breccias, thin discontinuous lava flows, and tuffs
Tlrf	Andesite flows - Medium-gray & brown platy-jointed lava flows & flow breccias of hypersthene-hornblende andesite & dacite
SEPULCHER FORMATION (EOCENE)	
Ts	Main body - Light-brown to yellowish-gray & greenish-gray epiclastic volcanic breccia, conglomerate, sandstone, and tuffs
Tlc	Lost Creek Tuff Member - Gray, green, purple, and yellow welded ash-flow tuff of trachyte-rhyodacite, with densely welded central zone

Figure 2b. Description of Map Units (modified from Prostka et al., 1975)

Quaternary deposits near Inkpot Spring (Feeley et al., 2002). Allen and Day (1935) were the first to recognize the abundance of andesitic cobbles in the drainages around the springs. They also attributed the dark color of the pools to iron derived from hydrothermal alteration of basaltic-andesite of the Absaroka Volcanics compared to the rhyolitic Yellowstone Volcanics.

The volcanic history of Yellowstone has been studied extensively but little is known about the underlying Paleozoic to mid-Tertiary stratigraphy. Drill holes completed by the USGS have been relatively shallow (maximum depth of 157m; Bargar and Beeson, 1985), reaching only the uppermost portion of the hydrothermal system and penetrating no deeper than the uppermost Yellowstone volcanics (Burnett, 2004). The Paleozoic Madison Limestone is the thickest sedimentary unit in the northern part of YNP. These Paleozoic limestones and dolostones are roughly 1000m thick and are overlain by approximately 1600m of shale, sandstone, mudstone, conglomerate, and limestone of Mesozoic age (Burnett, 2004). It is unknown whether these units underlie the volcanics in other parts of the park, but seismic data presented by Smith and Braile (1982) and stratigraphic interpolations (Tonnsen, 1982) suggest they that may be present (Burnett, 2004). Their presence near Inkpot Spring has important implications because subsurface water/rock interaction may have influenced the geochemistry of the subsurface fluids. The detection of high amounts of organic gases at Inkpot and Washburn Hot Springs has lead to speculation that distillation of hydrocarbons within these sedimentary units is occurring somewhere along the flow path (Allen and Day, 1935; Fournier, 1989; Burnett, 2004). Hydrocarbon discharges have been observed at Tower Bridge, Calcite Springs, and Rainbow Springs (Love and Good, 1970) which occur along the leading edge of the Gardiner Thrust trend, north and east of Inkpot Spring (Tonnsen, 1982). Two other occurrences of hydrocarbons in thermal areas east of YNP include Sweetwater Mineral Springs and Cedar

Mountain. These five occurrences lie in an arcuate southeastward- to eastward area 70 miles long (Love and Good, 1970). Rainbow Hot Springs is ~13 km west of Inkpot Spring and across the Grand Canyon of the Yellowstone River, just north of Hot Springs Basin. It is the closest known thermal area to Inkpot Spring that contains a hydrocarbon component.

The hydrocarbons have been used as evidence that sedimentary strata are present at depth beneath the surficial volcanics, and perhaps, beneath the springs (Clifton et al., 1990; Burnett, 2004). Clifton et al. (1990) suggest that the Permian Phosphoria Formation is a possible source of oil seeps at Calcite Springs, and that the Eocene Aycross Formation, with a minor contribution from bacteria or terrestrial plant material, is the source of oil at Rainbow Hot Springs. Marine facies of the Phosphoria Formation are thought to be a source of oil west of YNP (Tonnsen, 1982). The Eocene Aycross Formation is an alluvial facies of Absaroka volcanics found east and southeast of YNP (Smedes and Prostka, 1972), but is probably outside the circulation of Yellowstone's hydrothermal system (Burnett, (2004). Based on sulfur and nitrogen contents and the ratio of nitrogen to Ramsbottom carbon residue, Love and Good (1970) determined that hydrocarbons at Rainbow Hot Springs are post-Jurassic. Carbon isotopes suggest a marine origin for hydrocarbons at Rainbow Hot Springs, contrasting with their idea that bacteria or terrestrial plant material is the source. Post-Jurassic age marine shales and sandstones are found ~26.5 km northwest of Inkpot Spring on a trend parallel to the Solfatara Fault System. These Upper Cretaceous units including the Landslide Creek Formation, Mt. Everts Formation, and Cody Shale, among others, are exposed at Mount Everts near Mammoth Hot Springs and dip to the northwest. These rocks overlie Lower Cretaceous units including the Mowry Shale, Thermopolis Shale, and Kootenai Formation. Some coal beds have been observed in the Cretaceous section, as well (Ruppel, 1982). These Cretaceous shales and coal beds are a

potential source of hydrocarbons at Inkpot Spring and Washburn and Rainbow Hot Springs. Other potential, yet unlikely, source rocks for petroleum in Yellowstone include the Bakken Shale Formation of the Williston Basin, shales of the Big Snowy Formation corresponding to the Heath Shale of Central Montana, dolomites in the Upper Devonian Jefferson Formation, Mississippian Mission Canyon Formation, and Ordovician Big Horn Dolomite Formation (Tonnsen, 1982; Burnett, 2004). These Upper Devonian and Upper Ordovician units are found ~26 km north-northeast of Inkpot Spring along the YNP boundary where they overlie Cambrian shales and limestones and are overlain by the Eocene Absaroka volcanics and Quaternary detrital deposits.

3. HYDROTHERMAL BACKGROUND

Inkpot and Washburn Hot Springs are located just outside the Yellowstone caldera wall along Sulfur Creek, 2.4 km northwest of Sevenmile Hole, and 4.6 km southeast of Dunraven Pass (Fig. 2a and Fig. 3). The acid-sulfate, vapor-dominated springs are positioned on the southwest side of a northwest trending ridge, part of the Solfatara fault system (Fig. 3 and Fig. 4). Large, vapor-dominated systems like the one in this part of YNP develop when relatively impermeable rock and locally derived shallow groundwater provide a cap over a reservoir of considerable vertical extent (Fournier, 1981). Hydrothermal fluids emanating at both Inkpot Spring and unnamed springs along the Yellowstone River show a local vertical extent of at least 300 m within the Yellowstone hydrothermal system.

White et al. (1971) provide a general model for vapor-dominated geothermal systems that help explain the occurrence of acid-sulfate fluids at Inkpot Spring (Fig. 5). In these systems, steam is the continuous phase in open fractures while liquid water fills pore space (Fig. 6).

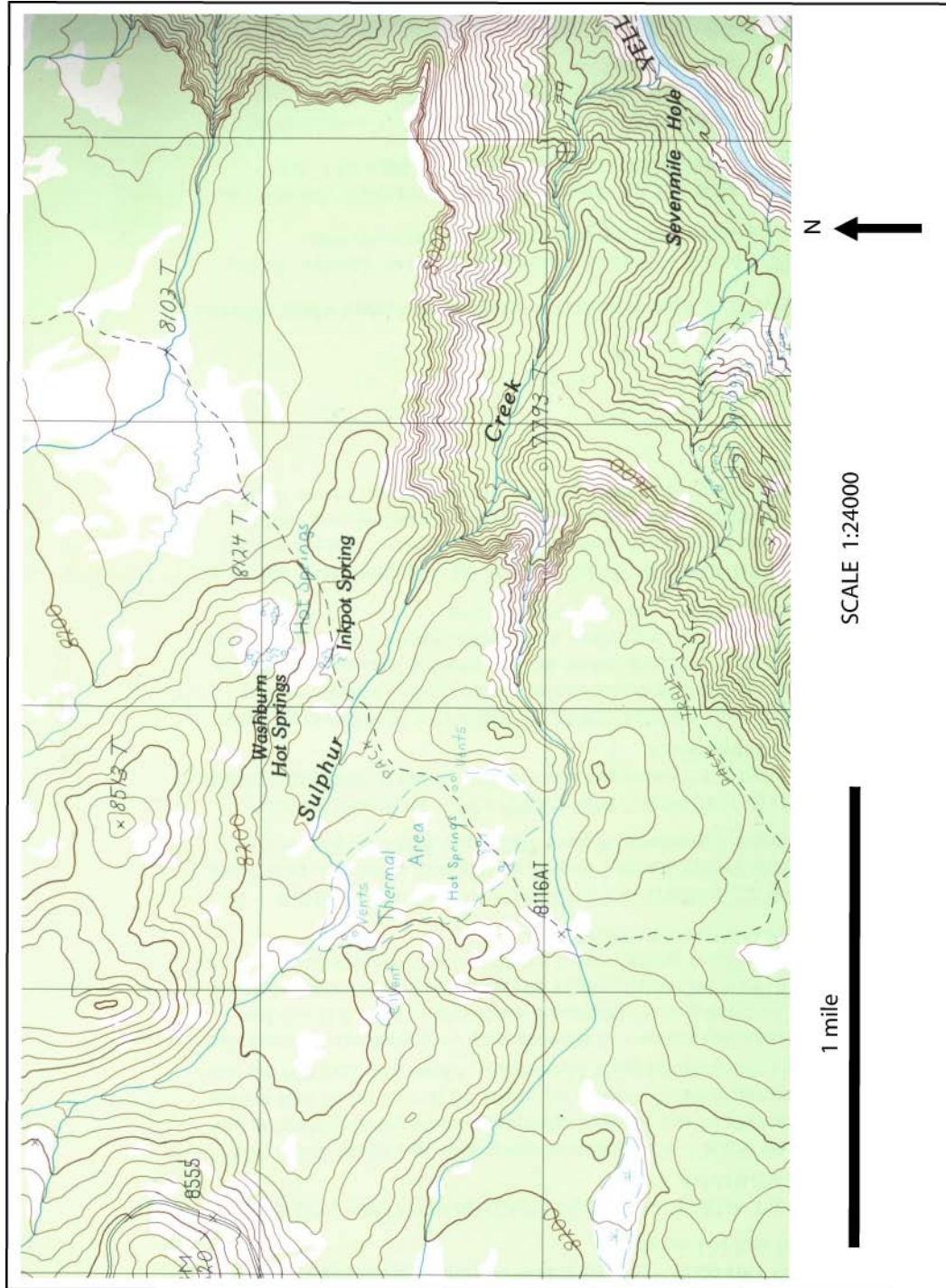


Figure 3. Topographic map of the Sulphur Creek -Sevenmile Hole area (from USGS Mount Washburn 7.5 Minute Quadrangle Map, 1986). Washburn Hot Springs are located near the top of a ridge trending northwest toward Dumraven Pass. Inkpot Spring is located on the southwest side of the ridge. Other thermal areas, mainly extinct, are located further to the southwest.

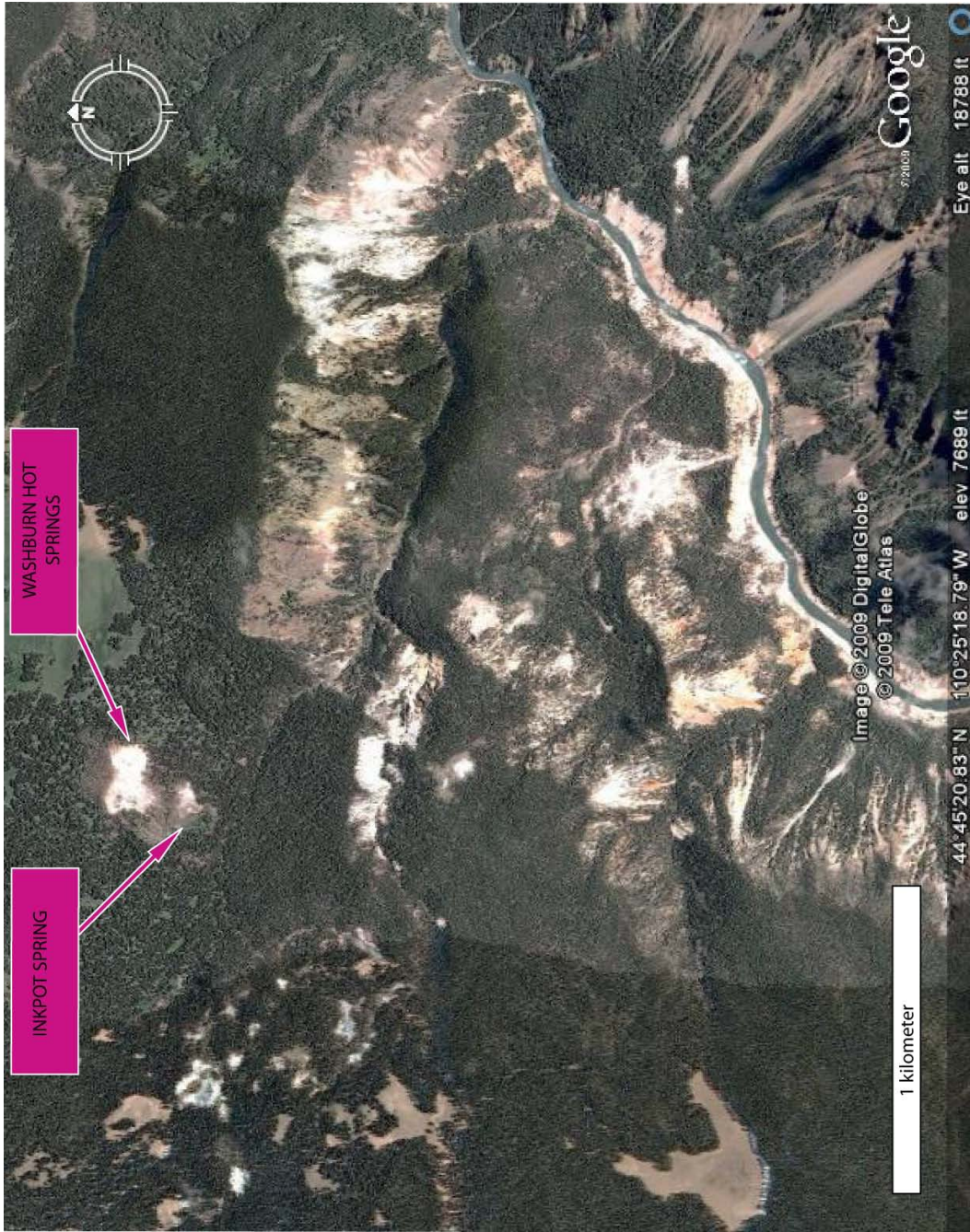


Figure 4. Aerial view of Sulphur Creek-Sevenmile Hole area near the Grand Canyon of the Yellowstone River (modified from Google Earth image). Siliceous sinter and acid-leached ground of active and extinct hydrothermal features appear as bright white areas.

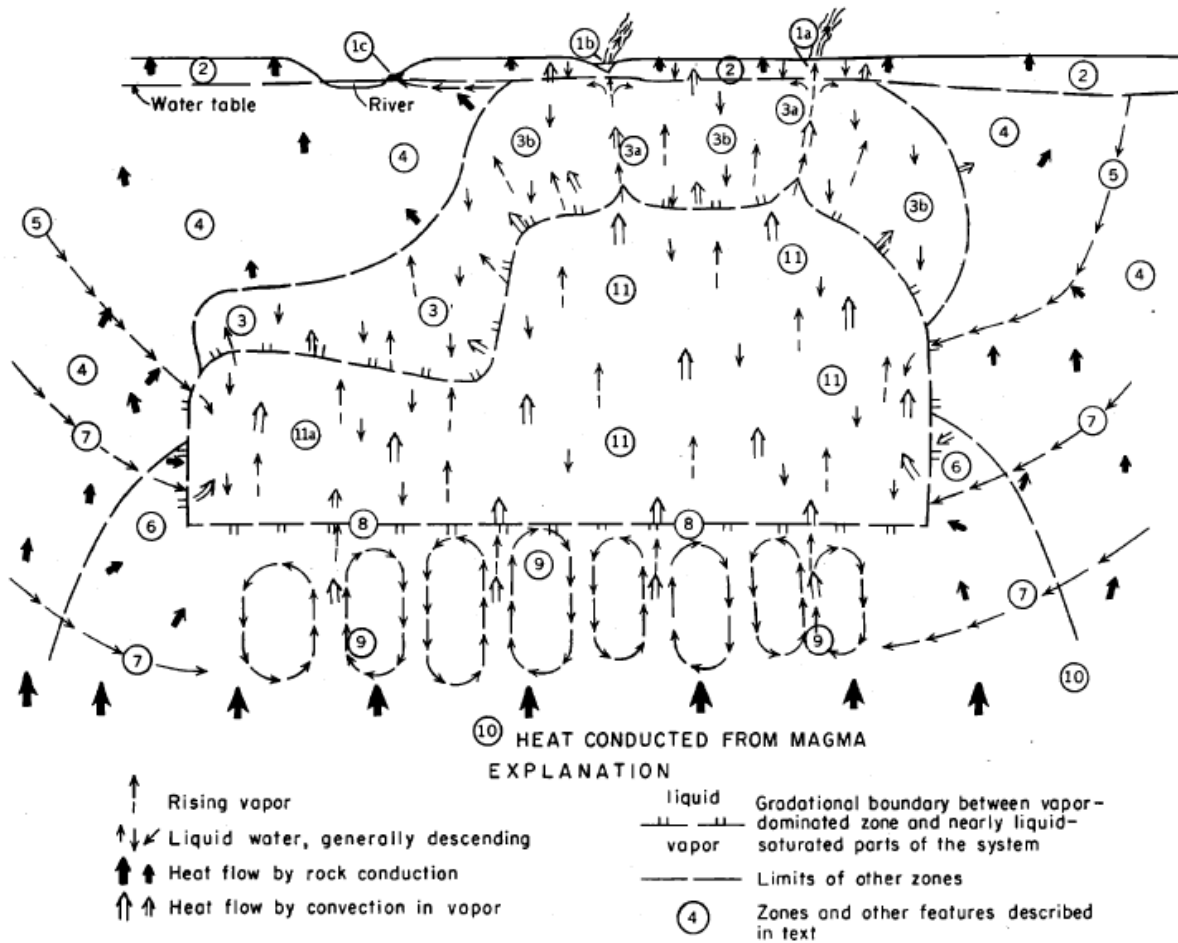


Figure 5. General model for vapor-dominated hydrothermal system from White et al. (1971).

Zones 1a, 1b, 1c: Fluids discharging at the surface; features include fumaroles, acid-sulfate mudpots and springs depositing little if any sinter, and strongly bleached ground.

Zone 2: Between the ground surface and water table where steam and other gases rise above the water table. Heat transfer is convective at the water table, but as temperature gradient increases upward and vapor condenses, near-surface heat transfer becomes largely conductive.

Zones 3, 3a, 3b: Saturated with liquid water derived from condensing CO₂-rich steam. Montmorillonite and kaolinite form by reaction of CO₂-rich condensate with silicate minerals. This material clogs most pore spaces impeding but not prohibiting further escape of gases. Near major zones of upflowing steam (3a), temperatures and pressures are somewhat above hydrostatic, and conductive heat flow and condensation of steam are high; some of the condensate is swept upward to the water-table or surface features. Zone 3b is dominated by downflowing condensate and some surface water. As temperature gradients increase outward and upward through zone 3, more heat of vaporization in the rising steam can be transferred by conduction. Water is continuously condensing and rate of vapor flow decreases upward. The dashed line within zone 3 marks the gradation from convective to conductive heat transfer.

Zone 4: Zone of conductive heat flow, with heat supplied from condensing steam in zone 3.

Zone 5: Channels of intermediate-level recharge are deep enough at points of entry for hydrostatic pressure to exceed the vapor pressure of about 31 to 35 kg/cm² in the reservoir (zone 11). Channels of inflow are enlarged by solution of SiO₂ as the inflowing water is heated by conduction (indicated by arrows in Figure 5). Channels are diminished, however, by deposition of CaCO₃ and CaSO₄, which decrease in solubility with increasing temperature.

Zone 6: Reservoir margins where temperatures decrease toward the reservoir. These reservoir margins contain channels of inflowing water at pressures that are close to hydrostatic and much greater than ~33 kg/cm² of the reservoir, therefore sharp pressure and temperature gradients decreasing toward the reservoir exist in zone 6. Heat is transmitted by conduction and inflowing water into the reservoir. Temperatures grade downward into, and are maintained by conduction from zone 10.

Zone 7: Channels of inflowing water are narrowed by precipitation of calcite and anhydrite but may be offset by solution of quartz which increases in solubility as long as the liquid water continues to rise in temperature. At the outer edge of this zone pressures and temperatures attain their maxima; boiling commences and temperature decreases with further flow toward the reservoir. In these channels, the flow of the two-phase mixture of steam and water is impeded by precipitation of quartz and other minerals.

Zone 8: The deep subsurface water table recedes as long as the heat supply is sufficient for net loss of liquid water and vapor from the system to exceed net inflow.

Zone 9: Deep zone of convective heat transfer, probably in brine.

Zone 10: Deep zone of conductive heat flow (too hot for open fractures to be maintained).

Zone 11: Main vapor-dominated reservoir, with convective upflow of heat in steam in larger channels, and downflow of condensate in small pores and fractures (surface tension effects).

Above the steam zone, fluid temperature and pressure increase with increasing depth, while there is little change in hydrostatic head within the steam zone because the density of steam is substantially less than that of liquid water (Fournier, 1981). Temperature and pressure again increase with increasing depth below the steam zone where liquid fills fractures and open channels (Fournier, 1981). Steam in vapor-dominated systems commonly carries volatiles such as NH₃, CO₂, H₂S, Hg, and B, which all occur at elevated concentrations in the pools of cooler surface water at Inkpot Spring. Surface manifestations of vapor-dominated systems commonly include fumaroles, mud pots, acid-sulfate springs with low rates of discharge, and acid-altered ground, all of which are found at Inkpot Spring.

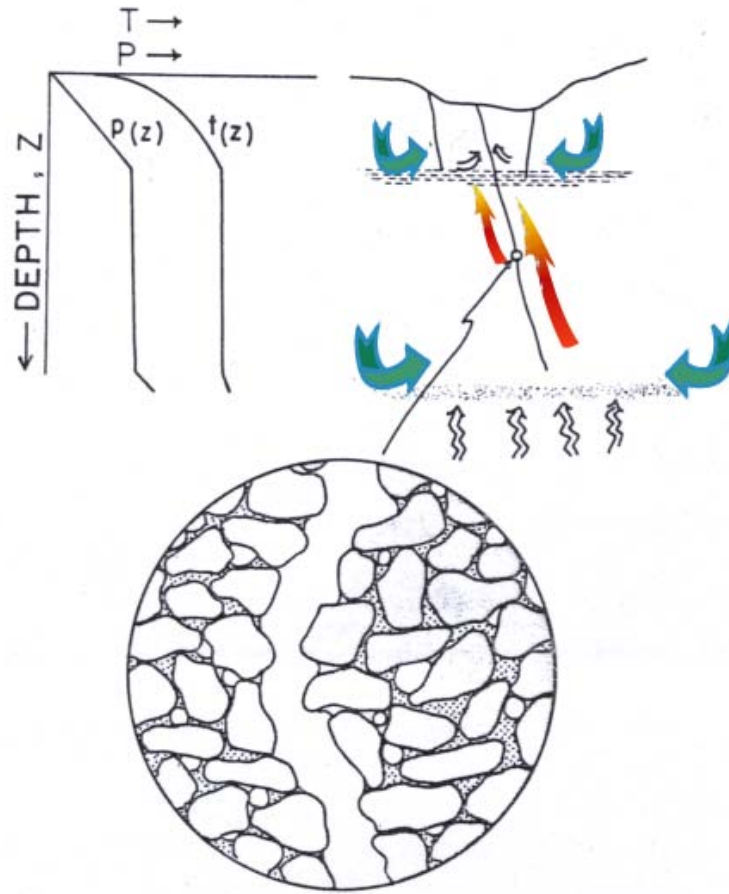


Figure 6. Schematic model of temperature and pressure conditions in a vapor-dominated geothermal system (modified from Fournier, 1981). Steam is the dominant phase in fractures, while liquid water fills pore space.

Yellowstone thermal waters are bimodally distributed between acid-sulfate and alkali-chloride waters although variable mixtures do exist (Nordstrom et al., 2009). In nearby Norris Geysir Basin, fluids of different chemistry can be found in close proximity. Other classifications have further subdivided Yellowstone's hydrothermal fluids. White et al. (1988) classified fluids from Norris Geysir Basin into four categories based on their major chemical and physical characteristics. These fluids include nearly neutral waters high in Cl and SiO₂, dilute recharging meteoric waters, acid Cl-SO₄ and acid SO₄-Cl waters, and acid-SO₄ waters. Nordstrom et al. (2009) provide a similar classification for Yellowstone thermal waters including (1) meteoric water containing minor solutes from weathering processes at low temperature and no contact with thermal fluids, (2) meteoric waters heated only by high-temperature gases, commonly containing high concentrations of SO₄ and high δ¹⁸O values, (3) deep hydrothermal waters with Cl concentrations of 310-400 mg/L and SO₄ concentrations of 10-100 mg/L, (4) deep hydrothermal waters that have boiled at depth with Cl concentrations greater than 400 mg/L, (5) hydrothermal waters that have boiled at depth and have been heated further with H₂S-enriched gases achieving higher SO₄ concentrations, (6) mixtures of these previous types, and (7) H₂SO₄ formed by oxidation of elemental S in hydrothermally altered areas that are no longer active.

Water-chemistry data have been collected at various times from the Washburn-Inkpot area since Allen and Day's study in 1935. Multiple USGS reports on the Yellowstone hydrothermal system include water-chemistry results from Washburn and Inkpot Hot Springs. For this study, we prefer to separate Inkpot Spring from Washburn Hot Springs, although a majority of the previous literature does not differentiate between the two because of proximity and indistinguishable chemistry. A compilation of previous Washburn and Inkpot water chemistry data from USGS and Carnegie Institute publications is included in Appendix B.

4. METHODS & PROCEDURES

4.1 Field Methods

Sample collection and field measurements took place from July 26, 2008, through August 9, 2009. Field methods and procedures followed those described in McCleskey et al. (2005) as closely as possible. Samples were collected from 8 separate pools at Inkpot Spring on 2 different days over the two-week period. With three additional samples collected at unnamed springs on altered ground several hundred meters west of Inkpot Spring, a total 19 samples were collected. Extreme care was taken to safely collect samples, protect fragile hot spring formations, and minimize changes in pH, temperature, and water chemistry during collection. Samples were collected from the center of the pool using a polyethylene bottle attached to an extendable aluminum pole (Fig. 7). Samples were filtered onsite by filling a 60-mL syringe at the source or with source water collected with the polyethylene container and extendable pole and immediately forcing the water through a 25-mm filter with a mixed cellulose-ester membrane with a pore size of 0.45 μm . Sample splits collected for determination of major cations and trace metals (Al, As, B, Ba, Ca, Co, Cu, Cr, Fe, Ga, Hg, K, Mg, Mn, Mo, Na, Ni, Pb, Rb, Sb, Si, Sn, Sr, Ti, Tl, V, W, and Zn), major anions (Br, Cl, F, NO_3 , and SO_4), alkalinity (as HCO_3), ammonium, nitrite, and water isotope ratios ($\delta^{18}\text{O}$ and δD) were filtered and then stabilizing reagents (nitric and diluted sulfuric acids), if needed, were added (McCleskey et al., 2005). Container preparation, stabilization, and filtration methods are summarized in Table 1. All samples were chilled as soon as practical after sample collection.

Field measurements of pH and temperature were performed on 7 different days during the two-week observation period using an Oakton 110 pH meter. Field measurement of pH in geothermal waters is challenging because of near boiling temperatures, complex sample matrices,



Figure 7. Sampling procedure using polyethylene bottle attached to an extendable aluminum pole.

Table 1. Container preparation and stabilization, filtration, and analytical methods				
Sample type(s)	Container preparation	Filtration	Stabilization treatment in addition to keeping on ice	Primary analytical method(s) & instrument(s)
Major cations and trace metals (Al, As, B, Ba, Ca, Co, Cu, Cr, Fe, Ga, K, Mg, Mn, Mo, Na, Ni, Pb, Rb, Sb, Si, Sn, Sr, Ti, Tl, V, W, and Zn)	High density polyethylene bottles soaked in 5% HCl and rinsed 3 times with distilled water	Filtered using disposable 25 mm mixed cellulose-ester membrane with 0.2 µm pore size, attached to a 60 mL syringe	1% (v/v) concentrated HNO ₃ added	ICP-MS ICP-AES
Major anions (Br, Cl, F, and SO ₄), alkalinity as HCO ₃ , nitrite	High density polyethylene bottles filled with distilled water and allowed to stand for 24 hours, then rinsed 3 times with distilled water	Same as major cations and trace metals	None	Ion Chromatography
Ammonia (NH ₃)	Same as major cations and trace metals	Same as major cations and trace metals	1% (v/v) 1:9 H ₂ SO ₄ added	Ion Chromatography
Oxygen isotopes (δ ¹⁸ O)	Same as major cations and trace metals	Same as major cations and trace metals	None	Finnegan MAT Delta S Gas Source IR-MS
Hydrogen isotopes (δD)	Same as major cations and trace metals	Same as major cations and trace metals	None	Finnegan MAT TC-EA Pyrolysis Unit
Mercury (Hg)	Same as major cations and trace metals	Same as major cations and trace metals	Same as major cations and trace metals	Direct Mercury Analysis (DMA-80 Pyrolysis Unit)
			None	
		Unfiltered	None	

and swelling water from gas discharge, therefore, electrodes specifically rated for boiling or near-boiling water temperatures were used (McCleskey et al., 2005). The meter was calibrated before each round of sampling and once midway through each round of sampling. The system was calibrated using two bracketing standard buffers having a pH of 4.01 and 7.00 corrected to their values at the sample temperature. After calibration, the electrodes were rinsed with deionized water, allowed to dry, and then submersed at the source until no change in temperature ($\pm 0.1^\circ\text{C}$) or pH (± 0.01 standard unit) was detected for 30 seconds. Temperature and pH of each pool were measured on at least 3 different days except for the 3 unnamed springs west of Inkpot Spring. A compilation of these pH and temperature results with averages for each pool over the two-week period along with photographs of each pool is presented in Appendix A.

Gases emanating from the hot spring pools, including CO_2 , CH_4 , NH_3 , C_2H_6 , and SO_2 , were measured to determine processes that occur along the path of upflow and to help identify different rock types fluids may be in contact with at depth. These gases were measured by infrared (IR) spectroscopy using a MIRAN 205B Series SapphIRe Portable Ambient Air Analyzer provided by the Oak Ridge National Laboratory. The IR analyzer's wavelength generator allows accurate and fast wavelength selection by matching the infrared frequency of tuning for vibration to the frequency of molecules. These results are reported in ppm, and are included in Appendix H. The IR analyzer's filter was attached to ~2 m pole and extended out over the pools (Fig. 8). Gas measurements determined by this method are qualitative as height above the pool and wind conditions strongly affected readings by the instrument. Previous gas results provided in Appendix G probably provide more accurate concentrations of gases at Inkpot Spring.



Figure 8. Gas chemistry measurement technique with MIRAN 205B Series SapphIRe Portable Ambient Air Analyzer provided by the Oak Ridge National Laboratory.

In addition to water collection and gas measurements, small sediment samples were collected around the edge of several pools, most of which were dark gray, clay-rich mud. Unfiltered samples were also collected directly from the pools for analysis of suspended sediment, precipitates, and mercury.

4.2 Analytical Procedures

Concentrations of major cations (Al, B, Ca, Fe, K, Mg, Na, and Si) were determined using an inductively coupled plasma atomic emission spectrometer (ICP-AES) at the University of Idaho Pedology Laboratory. Concentrations of trace metals (As, Ba, Co, Cu, Cr, Ga, Hg, Mn, Mo, Ni, Pb, Rb, Sb, Sn, Sr, Ti, Tl, V, W, and Zn) were determined using a HP4500 inductively coupled plasma mass spectrometer at Washington State University's GeoAnalytical Laboratory. Standard 3-point calibration curves were used for the ICPs. Low, mid, and high standards were used, as well as a quality control standard (QC). Working standards were prepared by dilution from 1,000 mg/L or 10,000 mg/L stock standards. All elements analyzed by either ICP-MS or ICP-AES were added to the same 100-mL or 250-mL volumetric flask after using a calibrated automatic pipette and weighing each stock standard on a calibrated digital scale. Working standards were brought to volume by adding triple distilled water into each volumetric flask. Accuracy and detection limits for the various analytical methods described above are included in Appendix C.

Inkpot Spring fluids were analyzed for major anions, alkalinity, pH, and ammonia at the University of Idaho's Analytical Sciences Laboratory. Hydroxide, carbonate, bicarbonate, and total alkalinity were measured by titration, following EPA method 310.1. Fluid pH was measured once again in the laboratory to record changes between the time of sampling and these

analyses. EPA method 150.1 was used for pH determination. Major anions including fluoride, chloride, nitrite-N, bromide, nitrate-N, o-Phosphate-P, and sulfate were determined using ion chromatography (IC), following EPA method 300.0. Ammonia-N was determined using a flow injection analyzer (FIA), following EPA method 350.1. All of the aforementioned EPA methods are outlined in EPA Report # 600/4-79-020 (U.S. EPA, 1983).

Oxygen isotope values were measured using a Finnegan MAT Delta S Gas Source Isotope Ratio Mass Spectrometer (Finnegan MAT IR-MS) at Washington State University's GeoAnalytical Laboratory. Hydrogen isotope values were measured using a Finnegan MAT high temperature conversion elemental analyzer pyrolysis unit (Finnegan MAT TC-EA) at the University of New Mexico Department of Earth and Planetary Sciences' Stable Isotope Laboratory. Analysis of δD is completed by placing the sample in silver capsules which are subsequently dropped into a 1325°C oven in a helium flow. During heating, reduction occurs forming H₂ and CO, which are then separated in a gas chromatograph and the H is analyzed for δD . Isotopic compositions are expressed in the δ -notation, which compares the isotope ratio of a sample to the Vienna Standard Mean Ocean Water (VSMOW) standard in parts per thousand (‰).

Sediment samples and precipitates were analyzed for major and trace elements by ALS-Chemex using method ME-MS41 which includes the use of both the ICP-MS and ICP-AES techniques in order to provide the widest concentration range. This method includes aqua regia digestion, therefore, data should be considered as representing only the leachable portion of the particular analyte. Fully quantitative Au concentrations were determined using method Au-ICP21, which includes fire assay fusion and the ICP-AES. Sediment sample #YS07AA15 was analyzed using the methods outlined above, as well as the X-ray Fluorescence Spectrometer at

WSU's GeoAnalytical Laboratory, for quality control purposes. The Siemens D-500 X-ray powder Diffractometer along with Materials Data Jade 8 software and searchable ICDD powder diffraction file at WSU's GeoAnalytical Laboratory was used for identification of different mineral phases in the sediment. Sediments were also analyzed by energy dispersive X-ray spectrometry (EDS) and backscattered electron imaging using a JEOL 8500F field emission electron microprobe in WSU's GeoAnalytical Laboratory.

Concentration of mercury in fluids, sediments and precipitates, and suspended sediment mud slurries is determined by thermal decomposition amalgamation and atomic absorption spectrophotometry, following EPA Method 7473. Mercury measurements were performed using a Direct Mercury Analyzer (DMA 80) in Washington State University's Department of Civil and Environmental Engineering. This method begins with the controlled heating of the sample in an oxygenated decomposition furnace, which is used to liberate mercury from solid and aqueous samples in the instrument. Once dried and thermally and chemically decomposed, products are carried by flowing oxygen to the catalytic section of the furnace where oxidation is completed and nitrogen/sulfur oxides are trapped (U.S. EPA, 2000). Remaining decomposition products are then carried to an amalgamator that selectively traps mercury. The amalgamator is rapidly heated, releasing mercury vapor, which is carried through absorbance cells positioned in the light path of a single wavelength atomic absorption spectrophotometer. Absorbance is measured at 253.7 nm as a function of mercury concentration (U.S. EPA, 2000).

5. RESULTS

5.1 Stable Isotope Ratios

The stable isotope ratios of water, especially when combined with the concentrations of other solutes, are good geochemical indicators of the origins, recharge locations, and flow paths of subsurface waters (Kharaka et al., 2002). The δD and $\delta^{18}O$ values of water are useful tools because the relations governing their distribution in surface and shallow ground waters, as well as their modifications in aquifers, are reasonably well known (Kharaka et al., 2002). Isotope ratios of meteoric water in YNP may be modified by evaporation and mixing at low temperatures and by mixing, boiling, and isotopic exchange with minerals at high temperatures. The isotopic concentration is reported in “delta notation”, which compares the isotope ratio of a sample to that of a reference standard. For the example of $^{18}O/^{16}O$ ratios, delta notation is:

$$\delta^{18}O\text{‰} = \left(\frac{\left(\frac{^{18}O}{^{16}O} \right)_{\text{sample}}}{\left(\frac{^{18}O}{^{16}O} \right)_{\text{standard}}} - 1 \right) \times 1000 \quad (5-1)$$

and in the case of hydrogen, the equation is:

$$\delta^{2}H\text{‰} = \left(\frac{\left(\frac{^2H}{^1H} \right)_{\text{sample}}}{\left(\frac{^2H}{^1H} \right)_{\text{standard}}} - 1 \right) \times 1000 \quad (5-2)$$

where ‰ is per mil, which is equivalent to parts per thousand. Oxygen and hydrogen isotopic results are reported relative to Vienna Standard Mean Ocean Water (VSMOW).

The δD and $\delta^{18}O$ values for meteoric recharge water in YNP, as calculated by Truesdell et al. (1977), are -149‰ and -19.9‰, respectively. These are generally accepted values,

however, hydrogen isotopic fractionation between water and steam at high temperatures could suggest a δD value higher than the -149‰ calculated by Truesdell et al. (1977) (Kharaka et al., 2002; Giggenbach, 1992). Current local meteoric water has isotopic values slightly higher than those calculated by Truesdell et al. (1977). Thordsen et al. (1992) found that modern cold meteoric water in YNP has δD and $\delta^{18}O$ values that range from -129 to -152 and -15.5 to -20.3‰, respectively. Snow samples were found to have δD and $\delta^{18}O$ values that range from -133 to -167 and -17.8 to -22.2‰, respectively. One possible explanation for the hydrothermal values that are lighter than present day precipitation may be that a majority of the water currently discharging in the Yellowstone caldera was recharged from the nearby Gallatin and Absaroka Ranges during the Little Ice Age (1250-1900 AD), when cooler temperatures would have resulted in lighter isotopic values (Kharaka et al., 2002).

Stable isotope ratios for Inkpot Spring fluids from previous USGS studies are included in Appendix B. Inkpot Spring thermal waters, from 1978 to 2003, had $\delta^{18}O$ values from -2.8 to -7.3‰ and δD values from -106 to -120‰. Results from this study are included in Appendix C and show similar results to previous USGS studies. Inkpot Spring fluids measured in 2008 had $\delta^{18}O$ values from -5.8 to 4.2‰ and δD values from -100 to -113‰. Stable isotope ratios from Inkpot Spring are recognized as some of the highest from hot spring fluids in YNP. Isotopic fractionation occurs when water is converted to steam in vapor-dominated systems like Inkpot Spring, which partially explains the variation between these fluids and other Yellowstone recharge waters. Isotopic compositions of the fluid depend on the ratio of steam to water, which is controlled by temperature and pressure. Using thermodynamic and isotopic fractionation data for water and steam, Truesdell et al. (1977) calculated increases in $\delta^{18}O$ and δD for both single-stage steam separation and continuous steam separation from 250° to 95°C. Single stage steam

separation was found to increase $\delta^{18}\text{O}$ values by as much as 1.75‰ and δD by 9.1‰, while continuous steam separation results in a $\delta^{18}\text{O}$ increase of 1.05‰ and δD increase of 3.1‰.

Continuous steam separation occurs when steam separates from water, with decreasing pressure and temperature, as soon as it is formed. This process may occur where boiling water moves upward along a fault with numerous offshoot faults allowing steam to escape as soon as it is formed, over a less restrictive temperature range. Single stage steam separation is more likely to occur along fewer restricted conduits or fractures where steam may remain with water until a certain temperature is reached (Truesdell et al., 1977). Multiple-stage steam separation is intermediate between single-stage and continuous steam separation and occurs along a finite number of faults and fractures (Truesdell et al., 1997). The significantly high oxygen isotope values coupled with the location along the caldera ring fault, suggest single-stage or multiple-stage steam separation at Inkpot Spring. If meteoric recharge water has $\delta^{18}\text{O}$ and δD values of -19.9 and -149, respectively, the higher isotope values at Inkpot Spring cannot be accounted for exclusively by steam separation.

These springs exhibit the “ $\delta^{18}\text{O}$ shift” typical of hydrothermal systems (Fig. 9). This shift can be explained primarily by boiling where fractionation leaves the liquid water enriched in the heavier isotope of oxygen (^{18}O) and the vapor enriched in the lighter isotope (^{16}O). Mixing with cooler, dilute groundwater generally lowers $\delta^{18}\text{O}$ values. Evidence of mixing at Inkpot Spring is not clearly reflected by the $\delta^{18}\text{O}$ values alone, which are very high. Possible explanations are that boiling occurs post-mixing or that the pools contain a significant thermal water component compared to the diluting groundwater component. A significant amount of the observed $\delta^{18}\text{O}$ shift may also be due to exchange of oxygen isotopes between water and rock, where the rock is shifted to lower $\delta^{18}\text{O}$ values and water is shifted to higher $\delta^{18}\text{O}$ values, depending on the

δD vs $\delta^{18}O$ of Hydrothermal Fluids at Inkpot Spring compared with other Thermal Areas in Yellowstone National Park

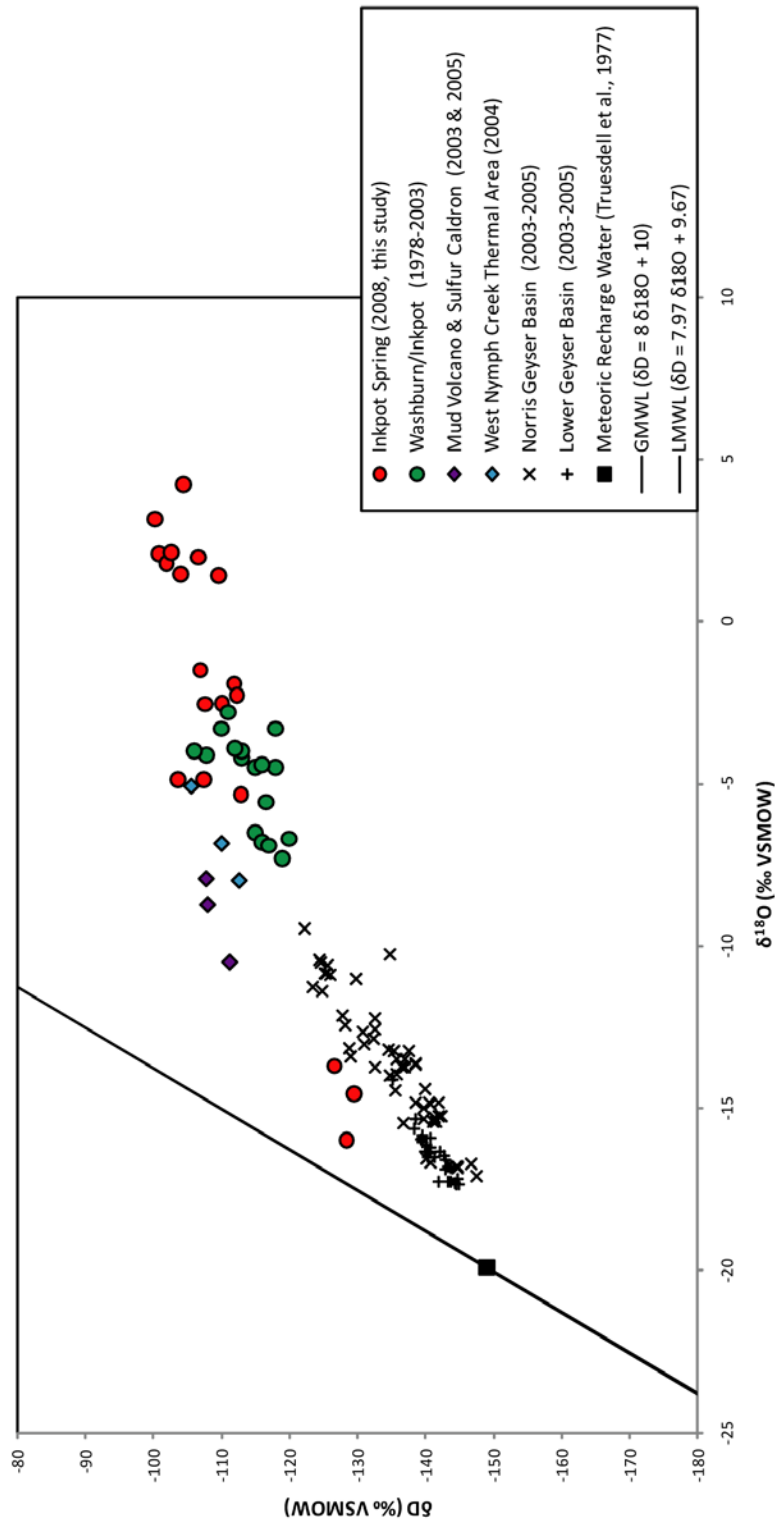


Figure 9. Graph showing δD versus $\delta^{18}O$ of Yellowstone hydrothermal fluids relative to the Global Meteoric Water Line (GMWL) and Local Meteoric Water Line (LMWL). Inkpot Spring fluids (red and green circles) show a strong shift away from the GMWL/LMWL. Three samples collected southwest of Inkpot Spring plot close to the GMWL/LMWL and probably consist of standing pools of groundwater slightly heated by steam. Other thermal areas within YNP share similar isotopic signatures, although Inkpot has the highest values. The significant isotopic shift observed at Inkpot is due to evaporation at near boiling conditions and water-rock interaction. Previous Washburn/Inkpot data are included in Appendix B and Inkpot Spring 2008 data are included in Appendix C. Previous data from Norris and Lower Geyser Basins, Mud Volcano and Sulfur Caldron, and West Nymph Creek Thermal Area were provided by J.W. Ball at the USGS, and are now available in Ball et al., 2007. Meteoric recharge water is from the calculated values of Truesdell et al., 1997.

temperature and water/rock ratio. Isotopic exchange with minerals in the wall rock and hydroxyl-bearing clay minerals lining conduits, may contribute to the variation in oxygen and hydrogen isotopes at Inkpot Spring. Much of this exchange probably occurs at the highest temperatures within the system where unaltered rock may be exposed due to thermal stress cracking, and little exchange may occur at lower temperatures where upflow channels have been established and coated with minerals in isotopic equilibrium with the fluids (Truesdell et al., 1977).

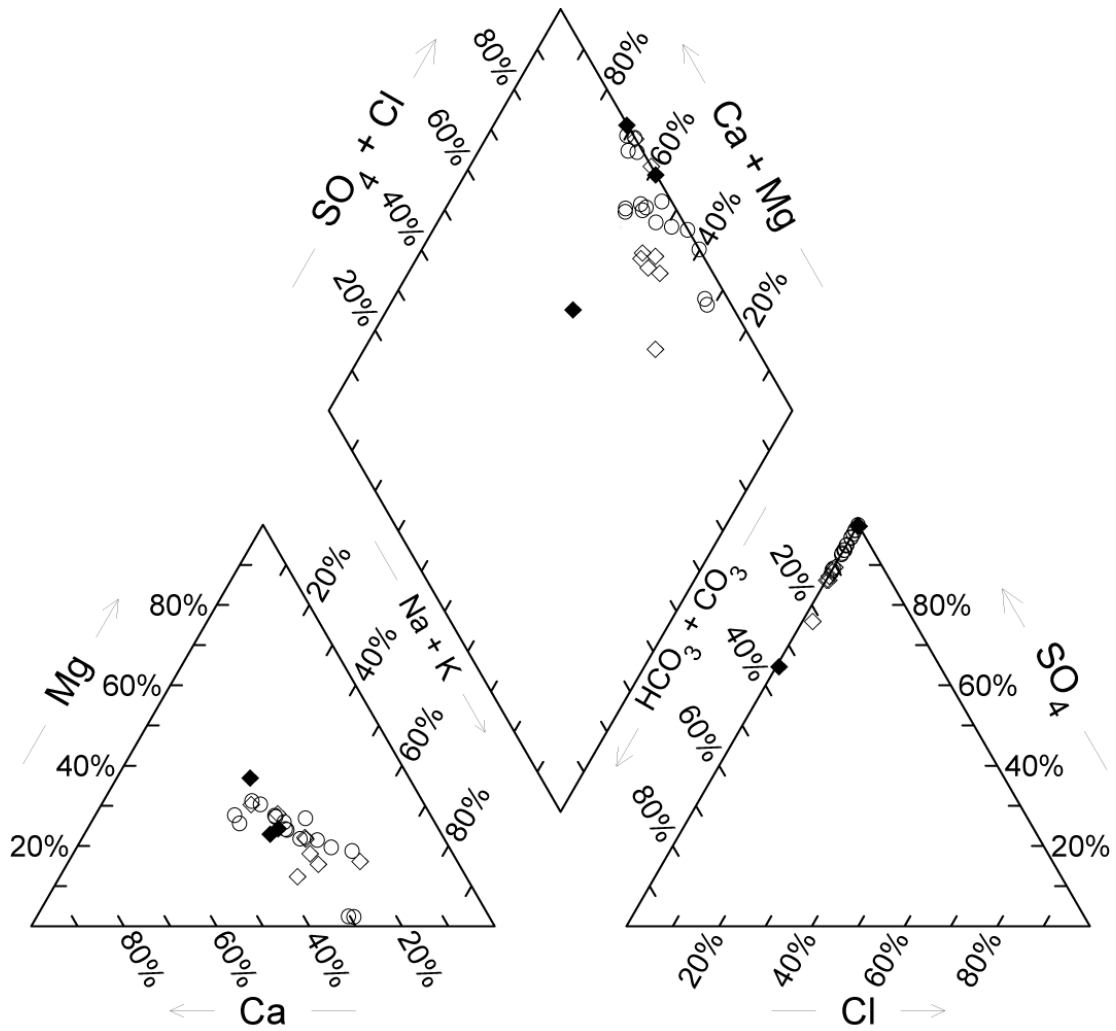
Fluids may also be flowing through Paleozoic and Mesozoic sedimentary units that underlie the younger volcanic units. Carbonates such as the Madison Limestone, found in the northern part of YNP, have relatively high $\delta^{18}\text{O}$ values (~25-30‰). Fluids reacting with these rocks rather than volcanic units could contribute to a greater oxygen isotope shift. These sedimentary units have been found to contain hydrocarbons which may also be the source of the anomalously high ammonia, methane, ethane, and other alkane levels at Inkpot Spring (Fournier, 1989; Love and Good, 1970).

Figure 9 shows the $\delta^{18}\text{O}$ shift of fluids at Washburn and Inkpot Hot Springs relative to the Global Meteoric Water Line (GMWL) and Local Meteoric Water Line (LMWL), which Kharaka et al. (1992) found to be almost identical. Alkali-chloride waters typically show a zero-slope shift away from the GMWL/LMWL while acid-sulfate waters typically show low positive slopes of 2-3 from the GMWL/LMWL, the latter being characteristic of evaporation at near-boiling temperatures (Criss, 1999). Data from Inkpot Spring show a cluster away from the GMWL/LMWL, suggesting boiling and steam separation may have a significant effect on fluid chemistry. Three samples, WTS01, WTS02, and WTS03, were sampled from relatively inactive standing pools of water with minor amounts of rising gas. These three samples plot near the

GMWL/LMWL and may represent a component of the fluids at Inkpot Spring. A combination of water-rock interaction at temperatures $>250^{\circ}\text{C}$ and single-stage steam separation, with possible minor contributions of water from other sources, could account for the high oxygen and hydrogen isotope values and significant $\delta^{18}\text{O}$ shift at Inkpot Spring.

5.2 Water Chemistry

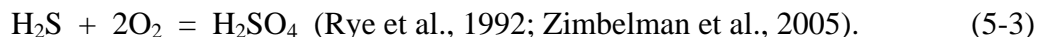
Water composition results from fluids collected at Inkpot Spring during July and August, 2008 (Appendix B) closely match water chemistry results from USGS studies conducted in 2001 and 2003 (Appendix A). Fluid chemistry at Inkpot Spring has not changed significantly since USGS studies were conducted in the late 1960's and early 1970's. Inkpot Spring fluids have pH values from 2.94 to 6.15 and significant levels of NH_3 (240-680 mg/L), SO_4 (900-3300 mg/L), SiO_2 (87.21-281.71 mg/L), B (0.7741-60.7 mg/L), and Hg (0.001-8.69 ng/L, unfiltered). Chemical compositions of the waters are plotted on the trilinear diagram of Piper (1944) (Fig. 10). Inkpot Spring fluids are of the acid- SO_4 type with variable cation concentrations. Most samples have the cation proportion: (Na>Ca>K>Mg). USGS studies reveal that the primary dissolved constituent is ammonium sulfate and our analyses confirm this. Silica is the next most abundant dissolved constituent. Based on oral communication with A.H. Truesdell, 1988, Fournier (1989) concludes that hot water flushes petroleum from a sedimentary source to the base of the vapor-dominated system at Washburn and Inkpot Springs, where distillation at high temperature and high pressure results in steam rich in organic gases and $\text{NH}_3 > \text{H}_2\text{S}$. Upon transport toward the surface, steam condenses and H_2S is oxidized to H_2SO_4 , which is immediately converted to ammonium sulfate by excess NH_3 (Fournier, 1989). H_2S from deep hydrothermal fluids is commonly oxidized to sulfuric acid by atmospheric oxygen in steam-



- 2008 Inkpot Spring samples. Data included in Appendix C.
- ◆ 2008 Unnamed thermal spring samples collected SW of Inkpot Spring along Howard Eaton Trail. Data included in Appendix C.
- ◇ 2003 & 2001 Washburn & Inkpot Spring water data from McCleskey et al. (2005) and Ball et al. (2007), included in Appendix B.

Figure 10. Trilinear “Piper” diagram showing the chemical composition of fluids at Inkpot Spring. Fluids are of the acid-sulfate type and have variable cation proportions, generally Na>Ca>K>Mg.

heated environments according to the reaction:



Sulfuric acid is converted to dissolved ammonium sulfate according to the reactions:



or



These reactions result in a fluid which is near-neutral to slightly alkaline and probably explains why these fluids, classified as acid-sulfate, are not always acidic. Figure 11 shows a linear relationship between ammonia and sulfate concentrations for pools at Inkpot Spring having a pH of approximately 6. Pools with lower ammonia/sulfate ratios have lower pH because of excess H_2SO_4 , which is not completely neutralized by ammonia. Without the addition of ammonia, all Inkpot Spring pools would probably have low pH and could truly be classified as “acid-sulfate.”

Other possible sources of dissolved sulfate at Inkpot Spring include disproportionation of SO_2 in magmatic vapor, oxidation of sulfide, and contact with old native sulfur deposits. In acid-sulfate systems sulfuric acid can be produced by disproportionation of SO_2 with decreasing temperature according to the reaction:



SO_2 is most likely derived from magma and transported in a vapor until temperature decreases, vapor condenses, and H_2S and H_2SO_4 are produced (Rye et al., 1992). Up to 7.0 ppm SO_2 gas was detected in 2008, and this process may provide a slight contribution of sulfate to the pools.

Ammonia vs Sulfate: Variable pH

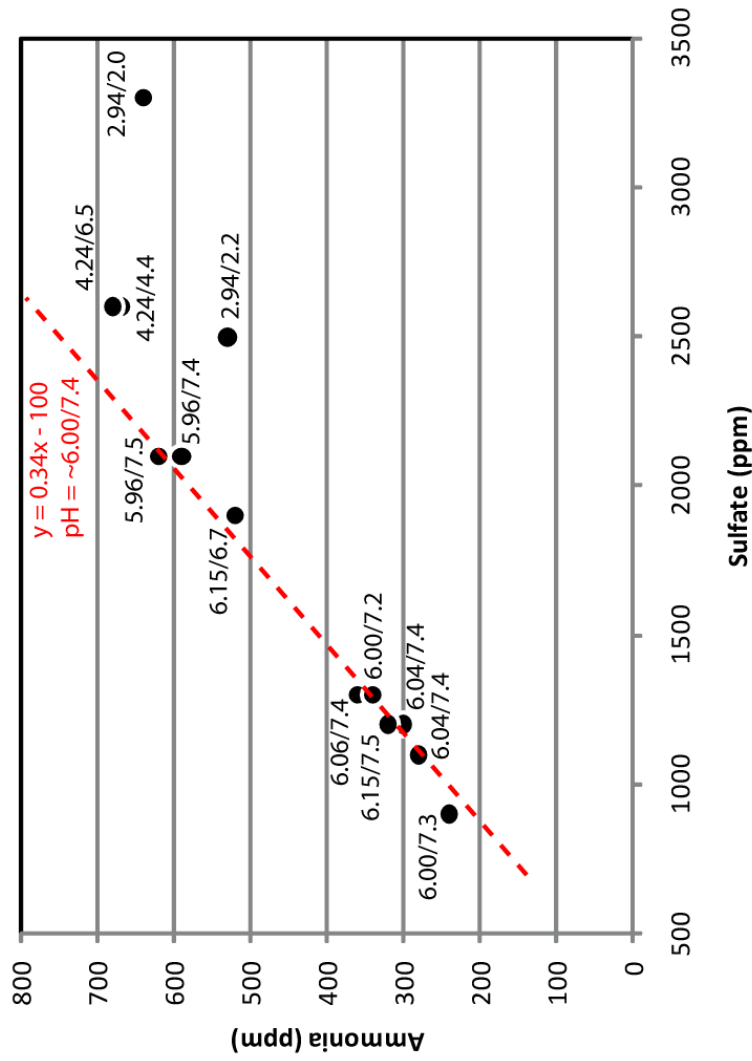


Figure 11. The ammonia versus sulfate diagram shows the control reactions (5-4) and (5-5) and the concentration of these constituents have on fluid pH. The dashed red line represents the ratio of ammonia to sulfate which produces near neutral (pH = 6.00-7.4) fluids. Inkpot Spring pools with lower ammonia/sulfate ratios lie below this line and contain excess sulfate (up to 3300 ppm). The excess sulfate is probably in the form H_2SO_4 , making the fluids acidic (pH = 2.94-4.24). All Inkpot Spring pools would probably be acidic without the presence of ammonia.

The oxidation of sulfides is a complex process not completely understood, but may contribute to elevated sulfate concentrations at Inkpot Spring. The oxidation of pyrite is in most cases the result of two reactions. The first, involving the oxidation of pyrite by oxygen, can be written:



Ferrous iron is not stable in the presence of free oxygen so it rapidly oxidizes to Fe^{+3} . The second reaction is the oxidation of pyrite by ferric iron:



A summary reaction producing a hydrous iron oxide phase and sulfuric acid can be written:



These reactions probably explain why the darkest pool, with pyrite coated pebbles at the bottom, has the highest amount of Fe^{+2} and SO_4^{-} and lowest pH. The concentrations of these constituents are highly variable from day to day. Fe^{+2} fluctuated from 6.88 to 13.94 ppm and SO_4^{-} from 2500 to 3300 ppm, in pool IKP10, over a 6 day period. Previous USGS analyses reveal that nearly all of the dissolved iron is Fe^{+2} . Ferrous iron concentrations can sometimes be abnormally high when acidifying the samples causes gradual dissolution of iron suspended as colloids, that may have passed through the 0.45 μm filter (Kennedy et al., 1974; Bethke, 2008).

Another way to increase sulfate while maintaining the low chloride concentrations is for groundwater to come into contact with native sulfur deposits that were formed in solfataras during earlier volcanic activity and subsequently covered by younger volcanic flows or glacial deposits (Fournier et al., 1992). Sulfur-consuming bacteria (*sulfolobus*) are effective at

generating H₂SO₄ from native sulfur and oxygen near the cooler margins of hydrothermal systems (Brock, 1978; Fournier, 1992).

Fluctuations in pH were also observed as a function of time. Fluid pH of individual Inkpot Spring pools was measured at various times on several different days during a two-week observation period. Seven of the eight pools at Inkpot Spring had an average pH variation of 0.37 and a maximum pH variation of 0.82. The average temperature variation for these pools was 4.66°C, and the maximum temperature variation was 10.70°C. Pool IKP04 had an observed pH range from 3.44 to 5.60 and temperature range from 74.2°C to 78.7°C. This pool's pH incrementally increased from 3.44 to 5.60 while the water level of the pool incrementally decreased during the first 10 observation days. Water level marks at the pool's edge are evident in the photograph of pool IKP04 in Appendix A, which also includes pH and temperature data. After 15 days, the pH of pool IKP04 had decreased to 3.47 and the water level had increased because of rain on the thirteenth, fourteenth, and fifteenth days of observation. These significant fluctuations were unique to pool IKP04 during the observation period and suggest other factors may be influencing pH in addition to the ammonia/sulfate ratio.

5.3 Geothermometry and Evidence of Mixing

Temperature of surface fluids at Inkpot Spring ranges from 70 to 90°C. Fluids that produced the alteration assemblages in nearby Sulfur Creek and the Grand Canyon of the Yellowstone River would have likely been 150-250°C. Two broad alteration assemblages have been identified in the canyon including an advanced argillic assemblage consisting of an association of quartz (opal) + kaolinite ± alunite ± dickite, and an argillic or potassic alteration assemblage consisting of quartz + illite ± adularia (Larson et al., 2008; Larson et al., 2009).

Reyes (1990) reports that kaolinite is found at temperatures up to about 200°C in active Philippine acid hydrothermal systems and dickite occurs with kaolinite from 120 to 200°C. Illite occurs at temperatures above 220°C in neutral pH Philippine systems (Reyes, 1990). The transition from shallower kaolinite and dickite to deeper illite in the Grand Canyon of the Yellowstone River occurs at temperatures that are estimated to range from 150 to 230°C (Larson et al., 2009).

Multiple geothermometers (Na-K, Na-K-Ca, and Quartz) have been used to estimate fluid temperature at depth in hydrothermal systems, however, their accuracy has been questioned in vapor-dominated systems and when fluids are likely to re-equilibrate with rocks at different points along upflow paths. Temperatures calculated from multiple geothermometers listed in Table 2b, are included in Table 2a. The Na-K and Na-K-Ca geothermometers give values too high and some Na, K, and Ca is probably introduced at shallow levels from local groundwaters. Quartz geothermometers give temperatures between ~140 and 205°C, which are temperatures commonly observed at the tops of small vapor-dominated zones explored by drilling worldwide (Fournier, 1989). These temperatures also compare well with temperatures that probably produced the alteration assemblages in the Grand Canyon of the Yellowstone River.

Silica can be used effectively to estimate the temperature of a reservoir feeding a group of hot springs because of the constraint that the solubility of quartz controls the concentration of silica in the reservoir fluid (Fournier, 1989). Silica concentrations and temperature are dependent on the degree of mixing in these types of hot spring fluids. Fournier and Truesdell (1974) published procedures for graphically and analytically estimating the temperature and proportion of hot and cold waters in a mixed fluid (Truesdell and Fournier, 1977). The silica versus enthalpy plot is used because the combined heat contents of two waters, at different

Table 2a. Fluid reservoir temperature estimates from chemical geothermometers. All values are presented in °C.

Sample #	Silica Geothermometers		Cation Geothermometers				Gas Geothermometer	
	Quartz-no steam loss ^a	Quartz-maximum steam loss ^b	Na/K (Fournier) ^c	Na/K (Truesdell) ^d	Na-K-Ca ($\beta=4/3$) ^e	Na-K-Ca (Mg) corrected ^f	Sample #	CO ₂ -H ₂ S-H ₂ -CH ₄ (D'Amore & Panichi) ^g
IKP01	160.33	152.02	394.18	441.05	84.59	83.43	YGS03-24	246.65
IKP02	149.49	143.02	367.21	398.02	77.02	77.02	YGS03-25	257.75
IKP03	202.93	186.73	441.72	521.50	100.06	n.c.	YGS03-26	233.71
IKP04	191.62	177.62	451.56	538.93	92.52	72.34	90	-----
IKP06	160.67	152.30	379.03	416.66	80.91	77.12	91	173.11
IKP07	149.72	143.20	424.19	491.12	84.34	84.34	Allen & Day	169.04
IKP09	161.93	153.34	369.88	402.19	79.55	79.55		
IKP10	201.93	185.93	583.58	803.32	113.14	100.50		
2IKP01	162.16	153.53	391.88	437.30	84.19	83.73		
2IKP02	146.19	140.26	411.38	469.46	83.06	81.39		
2IKP03	204.55	188.03	437.37	513.88	99.46	n.c.		
2IKP04	183.56	171.08	457.79	550.11	94.06	73.34		
2IKP06	161.39	152.89	376.29	412.30	80.34	77.71		
2IKP07	129.69	126.38	442.69	523.19	87.04	82.49		
2IKP09	160.64	152.28	385.85	427.56	83.65	74.42		
2IKP10	203.98	187.57	624.23	898.15	121.13	105.15		
WTS01	157.26	149.48	611.90	868.62	108.63	64.09		
WTS02	201.05	185.22	361.99	389.89	77.35	n.c.		
WTS03	182.03	169.84	302.04	301.03	64.69	n.c.		

Table 2a shows subsurface fluid temperatures estimated using silica, cation, and gas geothermometers. Geothermometers *a-g* correspond to geothermometer equations in Table 2b. Subsurface temperatures are calculated using equations in Table 2b, Inkpot Spring water chemistry data in Appendix C for equations *a-f*, and previous Washburn and Inkpot Hot Springs gas data compiled in Appendix F for equation *g*.

Table 2b. Chemical geothermometers applied to Inkpot Spring fluids to estimate fluid reservoir temperatures.			
	Geothermometer	Equation	Restrictions
a	Quartz-no steam loss	$t^{\circ}\text{C} = \frac{1309}{5.19 - \log(\text{SiO}_2)} - 273.15$	$t = 0\text{-}250^{\circ}\text{C}$
b	Quartz-maximum steam loss	$t^{\circ}\text{C} = \frac{1522}{5.75 - \log(\text{SiO}_2)} - 273.15$	$t = 0\text{-}250^{\circ}\text{C}$
c	Na/K (Fournier)	$t^{\circ}\text{C} = \frac{1217}{\log(\text{Na}/\text{K}) + 1.483} - 273.15$	$t > 150^{\circ}\text{C}$
d	Na/K (Truesdell)	$t^{\circ}\text{C} = \frac{855.6}{\log(\text{Na}/\text{K}) + 0.8573} - 273.15$	$t > 150^{\circ}\text{C}$
e	Na-K-Ca	$t^{\circ}\text{C} = \frac{1647}{\log(\text{Na}/\text{K}) + \beta[\log(\text{V}\text{Ca}/\text{Na}) + 2.06]} + 2.47 - 273.15$	$t < 100^{\circ}\text{C}, \beta = 4/3$ $t > 100^{\circ}\text{C}, \beta = 1/3$
f	Na-K-Ca (Mg corrected)	$t^{\circ}\text{C} = \frac{1647}{\log(\text{Na}/\text{K}) + \beta[\log(\text{V}\text{Ca}/\text{Na}) + 2.06]} + 2.47 - 273.15$	$t < 100^{\circ}\text{C}, \beta = 4/3$ $t > 100^{\circ}\text{C}, \beta = 1/3$
		$R = [\text{Mg}/(\text{Mg} + \text{Ca} + \text{K})] \times 100$ $\Delta t_{\text{Mg}} = 10.66 - 4.7415R + 325.87(\log R)^2 - 1.032 \times 10^5 (\log R)^2 / T - 1.968 \times 10^7 (\log R)^2 / T^2 + 1.605 \times 10^7 (\log R)^3 / T^2$	For R between 5 & 50
g	CO ₂ -H ₂ S-H ₂ -CH ₄ (D'Amore and Panichi)	$t^{\circ}\text{C} = (24775 / (\alpha + \beta + 36.05)) - 273$ $\alpha = 2\log(\text{CH}_4/\text{CO}_2) - 6\log(\text{H}_2/\text{CO}_2) - 3\log(\text{H}_2\text{S}/\text{CO}_2)$ $\beta = -7\log P_{\text{CO}_2}$	$P_{\text{CO}_2} = 0.1$ if % CO ₂ < 75 $P_{\text{CO}_2} = 1.0$ if % CO ₂ > 75 $P_{\text{CO}_2} = 10$ if % CO ₂ > 75 and CH ₄ > 2H ₂ and H ₂ S > 2H ₂

Table 2b shows chemical geothermometers used to estimate subsurface temperatures of Inkpot Spring fluids included in Table 2a. Geothermometer equations *a-f* are compiled from Table 4.1 in Fournier (1981). Geothermometer equation *g* is from D'Amore and Panichi (1980).

temperatures, is conserved when the two waters are mixed (neglecting the small heat of dilution), but the combined temperatures are not. Figure 12 shows the enthalpy and SiO₂ concentrations for mixing of cooler groundwater and thermal waters likely to take place at or near Inkpot Spring. The fraction of hot water (after steam loss) in Inkpot Spring pools is determined by dividing the distance AB by AC, which gives a maximum hot water component value of 88%. The weight fraction of original hot water lost as steam before mixing, x , is given by the equation:

$$x = 1 - \frac{\text{silica value at point E}}{\text{silica value at point D}} \quad (\text{Truesdell and Fournier, 1977}). \quad (5-10)$$

Approximately 21.6% of the original hot water is lost as steam at Inkpot Spring according to equation 5.10. Point D on Figure 12 represents the enthalpy of the hot water component before the onset of boiling. The temperature of the original hot water component at Inkpot is calculated to be 195°C, when enthalpy at point D is converted to temperature using steam tables in Appendix III of Henley et al. (1984). Point E represents a silica concentration of 248.7 ppm in the original hot water component before boiling at Inkpot Spring. The calculated hot water component temperature (195°C) is close to the maximum temperature (204.5°C) given by the quartz geothermometers in Table 2b. This value is close to estimated values for other geyser and hot spring basins throughout YNP, calculated using the silica geothermometer. Average temperatures for subsurface waters of Yellowstone geyser basins, presented in Table 3, were calculated by Truesdell and Fournier (1976) using the silica geothermometer.

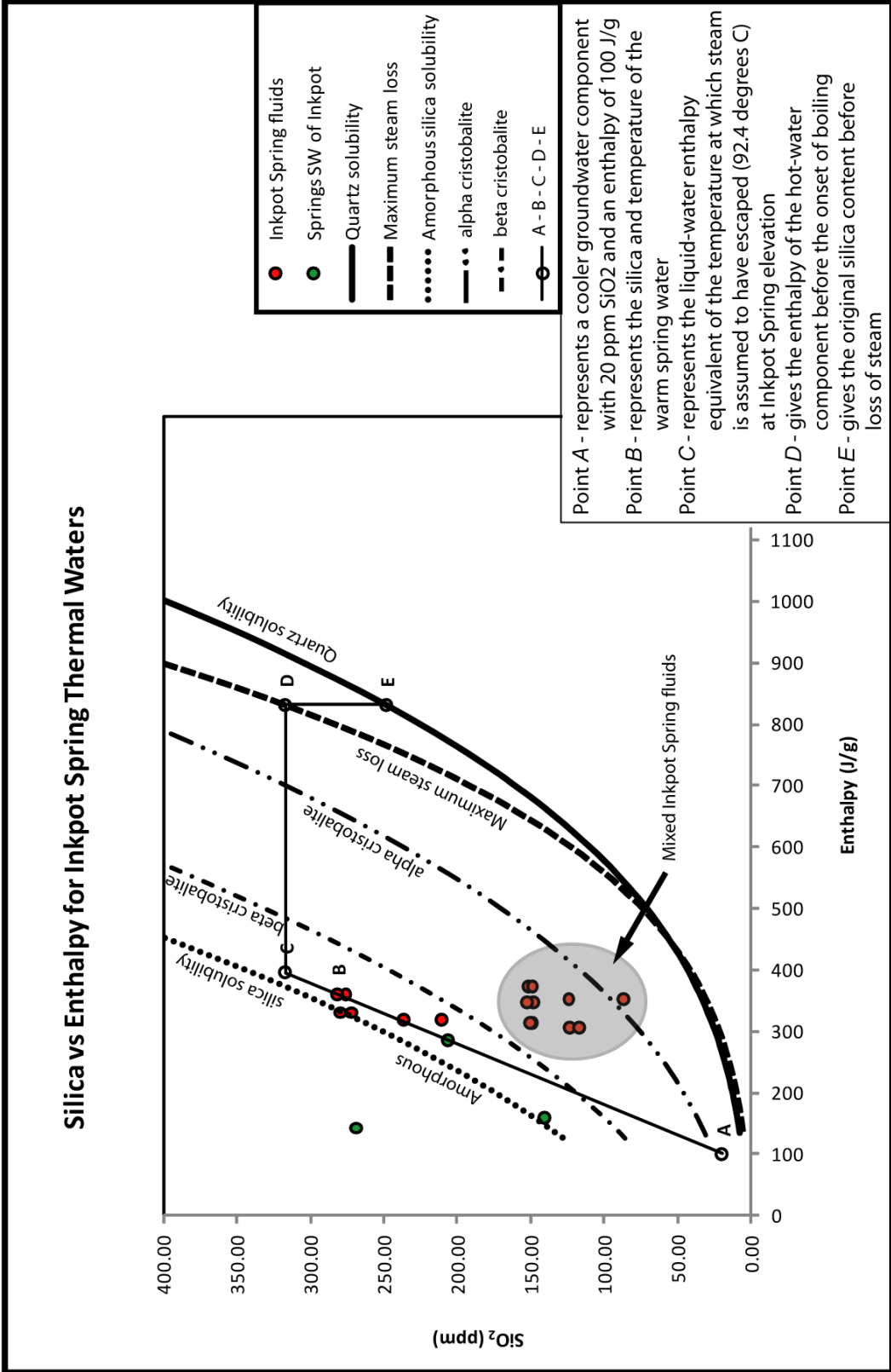


Figure 12. Dissolved silica versus enthalpy diagram showing estimated temperature and dissolved silica concentration of the hot water component in a mixed water. The fraction of hot water in the warm spring can be determined by dividing the distance AB by AC. The maximum hot water component calculated for Inkpot Spring is 88%. The enthalpy at point D is converted to temperature using steam tables in Henley et al. (1984), giving a value of 195°C. Point E represents an original silica concentration (248.7 ppm) before steam loss.

Geyser Basin	Average SiO₂ Geothermometer Temperature(°C)	Table 3. Average subsurface fluid temperatures calculated by Truesdell and Fournier (1976) using the silica geothermometer. Inkpot Spring reservoir temperatures calculated using Figure 12 and the silica geothermometers (Tables 2a and 2b) are close to subsurface temperatures calculated for other Yellowstone geyser basins.
West Thumb	188	
Heart Lake	196	
Shoshone	190	
Upper	195	
Lower	179	
Midway	179	
Norris	210	

The erroneous values given by some geothermometers may be due to boiling and dilution effects from mixing with local groundwaters. Silica and total carbonate concentrations can be used to investigate mixing in hot spring fluids. Arnórsson et al. (1983) found CO₂ concentrations in waters of geothermal reservoirs are only dependent on the temperatures of these waters and it is known that silica concentrations are determined by quartz solubility (Arnórsson, 1985). Assuming that this relationship between silica and total carbonate is valid, boiling of such waters will lead to reduction of carbonate when CO₂ is released as gas, but mixing without boiling will produce waters with high carbonate/silica ratios relative to equilibrated waters, due to the curvature of the silica/carbonate relationship, as shown in Figure 13 (Arnórsson, 1985). Inkpot Spring fluids plotting above this curve represent degassed or boiled waters, while fluids plotting below the curve represent mixed waters with increased total carbonate contents. Waters designated as mixed in Figure 13 are clearly shown as fluids with lesser silica contents, in the shaded oval of Figure 12. A possible explanation for this relationship between decreased silica concentration and higher total carbonate concentration is that the hot water component of Inkpot Spring is diluted by perched Na-HCO₃-rich groundwater which Fournier (1989) suggests keeps a “pressure lid” on the eastern vapor-dominated system.

Gas geothermometers have also been tested for fluids at Inkpot Spring, including the CO₂-CH₄ carbon isotope geothermometer and CO₂-H₂S-H₂-CH₄ gas geothermometer of

Silica vs Total Carbonate (Silica-Carbonate Mixing Model) for Inkpot Spring Thermal Waters

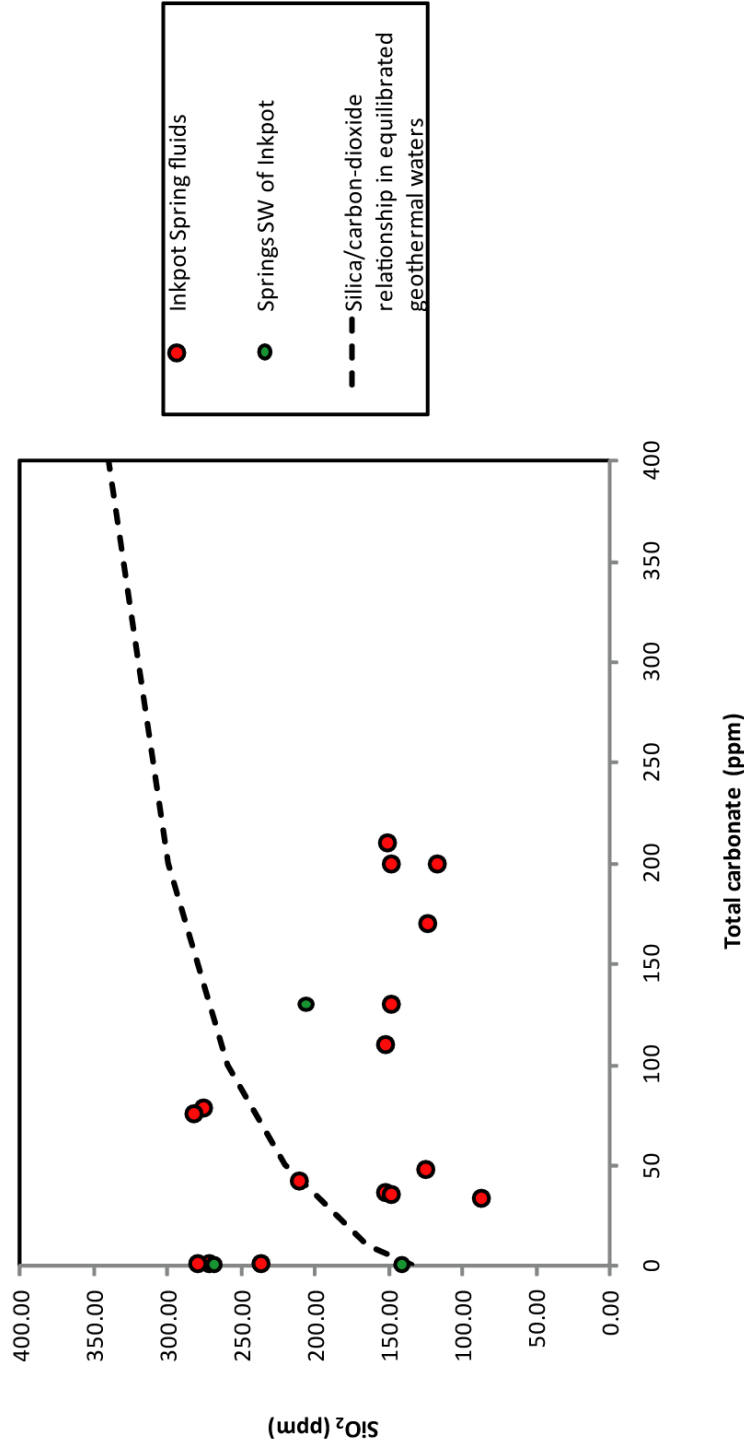


Figure 13. Silica versus total carbonate diagram (silica-carbonate mixing model of Arnórsson (1985)) for Inkpot Spring thermal waters. The dashed curve represents the silica/carbon-dioxide relationship in equilibrated geothermal waters. The temperature dependence of silica was assumed to be controlled by quartz solubility, and the temperature dependence of carbon dioxide is derived from the respective function in table 5 of Arnórsson et al. (1983). Data points plotting above the equilibrium curve represent degassed waters, and data points below represent mixed waters (Arnórsson, 1985). Data points plotting below the equilibrium curve in Figure 13 are shown in the shaded oval in Figure 12.

D'Amore and Panichi (1980). Burnett (2004) calculated a reservoir temperature of 380°C at Washburn Hot springs using the CO₂-CH₄ geothermometer and carbon isotope values. This number is higher than expected and should be interpreted with caution because there is no way of proving equilibrium between CO₂ and CH₄ and temperatures calculated using this method do not always compare well with measured down-hole temperatures in active hot spring areas elsewhere (Bergfield, 2001; Burnett, 2004). Burnett (2004) found a reservoir temperature of 258°C using the CO₂-H₂S-H₂-CH₄ gas geothermometer using data in Appendix F and the following equations.

$$T \text{ (}^\circ\text{C)} = (24775 / (\alpha + \beta + 36.05)) - 273 \quad (5-11)$$

$$\alpha = 2\log(\text{CH}_4/\text{CO}_2) - 6\log(\text{H}_2/\text{CO}_2) - 3\log(\text{H}_2\text{S}/\text{CO}_2) \quad (5-12)$$

$$\beta = -7 \log P_{\text{CO}_2} \quad (5-13)$$

When applying the above equations, the following assumptions are made regarding P_{CO₂}

(D'Amore and Panichi, 1980; Henley et al., 1984, Burnett, 2004):

- 1) P_{CO₂} = 0.1 if CO₂ (% by volume) < 75
- 2) P_{CO₂} = 1.0 if CO₂ (% by volume) > 75
- 3) P_{CO₂} = 10 if CO₂ (% by volume) > 75 and

$$\text{CH}_4 > 2\text{H}_2 \text{ and}$$

$$\text{H}_2\text{S} > 2\text{H}_2$$

The CO₂-H₂S-H₂-CH₄ gas geothermometer of D'Amore and Panichi (1980) was to used calculate reservoir temperatures (Table 2a) from other previous gas data compiled in Appendix F. These calculated temperatures compare with temperatures that would be close to equilibrium with the quartz + illite ± adularia alteration mineral assemblage observed in the Grand Canyon of the Yellowstone River and probably represents a deeper reservoir temperature.

6. FLUID-MINERAL EQUILIBRIA

6.1 Solubility-Activity Relationships

In order to study the equilibria between Inkpot Spring fluids and different mineral assemblages that may be present at the surface around the pools or at depth, equilibrium constants (K_{eq}) for important mineral reactions are calculated using The Geochemist's Workbench (GWB) computer program. The K_{eq} represents the point of minimum free energy for these mineral reactions. Simultaneous mass action equations for complexes and redox equilibria and mass balance equations on all components are solved to provide accurate values for activities of aqueous ions in a given water at high temperature (Reed and Spycher, 1984). Activities are used to calculate ion activity products (Q) for minerals. SpecE8, a GWB software program, was used to compute the distribution of species and calculate Q for Inkpot Spring fluids. The activity of individual species is defined by

$$a_i = \gamma_i m_i \quad (6-1)$$

where m_i is molality (number of moles of the species per kilogram solvent) and γ_i is the activity coefficient. Spec8 calculates ion activity coefficients using the Debye-Hückel expression

$$-\log \gamma_i = \frac{Az_i^2 \sqrt{I}}{1 + \hat{a}_i B \sqrt{I}} \quad (6-2)$$

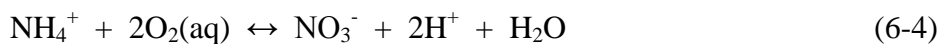
where z_i is ionic charge, A and B are constants that are functions of temperature and are characteristic of the solvent (H₂O), \hat{a}_i is the ion size parameter, and I is the solution's ionic strength (Garrels and Christ, 1965; Bethke, 2008). The solution's ionic strength is determined by

$$I = \frac{1}{2} \sum m_i z_i^2 \quad (6-3)$$

where m_i and z_i are defined previously in the Debye-Hückel expression (Garrels and Christ, 1965; Bethke, 2008). Here, the summation of molality and charge of all ions are considered.

6.2 Redox Disequilibrium

Interactions between hydrothermal fluids and elements present in the rock through which they pass, such as Fe, will affect redox potential (Burnett, 2004; Giggenbach, 1997). Redox reactions are unlikely to reach equilibrium at low temperatures making the determination of redox state in natural waters problematic. Complicating matters further, platinum electrodes used to measure Eh do not respond well to many redox couples (SO_4^{2-} - HS^- , NO_3^- - N_2 , N_2 - NH_4) (Bethke, 2008; Stumm and Morgan, 1996; Hostettler, 1984). Eh values measured by platinum electrode can also differ greatly from those calculated using the Nernst equation. The redox couple NH_4^+ - NO_3^- controlled by the coupling reaction



can be employed from 2008 water chemistry results. However, due to the disproportionate concentrations of NH_3^+ and NO_3^- and probable vapor-transport and organic source of NH_3^+ , previous Eh measurements from Inkpot Spring made in 2001 and 2003 are used to estimate redox state. These recent measurements gave Eh values around -165 mV and 165 mV. Inkpot Spring fluids are speciated using both values. The value of $\log(Q/K)$, a mineral's saturation index, provides a measure of proximity of the aqueous solution to equilibrium with the mineral (Reed and Spycher, 1984). Tables 4a and 4b show the saturation indices of important minerals at the surface thermo-chemical conditions of the multiple pools at Inkpot Spring. The actual form in which Fe occurs in high temperature hydrothermal systems is not well understood (Burnett, 2004; Giggenbach, 1997). Tables 4a and 4b are particularly useful in showing the effect redox potential has on the stability of Fe-bearing minerals. Analysis of precipitated sediment and observation of active pyrite precipitation and high ammonia concentrations gives some clues into the variable redox state in Inkpot Spring pools. Ammonium ion and ammonia are only present in

Table 4a								
Mineral	IKP01	IKP02	IKP03	IKP04	IKP06	IKP07	IKP09	IKP10
Cinnabar	12.8262	16.4613	12.4491	14.7151	14.1530	11.5078	11.9135	11.4267
Quicksilver	10.3302	11.8171	9.9379	10.8336	10.6316	9.6482	9.3980	10.1989
Clinoptilolite-K	1.8543	0.9475	4.3586	0.4170	2.2538	0.9598	0.9754	-2.1908
Mordenite-K	0.9222	0.4690	2.1742	0.2036	1.1221	0.4749	0.4826	-1.1003
Quartz	0.6579	0.6770	0.8920	0.9237	0.7392	0.5683	0.6091	0.9539
Pyrite	0.6152	4.9906	0.8109	4.1845	2.6207	0.7745	2.0951	0.8663
Tridymite	0.5358	0.5492	0.7721	0.7978	0.6124	0.4470	0.4905	0.8299
Chalcedony	0.4306	0.4435	0.6671	0.6923	0.5068	0.3419	0.3858	0.7245
Beidellite-Mg	0.2279	0.0022	0.4247	-0.0309	0.2282	0.1374	0.1845	-0.4962
Cristobalite	0.2146	0.2185	0.4547	0.4703	0.2833	0.1273	0.1756	0.5054
Pyrophyllite	0.1807	0.1457	0.6778	0.6634	0.2821	0.0122	0.1307	0.7473
Kaolinite	0.0000	0.0000	0.0000	0.0000	0.0000	0.0000	0.0000	0.0000
Barite	-0.0428	-0.1319	0.0893	-13.5385	0.0924	-0.1463	-0.1722	-26.1893
K-feldspar	-0.0640	-0.5362	0.7124	-1.3013	-0.0107	-0.3349	-0.4183	-2.6719
Amorphous silica	-0.3013	-0.3237	-0.0514	-0.0630	-0.2546	-0.3850	-0.3243	-0.0194
Muscovite	-0.3501	-0.8766	-0.0353	-2.1297	-0.4731	-0.4394	-0.5957	-3.5557
Nontronite-Mg	-0.3215	-1.4914	0.5121	-9.7907	-0.7304	2.6844	2.1056	-13.9017
Beidellite-K	-0.4547	-0.6622	-0.0138	-0.7254	-1.3622	-0.5956	-0.5626	-1.1365
Illite	-0.5507	-1.1219	-0.2985	-2.1629	-0.6056	-0.6820	-0.7902	-3.7814
Gypsum	-1.2783	-1.5721	-1.2619	-14.8142	-1.2615	-1.2715	-1.6006	-28.2414
Smectite	-1.2805	-3.6525	-1.8073	-10.7490	-1.7987	-0.1794	-0.9673	-18.4244
Diaspore	-1.4248	-1.4840	-1.6431	-1.7173	-1.5398	-1.3294	-1.3499	-1.7347
Albite	-1.7125	-2.2111	-1.0160	-3.1774	-1.7082	-2.0470	-1.9321	-4.7734
Calcite	-1.7672	-2.3725	-2.0089	-11.3734	-1.6481	-2.0683	-2.6479	-24.7734
Goethite	-2.2101	-2.7636	-2.1016	-7.1224	-2.5481	-0.5634	-0.8862	-8.9556
Pyrrhotite	-2.9677	-0.8243	-2.7790	-0.9328	-2.0438	-2.3403	-1.6399	-1.8223
Hematite	-3.2607	-4.4021	-3.0296	-13.1085	-3.9657	0.0380	-0.5895	-16.7639
Alunite	-7.7575	-7.2000	-8.0983	-30.8210	-7.7672	-7.9020	-7.8843	-52.7361

Table 4b								
Mineral	IKP01	IKP02	IKP03	IKP04	IKP06	IKP07	IKP09	IKP10
Cinnabar	-19.9009	-17.1528	-19.9321	-4.4049	-19.3172	-21.0910	-20.2440	5.2164
Quicksilver	5.6549	7.0149	5.3120	6.0214	5.8010	4.9912	4.8040	5.4285
Magnetite	3.3360	2.1990	3.5890	-10.3727	2.6715	8.0660	7.1859	-14.5301
Clinoptilolite-K	1.8543	0.9473	4.3586	0.2963	2.2538	0.9598	0.9754	-2.2943
Mordenite-K	0.9222	0.4689	2.1742	0.1433	1.1221	0.4749	0.4826	-1.1520
Quartz	0.6579	0.6770	0.8920	0.9269	0.7392	0.5683	0.6091	0.9566
Pyrite	-64.8888	-62.2440	-64.0085	-34.3321	-64.3364	-64.5105	-62.2851	-11.7913
Tridymite	0.5358	0.5493	0.7721	0.8011	0.6124	0.4470	0.4905	0.8326
Chalcedony	0.4306	0.4435	0.6671	0.6956	0.5068	0.3419	0.3858	0.7272
Beidellite-Mg	0.2279	0.0021	0.4247	-0.1020	0.2282	0.1374	0.1845	-0.5600
Cristobalite	0.2146	0.2185	0.4547	0.4736	0.2833	0.1273	0.1756	0.5081
Pyrophyllite	0.1807	0.1457	0.6778	0.6700	0.2820	0.0122	0.1307	0.7528
Kaolinite	0.0000	0.0000	0.0000	0.0000	0.0000	0.0000	0.0000	0.0000
Barite	-0.0428	-0.1316	0.0893	-0.1009	0.0925	-0.1463	-0.1722	-0.0648
K-feldspar	-0.0640	-0.5363	0.7124	-1.3682	-0.0107	-0.3349	-0.4183	-2.7290
Amorphous silica	-0.0130	-0.3237	-0.0514	-0.0597	-0.2546	-0.3850	-0.3243	-0.0167
Muscovite	-0.3501	-0.8767	-0.0353	-2.2032	-0.4730	-0.4394	-0.5957	-3.6184
Nontronite-Mg	8.9293	8.0999	9.6499	-1.0998	8.7993	11.8235	11.1633	-5.2014
Beidellite-K	-0.4547	-0.6622	-0.0138	-0.7453	-0.4360	-0.5956	-0.5626	-1.1535
Illite	-0.5507	-1.1221	-0.2985	-2.3174	-0.6056	-0.6820	-0.7902	-3.9178
Gypsum	-1.2783	-1.5716	-1.2619	-1.0988	-1.2614	-1.2714	-1.6006	-1.8506
Smectite	0.3219	-1.9776	-0.2270	-10.3054	-0.1366	1.3910	0.5962	-17.8677
Diaspore	-1.4248	-1.4840	-1.6431	-1.7206	-1.5398	-1.3294	-1.3499	-1.7375
Albite	-1.7125	-2.2112	-1.0160	-3.2249	-1.7082	-2.0470	-1.9321	-4.8147
Calcite	-1.7672	-2.3733	-2.0089	-7.4253	-1.6482	-2.0683	-2.6480	-10.6332
Goethite	2.4153	2.0322	2.4673	-2.7447	2.2167	4.0062	3.6427	-4.5764
Pyrrhotite	-39.2449	-38.0456	-38.6795	-23.9040	-39.1147	-38.5083	-37.2999	-11.8178
Hematite	5.9902	5.1894	6.1082	-4.3531	5.5639	9.1771	8.4682	-8.0053
Alunite	-7.7574	-7.1976	-8.0982	-2.4048	-7.7668	-7.9019	-7.8842	0.9425

Table 4a. Saturation indices (log Q/K) of hydrothermal minerals at Inkpot Spring assuming Eh = -165 mV. Table 4b. Saturation indices (log Q/K) of hydrothermal minerals at Inkpot Spring assuming Eh = 165 mV. Positive values indicate Inkpot fluids are supersaturated with respect to the mineral. Negative values indicate Inkpot fluids are undersaturated with respect to the mineral. A value of zero indicates Inkpot fluids are at saturation with the mineral.

very reducing waters, however, nearly all H₂S has been oxidized to SO₄, suggesting oxidizing conditions at Inkpot Spring surface waters. For most pools, current redox state is probably closer to the previously measured Eh values around -165 mV than those measured values around 165 mV.

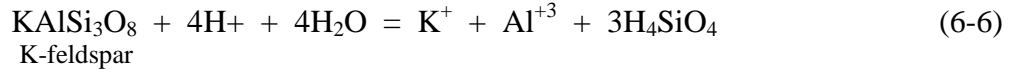
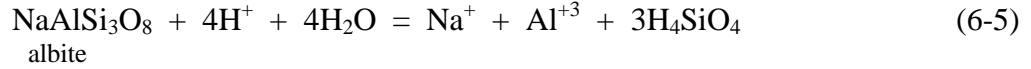
6.3 Activity–Mineral Stability Diagrams

To investigate fluid-mineral equilibria at Inkpot Spring, activity (stability) diagrams are constructed at 100°C, just above surface temperature, at 150°C, just below the temperature predicted from the silica geothermometer, at 225°C, the reservoir temperature estimated from alteration assemblages and at 250°C, calculated from the CO₂-H₂S-H₂-CH₄ gas geothermometer. A compilation of activity diagrams is included in Appendix D.

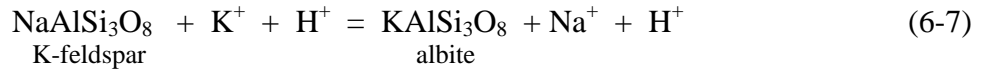
Fluid speciation calculations are based on some of the same equilibria used in the Na-K-Ca geothermometer. Equilibrium with feldspars at reservoir temperatures cannot be assumed for this system because of the erroneous values given by the Na-K-Ca geothermometer for Inkpot Spring fluids. Inkpot Spring fluids were speciated at surface temperatures, and chemistry of fluids at the surface is not defined by equilibrium processes deep in the reservoir, but by near surface processes.

Activity diagrams are constructed based on Al⁺³ conservation because Al⁺³ is relatively immobile in this type of environment. Muscovite is typically used as a proxy for illite in activity space, and this convention is followed in this study. The stability of Al-silicates in the system Na₂O-K₂O- Al₂O₃-SiO₂-H₂O at 100°C as a function of the activity ratios Na⁺/H⁺ and K⁺/H⁺ is shown in Figure 14. Inkpot Spring fluids have a bimodal compositional distribution and appear to be in equilibrium with kaolinite and illite. Boundaries between different mineral phases are

controlled by equilibrium reactions. In Figure 14, the slope of the boundary between albite and K-feldspar (maximum microcline) is defined by the two mineral hydrolysis reactions.



These are combined assuming Al^{+3} conservation and immobility.



The equilibrium constant for this reaction is

$$K_{\text{eq}} = \frac{\text{K-feldspar} a[\text{Na}^+] a[\text{H}^+]}{\text{albite} a[\text{K}^+] a[\text{H}^+]}. \quad (6-8)$$

Taking the log of each side of (6-8),

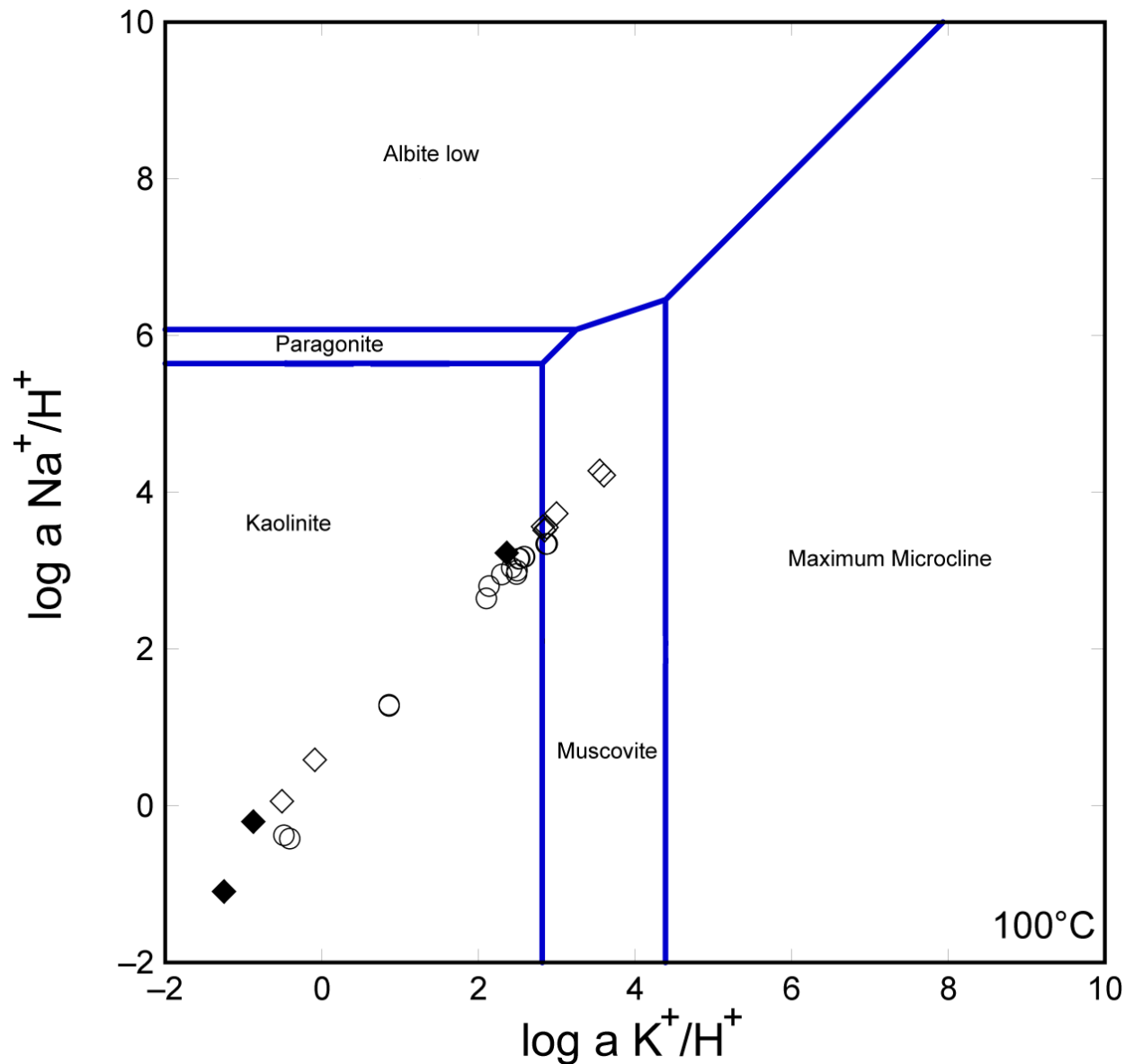
$$\log K = \log (a[\text{Na}^+]/a[\text{H}^+]) - \log ([a\text{K}^+]/a[\text{H}^+]), \quad (6-9)$$

allows us to place a linear boundary for this reaction in activity space.

$$\begin{array}{l} \log (a[\text{Na}^+]/a[\text{H}^+]) = \log ([a\text{K}^+]/a[\text{H}^+]) + \log K \\ y \qquad \qquad \qquad = \quad mx \qquad \qquad \qquad + \quad b \end{array} \quad (6-10)$$

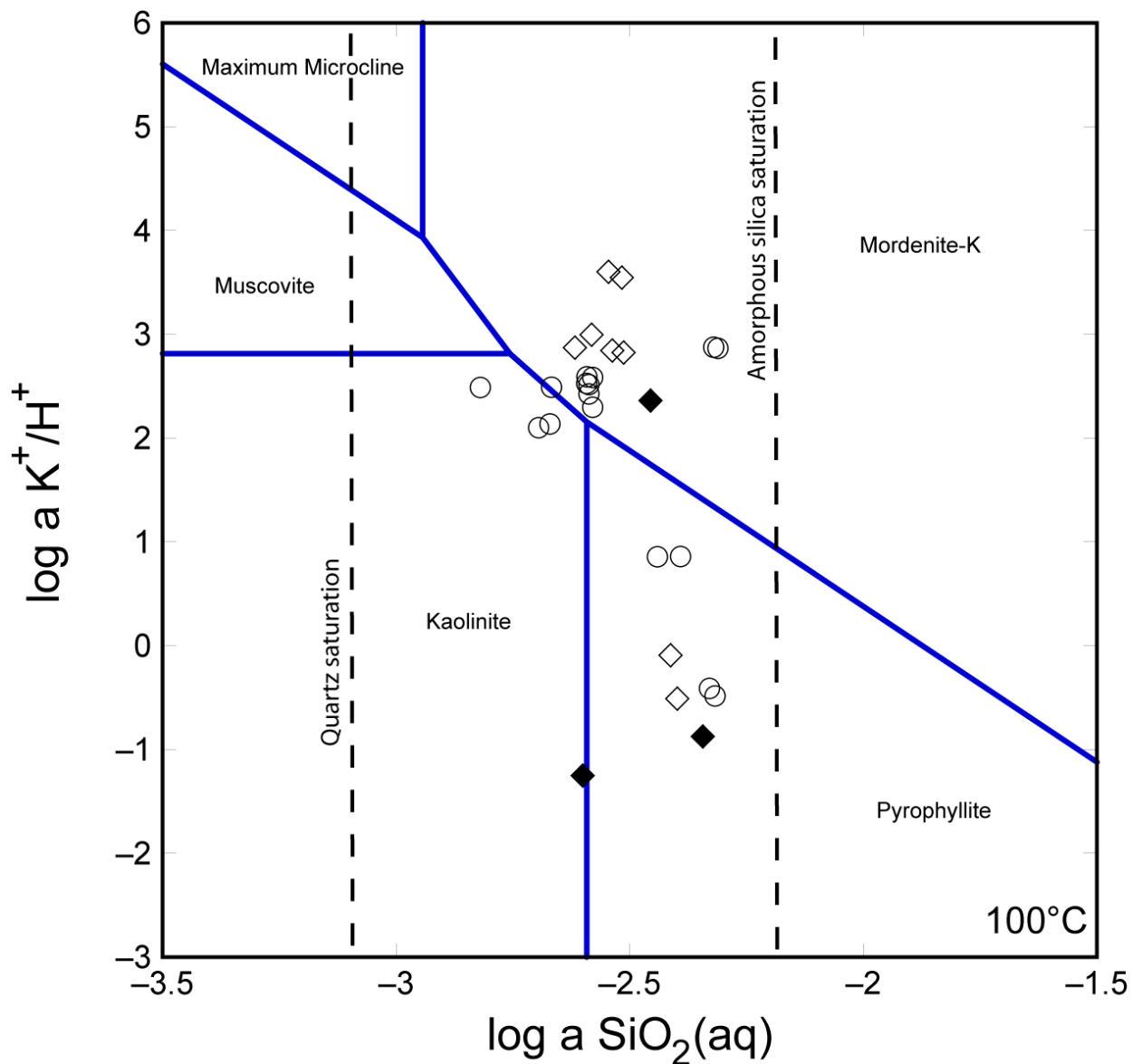
The slope of the boundary between albite and K-feldspar (maximum microcline) is 1. A similar approach is used to define the other minerals boundaries shown in the activity diagrams.

The stability of Al-silicate minerals in the system $\text{Al}_2\text{O}_3\text{-K}_2\text{O-SiO}_2\text{-H}_2\text{O}$ at 100°C as a function of the activity ratio K^+/H^+ and the activity of $\text{SiO}_2(\text{aq})$ is shown in Figure 15. Inkpot Spring fluids once again form a bimodal distribution and plot within the kaolinite and mordenite fields. Negating the neutralizing effect of ammonia, Inkpot Spring fluids would plot only in the kaolinite and pyrophyllite fields, two minerals characteristic of advanced argillic alteration.



- 2008 Inkpot Spring samples. Data included in Appendix C.
- ◆ 2008 Unnamed thermal spring samples collected SW of Inkpot Spring along Howard Eaton Trail. Data included in Appendix C.
- ◇ 2003 & 2001 Washburn & Inkpot Spring water data from McCleskey et al. (2005) and Ball et al. (2007), included in Appendix B.

Figure 14. Activity diagram showing the stability of aluminosilicate minerals in the system $\text{Na}_2\text{O}-\text{K}_2\text{O}-\text{Al}_2\text{O}_3-\text{H}_2\text{O}$ at 100°C as a function of the activity ratios Na^+/H^+ and K^+/H^+ . The diagram is constructed based on Al^{+3} conservation. Muscovite is used as a proxy for illite in activity space. Inkpot Spring fluids are in equilibrium with kaolinite and appear to be in equilibrium with illite.

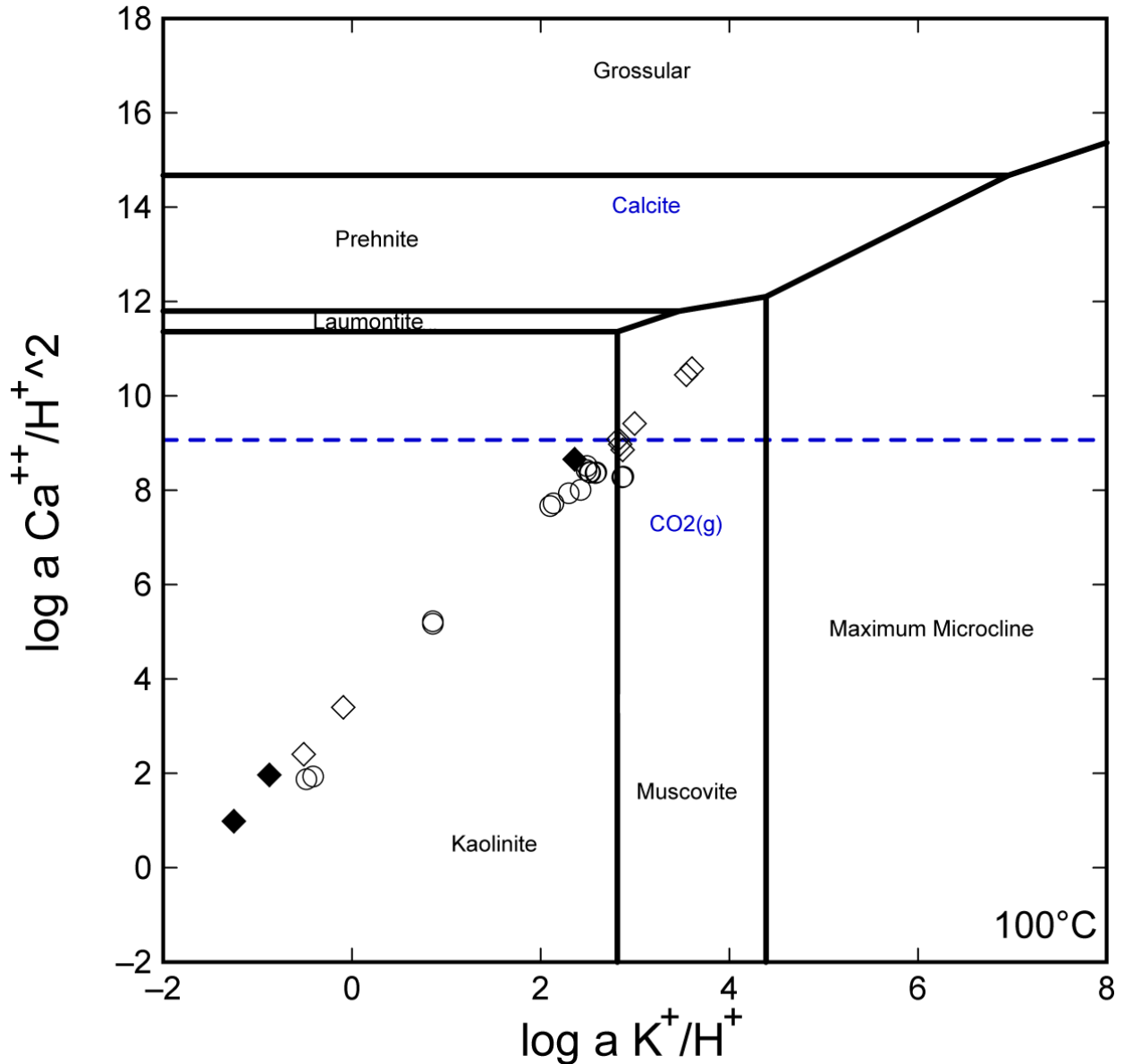


- 2008 Inkpot Spring samples. Data included in Appendix C.
- ◆ 2008 Unnamed thermal spring samples collected SW of Inkpot Spring along Howard Eaton Trail. Data included in Appendix C.
- ◇ 2003 & 2001 Washburn & Inkpot Spring water data from McCleskey et al. (2005) and Ball et al. (2007), included in Appendix B.

Figure 15. Activity diagram showing the stability of aluminosilicate minerals in the system $\text{Al}_2\text{O}_3\text{-K}_2\text{O-SiO}_2\text{-H}_2\text{O}$ at 100°C as a function of the activity ratio K^+/H^+ and the activity of SiO_2 (aqueous). The diagram is constructed based on Al^{+3} conservation. Muscovite is used as a proxy for illite in activity space. Inkpot Spring fluids are in equilibrium with kaolinite, pyrophyllite, and mordenite.

The bimodal distribution of Inkpot Spring fluids may show equilibrium with both the quartz-illite and quartz-kaolinite assemblages observed in the Grand Canyon of the Yellowstone River. Figures 14 and 15 show that the quartz-illite assemblage may form from a higher K^+ activity or a higher pH hydrothermal fluid than that which produced the quartz-kaolinite assemblage. However, the bimodal distribution is most likely controlled by the neutralizing effect of ammonia. If ammonia does not occur in sufficient quantities to neutralize the H_2SO_4 , then the data points that plot within the illite (muscovite) and mordenite fields would probably plot within the kaolinite and pyrophyllite fields among the other data points at higher H^+ activity. This effect may be seen on Figures 14, 15, 16, and any other activity diagram controlled in part by H^+ activity. The neutralizing effect of ammonia suggests Inkpot Spring fluids may be in equilibrium with only the quartz-kaolinite assemblage. The stability of Al-silicates in the system CaO-K₂O- Al₂O₃-SiO₂-H₂O at 100°C as a function of the activity ratios Ca^{++}/H^{+^2} and K^+/H^+ is shown in Figure 16. At near-surface temperatures, fluids plot in the kaolinite and illite fields. At 200, 225, and 250°C fluids plot within the kaolinite, beidellite, heulandite, and prehnite fields.

Another explanation for increased Ca^{++} activity at Inkpot Spring is exchange with anorthitic plagioclase in the Sulphur Creek Stock. Equilibrium with calcite, indicated by blue boundaries in Figure 16, is also possible. Travertine is not observed at the surface at Inkpot Spring but $CaCO_3$ may line conduits at depth as calcite solubility decreases with increasing temperature. Surface deposits of travertine have been observed within 1 km of Inkpot Spring. Gypsum mounds have been observed around fumarolic vents developed on basaltic-andesite of the Absaroka volcanics not far from Inkpot Spring, but at a lower elevation, and may explain the increased Ca^{++} activity. Gypsum solubility also decreases with increasing temperature.



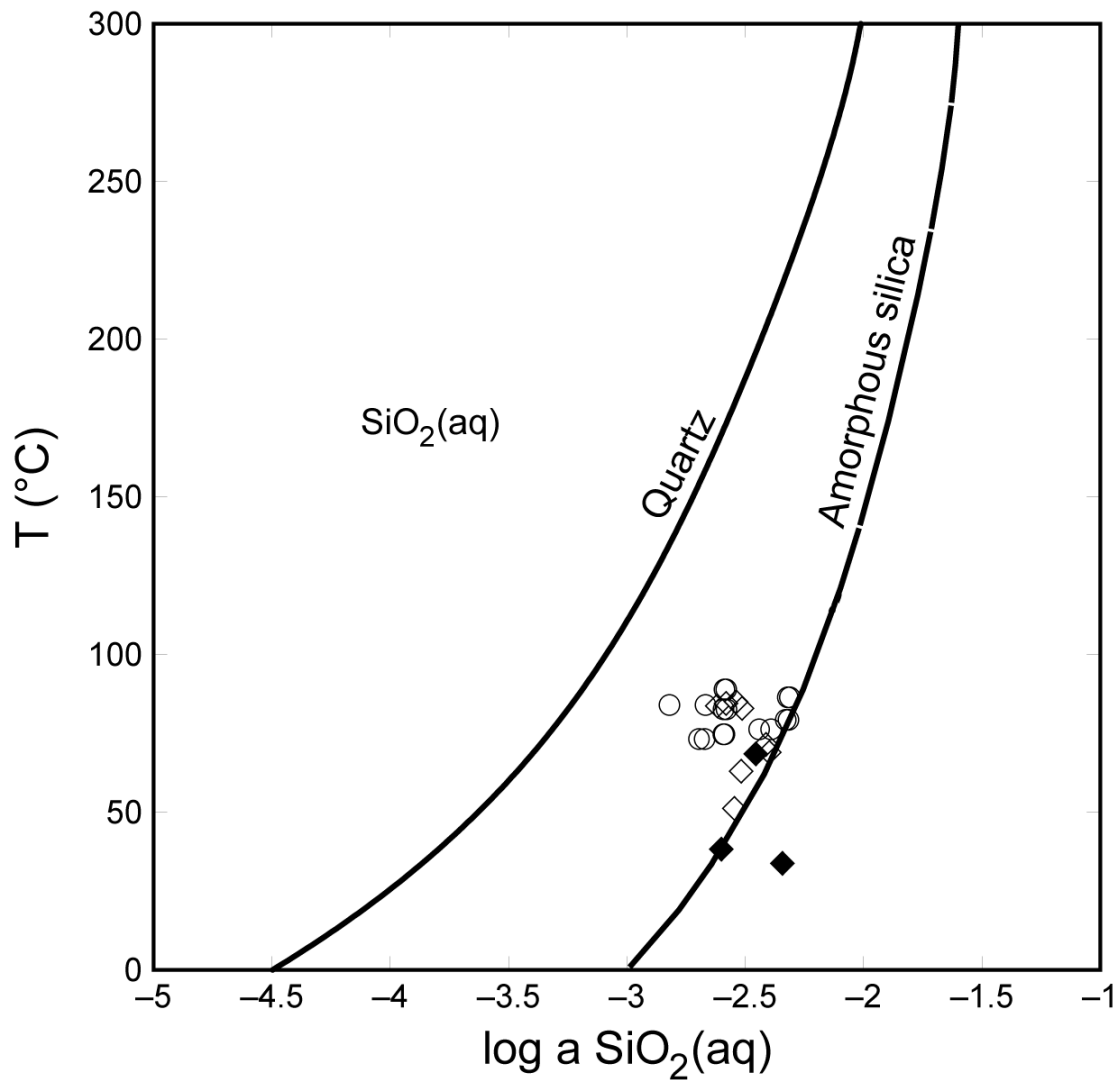
- 2008 Inkpot Spring samples. Data included in Appendix C.
- ◆ 2008 Unnamed thermal spring samples collected SW of Inkpot Spring along Howard Eaton Trail. Data included in Appendix C.
- ◇ 2003 & 2001 Washburn & Inkpot Spring water data from McCleskey et al. (2005) and Ball et al. (2007), included in Appendix B.

Figure 16. Activity diagram showing the stability of aluminosilicate minerals in the system CaO-Al₂O₃-K₂O-H₂O at 100°C as a function of the activity ratios Ca⁺⁺/H⁺² and K⁺/H⁺. The diagram is constructed based on Al⁺³ conservation. Muscovite is used as a proxy for illite in activity space. Inkpot Spring fluids are in equilibrium with kaolinite and appear to be in equilibrium illite. Instead of equilibrium with illite, Ca⁺⁺ activity may also be explained by equilibrium with calcite, gypsum, or anorthitic plagioclase.

Mineral saturation indices ($\log Q/K$) indicate amorphous silica is near saturation in Inkpot Spring fluids. Minimal sinter deposits are present on altered ground around Inkpot Spring pools. Pool IKP03, the most vigorously bubbling pool, is rimmed with layered siliceous sinter. Figure 17, in conjunction with mineral saturation indices and observed sinter deposits, indicates Inkpot Spring fluids are saturated with respect to quartz and are at or just below saturation with amorphous silica at the surface thermo-chemical conditions.

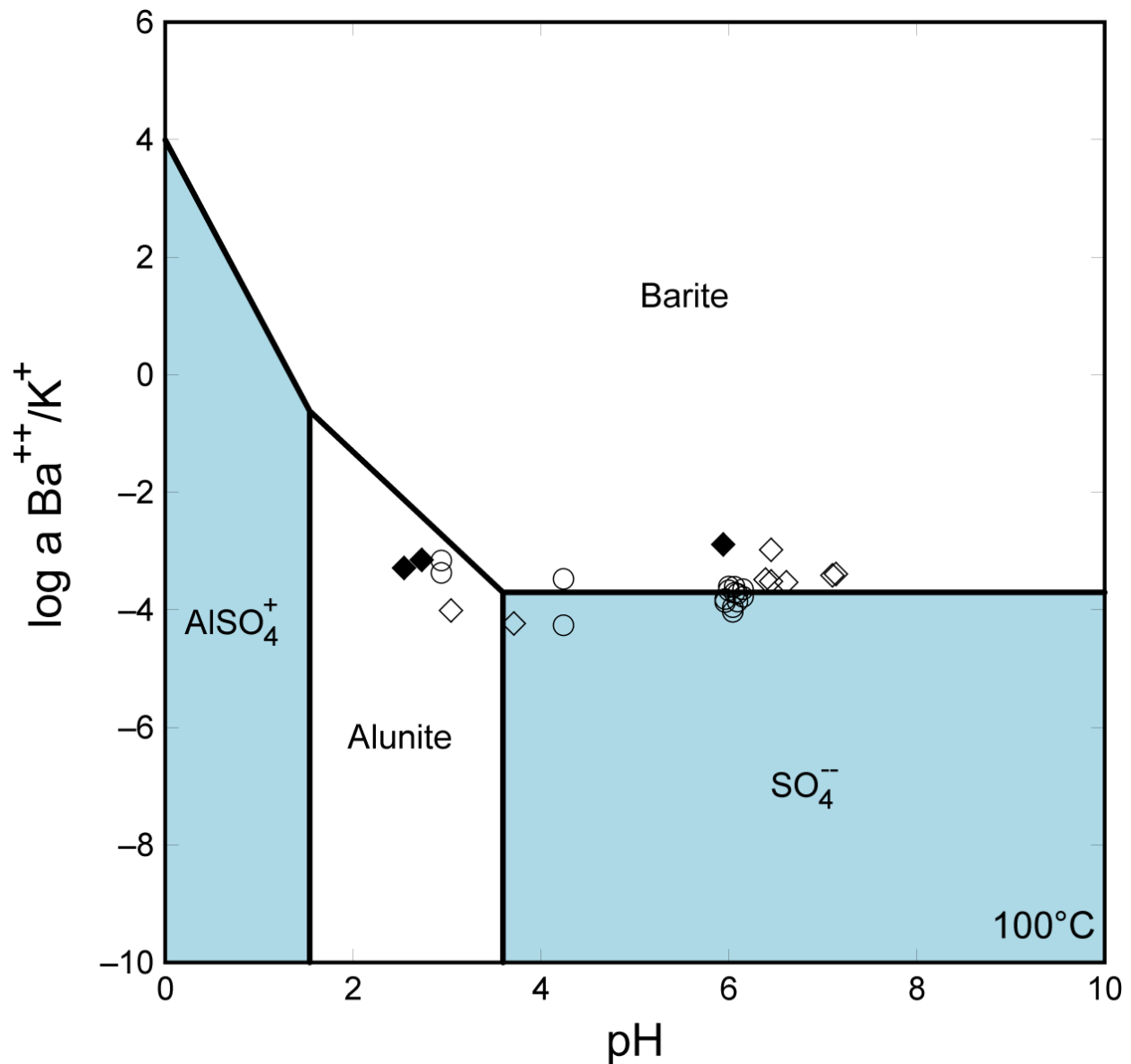
Activity diagrams and mineral saturation indices show three zeolite minerals, mordenite, heulandite, and clinoptilolite, are stable in these fluids. Saturation indices should be interpreted with caution as a mineral's saturation index depends on the choice of its formula unit. Large formula units are used for many clay and zeolite minerals in The Geochemist's Workbench LLNL database, which explains why these minerals often appear at the top of the supersaturation list (Bethke, 2008). However, all zeolites and clays at or near saturation in Inkpot Spring fluids have been observed in Yellowstone research drill holes. Zeolites such as mordenite, heulandite, and clinoptilolite are common devitrification products of silicic tuffs. Devitrification and pervasive alteration of the local Plateau Rhyolites is the likely location of these zeolites. Surficial sediments in Yellowstone are often cemented with hydrothermal zeolites and silica, as well.

Alteration mineral assemblages in the Grand Canyon of the Yellowstone River contain several sulfate minerals, including barite, alunite, walthierite, and huangite. These minerals are also found in the sediment in and around the pools at Inkpot Spring. Dissolved sulfate at concentrations from 900 to 3300 mg/L at Inkpot Spring allows precipitation of these sulfate minerals. Figure 18 shows that Inkpot Spring fluids are at or near equilibrium with barite and some are in equilibrium with alunite just above surface temperatures. Excess Ba^{++} available to



- 2008 Inkpot Spring samples. Data included in Appendix C.
- ◆ 2008 Unnamed thermal spring samples collected SW of Inkpot Spring along Howard Eaton Trail. Data included in Appendix C.
- ◇ 2003 & 2001 Washburn & Inkpot Spring water data from McCleskey et al. (2005) and Ball et al. (2007), included in Appendix B.

Figure 17. Activity diagram showing calculated solubilities of quartz and amorphous silica. Silica activity at Inkpot Spring is just below amorphous silica saturation. Some pools are probably closest to equilibrium with cristobalite.



- 2008 Inkpot Spring samples. Data included in Appendix C.
- ◆ 2008 Unnamed thermal spring samples collected SW of Inkpot Spring along Howard Eaton Trail. Data included in Appendix C.
- ◇ 2003 & 2001 Washburn & Inkpot Spring water data from McCleskey et al. (2005) and Ball et al. (2007), included in Appendix B.

Figure 18. Activity diagram showing the stability of sulfate species as a function of pH and Ba^{++}/K^+ . Diagram calculated for a temperature of 100°C, with an average $\log SO_4^{2-}$ activity of -2.2483, average $\log K^+$ activity of -3.5562, activity of silica set by cristobalite, and activity of Al^{+3} is fixed by kaolinite. Fields shaded blue are species in solution. Inkpot Spring fluids appear to be at or close to equilibrium with barite and some pools are in equilibrium with alunite. Ba^{++} activity is probably controlled by walthierite and not barite. Walthierite is the Ba-rich sulfate abundant in sediment around the pools. Without the neutralizing effect of ammonia most Inkpot Spring fluids would plot closer to the alunite stability field.

form barite is probably derived from the nearby Tuff of Sulfur Creek, however, walthierite is the more abundant Ba-rich sulfate in this area probably due to available aluminum and sulfur.

Variable pH and redox conditions at Inkpot Spring may allow for near equilibrium conditions with alunite in one pool but not another. Thermodynamic data for walthierite and huangite are not available. So, although it cannot be demonstrated using thermodynamic equilibrium relationships, it is likely that these alunite group minerals are in equilibrium with the fluids.

7. SUSPENDED SEDIMENT AND PARTICULATES

One of the most striking features at Inkpot Spring is the dark gray to black color of the water and surrounding sediment, described in detail as early as 1888 by Gooch and Whitfield and later by Allen and Day (1935). Photos from Allen and Day's 1935 study show that the ground around Inkpot Spring has changed dramatically since that time. In 1935, there appears to have been only one main pool 20 by 27 feet in size and choked with fine black sediment (Allen and Day, 1935) (Fig. 19). This is thought to be the pool named Devil's Ink Pot by Gooch and Whitfield (1888) and later referred to as Inkpot Spring on topographic maps. In 2008, Inkpot Spring consisted of approximately 6 main pools of bubbling water, 1 large mudpot, 1 fumarole, and numerous areas of steaming and sizzling ground. Pool IKP10 is the blackest pool and IKP04, IKP10, and a deep mudpot appear to be located at what was once Devil's Ink Pot (Fig. 20a and 20b). Minor changes in the pools at Inkpot Spring can occur from year to year, partly depending on the amount of precipitation. Figure 21a and 21b show changes at Inkpot between 2001 and 2008. Some pools at Inkpot Spring were observed filling with water overnight and then dropping throughout the day. On several days, a small pool (IKP11), approximately 1.5 feet in diameter, contained several inches of water at 10:30 AM, was completely drained by 1:30 PM, revealing pyrite coated pebbles in the bottom (Fig. 22a,b,c, and d). A chemical analysis of pyrite coated pebbles from pool IKP11 is included in Appendix E. Backscattered electron images (Fig. 23a and 23b) show precipitated pyrite coatings at 10 and 100 μ m. Most of the ground around the pools at Inkpot is bleached white, but cobbles that are not completely altered are basaltic-andesite of the Absaroka volcanics. Since Allen and Day's study in 1935, this basaltic-andesite has been considered to be the source of excess iron which combines with sulfur to give the pools their distinct "ink" color.



Figure 19. Photograph of largest Inkpot Spring pool from Allen and Day (1935). This photograph shows the largest and darkest pool in this area in 1935, which has become known as Inkpot Spring. Allen and Day (1935) conclude that this is the pool named Devil's Ink Pot by Gooch and Whitfield (1888).

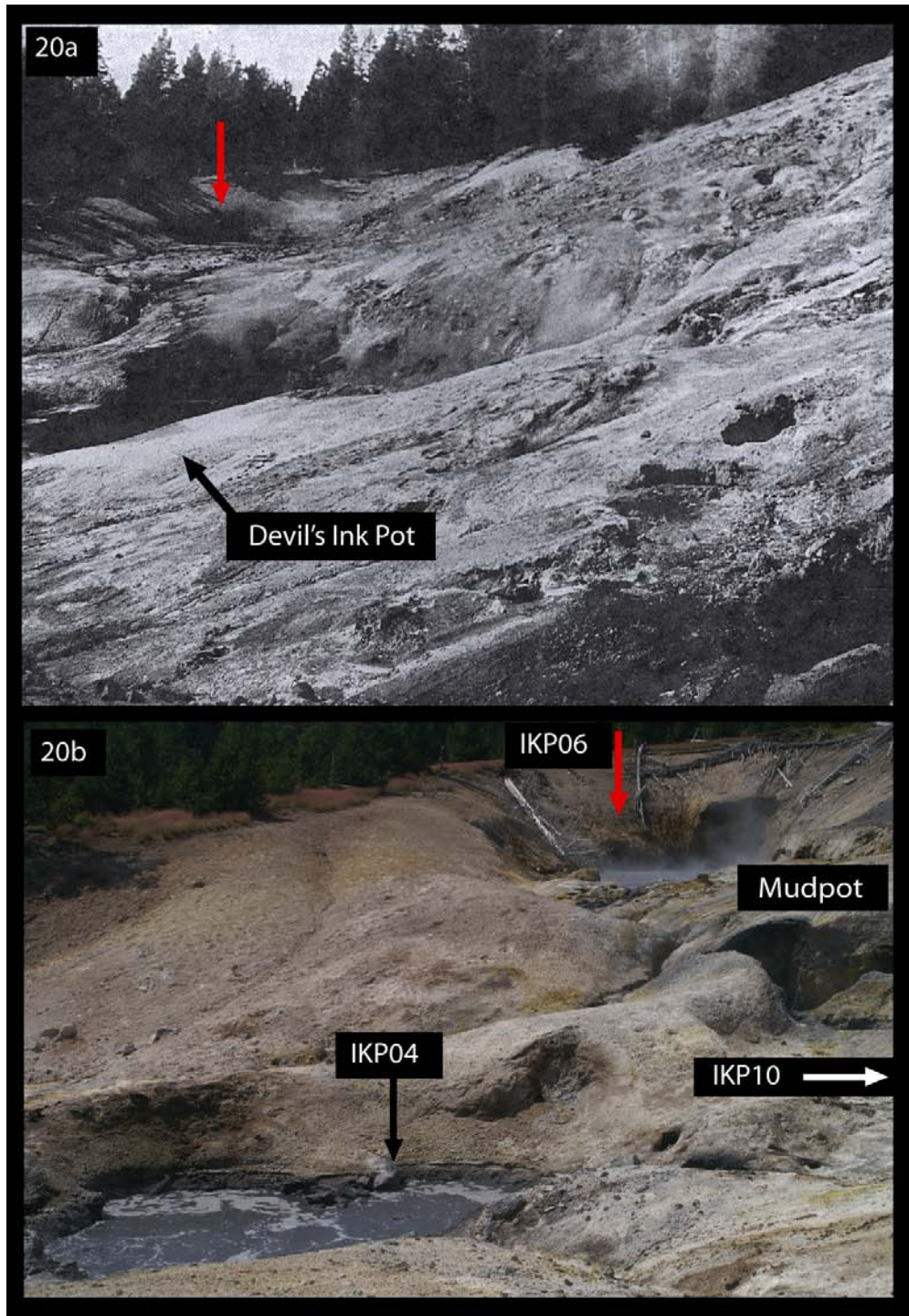


Figure 20a and b. Photographs of Devil's Ink Pot (Inkpot Spring) from Allen and Day (1935) (Fig. 20a) and Inkpot Spring during 2008 (Fig. 20b) show dramatic changes of the altered ground and pools during the time between these two studies. Only a depression exists in 1935 in the altered ground where pool IKP06 has formed. The Devil's Ink Pot pool has retreated since 1935 and would probably occupy pools IKP04 and IKP10 and a nearby mudpot today. Pool IKP10 still has the darkest colored water and probably represents the fluid most similar to that of the 1935 Devil's Ink Pot.



Figure 21a and b. Photographs of the largest Inkpot Spring pool (IKP06) during 2001 from McCleskey et al. (2005) (Fig. 21a), and this study during 2008 (Fig. 21b) show changes over a 7 year period. The water surface during 2001 appears to be in a state of constant agitation with intense bubbling and possibly boiling, while the pool contains more water during 2008, and has reached a stage of quiescence. Minor bubbling and turbulence of the water surface was observed in 2008.

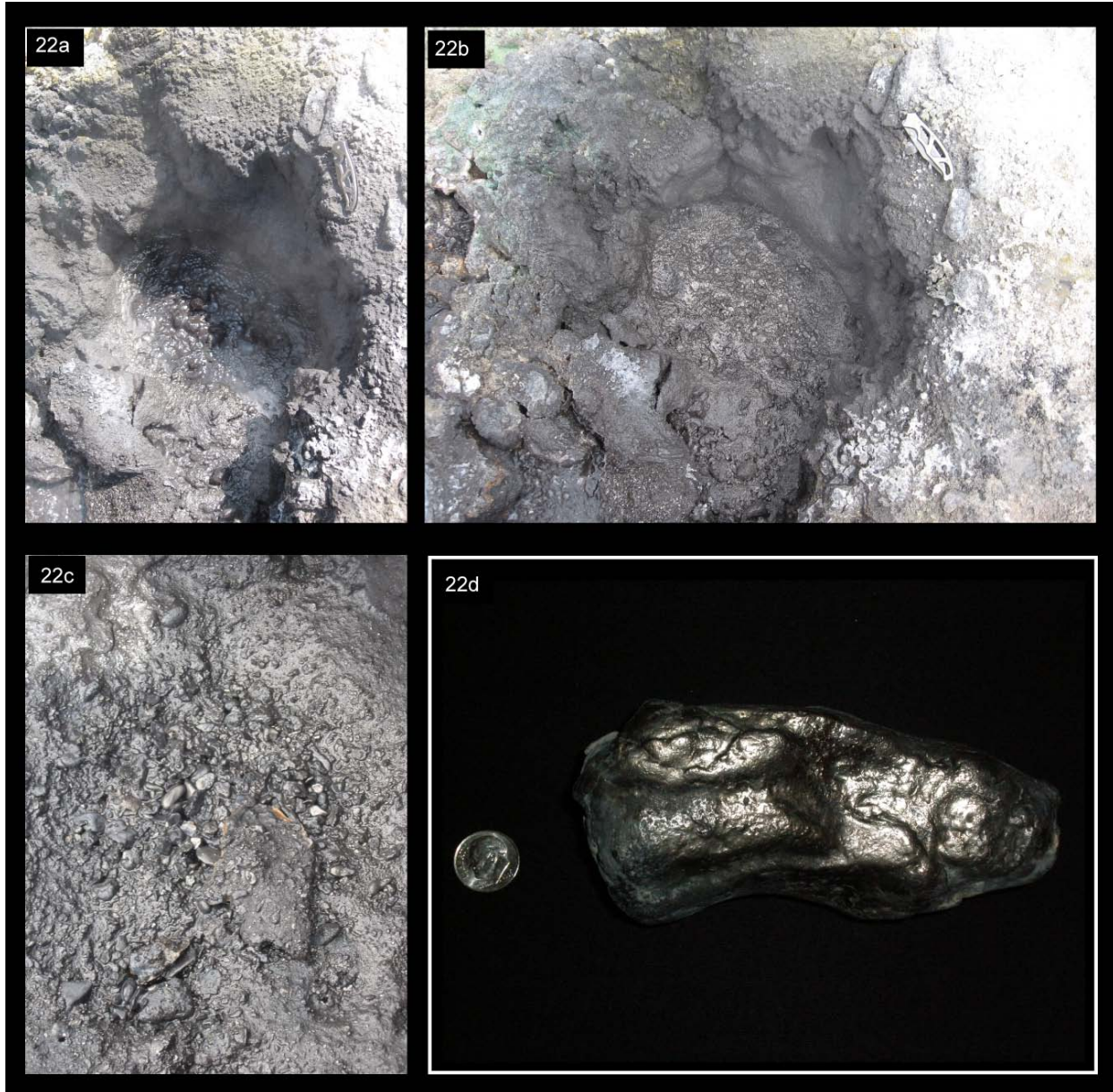
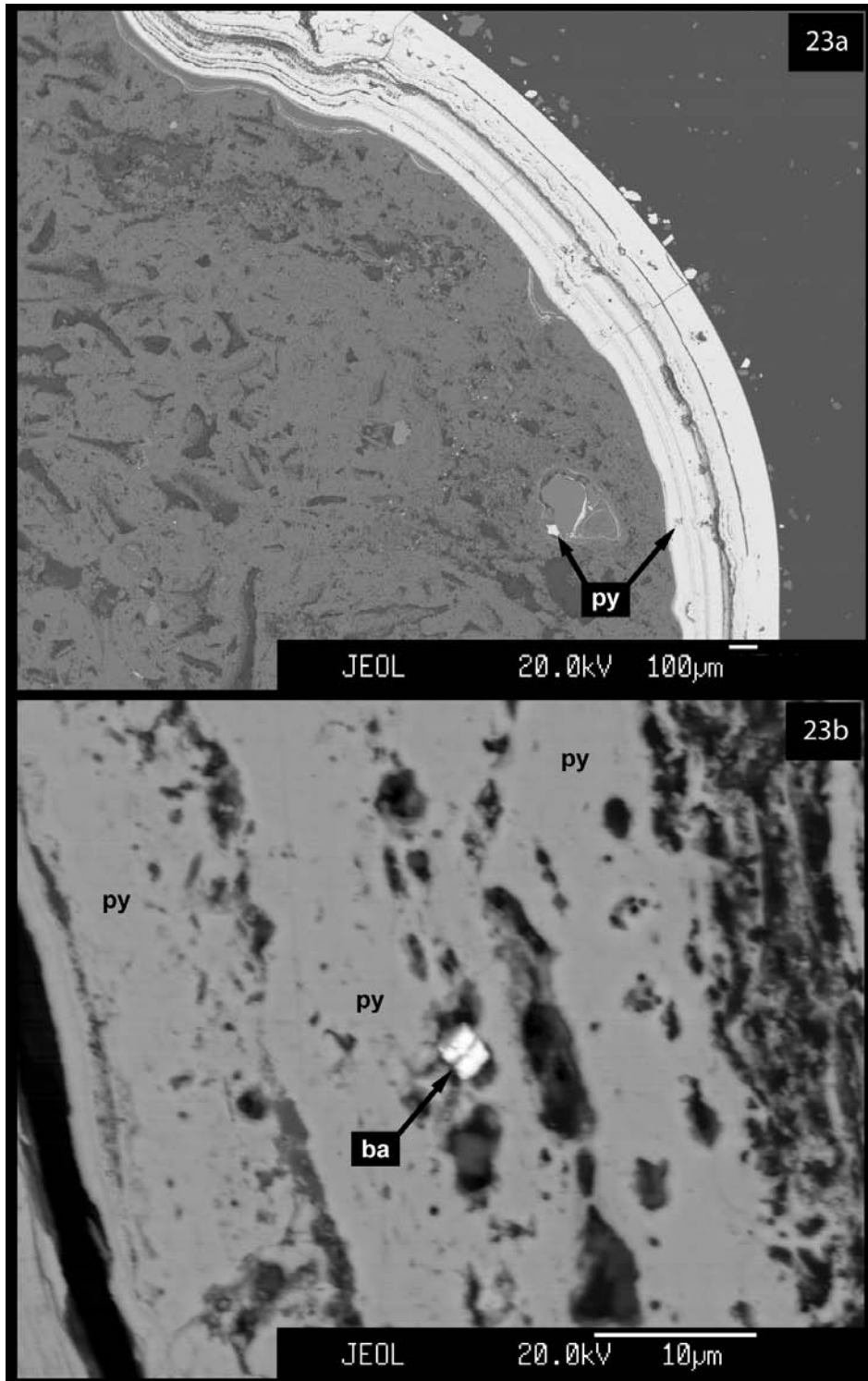


Figure 22a,b,c, and d. Photographs of a small pool (IKP11), which was observed with boiling water around 10:30-11:00 AM (Fig. 22a), and completely drained by 1:30 PM (Fig. 22b) on several days during late July and early August, 2008. Once drained, pyrite coated pebbles are revealed in the bottom of the pool (Fig 22c). Figure 22d shows a close-up view of a cobble coated with pyrite from pool IKP11. A chemical analysis of these pyrite coated pebbles from pool IKP11 is included in Appendix E. Backscattered electron images of the pyrite coatings are shown in Figures 23a and 23b.



In conjunction with water analyses, various sediments were collected in and around Inkpot Spring in order to investigate fluid-mineral equilibria and similarities with hydrothermal ore deposits. Unfiltered water samples were collected for measurement of suspended sediment. This sediment has been analyzed using X-ray powder diffraction (XRD), scanning electron microscopy (SEM), and energy dispersive X-ray spectrometry (EDS) coupled with backscattered electron imaging. Small sediment samples were also collected at the edge of several pools and analyzed using ICP-MS, ICP-AES, XRD, EDS, and X-ray Fluorescence (XRF). Inkpot Spring sediment analyses are included in Appendix E. Table 5 shows a list of minerals in Inkpot spring sediments identified using XRD and EDS.

Table 5. Minerals identified in Inkpot Spring sediment using XRD and EDS	
<i>Tectosilicates</i>	<i>Sulfates</i>
Quartz	SiO ₂
Cristobalite	SiO ₂
Tridymite	SiO ₂
Mordenite	Na _{1.1} Ca _{0.5} K _{0.1} Al _{2.2} Si _{9.8} O ₂₄ •5.9(H ₂ O)
Ca-plagioclase	(Ca,Na)(Si,Al) ₄ O ₈
K-feldspar	(K,Na)(Si,Al) ₄ O ₈
<i>Phyllosilicates (clays)</i>	
Kaolinite	Al ₂ Si ₂ O ₅ (OH) ₄
Dickite	Al ₂ Si ₂ O ₅ (OH) ₄
<i>Sulfides and Sulfur</i>	
Pyrite	FeS ₂
Cinnabar	HgS
Sulfur	S
	Alunite
	Ammonioalunite
	Walthierite
	Huangite
	Letovicite
	Barite
	Potassium alum
	Tschermigite
	(Ammonia alum)
	KAl ₃ (SO ₄) ₂ (OH) ₆
	(NH ₄)Al ₃ (SO ₄) ₂ (OH) ₆
	BaAl ₆ (SO ₄) ₄ (OH) ₁₂
	Ca _{0.5} Al ₃ (SO ₄) ₂ (OH) ₆
	(NH ₄) ₃ H(SO ₄) ₂
	BaSO ₄
	KAl(SO ₄) ₂ •12(H ₂ O)
	(NH ₄)Al(SO ₄) ₂ •12(H ₂ O)

Table 5. Minerals identified in sediments collected around Inkpot Spring and in suspended sediment filtered from Inkpot Spring fluids.

Multiple forms of silica are found in the sediment around the springs. Opaline silica is actively precipitating around pool IKP03 and this finely layered deposit may contain metastable opal C-T

with microscopic stacking of the high temperature polymorphs, cristobalite and tridymite, in varying proportions. Non-crystalline silica transforms to opal C-T as a result of diagenesis due to overburden and pressure (Cady et al., 1996). Weathering of old, buried sinter deposits in the vicinity of Inkpot Spring may explain the presence of cristobalite and tridymite in loose sediments around the pools. Other pools at Inkpot Spring have probably precipitated opal in the past adding to the amount of silica in the surrounding sediments.

The Tuff of Sulphur Creek contains approximately 5-15% quartz phenocrysts and the Sulphur Creek Stock contains approximately 25% quartz phenocrysts (Christensen, 2001; Larson et al., 2009). Both of these units may also contribute to the amount of silica in the sediment. The Tuff of Sulfur Creek also contains approximately 20-35% sanidine and 5% sodic plagioclase phenocrysts (Larson et al., 2009). No outcrops of the Tuff of Sulphur Creek are mapped within a few hundred meters of Inkpot Spring; however, this unit may have been present in drainages outside the caldera rim, including those around Inkpot Spring. Quaternary glacial deposits in the vicinity of Inkpot Spring include material transported from the Tuff of Sulphur Creek and other rhyolitic units and are the likely source of K- and Na-feldspar in the sediment. Feeley et al. (2001) found plagioclase compositions from the Mt. Washburn volcanic rocks to range from An₈₃-An₄₀ with greater than two-thirds of phenocryst cores between An₆₅ and An₅₀.

Four sulfate minerals of the alunite group are identified in Inkpot Spring sediments, including alunite, ammonioalunite, walthierite, and huangite. Excess sulfate allows for precipitation of these minerals from Inkpot Spring pools. Alunite, walthierite, and huangite also occur as alteration phases in the nearby Tuff of Sulphur Creek (Larson et al., 2009). Letovicite, an ammonium sulfate, and barite were also identified in the sediments. Letovicite from Inkpot Spring has a strong odor of ammonia and significant amounts are found on the altered ground

surrounding the pools. Although not identified during this study, other sulfates such as mascagnite and natroalunite may form at Inkpot Spring.

Pyrite is actively precipitating from pool IKP11 and other small surrounding pools (Fig. 22 and 23). It was the only sulfide identified using XRD, however, marcasite is abundant in veins in the Tuff of Sulphur Creek (TSC). Microscopic cinnabar was identified using EDS and is discussed in the following chapter. Clay minerals, kaolinite and dickite, are both identified in Inkpot sediment and in the TSC. Although As and Sb occur at low concentrations compared to similar acid-sulfate systems, minerals such as realgar may form in minor amounts at Inkpot Spring, but have not been identified. Elemental sulfur is identified in suspended material, similar to other hot springs in Yellowstone.

In order to identify the major components directly contributing to the dark color of the pools, suspended sediment was collected by pouring unfiltered water samples onto filter paper, leaving behind dark gray mud slurries. This material was dried in an oven at 100°C over 24 hours and then analyzed using XRD and SEM. XRD revealed the presence of several of the same minerals in Table 5, including pyrite, thought to be the major contributor to the pool's dark color. SEM images (Fig. 24), in conjunction with XRD analyses, and backscattered electron imaging coupled with EDS analyses suggest that a variety of minerals are in suspension in the pools. Figure 25 shows backscattered electron images of the fine suspended material from some of the darker pools at Inkpot Spring.

Sediments collected around the edge of several pools were also analyzed for a suite of major and trace elements by ALS Chemex using a combination of ICP-MS and ICP-AES techniques. Exceptions include Au, which was analyzed by fire assay (FA), and Hg, which was analyzed by Cold Vapor Atomic Absorption (CVAA) and Direct Mercury Analysis (DMA).

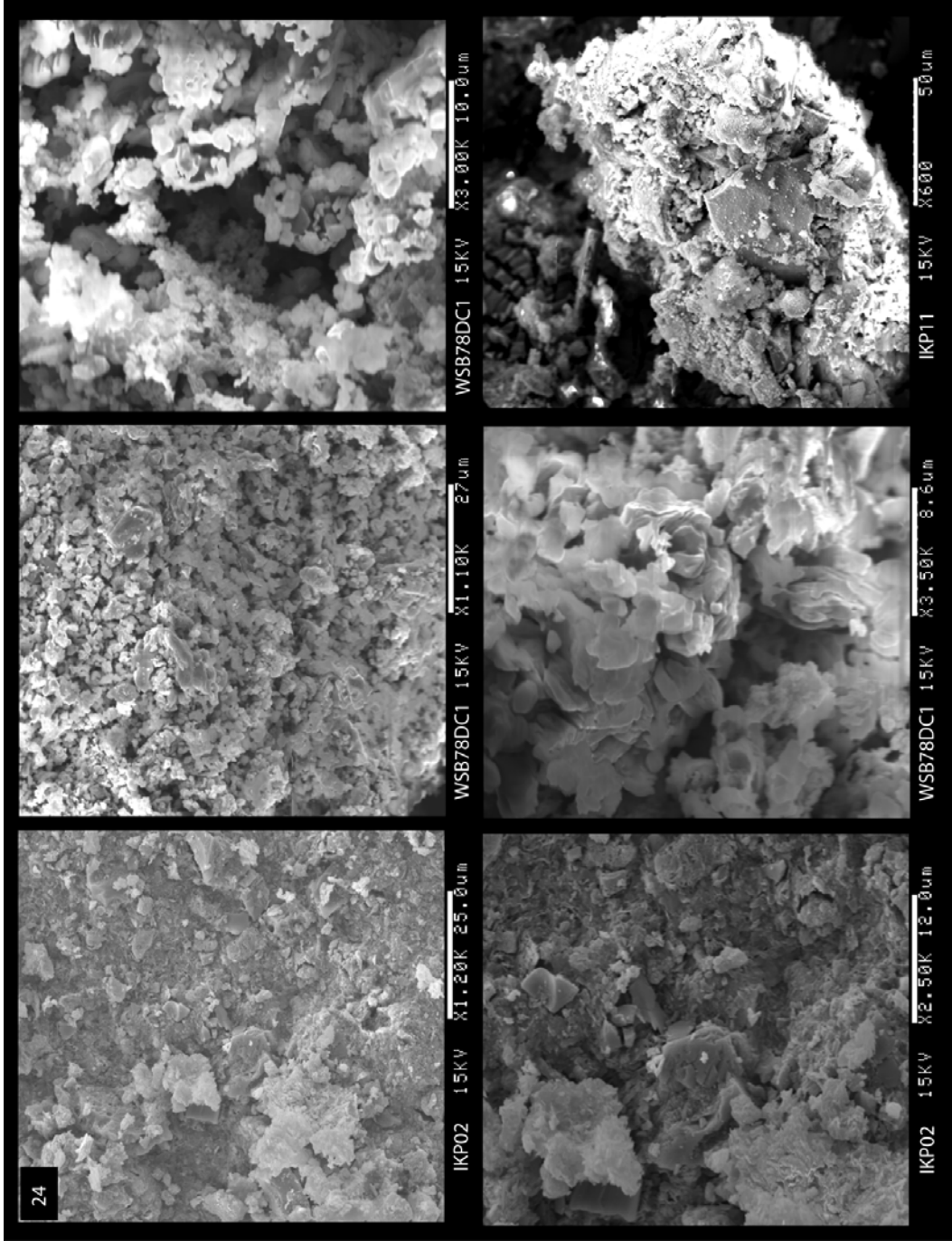


Figure 24. Scanning electron micrographs of suspended sediments filtered from Inkpot Spring fluids. In conjunction with XRD and EDS analyses, these images suggest several minerals including opal, quartz, pyrite, sulfur, and various clays and sulfates may be suspended in Inkpot Spring fluids.

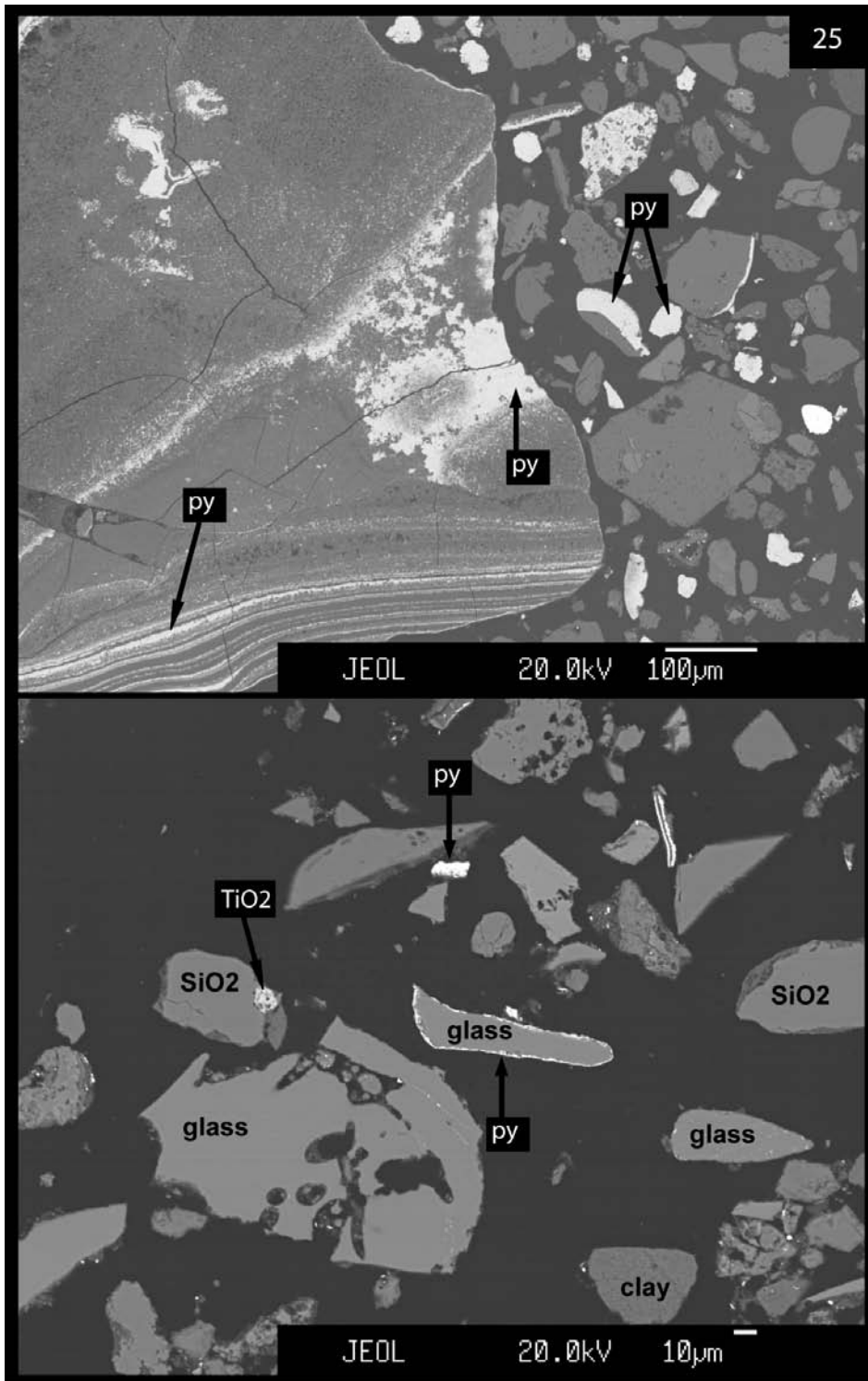


Figure 25. Backscattered electron images showing fine suspended material from IKP10 and IKP11. Glass fragments appear to represent a major component in these pools. Multiple generations of pyrite (py) precipitation have occurred and fine suspended pyrite produces the dark “ink” color of the fluids.

Most of the sediment is dark gray, Fe-sulfide-rich, and water saturated. Similar hot spring deposits have been observed at Growler Hot Springs in Lassen Volcanic National Park, California (LVNP) (D. John, USGS, oral communication, 2007). Major and trace element analyses of Inkpot Spring sediments are presented in Appendix E with additional data from Growler Hot Spring sediments for comparison.

Major and trace element abundances in the sediment reflect the composition and mineralogy of the major geologic units around Inkpot Spring. Appendix E includes a comparison of Inkpot Spring sediment to basaltic andesite of the Lamar River Formation (LRF) and rhyolitic Tuff of Sulphur Creek (TSC). The silica concentration of the sediments is approximately 68 weight percent, between the ~74% of the TSC and ~54% of the LRF. The data suggest that elements, including Ti, Fe, Mg, and Ca, are primarily derived from the LRF, while K may be primarily derived from the TSC. Trace element data suggest that Ni, Cr, Sc, V, Sr, and Cu may be primarily derived from the LRF, while Zr, Rb, Y, Nb, Ce, and Th are probably derived from the TSC. Other trace elements including Ba, Ga, Zn, Pb, La, Nd, and U occur at similar concentrations in both the LRF and TSC, and both probably contribute to the concentrations of these elements in Inkpot Spring sediments.

Acid-sulfate or high-sulfidation systems similar to that at Inkpot Spring have produced several high-tonnage Au deposits worldwide including Yanacocha, Peru; Summitville, CO, USA; La Coipa, Chile; Rodalquilar, Spain; Akaiwa, Japan; and Temora, Australia (Hedenquist et al., 2000). Inkpot Spring sediments and precipitates have low gold concentrations with the highest at 0.023 ppm around IKP02. One major difference between Inkpot Spring sediments and common precipitates associated with other high-sulfidation systems is the concentration of As and Sb, which commonly occur with Au. Similar sediments and precipitates from Growler Hot

Springs in LVNP have As concentrations from 109 to 1430 ppm and Sb concentrations from 107 to 5700 ppm. Inkpot Spring sediment As concentrations range from 1.8 to 15 ppm, and Sb concentrations range from 0.07 to 1.09 ppm. In addition to the highest concentrations of Fe (7.54%) and S (9.61%), sediment from pool IKP10 contains the highest concentrations of metals of economic interest including Zn (126 ppm), Ni (91.3 ppm), and Co (24.3 ppm). Ni may substitute for Fe in pyrite as observed in veins in the TSC during microprobe analysis (J. Manion, oral communication, 2009). Sphalerite was also observed in veins in the TSC and may precipitate from this pool.

8. MERCURY

8.1 Comparisons to other Hg-depositing Geothermal Systems

Mercury is the primary anomalous trace element at Inkpot Spring, occurring at high concentrations in fluids, sediments, and precipitates. Data from Direct Mercury Analysis (DMA) of filtered fluids, unfiltered fluids (mud-suspended sediment slurries), and sediments are included in Appendix F. Mercury concentrations at Inkpot are similar to those from large Hg deposits in volcanic environments and other Hg-depositing waters worldwide. Inkpot Spring shares several similarities with Hg-depositing systems of the Coast Ranges, CA, including Sulphur Bank, The Geysers-Clear Lake area (Myacmas district), Wilber Springs district, Skaggs Springs, Mt. Diablo, and the Cymric oil field. Other similar Hg-depositing systems include Ngawha, New Zealand; Mendeleev, Kunashir, Russia; Apapel'sk Springs, Kamchatka, Russia; Steamboat Spring, Nevada, USA; and Boiling Springs, Idaho, USA. Table 6 shows the comparison between worldwide waters associated with Hg and Inkpot Spring fluids. In addition to Hg, many of these Hg-depositing systems include elevated concentrations of SiO₂, CO₂, NH₃,

Locality	Sample #	Units	Temp (°C)	pH	Na	K	NH ₄	Ca	Mg	Fe	Mn	HCO ₃	Cl
Sulfur Bank, Lake Co., CA	-----	ppm	69.5	6.8	1190	23	464	20	55	0.1	0.2	3290	664
Abbott mine, Wilber Springs district, Colusa Co., CA	-----	ppm	35	7.1	1500	39	22	64	443	0.04	0.0	2710	1900
Wilber Springs (Sulphur Creek grp.), Colusa Co., CA	-----	ppm	57	7.2	9140	460	303	1.4	58	0.1	0.3	7390	11000
Elgin mine, Wilber Springs district, Colusa Co., CA	-----	ppm	68.5	7.4	9110	506	243	5.9	29	0.04	0.0	7240	11000
Valley mine, Mayacmas district, Napa Co., CA	-----	ppm	32	6.5	476	8.2	2.5	19	90	0.6	0.1	1490	229
Big Injun mine, Mayacmas district, Lake Co., CA	-----	ppm	21	6.8	26	0.9	-----	34	142	-----	-----	708	2
The Geysers, Mayacmas district, Sonoma Co., CA	-----	ppm	100	1.8	12	5	1400	47	281	63	1.4	-----	0.5
Skaggs Springs, Sonoma Co., CA	-----	ppm	54	7.2	912	33	-----	14	5.4	-----	-----	2480	58
Altoona mine, Trinity Co., CA	-----	ppm	12.5	7.0	3710	220	18	28	39	0.07	0.01	8060	1560
Mt. Diablo mine, Contra Costa Co., CA	-----	ppm	21	7.7	3100	53	57	431	12	0.3	0.1	203	5770
Steamboat Springs, Washoe Co., NV	-----	ppm	60	6.1	637	61	<1	16	1.0	-----	-----	314	824
Cordero mine, Humboldt Co., NV	-----	ppm	56	8.1	115	2.4	0.3	3.2	0.2	0.06	0.01	199	26
Amedee Springs, Lassen Co., CA	-----	ppm	92	8.5	227	6.8	0.5	16	0.0	0.01	0.00	37	160
Boiling Springs, Valley Co., ID	-----	ppm	88	9.2	74	1.9	-----	2.2	0.0	0.4	0.004	106	14
Apapel'sk Springs, Kamchatka, Russia	-----	ppm	96	8.1	372	22	0	16	5.2	0.7	0	174	168
Ngawha Springs, New Zealand	-----	ppm	48	6.4	830	63	148	7.8	2.5	-----	-----	340	1250
Cymric Oilfield, Kern Co., CA	-----	ppm	81	7.5	5820	132	51	373	115	1.2	0.08	535	9840
Ourray Springs, San Juan Mountains., Ouray Co., CO	-----	ppm	62	6.8	111	8.0	-----	376	6.1	0.4	0.9	128	45
Growler Hot Spring, Lassen Volcanic National Park	LJ-82-01	ppm	95.5	8.0	1380	185	3.0	59.8	0.01	0.16	0.01	66	2430
Little Growler, Lassen Volcanic National Park	LJ-82-04	ppm	95	7.2	1380	153	4.2	69.7	0.66	0.08	0.03	61	2250
Inkpot Spring, Yellowstone National Park	IKP01	ppm	82.6	6.09	34.03	15.53	350	29.05	12.92	0.0194	0.1205	130	0.53
Inkpot Spring, Yellowstone National Park	IKP02	ppm	73.2	5.96	20.45	7.82	590	14.36	6.12	0.0395	0.0537	170	4.4
Inkpot Spring, Yellowstone National Park	IKP03	ppm	86.4	6.04	55.47	33.47	300	29.51	1.453	0.0245	0.0306	79	0.24
Inkpot Spring, Yellowstone National Park	IKP04	ppm	76.3	4.24	29.59	18.83	670	40.66	20.92	0.0838	0.1430	<3	<0.2
Inkpot Spring, Yellowstone National Park	IKP06	ppm	74.7	6.06	34.69	14.36	360	32.55	16.17	0.0224	0.0533	200	0.63
Inkpot Spring, Yellowstone National Park	IKP07	ppm	84.0	6.15	19.46	10.64	320	29.37	10.8	0.485	0.0172	48	0.39
Inkpot Spring, Yellowstone National Park	IKP09	ppm	88.9	6.00	24.04	9.361	240	13.87	6.564	0.3799	0.0157	37	0.86
Inkpot Spring, Yellowstone National Park	IKP10	ppm	79.3	2.94	11.31	13.06	530	7.645	3.595	6.879	0.0153	<3	NA
Inkpot Spring, Yellowstone National Park	2IKP01	ppm	82.6	6.09	33.95	15.27	360	28.46	12.62	0.0087	0.0185	110	0.36
Inkpot Spring, Yellowstone National Park	2IKP02	ppm	73.2	5.96	14.24	7.222	620	12.58	6.085	0.0244	0.0137	200	0.22
Inkpot Spring, Yellowstone National Park	2IKP03	ppm	86.4	6.04	54.56	32.14	280	27.28	1.334	0.0154	0.0098	76	NA
Inkpot Spring, Yellowstone National Park	2IKP04	ppm	76.3	4.24	28.57	18.79	680	35.55	18.52	0.0092	0.0184	42	<0.2
Inkpot Spring, Yellowstone National Park	2IKP06	ppm	74.7	6.06	34.44	14	360	31.89	15.68	0.009	0.0137	210	0.36
Inkpot Spring, Yellowstone National Park	2IKP07	ppm	84.0	6.15	18.53	11.24	520	30.78	12.23	0.023	0.0088	34	<0.2
Inkpot Spring, Yellowstone National Park	2IKP09	ppm	88.9	6.00	30.27	13.1	340	19.77	11.77	0.0217	0.0084	36	0.27
Inkpot Spring, Yellowstone National Park	2IKP10	ppm	79.3	2.94	12.62	16.9	640	7.02	3.737	13.94	0.0085	<3	NA

Table 6. Geochemical analyses of waters associated with mercury deposits compared with Inkpot Spring fluids. Data for un-numbered samples are from Table 13.1 in White (1967). Data for Growler and Little Growler Hot Springs, Lassen Volcanic National Park are from Table 1 in Thompson (1985). Inkpot Spring water chemistry data from this study is included in Appendix C with additional Hg data in Appendix F.

Locality	Sample #	Units	SO ₄	H ₂ S	B	SiO ₂	As	Sb	Hg	Analyst/Reference
Sulfer Bank, Lake Co., CA	-----	ppm	598	12	620	42	0.00	<0.02	<0.02	White and Robertson, 1962
Abbott mine, Wilber Springs district, Colusa Co., CA	-----	ppm	467	<1	56	16	0.00	-----	-----	White and others, 1963
Wilber Springs (Sulphur Creek grp.), Colusa Co., CA	-----	ppm	23	178	292	190	0.0	0.0	0.22	White and others, 1963
Elgin mine, Wilber Springs district, Colusa Co., CA	-----	ppm	6.8	170	240	244	-----	-----	0.04	C.E. Robertson, USGS
Valley mine, Mayacmas district, Napa Co., CA	-----	ppm	16	<1	67	95	0.00	-----	-----	White and others, 1963
Big Injun mine, Mayacmas district, Lake Co., CA	-----	ppm	154	-----	0.7	74	-----	-----	-----	C.E. Robertson, USGS
The Geysers, Mayacmas district, Sonoma Co., CA	-----	ppm	5710	-----	3.1	225	-----	-----	0.07	White and others, 1963
Skaggs Springs, Sonoma Co., CA	-----	ppm	6.5	<1	92	74	<0.02	0.01	<0.02, 0.06	White, 1957b
Altoona mine, Trinity Co., CA	-----	ppm	352	18	121	60	0.05	-----	-----	H.C. Whitehead, USGS
Mt. Diablo mine, Contra Costa Co., CA	-----	ppm	1.6	0.4	191	16	0.00	-----	-----	Pampeyan, 1963
Steamboat Springs, Washoe Co., NV	-----	ppm	107	8	48	220	1.7	0.3	0.00, 0.10	W.W. Brannock, USGS
Cordero mine, Humboldt Co., NV	-----	ppm	59	0.2	0.7	60	0.07	-----	-----	H.C. Whitehead, USGS
Amedee Springs, Lassen Co., CA	-----	ppm	288	<1	4.1	96	0.15	0.01	-----	White and others, 1963
Boiling Springs, Valley Co., ID	-----	ppm	12	<1	0.1	81	<0.1	<0.1	-----	White and others, 1963
Apapel'sk Springs, Kamchatka, Russia	-----	ppm	499	-----	16	182	1.6	-----	-----	Ivanov, 1958
Ngawha Springs, New Zealand	-----	ppm	347	6	912	178	0.2	-----	0.1	A.J. Ellis (written comm., 1964)
Cymric Oilfield, Kern Co., CA	-----	ppm	1.6	0	140	47	0.0	-----	0.1, 0.4	Bailey and others, 1961
Ourray Springs, San Juan Mountains., Ouray Co., CO	-----	ppm	1030	0.0	0.2	49	0.00	-----	-----	Burbank and Luedke, 1961
Growler Hot Spring, Lassen Volcanic National Park	LJ-82-01	ppm	90	0.36	71	274	12.7	-----	-----	Thompson, 1985
Little Growler, Lassen Volcanic National Park	LJ-82-04	ppm	102	0.22	67	199	10.4	-----	-----	Thompson, 1985
Inkpot Spring, Yellowstone National Park	IKP01	ppm	1300	-----	15.71	148.00	0.003	0.0001	0.00084, 0.033	this study
Inkpot Spring, Yellowstone National Park	IKP02	ppm	2100	-----	0.7741	123.83	0.007	0.0003	0.00022, 8.691	this study
Inkpot Spring, Yellowstone National Park	IKP03	ppm	1200	-----	4.482	275.72	0.002	<0.00005	0.00029, 0.009	this study
Inkpot Spring, Yellowstone National Park	IKP04	ppm	2600	-----	14.66	236.36	0.005	<0.00005	0.00021, 0.126	this study
Inkpot Spring, Yellowstone National Park	IKP06	ppm	1300	-----	8.087	148.81	0.002	<0.00005	0.00024, 0.041	this study
Inkpot Spring, Yellowstone National Park	IKP07	ppm	1200	-----	12.76	124.30	0.004	0.0001	0.00020, 0.002	this study
Inkpot Spring, Yellowstone National Park	IKP09	ppm	900	-----	59.71	151.83	0.002	<0.00005	0.00019, 0.001	this study
Inkpot Spring, Yellowstone National Park	IKP10	ppm	2500	-----	3.138	272.08	0.005	<0.00005	0.00019, 0.010	this study
Inkpot Spring, Yellowstone National Park	2IKP01	ppm	1300	-----	17.22	152.38	0.002	<0.00005	0.00025, 0.033	this study
Inkpot Spring, Yellowstone National Park	2IKP02	ppm	2100	-----	0.8052	117.07	0.003	0.0001	0.00021, 8.691	this study
Inkpot Spring, Yellowstone National Park	2IKP03	ppm	1100	-----	4.706	281.71	0.002	<0.00005	0.00028, 0.009	this study
Inkpot Spring, Yellowstone National Park	2IKP04	ppm	2600	-----	15.1	210.78	0.007	<0.00005	0.00023, 0.126	this study
Inkpot Spring, Yellowstone National Park	2IKP06	ppm	1300	-----	7.954	150.52	0.002	<0.00005	0.00022, 0.041	this study
Inkpot Spring, Yellowstone National Park	2IKP07	ppm	1900	-----	11.69	87.21	0.005	0.0001	0.00023, 0.002	this study
Inkpot Spring, Yellowstone National Park	2IKP09	ppm	1300	-----	60.7	148.75	0.003	0.0001	0.00018, 0.001	this study
Inkpot Spring, Yellowstone National Park	2IKP10	ppm	3300	-----	3.645	279.57	0.004	<0.00005	0.00019, 0.010	this study

Table 6 continued. Geochemical analyses of waters associated with mercury deposits compared with Inkpot spring fluids. Mercury data for both filtered and unfiltered Inkpot Spring water samples are included in Table 6. Mercury concentrations of filtered Inkpot samples are several orders of magnitude lower than unfiltered samples, suggesting Hg particles are greater than the 0.45 μm pore-size of the filters used during collection.

B, various hydrocarbon gases, oils, and bitumen, and sometimes Mg (Barnes and Seward, 1997). NH₃, B, Hg, and hydrocarbons are found at high concentrations in shales (Table 7). Significant levels of these elements and compounds are found in Inkpot Spring fluids, and support the conclusion that distillation of petroleum-water mixtures flushed from sediments (shales) at high temperatures is the source of organic components (NH₃ and hydrocarbon gases) at Inkpot Spring, made by A.H. Truesdell and R.O. Fournier in Fournier (1989).

Table 7. Mercury and boron abundances in different geologic environments.		
ROCK TYPE	AVERAGE CONCENTRATION	
	Hg (ppb)	B (ppm) ^b
<u>Igneous</u>		
Granites	77, ^a 80 ^b	9
Basalts	70, ^a 90 ^b	5
Ultramafics	4 ^a	-----
<u>Sedimentary</u>		
Shales	400 ^{a,b}	100
Graywackes	280 ^a	-----
Sandstones	30 ^b	35
Limestones/Carbonates	40 ^{a,b}	20
Deep sea clays	-----	230
Deep sea carbonates	-----	55

Table 7. Mercury and boron abundances in different geologic environments. Data compiled from Barnes and Seward (1997).
a Marowsky and Wedepohl (1971)
b Turekian and Wedepohl (1961)

The chemistry of waters from The Geysers-Clear Lake area, CA, is most similar to that of fluids from Inkpot Spring. Both contain significant concentrations of NH₄ and SO₄, SiO₂, and Hg, while maintaining low to moderate concentrations of Na, K, Ca, and Cl. The Geysers-Clear Lake area is a vapor dominated geothermal system, thought to be underlain by a large, partially

molten, silicic magma chamber similar to Yellowstone (White, 1981). Mercury deposits at The Geysers are thought to be unrelated to the active hydrothermal system, but were probably deposited during a hypothesized earlier hot water period. Hydrothermal systems such as The Geysers and Yellowstone are initially hot water systems that evolve into vapor-dominated systems as a result of increasing heat supply and permeability lowered by precipitation of hydrothermal minerals in channels of meteoric inflow (White et al., 1971; White, 1981).

The Sulphur Bank system is located approximately 15 km northwest of the vapor-dominated system of The Geysers, and both are associated with the Clear Lake volcanic field which includes rhyolitic flows and tuffs of Pliocene and Pleistocene age (White, 1967; White, 1981). Mercury deposits at Sulphur Bank are mainly hosted by an augite andesite flow (White, 1981). Both Sulphur Bank and The Geysers geothermal areas are underlain by serpentine and Mesozoic graywacke and shale of the Franciscan Formation, which is the likely source of the Hg (White, 1967; White, 1981). Similar rock types including rhyolitic flows and tuffs, andesite flows, and shales are found at both the Inkpot/Washburn Springs area in YNP and the Sulphur Bank and The Geysers areas in California. Elemental sulfur with minimal cinnabar was mined near the original surface at Sulphur Bank and native sulfur formed in condensing steam of a power plant in the Mayacmas district (The Geysers) contained 50 ppm Hg (H. McCarthy, U.S. Geological Survey, 1967; White, 1967; White, 1981). Similar vapor-dominated conditions have produced large mounds of native sulfur (Fig. 26) in fumarolic areas at Inkpot Spring. A native sulfur sample, similar to those in Figure 26, was analyzed for Hg using DMA. The concentration was above the limit of detection and the sulfur is assumed to contain at least 100 ppm mercury.

Ngawha, New Zealand, is another example of a fracture-controlled, vapor-dominated system similar to the Inkpot-Washburn Spring area of YNP. Drill data from Ngawha has shown



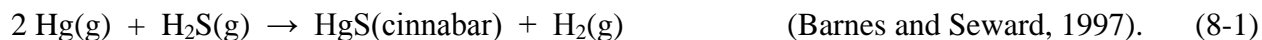
26

Figure 26. Sulfur crystals lining fumaroles and mounds of native sulfur produced from fumarolic activity around Inkpot Spring.

that the geothermal reservoir has a large depth range of hundreds of meters with temperatures near 230°C, not dissimilar from the hypothesized geothermal reservoir in parts of YNP (Barnes and Seward, 1997). In this part of the Ngawha system, there is a vapor that separated from a NH₃- and B-rich liquid, which leaves behind less volatile solutes like SiO₂, Mg, and B (Barnes and Seward, 1997). Describing the hydrothermal environment at Ngawha, Barnes and Seward (1997) state;

Near the surface, sometimes vigorous discharge of the vapor emerges into pools or ponds sitting in hydrothermal explosion craters and oxidation of the accompanying H₂S produces sulfuric acid and consequent advanced argillic alteration.

This description could be written nearly word-for-word for the conditions at Inkpot Spring. At Ngawha, mercury in the vapor, at concentrations up to 785 µg/L, rises to surface pools and condenses to native mercury (Hg⁰) or reacts to form cinnabar by the following process:



Perhaps the best locality to examine Hg occurrence with hydrocarbons is the Cymric oil field, CA. Petroleum, natural gas, and brine of the Cymric oil field contain Hg⁰ and possibly other forms of Hg (White, 1967; White, 1981). Petroleum occurs in interbedded sandstone and silty sandstone, shale, and sandstone and Hg concentrations in the petroleum range from 1.9 to 21 ppm (White, 1967). Dark-colored sediment recovered from water sample bottles ranges from 470 to 3600 ppm Hg, much higher than normal sedimentary rocks (White, 1967). The occurrence of Hg with hydrocarbon gases at Inkpot Spring suggests the presence of heated petroleum at depth.

The Wilber Springs district, CA, includes mercury deposits in which cinnabar is associated with thermal waters, petroleum, and hydrocarbon gases (White, 1981). At the Abbott mine in the Wilber Springs district, unusual frothy vein material is abundant in parts of the ore bodies. The vein material consists of small, tightly packed spherical shells of cristobalite filled with petroleum, usually containing a gas bubble (White, 1981). Baily (1959) concluded that the siliceous shells were deposited between a hydrous fluid and immiscible droplets of oil, and cinnabar within layers of the shells indicates contemporaneous transport of Hg (White, 1981). Siliceous sinter at Inkpot Spring is almost non-existent, however, the edge of pool IKP03 is lined with layered opaline silica and unusual silica spires (~2-4 mm). This layered silica deposit yielded one of the highest Hg concentrations (235 ppm) of all sediments and precipitates analyzed at Inkpot Spring. A second sample, of small, silver-colored flakes washing aside from vigorously bubbling IKP03, yielded a Hg concentration of 122.5 ppm.

Data from filtered and unfiltered water samples in Table 6 and Appendix F indicates that mercury probably occurs as or adheres to particles larger than 0.45 μ m because unfiltered samples have Hg concentrations several orders of magnitude greater than filtered samples. Energy dispersive X-ray spectrometric analysis of the layered silica from Inkpot Spring revealed microscopic grains (~0.5-1 μ m) of cinnabar. Backscattered electron images of these grains are included in Figure 27. Sampling methods, including filtration, may have varied between the analyses performed at the different localities included in Table 6 from White et al. (1967). These methods may also differ from this study; however, Hg concentrations in unfiltered Inkpot Spring samples compare well with Hg concentrations in waters from Hg-depositing geothermal systems of the Coast Ranges, CA included in Table 6.

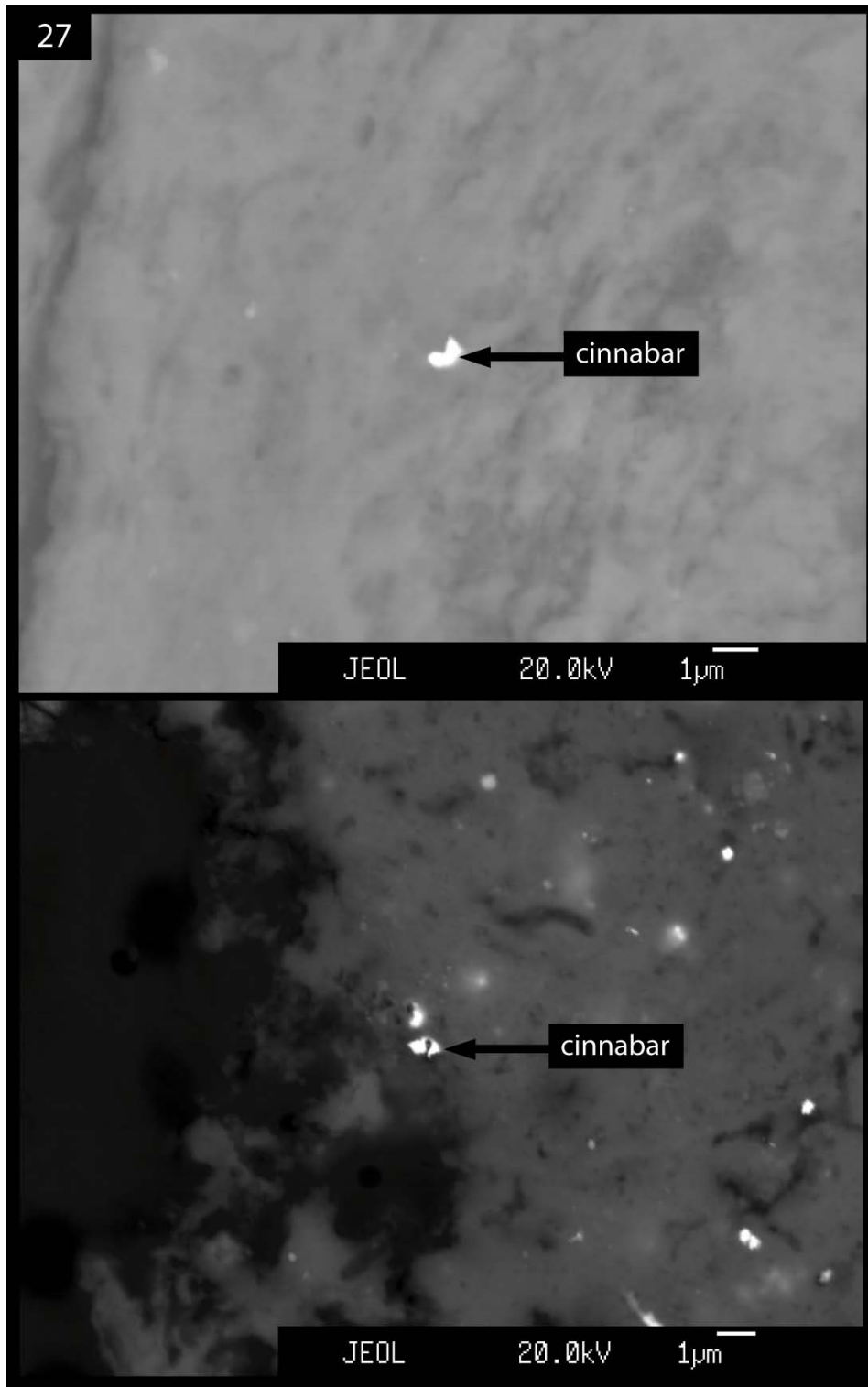


Figure 27. Backscattered electron images showing sub-micron-sized cinnabar grains in layered silica deposit surrounding pool IKP03. Sample also contains significant amounts of clay and similarly sub-micron-sized pyrite grains.

8.2 Mercury Transport Mechanisms

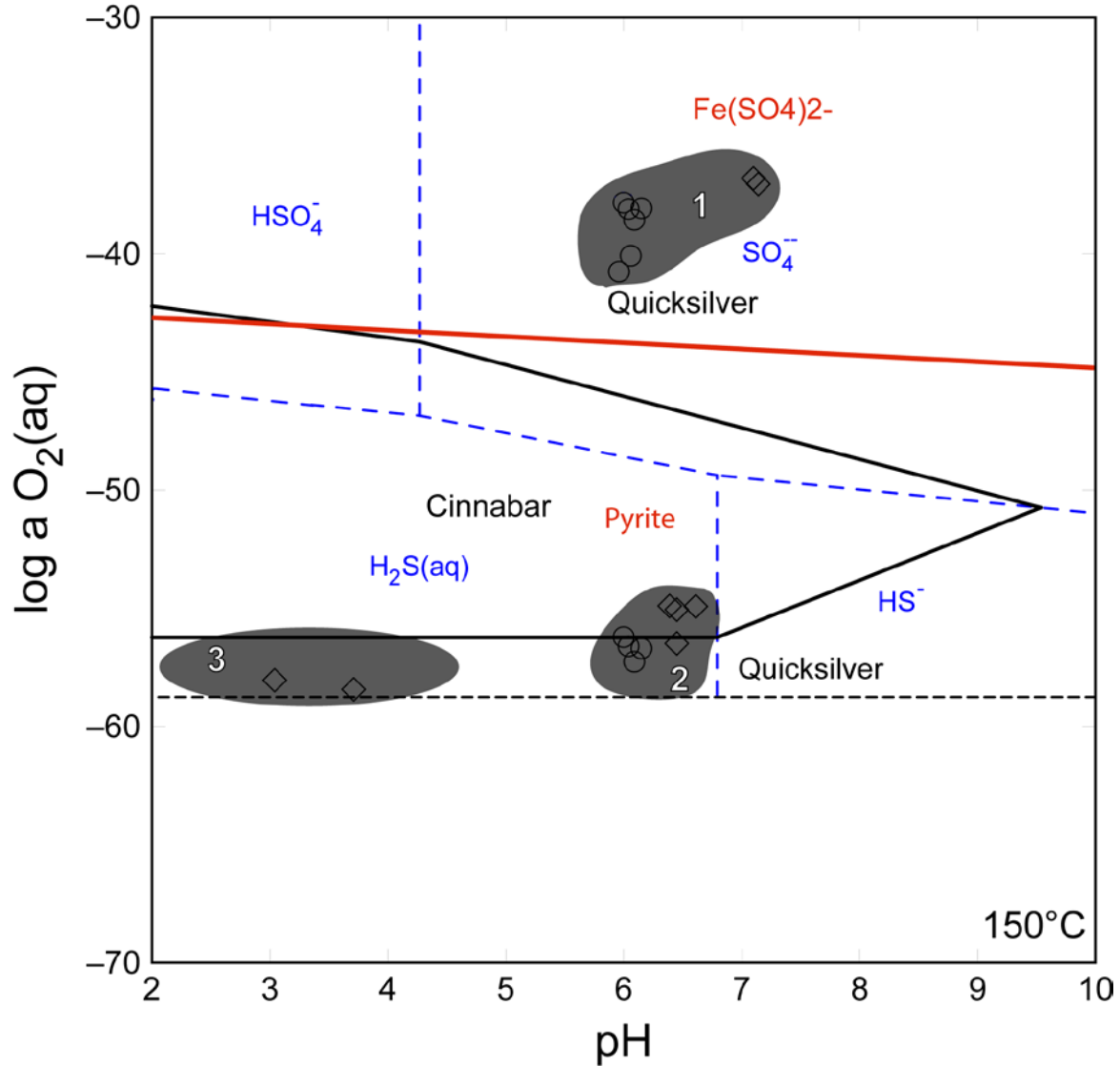
Partitioning of mercury among aqueous liquid, aqueous vapor, and an organic phase may have variable importance with respect to transport of mercury in hydrothermal environments. Transport of mercury as $\text{Hg}^0_{(\text{aq})}$ in aqueous liquid is only possible under oxidizing and alkaline conditions, but the presence of hydrocarbons in these systems implies reducing conditions, and suggests that liquid transport may be unimportant (Fein and Williams-Jones, 1997). Mercury can also partition into a vapor phase, however, boiling rarely occurs at greater depth, suggesting that a vapor phase may be of lesser importance to mercury transport (Fein and Williams-Jones, 1997). Fein and Williams-Jones (1997) conclude that extremely high concentrations of mercury may be dissolved into, and transported by, an organic phase based on extrapolation of low-temperature mercury solubility experiments.

In reviewing the literature of the solubility of liquid metallic mercury in organic phases, Clever and Iwamoto (1987) found that the solubility of mercury in C_5 to C_{10} normal alkanes increases greatly with increasing temperature (Fein and Williams-Jones, 1997). Burnett (2004) found anomalous concentrations of two C_5 to C_{10} normal alkanes in gases at Washburn-Inkpot Hot Springs. Washburn-Inkpot gases have reported pentane (C_5H_{12}) and hexane (C_6H_{14}) concentrations of 12.4 ppm and 4.13 ppm, respectively (Appendix G). Data in Appendix G shows other organic gases at high concentrations including ethane (521-1820 ppm), propane (175-365 ppm), n-butane (34.0-69.9 ppm), benzene (13.1-22.5 ppm), and toluene (0.121 ppm), and other previous gas data from Washburn-Inkpot Hot Springs. Fein and Williams-Jones (1997) present the overall equilibrium which quantifies the relative thermodynamic stabilities of cinnabar and mercury in an alkane organic phase:



Equation (8-2) shows that cinnabar in an alkane organic phase varies with pH and oxygen fugacity (Fein and Williams-Jones, 1997). The oxygen fugacity in this system is difficult to constrain, however, the coexistence of cinnabar and pyrite and high ammonia and ammonium concentrations may be used to place some limits on f_{O_2} . Figure 28 illustrates the iron sulfide, cinnabar, and native mercury (quicksilver) stability fields in terms of oxygen fugacity and pH at 150°C. Figure 28 shows Inkpot Spring fluids may be in equilibrium with native mercury or cinnabar and pyrite at 150°C and the relatively reducing conditions indicated by the presence of ammonia and ammonium. Previous data from McCleskey et al. (2005) and Ball et al. (2007) in addition to data from this study are included in Figure 28 and show that our estimates of redox state in Inkpot fluids are in good agreement with previous data.

Fein and Williams-Jones (1997) illustrate that the molality of mercury in normal alkanes is approximately two orders of magnitude greater than the corresponding molality in the aqueous phase. Extremely high concentrations of mercury can dissolve into an organic phase at high pH (6 to 7) and low oxygen fugacity. These conditions are observed at Inkpot Spring, and are likely due to a strong influence from ammonia and other organic gases. These observations, in conjunction with the widespread occurrence of hydrocarbons with mercury ore deposits and mercury-depositing waters, suggests that organic phase transport plays a significant role in mercury mobility in organic-bearing ore-forming environments and may play a significant role at Inkpot Spring.



—	Cinnabar and quicksilver stability boundaries	○	2008 Inkpot Spring samples. Data included in Appendix C.
—	Pyrite and Fe(SO ₄) ₂ - stability boundaries	◇	2003 & 2001 Washburn & Inkpot Spring water data from McCleskey et al. (2005) and Ball et al. (2007), included in Appendix B.
- - -	Aqueous sulfur speciation boundaries		
- - - - -	Lower water stability limit		

Figure 28. Log f_{O_2} vs pH stability diagram for the system Hg-Fe-S-H₂O-O at 150°C assuming Fe²⁺ is controlled by pyrite with a average log Fe²⁺ activity of -6.85, and an average log SO₄⁻ activity of -2.248. Aqueous sulfur speciation is shown for reference. Most Washburn-Inkpot Hot Spring fluid samples plot at reducing conditions near the lower limit of water stability (Groups 2 and 3). The presence of ammonia and ammonium in high concentrations agree with these fluids near the lower limit of water stability. These fluids also plot near the lower cinnabar-quicksilver boundary within pyrite stability. Washburn-Inkpot Hot Spring fluids in Group 1 fluids have higher f_{O_2} values due to speciation using higher Eh values and/or low ammonia concentrations. Fluids at the surface are experiencing oxidizing conditions, confirmed by the high SO₄ and very low H₂S concentrations. Washburn-Inkpot Hot Spring fluids may exist at any point between Group 1 and Groups 2 and 3 and may be in equilibrium with pyrite and cinnabar or native mercury at temperatures near 150°C.

9. ORGANIC AND INORGANIC GAS GEOCHEMISTRY

Organic and inorganic gases emanating from Inkpot Spring have been observed since Allen and Day's 1935 study. However, few Yellowstone studies have included an analysis of these gases at Inkpot Spring. Previous organic and inorganic gas geochemistry data compiled from three studies are included in Appendix G. Because Inkpot has a significant vapor component, gas geochemistry is useful in determining the source and pathway of inorganic compounds and volatiles. Nitrogen and carbon isotopes of gas compounds are useful in determining the origin of hydrocarbon components at Inkpot Spring.

Gas collection from hot springs by previous workers in YNP has typically involved a partially-submerged funnel that allows for the transmission of gas and steam without mixing with air (Werner et al., 2008). Tubing is attached to the funnel and connected to an evacuated sampling bottle filled with NaOH solution. Steam and major inorganic species in the gas (CO_2 , SO_2 , H_2S , and HCl) are collected in the NaOH solution, and the more inert gases (H_2 , He , N_2 , Ar , O_2 , and CH_4) and hydrocarbons (C2-C9 normal and iso alkanes, benzene, and toluene) are collected in the head space (Burnett, 2004; Werner et al., 2008). Gases trapped in the headspace, including hydrocarbons, are generally analyzed using a gas chromatograph and/or a flame ionization detector (Burnett, 2004; Werner et al., 2008). After removal of the NaOH solution under vacuum, wet chemical analysis is commonly used for determination CO_2 , H_2S , SO_2 , and HCl , and a gas sensing electrode is used for measuring NH_3 concentrations. Much of the previous Washburn-Inkpot Hot Springs gas data presented in Appendix G was obtained using these methods.

Our 2008 study tested a new method of gas analysis. Following the techniques outlined in Chapter 3 (Methods), gases including CO_2 , CH_4 , NH_3 , C_2H_6 , and SO_2 were measured by infrared

(IR) spectroscopy using a MIRAN 205B Series SapphIRe Portable Ambient Air Analyzer provided by the Oak Ridge National Laboratory. This instrument is commonly used for real-time detection of vapors in the work environment, emergency response analysis, detection of waste anesthetic gases, fume hood/tracer gas analysis, and detection of decaying organic compounds. Its application to the detection of decaying, buried organic compounds prompted interest in its application to detection of organic and inorganic compounds in the Inkpot Spring vapor-dominated hydrothermal system. The IR analyzer's filter was attached to a 2m pole and extended out over Inkpot Spring pools. Measurements were recorded at different heights (0.5, 1.0, and 1.5 meters) above the pools. Gas geochemistry data (Appendix H) collected by this method is qualitative due to the effect wind conditions and height above the pools had on instrument readings. These effects are eliminated by the submerged-funnel apparatus used by previous workers. This apparatus has not been tested in conjunction with the MIRAN air analyzer. Previous data presented in Appendix G is probably more accurate than the data in Appendix H because of these effects.

One trend between ammonia and pH can be observed in 2008 gas chemistry data. Our gas data shows that the two pools with the lowest pH have the highest ammonia emanations. It is possible that more ammonia is escaping as gas and less is retained in the fluid to combine with and neutralize H_2SO_4 in the pools. However, oxidation of pyrite and other factors may also be contributing to the low pH of these pools.

With the exception of a positive relationship between ammonia and methane, no other direct relationship is observed between any organic and inorganic compounds at Inkpot Spring, suggesting different sources for organic and inorganic compounds or that these compounds are influenced by different factors. High concentrations of CO_2 , CH_4 , HCl , H_2S , and N_2 and low

concentrations of He are found at Inkpot and Washburn Hot Springs. Hydrocarbons present in high concentrations at Inkpot and Washburn Hot Springs include ethane, propane, butane, pentane, and benzene (Appendix G). Other hydrocarbons present at Inkpot and Washburn Hot Springs are hexane, toluene, and dimethylbutane. Some of the most positive $\delta^{15}\text{N-N}_2$ values in YNP are found at Washburn-Inkpot Hot Springs. Burnett (2004) found low $\delta^{13}\text{C-CO}_2$ values (-4.0‰) and high $\delta^{13}\text{C-CH}_4$ values (-24.2‰) at Washburn Hot Springs, which suggest a thermogenic origin for the hydrocarbons. These values combined with the ^{15}N enriched nitrogen indicate that the hydrocarbons are likely derived from a relatively deep, mature source, which is not consistent with the low He concentrations (Burnett, 2004). These data suggest that the hydrocarbons detected at Inkpot and Washburn Hot Springs could have multiple sources, with thermogenic degradation of buried organic material serving as the primary source of hydrocarbons (Burnett, 2004). This is consistent with the conclusion by Fournier (1989) that distillation of buried, petroleum-bearing sediments is the source of organic gases at Inkpot and Washburn Hot Springs.

The closest sedimentary outcrop to Inkpot Spring is approximately 26 km north and northwest. In northern YNP there are approximately 1000m of Paleozoic limestones and dolostones overlain by 1600m of Mesozoic shale, sandstone, mudstone, conglomerate, and limestone. Several units within these sections including shale above the late Devonian Sappington Member of the Three Forks Formation, shales of the late Mississippian Big Snowy Formation, oil-bearing marine shales of the Permian Phosphoria Formation, dolomites of the Upper Devonian Jefferson Formation and Mississippian Mission Canyon Formation, and shales of the Upper Cretaceous Thermopolis Formation, Mowry Shale Formation, and Lower and Upper Cody Shale Formation, have been suggested as possible sources of oil seeps and

hydrocarbons at hot springs in northeastern YNP (Tonnsen, 1982). Some of these units may underlie the Eocene Absaroka volcanics and may exist much closer to Inkpot Spring. Further research is needed to distinguish between possible sedimentary sources of hydrocarbons in this area.

10. DISCUSSION

10.1 Overview

The acid-sulfate pools at Inkpot Spring are part of a vapor-dominated hydrothermal system influenced by multiple processes including mixing, boiling, and water/rock interaction. Inkpot Spring is located in close proximity to the Yellowstone caldera, which provides a path for upflow of fluids and gases. Multiple fluid types may influence the water chemistry at the surface including meteoric water containing minor solutes from weathering processes at low temperature, meteoric waters heated only by high-temperature gases, commonly containing high concentrations of SO_4 and high $\delta^{18}\text{O}$ values, and hydrothermal waters that have boiled at depth and have been heated further with H_2S -enriched gases achieving higher SO_4 concentrations.

Major and trace element concentrations suggest Inkpot fluids may react with a variety of rock types including oil-bearing marine shales and other Paleozoic and Mesozoic sediments, basaltic-andesite of the Absaroka volcanics, and rhyolitic lava flows and tuffs of the Plateau Rhyolites, on their way to the surface. Significant levels of mercury, boron, ammonia, ethane, propane, hexane, and other hydrocarbons are probably derived from the distillation of petroleum-bearing sediments at depth. A group of small pools at Inkpot Spring is currently precipitating pyrite. To our knowledge, this is the first record of active precipitation of pyrite at Inkpot Spring, although the “ink” color of the pools has been attributed to iron sulfide since the study of

Allen and Day (1935). Higher concentrations of iron, which combine with sulfur to form pyrite, are derived from hydrothermal alteration of basaltic-andesite or tonalite of the Absaroka volcanics.

10.2 Stable Isotope Ratios, Boiling, and Mixing

Stable oxygen and hydrogen isotope values of Inkpot Spring fluids are some of the highest of all Yellowstone thermal fluids and a significant $\delta^{18}\text{O}$ shift suggests boiling is an important process controlling stable isotope distribution. Evidence of mixing at Inkpot Spring is more ambiguous. Inkpot Spring pools are essentially flooded fumaroles with significant amounts of steam and hot water with a contribution from local meteoric water. Perched Na-Ca- HCO_3 groundwaters are known to exist in this area. Mixing of meteoric water with the steam condensate component at Inkpot Spring may be expected to lower $\delta^{18}\text{O}$ and δD values, however, as stated above, stable isotope values are much higher than those of local meteoric water. If Na-Ca- HCO_3 groundwaters are mixing with stream condensate, then boiling most likely occurs post mixing because of the high $\delta^{18}\text{O}$ values. Mixing relationships are commonly resolved using enthalpy versus chloride diagrams, however, chloride concentrations in Inkpot Spring fluids are so low that this technique is not practical. Assuming an equilibrium relationship between silica and total carbonate based on temperature and quartz solubility, Arnórsson (1985) shows that boiling will lead to reduction of carbonate when CO_2 is released as gas, but mixing without boiling will produce waters with high carbonate/silica ratios relative to equilibrated waters, due to the curvature of the silica/carbonate relationship. Boiled fluids with high silica and low carbonate concentrations and mixed fluids with higher carbonate are both present at Inkpot Spring (Fig. 13).

Surface temperatures at Inkpot Spring range from 70 to 90°C and the boiling temperature at these elevations is 92.4°C, which suggests these fluids may be boiling at shallow depths (they are vigorously bubbling at the surface). These conditions may allow for mixing of a steam condensate component and local meteoric groundwater at fairly shallow depths (tens of meters), followed by boiling at or near the surface. These conditions account for the observed trajectory of the $\delta^{18}\text{O}$ and δD values.

10.3 Variable pH Conditions

Inkpot Spring fluids are characterized by variable pH and redox conditions controlled by multiple factors. Fluids at Inkpot Spring have previously been characterized as acid-sulfate waters, but our data show most pools have a pH near 6, and two others have a pH of 2.94 and 4.24. Fournier (1989) concluded that H_2S is oxidized to H_2SO_4 near the surface, which combines with excess ammonia in rising vapor to form ammonium sulfate, effectively neutralizing the H_2SO_4 and resulting in a water that may be slightly alkaline. Water chemistry data show that nearly all of the H_2S has been converted to H_2SO_4 at the surface and that these waters contain high concentrations of ammonia (240-680 mg/L). Gas geochemistry data also confirm high concentrations of ammonia. Pool IKP10, the darkest “ink” colored pool, has a pH of 2.94 and contains pyrite coated pebbles. Oxidation of pyrite following reactions (5-7), (5-8), and (5-9) may contribute to the low pH in this pool as well pool IKP04 which has a pH of 4.24. These two pools with $\text{pH} < 6$ also have some of the highest measured ammonia and sulfate values, which suggests excess H_2SO_4 is producing the acidic conditions or perhaps less ammonia is combining with H_2SO_4 to form ammonium sulfate, leaving the fluids more acidic.

10.4 Redox Conditions

Redox conditions at Inkpot Spring are difficult to constrain. Previous Eh measurements (-0.165 to 0.165 V) coupled with the presence of ammonia and hydrocarbon compounds suggest that reducing conditions are present at Inkpot Spring. However, as previously mentioned, nearly all H₂S is oxidized to H₂SO₄ at the surface, suggesting oxidizing conditions. Ammonia and various hydrocarbons are mainly transported in vapor at Inkpot Spring and may have separated from a reduced fluid at depth, while oxidation of H₂S is occurring only at the surface. Calculated mineral saturation indices show that pyrite is supersaturated in fluids assuming an Eh of -0.165 V, but undersaturated when assuming an Eh of 0.165 V. The observation of precipitated pyrite at Inkpot suggests reducing conditions are present in at least some of the pools.

10.5 Subsurface Temperatures and Silica Concentrations

Various geothermometers can be applied to Inkpot Spring fluids, however, cation geothermometers give unreasonably high values. The silica geothermometer gives a reasonable subsurface temperature estimate (195°C) for the Inkpot system. This temperature has been calculated for other hot spring basins within the Yellowstone caldera using the silica geothermometer. Following the techniques of Truesdell and Fournier (1977), the silica-enthalpy diagram is used to determine the fraction of hot and cold water components in addition to subsurface temperature and silica concentration at depth. Assuming meteoric groundwater has an initial enthalpy of ~100 J/g and silica concentration of 20 ppm, Inkpot Spring fluids are calculated to have an ~88% hot water component and ~12% cooler meteoric water component. The temperature of the original hot water component was calculated to 195°C with a silica concentration of 248.7 ppm (Fig. 12). This temperature probably represents the last equilibrium

with quartz, and may not reflect the deepest, hottest parts of the system.

Inkpot Spring pools with silica concentrations ranging from ~200 to 300 ppm seemed to be controlled by amorphous silica saturation (Fig. 12). Pools with silica concentrations between ~75 and ~160 ppm may be controlled by α - and β - cristobalite phases or may simply be experiencing greater dilution effects.

A temperature of ~250°C is calculated for deep fluids feeding Inkpot Spring, using the CO₂-H₂S-H₂-CH₄ gas geothermometer of D'Amore and Panichi (1980), which has been found to compare well with drill hole data in other geothermal systems. This temperature compares with temperatures that would be close to equilibrium with the quartz + illite ± adularia alteration mineral assemblage observed in the Grand Canyon of the Yellowstone River.

10.6 Fluid-Mineral Equilibria

Mineral stability relationships at Inkpot Spring are investigated using activity diagrams. When comparing the activity of Na⁺ and Ca⁺⁺ with the activity of K⁺, Inkpot Spring fluids have a bimodal distribution along a linear trend (Fig. 14 and Fig. 16). These bimodal and linear trends can be explained by the variable pH conditions. For example, fluids appear to be in equilibrium with muscovite (illite) on Figure 14 because of higher H⁺ activities, however, pH is controlled by other factors at Inkpot Spring (formation of ammonium sulfate). If the neutralization of H₂SO₄ by NH₃ is ignored, most Inkpot fluids would have lower pH, and therefore would plot in the kaolinite field instead of the muscovite (illite) field. The control of pH is also exhibited in Figure 17, where fluids appear to be in equilibrium with barite and alunite, but are probably only in equilibrium with alunite. High Ca⁺⁺ activity can be explained by equilibrium with calcite or gypsum, but may be derived from Na-Ca-HCO₃ groundwater.

Assuming redox conditions can reasonably be estimated using previous Eh measurements, Inkpot Spring fluids are in equilibrium with pyrite. This agrees with the fact that pyrite has precipitated in the bottom of some pools and that the “ink” color of the pools is attributed to very fine pyrite. Mercury occurs at anomalously high concentrations in Inkpot Spring fluids and sediments. The presence of ammonia and hydrocarbon compounds in fluids and gases suggest reducing conditions at Inkpot Spring. Assuming low oxygen fugacity and accounting for acidic to near-neutral conditions, Inkpot Spring fluids may be in equilibrium with cinnabar or native mercury at depth, where temperatures are near 150°C. Significant mercury is probably transported to the surface in vapor or dissolved in hydrocarbons and transported in vapor.

10.7 Sediments

Sediments surrounding Inkpot Spring pools are weathering and alteration products of the basaltic-andesites of the Absaroka volcanics and Quaternary gravels containing fragments of rhyolitic tuffs and lava flows and basaltic-andesites of the Absaroka volcanics. In addition to the weathered material, Inkpot Spring fluids have contributed several alteration minerals to the surrounding sediment including kaolinite, dickite, alunite, walthierite, huangite, pyrite, and opal. Many of these minerals were also identified in suspensions from the pools using XRD and EDS.

10.8 Gas Geochemistry

High concentrations of CO₂, CH₄, HCl, H₂S, and N₂ and low concentrations of He are found at Inkpot and Washburn Hot Springs. Hydrocarbons present in high concentrations at Inkpot and Washburn Hot Springs include ethane, propane, butane, pentane, and benzene. The

presence of these compounds has been attributed to the distillation of petroleum-water mixtures flushed from buried sediments at depth. Paleozoic and Mesozoic sedimentary rock is present 26 km to the north of Inkpot Spring and may underlie the Eocene Absaroka volcanics closer to the spring. High concentrations of mercury also suggest fluids may be reacting with petroleum-bearing sediments. Shales are known to have some of the highest concentrations of mercury (up to 400 ppb).

11. CONCLUSIONS

The main conclusions of this study are:

1. Inkpot Spring fluids are produced from multiple water types. Our research suggests surface fluids are probably a combination of the following waters classified by White et al. (1988) and Nordstrom et al. (2009).
 - I. Dilute, recharging meteoric groundwater containing minor solutes from weathering processes at lower temperatures (perched Na-Ca-HCO₃ aquifers)
 - II. Meteoric waters heated only by high-temperature gases, commonly containing high concentrations of SO₄ and high $\delta^{18}\text{O}$ values
 - III. Hydrothermal waters that have boiled at depth and have been heated further with H₂S-enriched gases achieving higher SO₄ concentrations
 - IV. H₂SO₄ formed by oxidation of elemental sulfur or sulfide in hydrothermally altered areas

Silica-enthalpy relationships indicate surface fluids contain an ~88% deeply-circulated heated meteoric water component and an ~12% cooler, low-silica groundwater component.

2. A subsurface temperature of 195°C was calculated using the silica geothermometer and silica-enthalpy diagram and compares well with subsurface temperatures of other major geyser and hot spring basins in YNP. A subsurface temperature of ~250°C was calculated using the CO₂-H₂S-H₂-CH₄ gas geothermometer and may represent deeper conditions beneath Inkpot Spring.

3. Water-rock interaction has a significant effect on fluid chemistry. There is evidence that Inkpot Spring fluids are reacting with the following rock types.

I. Basaltic-andesite of the Lamar River Formation and biotite tonalite of the Sulphur Creek Stock, both of which are constituents of the Eocene Absaroka volcanics exposed in the Washburn Range, contribute Fe, Mg, Ca, and Ti to fluids.

II. Oil-bearing marine shales or other sedimentary rocks of Paleozoic or Mesozoic age contribute Hg, B, NH₃, CH₄, and hydrocarbon compounds to vapor and fluids.

Other rocks that may provide a lesser contribution to Inkpot Spring fluids include:

III. Quaternary gravels present in drainages containing fragments of the Absaroka volcanics and tuffs and lava flows of the Plateau Rhyolites.

IV. Tuffs and lava flows of the Plateau Rhyolites (The Tuff of Sulphur Creek)

4. At least one of the observed alteration mineral assemblages observed in the Grand Canyon of the Yellowstone River could have been produced by fluids similar to those at Inkpot Spring. Advanced argillic alteration consisting of an association with quartz (opal) + kaolinite ± alunite ± dickite (Larson et al., 2009) can be produced by these fluids. Activity relationships show Inkpot fluids are at or near equilibrium with kaolinite, alunite, pyrophyllite, opal, and montmorillonite (beidellite).

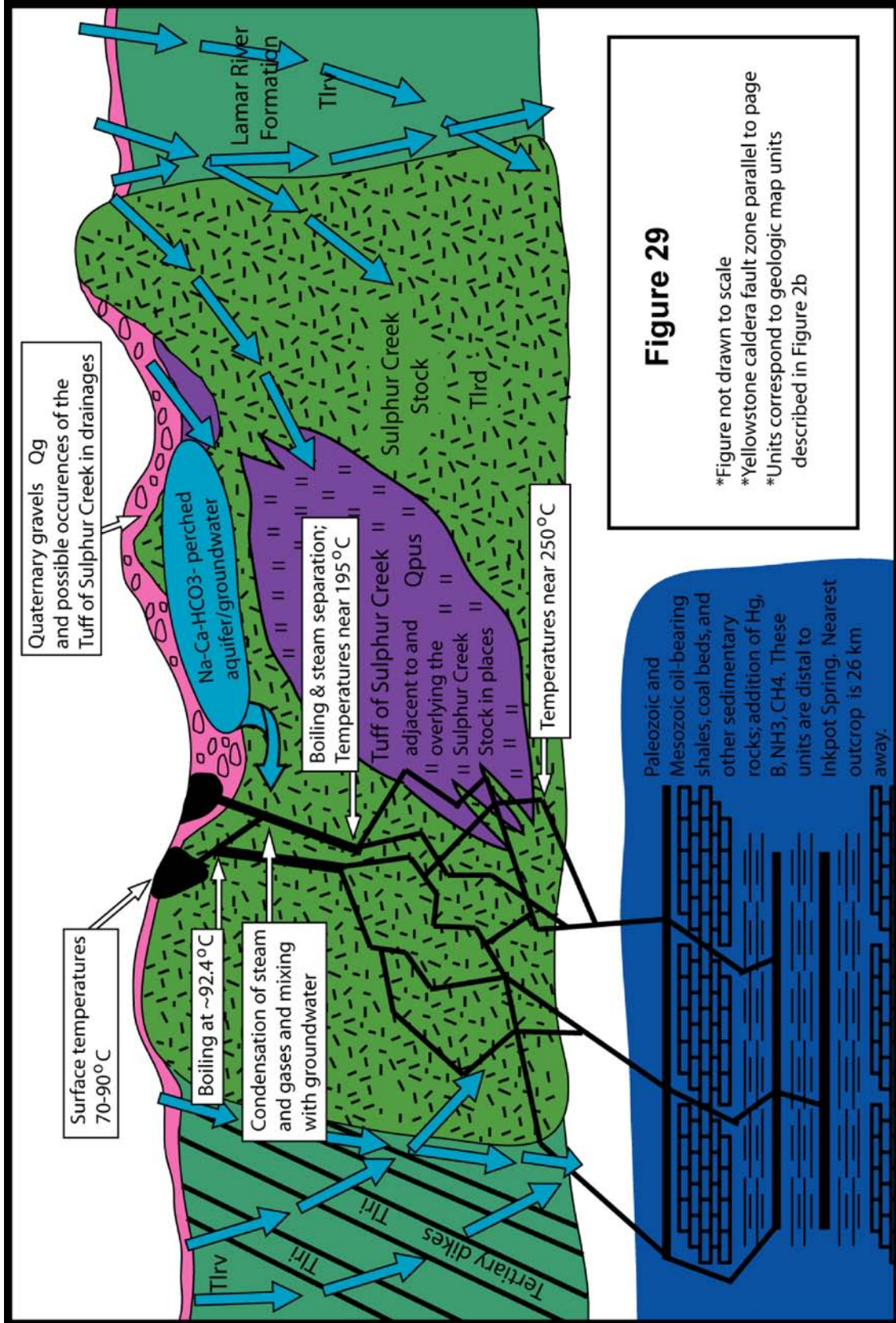
5. Many factors may control the variable pH conditions observed at Inkpot Spring. The dominant factors include the oxidation of H_2S to H_2SO_4 near the surface, which is immediately converted to ammonium sulfate by excess NH_3 , producing a near neutral fluid. The more acidic pools are found to have higher sulfate/ammonia ratios. This suggests that excess H_2SO_4 is producing the acidic conditions or perhaps less ammonia is combining with H_2SO_4 to form ammonium sulfate, leaving the fluids more acidic.

6. Sulfate occurs in concentrations from 900 to 3300 ppm in Inkpot Springs fluids. Multiple sources may contribute to the high levels of sulfate including H_2S from deep hydrothermal fluids oxidized to sulfuric acid by atmospheric oxygen, disproportionation of SO_2 in magmatic vapor, oxidation of pyrite, and buried native sulfur deposits from which sulfur-consuming bacteria can generate H_2SO_4 . Atmospheric oxidation of H_2S is probably the largest contributor to sulfate, but oxidation of pyrite appears to be a factor in at least some pools. Other sources of sulfate cannot be ruled out.

7. It has long been hypothesized that the “ink” color of the pools is produced by iron sulfide. XRD and EDS analysis of suspended sediment confirms the presence of pyrite in the pools. Pyrite coated material is also observed in pools which are thought to be the remnants of Gooch and Whitfield’s “Devil’s Ink Pot.” Coatings of layered pyrite bands indicate multiple episodes of pyrite precipitation from the fluids.

8. Mercury is the only trace element of economic importance that occurs in significant concentrations at Inkpot Spring. Inkpot Spring fluids are similar in many respects to Hg-depositing hydrothermal systems worldwide, particularly those in the Coast Ranges of California. Mercury is most likely derived from oil-bearing marine shales, which also contribute to elevated concentrations of hydrocarbon compounds and ammonia in vapors at Inkpot Spring. Various mercury transport mechanisms have been suggested, and Inkpot Spring may provide an ideal field area to study organic and vapor phase transport of mercury.

A hypothesized cross section of the Yellowstone hydrothermal system at Inkpot Spring is shown in Figure 29. The caldera fault zone provides the network of fractures necessary for the local vapor-dominated hydrothermal system. The fine-grained biotite tonalite of the Sulphur Creek Stock is less permeable than the Yellowstone tuffs and rhyolite flows and contributes to the vapor-dominated conditions as greater amounts of vapor and fluid ascend through a network of fractures rather than pore space. Inkpot Spring fluids are probably not limited to contact with the Sulphur Creek Stock during ascension and may be in contact with significant intervals of Yellowstone rhyolitic tuffs and lava flows, adjacent to the page in Figure 29. Deeply circulating meteoric water with heat supplied by magma at 5-6 km is the main source of fluids at Inkpot Spring. Paleozoic and Mesozoic sediments contributing Hg, B, NH₃, CH₄, and volatile light hydrocarbons to Inkpot Spring fluids underlie the Eocene Absaroka volcanics in northeast YNP. The closest outcrop of these units is ~26 km north and northwest of Inkpot Spring.



REFERENCES

- Arnórsson, S., 1985, The use of mixing models and chemical geothermometers for estimating underground temperatures in geothermal systems: *Journal of Volcanology and Geothermal Research*, v. 23, p. 299-335.
- Arnórsson, S., Gunnlaugsson, E., and Svavarsson, H., 1983, The chemistry of geothermal waters in Iceland. II. Mineral equilibria and independent variables controlling water compositions: *Geochimica et Cosmochimica Acta*, v. 47, p. 547-566.
- Allen, E.T., and Day, A.L., 1935, Hot springs of the Yellowstone National Park: Carnegie Institute of Washington Publication 466, 525 p.
- Baily, E.H., 1959, Froth veins, formed by immiscible hydrothermal fluids, in mercury deposits, California: *Geological Society of America Bulletin*, v. 70, p. 661-663.
- Ball, J.W., McCleskey, R.B., Nordstrom, D.K., and Holloway, J.M., 2007, Water-chemistry data for selected springs, geysers, and streams in Yellowstone National Park, Wyoming, 2003-2005: U.S. Geological Survey Open-File Report 2006-1339, 183 p.
- Ball, J.W., Nordstrom, D.K., Cunningham, K.M., Schoonen, M.A.A., Xu, Y., and DeMonge, J.M., 1998, Water-chemistry and on-site sulfur-speciation data for selected springs in Yellowstone National Park, Wyoming, 1994-1995: U.S. Geological Survey Open-File Report 98-574, 35 p.
- Bargar, K.E., and Beeson, M.H., 1985, Hydrothermal alteration in research drill hole Y-3, Lower Geyser Basin, Yellowstone National Park, Wyoming: U.S. Geological Survey Professional Paper 1054-C, 23 p.
- Barnes, H.L., and Seward, T.M., 1997, Geothermal systems and mercury deposits, in Barnes, H.L., ed, *Geochemistry of Hydrothermal Ore Deposits*, 3rd Edition: Wiley and Sons, New York, 972 p.
- Bethke, C.M., 2007, The Geochemist's Workbench, Release 7.0.2, University of Illinois at Urbana-Champaign.
- Bethke, C.M., 2008, *Geochemical and Biogeochemical Reaction Modeling*, Second Edition: Cambridge University Press, Cambridge, UK, 543 p.
- Bergfield, D., Goff, F., and Janik, C.J., 2001, Carbon isotope systematic and CO₂ sources in The Geysers-Clear Lake region, northern California, USA: *Geothermics*, v. 13, p. 303-331.
- Bindeman, I.N., and Valley, J.W., 2000, Formation of low-d¹⁸O rhyolites after caldera collapse at Yellowstone, Wyoming, USA: *Geology*, v. 28, p. 719-722.

- Bindeman, I.N., and Valley, J.W., 2001, Low-¹⁸O rhyolites from Yellowstone: Magmatic evolution based on analyses of zircons and individual phenocrysts: *Journal of Petrology*, v. 42, p. 1491-1517.
- Bindeman, I.N., Valley, J.W., Wooden, J.L., and Persing, H.M., 2001, Post-caldera volcanism: in situ measurement of U-Pb age and oxygen isotope ratio in Pleistocene zircons from Yellowstone caldera: *Earth and Planetary Science Letters*, v. 189, p. 197-206.
- Brock, T.D., 1978, *Thermophilic micro-organisms and life at high temperatures*, Springer-Verlag New York, 465 p.
- Burnett, B.J., 2004, Volatile light hydrocarbons in geothermal gas emissions from Yellowstone National Park, USA, and Comparisons to El Salvador and Honduras, M.S. Thesis, University of New Mexico, 95 p.
- Cady, S.L., Wenk, H.-R., and Downing, K.H., 1996, HRTEM of microcrystalline opal in chert and porcelanite from the Monterey Formation, California: *American Mineralogist*, v. 81, p. 1380-1395.
- Chang, W.L., Smith, R.B., Wicks, C., Farrell, J.M., Puskas, C.M., 2007, Accelerated uplift and magmatic intrusion of the Yellowstone caldera, 2004 to 2006: *Science*, v. 318, p. 952- 956.
- Christiansen, R.L., 1975, Geologic map of the Norris Junction Quadrangle, Yellowstone National Park, Wyoming: U.S. Geological Survey Map GQ-1193.
- Christiansen, R.L., 2001, The Quaternary and Pliocene Yellowstone plateau volcanic field of Wyoming, Idaho, and Montana: U.S. Geological Survey Professional Paper 729-G, 145 p.
- Christiansen, R.L., and Blank, H.R., Jr., 1975, Geologic map of the Canyon Village Quadrangle, Yellowstone National Park, Wyoming: U.S. Geological Survey Map GQ-1192.
- Clever, H.L., and Iwamoto, M., 1987, Solubility of mercury in normal alkanes: *Industrial Engineering Chemistry Research*, v. 26, p. 336-337.
- Clifton, C.G., Walters, C.C., Simoneit, B.R.T., 1990, Hydrothermal petroleum from Yellowstone National Park, Wyoming, U.S.A.: *Applied Geochemistry*, v. 5, p. 169-191.
- Criss, R.E., 1999, *Principles of Stable Isotope Distribution*: Oxford University Press, New York, 254 p.
- D'Amore, F., and Panichi, C., 1980, Evaluation of deep temperatures of hydrothermal systems by a new gas geothermometer: *Geochimica et Cosmochimica Acta*, v. 44, p. 549-556.
- Feeley, T.C., Cosca, M.A., and Lindsay, C.R., 2002, Petrogenesis and implications of cryptic hybrid magmas from Washburn volcano, Yellowstone National Park, USA. *Journal of Petrology*, v. 43, p. 663-703.

- Feeley, T.C., and Cosca, M.A., 2003, Time vs composition trends of magmatism at Sunlight volcano, Absaroka volcanic province, Wyoming: *Geological Society of America Bulletin*, v. 115, 714-728.
- Fein J.B., and Williams-Jones, A.E., 1997, The role of mercury-organic interactions in the hydrothermal transport of mercury: *Economic Geology*, v. 92, p. 20-28.
- Fournier, R.O., 1981, Application of water geochemistry to geothermal exploration and reservoir engineering, in Rybach, L., and Muffler, L.J.P., eds, *Geothermal Systems: Principals and Case Histories*: Wiley and Sons, Chichester, p. 109-143.
- Fournier, R.O., 1989, Geochemistry and dynamics of the Yellowstone National Park hydrothermal system: *Annual Review of Earth and Planetary Sciences*, v. 17, p. 13-53.
- Fournier, R.O., Thompson, J.M., and Hutchinson, R.A., 1992, The geochemistry of hot spring waters at Norris Geyser Basin, Yellowstone National Park, USA, in Kharaka, Y.K. and Maest, A.S., eds., *Proceedings of the 7th International Symposium on Water-Rock Interaction*: Rotterdam, A.A. Balkema, p. 1289-1292.
- Fournier, R.O., and Truesdell, A.H., 1974, Geochemical indicators of subsurface temperature – Part 2, Estimation of temperature of fraction of hot water mixed with cold water: *U.S. Geological Survey Journal of Research*, v. 2, no. 3, p. 263-270.
- Friedman, I., Lipman, P.W., Obradovich, J.D., Gleason, J.D., and Christiansen, R.L., 1974, Meteoric water in magmas: *Science*, v. 184, p. 1069-1072.
- Gansecki, C.A., Mahood, G.A., and McWilliams, M.O., 1996, $^{40}\text{Ar}/^{39}\text{Ar}$ geochronology of rhyolites erupted following collapse of the Yellowstone caldera, Yellowstone Plateau volcanic field: Implications for crustal contamination: *Earth and Planetary Science Letters*, v. 42, p. 91-107.
- Garrels, R.M., and Christ, C.L., 1965, *Solutions, Minerals, and Equilibria*: Harper and Row, New York, 450 p.
- Giggenbach, W.F., 1992, Isotopic composition of water and steam discharges, in D'Amore, F., Coordinator, *Application of Geochemistry in Geothermal Reservoirs Development*, UNITAR/UNDP, p. 253-273.
- Giggenbach, W.F., 1997, Relative importance of thermodynamic and kinetic processes in governing the chemical and isotopic composition of carbon gases in high-heatflow sedimentary basins: *Geochimica et Cosmochimica Acta*, v. 61, p. 3763-3785.
- Goff, F., and Gardner, J.N., 1994, Evolution of a mineralized geothermal system, Valles Caldera, New Mexico: *Economic Geology*, v. 89, p. 1803-1832.

- Gooch, F.A., and Whitfield, J.E., 1888, Analyses of waters of the Yellowstone National Park, with an account of the methods of analysis employed: U.S. Geological Survey Bulletin, v. 47, 84 p.
- Gunter, B.D., and Musgrave, B.C., 1966, Gas chromatographic measurements of hydrothermal emanations at Yellowstone National Park: *Geochimica et Cosmochimica Acta*, v. 30, p. 1175-1189.
- Hedenquist, J.W., Arribas, A.R., Gonzalez-Urien, E., 2000, Exploration for epithermal gold deposits: *SEG Reviews in Economic Geology*, v. 13, p. 245-277.
- Henley, R.W., Truesdell, A.H., Barton, P.B. Jr., Whitney, J.A., 1984, Fluid-mineral equilibria in hydrothermal systems: *Reviews in Economic Geology*, v. 1, 267 p.
- Hildreth, W., Christiansen, R.L., and O'Neil, J.R., 1984, Oxygen isotopic study of the Yellowstone Plateau volcanic field: *Journal of Geophysical Research*, v. 89, p. 8339-8369.
- Hildreth, W., Halliday, A.N., and Christiansen, R.L., 1991, Isotopic and chemical evidence concerning the genesis and contamination of basaltic and rhyolitic magma beneath the Yellowstone Plateau volcanic field: *Journal of Petrology*, v. 32, p. 63-138.
- Hostettler, J.D., 1984, Electrode electrons, aqueous electrons, and redox potentials in natural waters: *American Journal of Science*, v. 284, p. 734-759.
- Kennedy, V.C., Zellweger, G.W., Jones, B.F., 1974, Filter pore-size effects on the analysis of Al, Fe, Mn, and Ti in water: *Water Resources Research*, v. 10, p. 785-790.
- Kharaka Y.K., Thordsen, J. J., and White L.D., 2002, Isotope and chemical compositions of meteoric and thermal waters and snow from the greater Yellowstone National Park Region: U.S. Geological Survey Open-File Report 02-194, 75 p.
- Larson P.B., Phillips, A., John, D., Cosca, M., Pritchard, C., Andersen, A., and Manion, J., 2008, Older hydrothermal alteration in the Yellowstone caldera, Wyoming [abstract]: *Goldschmidt Conference Abstracts 2008*, p. A518.
- Larson P.B., Phillips, A., John, D., Cosca, M., Pritchard, C., Andersen, A., and Manion, J., 2009, A preliminary study of older hot spring alteration in Sevenmile Hole, Grand Canyon of the Yellowstone River, Yellowstone Caldera, Wyoming: *Journal of Volcanology and Geothermal Research*, v. 188, p. 225-236.
- Larson, P.B., and Taylor, H.P., Jr., 1986a, An oxygen isotope study of hydrothermal alteration in the Lake City Caldera, San Juan Mountains, Colorado: *Journal of Volcanology and Geothermal Research*, v. 30, p. 47-82.

- Larson, P.B., and Taylor, H.P., Jr., 1986b, An oxygen study of water/rock interaction in the granite of Cataract Gulch, western San Juan Mountains, Colorado: Geological Society of America Bulletin, v. 97, p. 505-515.
- Larson, P.B., and Taylor, H.P., Jr., 1987, Solfataric alteration in the San Juan Mountains, Colorado: Oxygen isotope variations in a boiling hydrothermal environment: Economic Geology, v. 82, p. 1019-1036.
- Love, J.D., 1961, Reconnaissance study of Quaternary faults in and south of Yellowstone National Park, Wyoming: Geological Society of America Bulletin, v. 72, p. 1749-1764.
- Love, J.D. and Good, J.M., 1970, Hydrocarbons in thermal areas, northwestern Wyoming: U.S. Geological Survey Professional Paper 644-B, 23 p.
- Love, J.D., Tschudy, R.H., and Obradovich, J.D., 1975, Dating a Laramide orogeny, northwestern Wyoming: U.S. Geological Survey Professional Paper 975, 51 p.
- Marowsky, G., Wedepohl, K.H., 1971, General trends in the behavior of Cd, Hg, Tl, and Bi in some major rock forming processes: Geochimica et Cosmochimica Acta, v. 35, p. 1255-1267.
- McCleskey, R.B., Ball, J.W., Nordstrom, D.K., Holloway, J.M., and Taylor, H.E., 2005, Water-chemistry data for selected hot Springs, geysers, and streams in Yellowstone National Park, Wyoming, 2001-2002: U.S. Geological Survey Open-File Report 2004-1316, 94 p.
- Nordstrom D.K., McCleskey, B.R., Ball, J.W., 2009, Sulfur geochemistry of hydrothermal waters in Yellowstone National Park: IV Acid-sulfate waters: Applied Geochemistry, v. 24, p. 191-207.
- Phillips, A., Larson, P., John, D., Cosca, M., Pauley, B., Manion, J., Pritchard, C., Andersen, A., 2007, Distribution of hydrothermal mineral assemblages in the Sevenmile Hole area, Grand Canyon of the Yellowstone River, Yellowstone National Park [abstract]: American Geophysical Union Annual Fall Meeting, San Francisco.
- Piper, A.M., 1944, A graphical procedure in the geochemical interpretation of water analysis: American Geophysical Union Transactions, v. 25, p. 914-928.
- Prostka, H.J., Blank, H.R., Jr., Christiansen, R.L., and Ruppel, E.T., 1975, Geologic map of the Tower Junction Quadrangle, Yellowstone National Park, Wyoming and Montana: U.S. Geological Survey Map GQ-1247.
- Puskas, C.M., Smith, R.B., Meertens, C.M., and Chang, W.L., 2007, Crustal deformation of the Yellowstone-Snake River Plain volcano-tectonic system: Campaign and continuous GPS observations, 1987-2004: Journal of Geophysical Research, v. 112, B03401, doi: 10.1029/2006JB004325.

- Reed, M.H., and Spycher, N.F., 1984, Calculation of pH and mineral equilibria in hydrothermal waters with application to geothermometry and studies of boiling and dilution: *Geochimica et Cosmochimica Acta*, v. 48, p. 1479-1492.
- Reyes, A.G., 1990, Petrology of the Philippine geothermal systems and the application of alteration mineralogy to their assessment: *Journal of Volcanology and Geothermal Research*, v. 43, p. 279-309.
- Ruppel, E.T., 1982, Geology of Pre-Tertiary rocks in the northern part of the Yellowstone National Park, Wyoming, *in Wyoming Geological Association Guidebook, Thirty-third Annual Conference 1982*, p. 111-137.
- Rye, R.O., Bethke, P.M., Wasserman, M.D., 1992, The stable isotope geochemistry of acid sulfate alteration: *Economic Geology*, v. 87, p. 225-262.
- Simmons, S.F., White, N.C., and John, D.A., 2005, Geological characteristics of epithermal precious and base metal deposits: *Economic Geology 100th Anniversary Volume*, p. 485-522.
- Smedes, H.W., and Prostka, H.J., 1972, Stratigraphic framework of the Absaroka Volcanic Supergroup in the Yellowstone National Park region: U.S. Geological Survey Professional Paper 729-C, 33 p.
- Smith, B.R., Braile, L.W., 1982, Crustal structure and evolution of an explosive silicic volcanic system at Yellowstone National Park, *in Wyoming Geological Association Guidebook, Thirty-third Annual Conference 1982*, p. 230-250.
- Stumm, W., and Morgan, J.J., 1996, *Aquatic Chemistry, Chemical Equilibria and Rates in Natural Waters*, 3rd edition: Wiley Interscience, New York, 1022 p.
- Thompson, J.M., 1985, Chemistry of thermal and nonthermal springs in the vicinity of Lassen Volcanic National Park: *Journal of Volcanology and Geothermal Research*, v. 25, p. 81-104.
- Thompson, J.M. and DeMonge, J.M., 1996, Chemical analyses of hot springs, pools, and geysers from Yellowstone National Park, Wyoming, and vicinity, 1980-1993: U.S. Geological Survey Open-File Report 96-68, 66 p.
- Thompson, J. M., Presser, T. S., Barnes, R. B., Bird, D. B., 1975, Chemical analysis of the waters of Yellowstone National Park, Wyoming from 1965 to 1973: U.S. Geological Survey Open-File Report 75-25, 59 p.
- Thordsen, J.J., Kharaka, Y.K., Mariner, R.H., White, L.D., 1992, Controls on the distribution of stable isotopes of meteoric water and snow in the greater Yellowstone National Park region, USA, *in Kharaka, Y.K. and Maest, A.S., eds., Proceedings of the 7th International Symposium on Water-Rock Interaction: Rotterdam, A.A. Balkema*, p. 591-595.

- Tonnson, J.J., 1982, Petroleum geology of the northern part of Yellowstone National Park, *in* Wyoming Geological Association Guidebook, Thirty-third Annual Conference 1982, p. 289-295.
- Truesdell, A.H., Fournier, R.O., 1976, Conditions in the deeper parts of the hot spring systems of Yellowstone National Park, Wyoming: U.S. Geological Survey Open-File Report 76-428, 29 p.
- Truesdell, A.H., and Fournier, R.O., 1977, Procedure for estimating the temperature of a hot-water component in a mixed water by using a plot of dissolved silica versus enthalpy: U.S. Geological Survey Journal of Research, v. 5, no. 1, p. 49-52.
- Truesdell, A.H., Nathenson, M., Rye, R.O., 1977, The effects of subsurface boiling and dilution on the isotopic compositions of Yellowstone thermal waters: Journal of Geophysical Resources, v. 82, p. 3694-3704.
- Turekian, K.K., and Wedepohl, K.H., 1961, Distribution of the elements in some major units of the earth's crust: Geological Society of America Bulletin, v. 72, p. 175-192.
- U.S. Environmental Protection Agency, 1983, Methods for Chemical Analysis of Water and Wastes, EPA Report # 600/4-79-020, Environmental Monitoring and Support Laboratory, Office of Research and Development, USEPA, Cincinnati, OH, 491 p.
- U.S. Environmental Protection Agency, 2000, Method 7473, Mercury in solids and solutions by thermal decomposition, amalgamation, and atomic absorption spectrometry, *in* Test Methods for Evaluating Solid Waste, Physical/Chemical Methods, SW-846, Update IVA: U.S. Government Printing Office, Washington, D.C., 15 p.
- U.S. Geological Survey, Mount Washburn Quadrangle, Wyoming-Park Co. [map], Provisional Edition, 1986, 1:24,000, 7.5 Minute Series, Reston, VA: United States Department of the Interior, USGS, 1986.
- Werner, C., Hurwitz, S., Evans, W.C., Lowenstern, J.B., Bergfeld, D., Heasler, H., Jaworowski, C., Hunt, A., 2008, Volatile emissions and gas geochemistry of Hot Springs Basin, Yellowstone National Park, USA: Journal of Volcanology and Geothermal Research, v. 178, p. 751-762.
- White, D.E., 1967, Mercury and base-metal deposits with associated thermal and mineral waters, *in* Barnes, H.L., ed, Geochemistry of Hydrothermal Ore Deposits, 1st Edition: Rinehart and Winston, Inc., New York, 670 p.
- White, D.E., 1981, Active geothermal systems and hydrothermal ore deposits: Economic 75th Anniversary Volume, p. 392-423.

White, D.E., Hutchinson, R.A., and Keith, T.E.C., 1988, The geology and remarkable thermal activity of Norris Geyser Basin, Yellowstone National Park, Wyoming: U.S. Geological Survey Professional Paper 1456, 84 p.

White, D.E., Muffler, L.J.P., and Truesdell, A.H., 1971, Vapor-dominated hydrothermal systems compared with hot-water systems: *Economic Geology*, v. 66, p. 75-97.

Zimbelman, D.R., Rye, R.O., and Breit, G.N., 2005, Origin of secondary sulfate minerals on active andesitic stratovolcanoes: *Chemical Geology*, v. 215, p. 37-60.

**APPENDIX A: Photographs, coordinates, and pH and temperature measurements
at Inkpot Spring from July 26, 2008 to August 9, 2008**

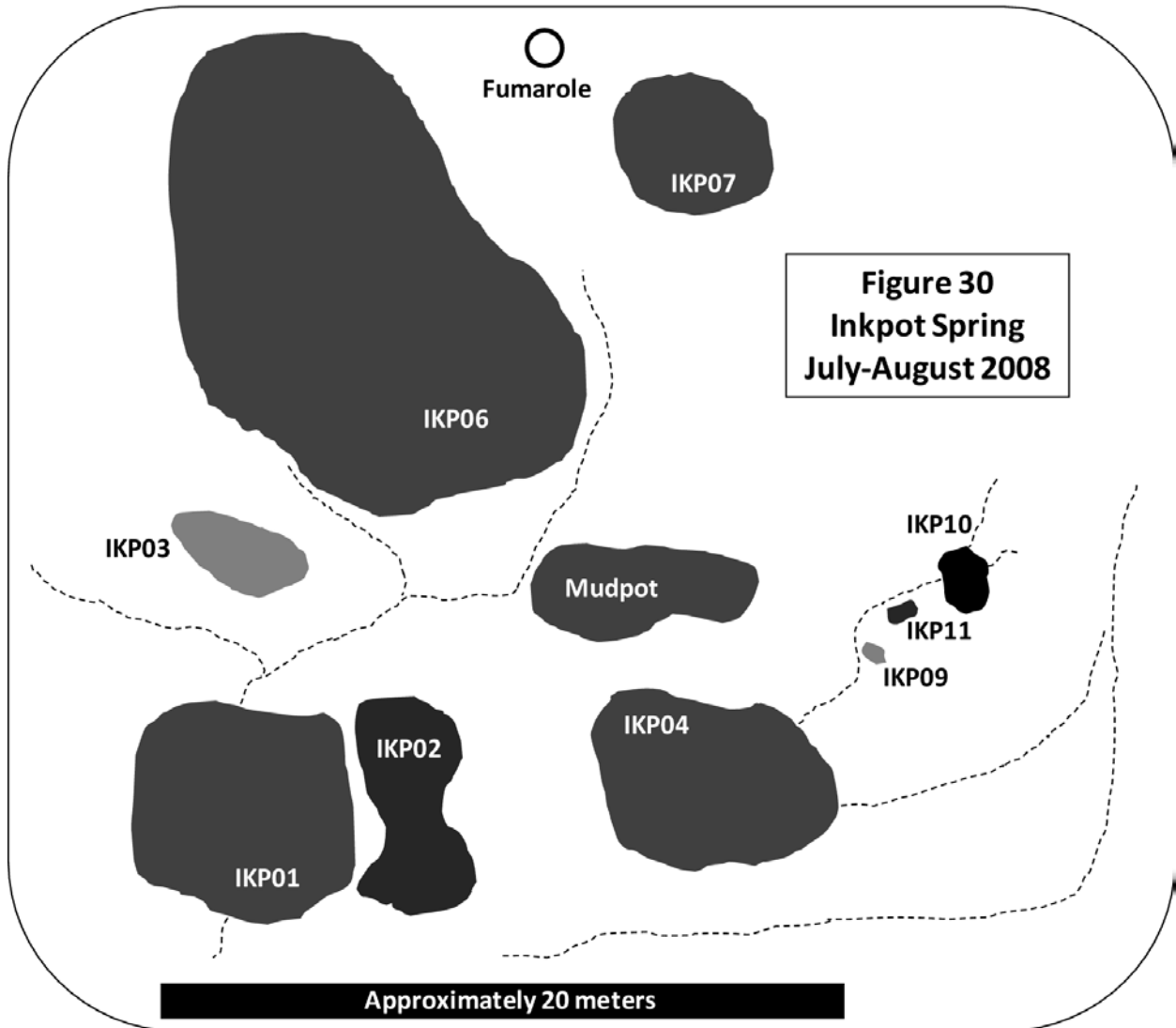


Figure 30. Schematic drawing of Inkpot Spring pool distribution during July and August, 2008.

IKP01

Easting: 0545156

Northing: 4956751



POOL	pH	TEMP (°C)	DATE	TIME
IKP01	6.27	80.3	7/26/2008	4:30 PM
IKP01	6.40	87.5	7/26/2008	4:30 PM
IKP01	6.06	78.9	7/29/2008	1:53 PM
IKP01	6.04	78.8	7/29/2008	1:53 PM
IKP01	6.10	77.9	7/30/2008	1:30 PM
IKP01	6.26	88.6	7/30/2008	1:30 PM
IKP01	6.10	79.4	8/1/2008	3:28 PM
IKP01	6.14	87.9	8/1/2008	3:28 PM
IKP01	5.99	79.4	8/3/2008	3:11 PM
IKP01	6.03	88.2	8/3/2008	3:11 PM
IKP01	6.06	81.8	8/9/2008	12:20 PM
IKP01	5.58	82.1	8/9/2008	12:20 PM
IKP01 AVG	6.09	82.6	-----	-----

IKP02

Easting: 0545167

Northing: 4956762



POOL	pH	TEMP (°C)	DATE	TIME
IKP02	5.99	71.4	7/26/2008	4:35 PM
IKP02	6.06	74.2	7/26/2008	4:35PM
IKP02	5.96	72.1	7/27/2008	11:40 AM
IKP02	6.04	75.4	7/27/2008	11:40 AM
IKP02	5.96	74.4	7/29/2008	1:50 PM
IKP02	5.86	71.5	7/29/2008	1:50 PM
IKP02	6.00	74.1	7/30/2008	1:33 PM
IKP02	5.86	70.0	7/30/2008	1:33 PM
IKP02	5.91	71.2	8/1/2008	3:24 PM
IKP02	5.98	74.7	8/1/2008	3:24 PM
IKP02	6.01	74.9	8/3/2008	3:08 PM
IKP02	5.90	71.1	8/3/2008	3:08 PM
IKP02	5.92	73.3	8/9/2008	12:25 PM
IKP02	5.95	77.1	8/9/2008	12:25 PM
IKP02 AVG	5.96	73.2	-----	-----

IKP03

Easting: 0545153

Northing: 4956773



POOL	pH	TEMP (°C)	DATE	TIME
IKP03	5.92	86.5	7/26/2008	4:40 PM
IKP03	6.18	86.6	7/27/2008	11:45 AM
IKP03	6.03	86.3	7/29/2008	1:46PM
IKP03	6.00	86.4	7/29/2008	1:46PM
IKP03	6.15	85.6	7/30/2008	1:39 PM
IKP03	6.07	86.4	7/30/2008	1:39 PM
IKP03	6.05	86.3	8/1/2008	3:30 PM
IKP03	5.98	86.2	8/3/2008	3:15 PM
IKP03	5.93	86.6	8/3/2008	3:15 PM
IKP03	6.11	86.7	8/9/2008	12:30 PM
IKP03 AVG	6.04	86.36	-----	-----

IKP04

Easting: 0545169

Northing: 4956774



POOL	pH	TEMP (°C)	DATE	TIME
IKP04	3.45	74.5	7/26/2008	4:45PM
IKP04	3.44	74.2	7/26/2008	4:45 PM
IKP04	3.50	75.2	7/27/2008	11:50 AM
IKP04	3.51	75.1	7/27/2008	11:50 AM
IKP04	4.05	76	7/29/2008	1:42 PM
IKP04	4.01	76	7/29/2008	1:42 PM
IKP04	4.01	75.6	7/29/2008	1:42 PM
IKP04	4.62	75.7	7/30/2008	1:36 PM
IKP04	4.62	75.3	7/30/2008	1:36 PM
IKP04	5.43	77.8	8/1/2008	3:12 PM
IKP04	5.44	77.5	8/1/2008	3:12 PM
IKP04	5.60	78.7	8/3/2008	2:58 PM
IKP04	5.56	78.1	8/3/2008	2:58 PM
IKP04	3.62	77.5	8/9/2008	12:11 PM
IKP04	3.56	77.1	8/9/2008	12:11 PM
IKP04	3.47	76.4	8/9/2008	1:04 PM
IKP04 AVG	4.24	76.29	-----	-----

IKP06

Easting: 0545126

Northing: 4956806



POOL	pH	TEMP (°C)	DATE	TIME
IKP06	6.24	74.8	7/29/2008	1:35 PM
IKP06	6.20	74.6	7/29/2008	1:35 PM
IKP06	6.02	73.6	7/30/2008	1:42 PM
IKP06	5.99	73.2	7/30/2008	1:42 PM
IKP06	6.06	73.7	8/1/2008	3:33PM
IKP06	6.00	74.2	8/1/2008	3:33PM
IKP06	6.04	74.6	8/3/2008	3:23 PM
IKP06	6.00	74.7	8/3/2008	3:23 PM
IKP06	5.98	75.6	8/9/2008	12:33 PM
IKP06	5.98	75.9	8/9/2008	12:33 PM
IKP06	6.12	76.4	8/9/2008	12:58 PM
IKP06 AVG	6.06	74.7	-----	-----

IKP07

Easting: 0545155

Northing: 4956812

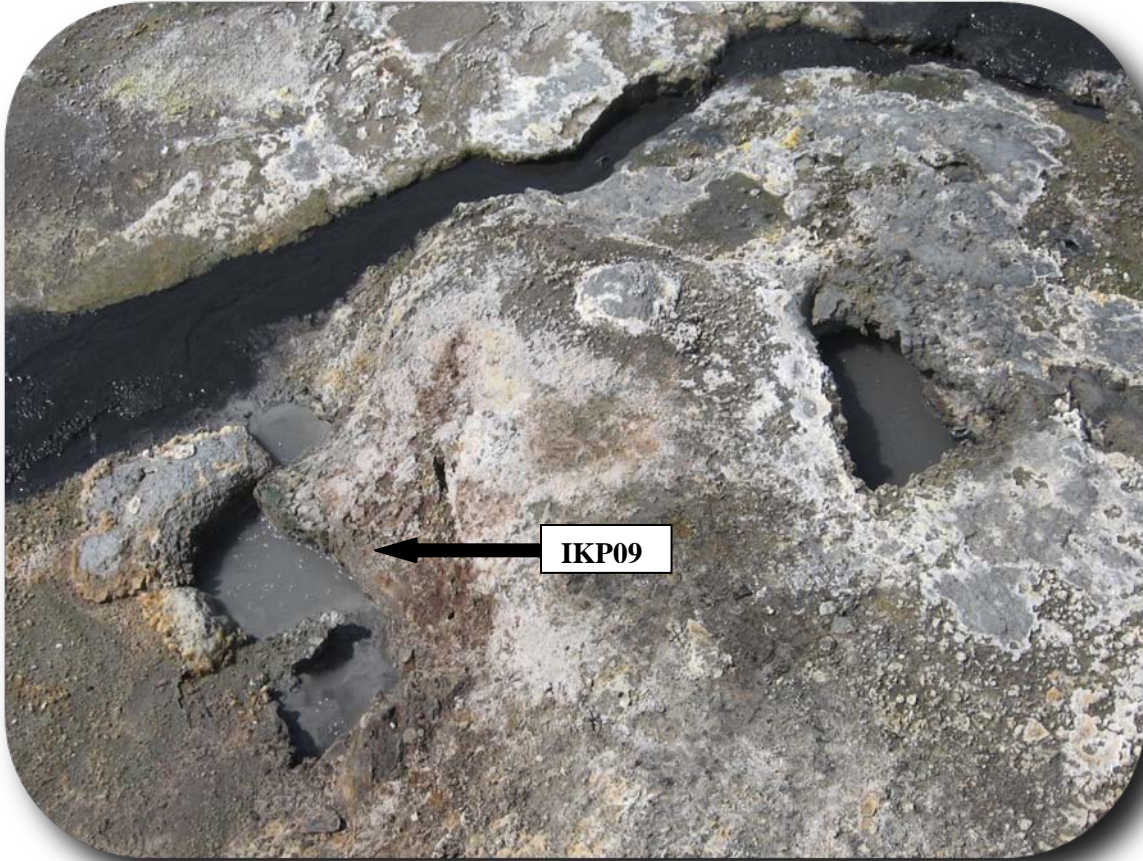


POOL	pH	TEMP (°C)	DATE	TIME
IKP07	6.16	85.3	7/29/2008	2:15PM
IKP07	6.19	86.6	7/29/2008	2:15PM
IKP07	6.25	81.1	7/30/2008	1:50 PM
IKP07	6.18	84.9	8/3/2008	3:30 PM
IKP07	6.13	83.3	8/9/2008	12:51 PM
IKP07	5.99	82.5	8/9/2008	12:51 PM
IKP07 AVG	6.15	83.95	-----	-----

IKP09

Easting: 0545171

Northing: 4956785



POOL	pH	TEMP (°C)	DATE	TIME
IKP09	6.05	88.5	8/1/2008	3:20 PM
IKP09	6.01	88.0	8/1/2008	3:20 PM
IKP09	6.06	89.3	8/3/2008	3:04 PM
IKP09	6.00	88.3	8/3/2008	3:04 PM
IKP09	5.98	89.7	8/9/2008	12:40 PM
IKP09	5.92	89.7	8/9/2008	12:40 PM
IKP09 AVG	6.00	88.92	-----	-----

IKP10

Easting: 0545168

Northing: 4956784



POOL	pH	TEMP (°C)	DATE	TIME
IKP10	3.20	80.9	8/1/2008	3:16 PM
IKP10	3.19	81.0	8/1/2008	3:16 PM
IKP10	2.92	77.7	8/3/2008	3:01 PM
IKP10	2.88	77.8	8/3/2008	3:01 PM
IKP10	2.52	79.1	8/9/2008	12:45 PM
IKP10 AVG	2.94	79.30	-----	-----

WTS01

Easting: 0544430

Northing: 4956125

No photograph available

POOL	pH	TEMP (°C)	DATE	TIME
WTS01	2.49	36.6	7/29/2008	11:40 AM
WTS01	2.57	41.8	7/29/2008	11:40 AM
WTS01	2.55	36.6	7/29/2008	11:40 AM
WTS01 AVG	2.54	38.33	-----	-----

WTS02

Easting: 0544460

Northing: 4956194



POOL	pH	TEMP (°C)	DATE	TIME
WTS02	2.74	33.9	7/29/2008	5:00 PM
WTS02	2.72	33.6	7/29/2008	5:00 PM
WTS02 AVG	2.73	33.75	-----	-----

WTS03

Easting: 0544263

Northing: 4956501



POOL	pH	TEMP (°C)	DATE	TIME
WTS03	5.82	72.1	8/3/2008	11:10 AM
WTS03	6.05	64.8	8/3/2008	11:10 AM
WTS03 AVG	5.94	68.45	-----	-----

**APPENDIX B: Previous USGS and Carnegie Institute data from Washburn-Inkpot
Spring geothermal area**

Sample #	03WA127	03WA128	03WA129	03WA130	01WA110	01WA117	01WA116	01WA115
Corresponding # in this study	IKP01	IKP06	IKP02	IKP02	IKP01	IKP01	IKP01	-----
Publication/Report†	2006-1339	2006-1339	2006-1339	2006-1339	2004-1316	2004-1316	2004-1316	2004-1316
Date collected	6/3/2003	6/3/2003	6/3/2003	6/3/2003	5/23/2001	5/25/2001	5/25/2001	5/25/2001
Latitude	44°45'53.1"	44°45'53.9"	44°45'53.5"	44°45'52.2"	44°45'52.8"	44°45'52.5"	44°45'52.2"	44°45'49.2"
Longitude	110°25'46.0"	110°25'46.2"	110°25'45.2"	110°25'45.8"	110°25'48.9"	110°25'48.8"	110°25'48.8"	110°25'51.5"
Temp (°C)	82.9	84.5	69	-----	85.0	63.0	51.2	19.4
pH - field	6.45	6.61	3.04	-----	6.39	7.1	7.14	7.97
pH - lab	8.09	8.01	2.74	8.24	7.77	7.8	7.74	7.55
S. conductance (µS/cm)	2135/2260	2050/2100	4460/5170	---/2350	2020/2210	2230/2300	2250/2290	2370/2330
Redox potential, Eh (V)	-0.178	-0.168	0.083	-----	-0.154	0.187	0.218	0.369
Constituents (mg/L)*								
Silica (SiO ₂)	178	152	233	89.3	168	180	170	170
Aluminum (Al)	0.076	0.092	16.8	0.003	<0.07	<0.07	0.09	0.09
Calcium (Ca)	22.2	22.6	38.4	15.5	22.7	23.4	25	26.1
Magnesium (Mg)	9.76	10.1	18.9	5.52	8.08	7.20	5.13	5.87
Sodium (Na)	34.7	35.0	29.8	20.8	35.5	40.4	32.4	34.9
Potassium (K)	11.1	11.3	14.2	7.76	13.2	13.1	13.6	14.1
Lithium (Li)	0.019	0.018	0.040	0.005	0.034	0.035	0.037	0.037
Sulfate (SO ₄)	830	783	2050	809	774	853	859	892
Thiosulfate (S ₂ O ₃)	0.8	1.2	<0.1	-----	2.6	<0.1	<0.1	<0.1
Polythionate (S ₅ O ₆)	0.9/4 mg/L / n	<0.5 mg/L / n	<0.5 mg/L / n	-----	<0.002 mM/n	<0.002 mM/n	<0.002 mM/n	<0.002 mM/n
Hydrogen sulfide (H ₂ S)	2.3	1.0	4.6	-----	1.3	0.005	0.007	0.003
Alkalinity (HCO ₃)	168	145	-----	140	152	141	126	80.0
Ammonium (NH ₄)	281	263	571	329	285	290	284	286
Barium (Ba)	0.064	0.062	0.031	0.016	0.08	0.081	0.081	0.081
Strontium (Sr)	0.142	0.144	0.201	0.111	0.178	0.178	0.182	0.191
Fluoride (F)	0.500	0.500	0.400	0.300	0.34	0.31	0.42	0.35
Chloride (Cl)	0.856	0.821	5.81	0.722	3.5	2.1	2.0	1.0
Bromide (Br)	0.102	0.102	0.102	0.102	<0.03	<0.03	<0.03	<0.03
Nitrate (NO ₃)	<0.1	0.147	<0.1	<0.1	<0.1	<0.1	<0.1	<0.1
Nitrite (NO ₂)	0.122	0.020	0.001	0.002	0.0285	0.0428	0.0287	0.374
Boron (B)	5.67	4.27	6.52	1.18	7.56	8.27	8.47	8.66
Rubidium (Rb)	-----	-----	-----	-----	-----	-----	-----	-----
Cesium (Cs)	-----	-----	-----	-----	-----	-----	-----	-----
Phosphate (PO ₄)	-----	-----	-----	-----	-----	-----	-----	-----
Iron total (Fe(T))	<0.002	0.012	14.9	0.020	0.007	0.003	0.004	0.017
Ferrous iron (Fe(II))	<0.002	0.010	14.9	---	0.007	0.003	0.003	0.009
Manganese (Mn)	0.124	0.141	0.712	0.091	0.124	0.117	0.118	0.115
Copper (Cu)	<0.0005	<0.0005	<0.0005	<0.0005	0.0008	<0.0005	<0.0005	<0.0133
Zinc (Zn)	<0.004	<0.004	0.081	<0.004	<0.001	<0.001	<0.001	<0.001
Cadmium (Cd)	<0.0001	0.0016	0.0002	0.0002	<0.0001	<0.0001	<0.0001	0.0006
Chromium (Cr)	0.0037	0.0043	0.030	<0.0005	<0.0005	0.0008	0.0012	0.0012
Cobalt (Co)	<0.0007	<0.0007	<0.0007	<0.0007	0.0008	<0.0007	<0.0007	<0.0007
Mercury (Hg), ng/L	2100	510	83	-----	-----	-----	-----	-----
Nickel (Ni)	<0.002	<0.002	0.0050	<0.002	<0.002	<0.002	<0.002	<0.002
Lead (Pb)	<0.0008	<0.0008	<0.0008	<0.0008	<0.0008	<0.0008	<0.0008	<0.0008
Beryllium (Be)	<0.001	<0.001	0.005	<0.001	<0.001	<0.001	<0.001	<0.001
Vanadium (V)	<0.005	0.011	0.033	0.008	<0.002	0.002	0.002	0.003
Molybdenum (Mo)	<0.007	<0.007	<0.007	<0.007	-----	-----	-----	-----
Antimony (Sb)	0.0020	<0.001	<0.001	<0.001	0.001	0.003	0.003	0.002
Arsenic total (As(T))	0.003	0.003	0.0004	<0.04	0.0008	0.0007	0.0008	0.0009
Arsenite (As(III))	0.003	0.003	<0.001	-----	0.0005	0.0007	0.0008	0.0007
Selenium (Se)	<0.001	<0.001	<0.001	<0.001	<0.001	<0.001	<0.001	<0.001
Dissolved organic carbon	17.0	21.0	-----	10	4.1	4.0	4.5	5.5
δ ¹⁸ O, per mil	-4.21	-5.57	-4.12	-----	-4.5	-4.0	-----	-3.3
δD, per mil	-112.95	-116.52	-107.75	-----	-115	-113	-----	-110
sum cations, meq/L	17.2	16.2	34.6	18.2	17.4	17.5	17.2	17.7
sum anions, meq/L	18.5	17.2	35.3	17.9	17.2	18.6	18.6	18.5
Charge imbalance, percent	-7.1	-5.5	-2.0	1.6	1.2	-6.4	-7.7	-4.6

†References for each report/publication are included on the final page of this appendix.

*An explanation of all symbols and abbreviations is included in Appendix I.

Sample #	01WA111	01WA118	95WA111	95WA112	95WA113	90YNP-112	90YNP-113	J7806
Corresponding # in this study	IKP02	IKP04	----	----	----	----	----	----
Publication/Report†	2004-1316	2004-1316	98-574	98-574	98-574	02-194	02-194	96-68
Date collected	5/23/2001	5/25/2001	8/23/1995	8/23/1995	8/23/1995	6/14/1990	6/14/1990	9/29/1978
Latitude	44°45'52.9"	44°45'53.2"	----	----	----	44°46'0.6"	44°45'58.3"	- ? - ? - ? -
Longitude	110°25'48.7"	110°25'48.1"	----	----	----	110°25'37.8"	110°25'44.3"	110°25.804"
Temp (°C)	83.7	71.5	75.5	93	82	80.0	----	82.0
pH - field	6.45	3.71	2.92	6.71	1.83	----	3.15	6.0
pH - lab	8.14	3.35	2.49	6.77	1.63	----	----	6.57
S. conductance (µS/cm)	1980/----	4070/4450	5790/7260	3250/3300	7670/13600	3490	4300	----
Redox potential, Eh (V)	-0.156	0.022	0.067	0.157	0.223	----	----	----
Constituents (mg/L)*								
Silica (SiO ₂)	140	225	262	263	316	58.7	280	197
Aluminum (Al)	0.11	3.31	34.0	0.820	68.0	----	----	0.06
Calcium (Ca)	11.7	19.3	42.0	7.0	14.6	3.97	18.8	3.45
Magnesium (Mg)	5.45	10.0	19.7	4.40	9.30	0.23	9.07	12.2
Sodium (Na)	33.2	21.7	31.0	11.0	11.0	1.0	14.5	20.0
Potassium (K)	12.0	8.07	18.3	12.5	13.1	1.58	4.44	5.0
Lithium (Li)	<0.003	0.018	0.050	0.050	<0.070	0.008	<0.002	0.0
Sulfate (SO ₄)	606	1920	3120	1280	4200	1200	1790	1800
Thiosulfate (S ₂ O ₃)	12	<0.1	0.09	0.13	n.a.	----	----	----
Polythionate (S _n O ₆)	<0.002 mM/n	<0.002 mM/n	----	----	----	----	----	----
Hydrogen sulfide (H ₂ S)	----	2.8	8	<0.03	5.7	----	----	0.25
Alkalinity (HCO ₃)	222	----	n.a.	9.25	n.a.	216	----	45
Ammonium (NH ₄)	289	618	884	478	628	567	560	625
Barium (Ba)	0.206	0.012	0.030	<0.015	0.070	0.035	0.011	----
Strontium (Sr)	0.079	0.103	0.240	0.050	0.490	0.125	0.06	0.20
Fluoride (F)	0.56	0.22	0.338	0.222	0.182	<0.05	<0.05	0.1
Chloride (Cl)	13.2	3.6	<10	1.8	6.7	0.8	0.9	5.0
Bromide (Br)	<0.03	<0.03	<22	<0.2	<0.2	<0.03	<0.03	----
Nitrate (NO ₃)	1.6	<0.1	0.26	0.30	0.42	0.2	<0.02	----
Nitrite (NO ₂)	<0.01	0.0271	----	----	----	----	----	----
Boron (B)	1.44	5.56	9.40	14.3	15.0	0.2	6.87	3.9
Rubidium (Rb)	----	----	----	----	----	----	----	0.1
Cesium (Cs)	----	----	----	----	----	----	----	0.10
Phosphate (PO ₄)	----	----	----	----	----	<0.25	<0.25	----
Iron total (Fe(T))	0.022	1.02	23.6	2.22	71.0	0.01	21.5	----
Ferrous iron (Fe(II))	0.02	1.01	23.6	2.21	65.0	----	----	----
Manganese (Mn)	0.056	0.286	0.510	0.120	0.34	0.006	0.29	0.18
Copper (Cu)	----	0.0005	<0.20	<0.20	<0.20	----	----	----
Zinc (Zn)	0.014	0.012	0.080	<0.009	0.060	----	----	<0.01
Cadmium (Cd)	----	<0.0001	<0.009	<0.009	<0.009	----	----	----
Chromium (Cr)	----	0.0077	<0.21	<0.21	<0.21	----	----	----
Cobalt (Co)	----	<0.0007	<0.024	<0.024	0.060	----	----	----
Mercury (Hg), ng/L	----	----	----	----	----	----	----	----
Nickel (Ni)	<0.002	0.004	<0.042	<0.042	0.18	----	----	----
Lead (Pb)	----	<0.0008	<0.11	<0.11	<0.11	----	----	----
Beryllium (Be)	<0.001	0.001	<0.001	<0.001	<0.001	----	----	----
Vanadium (V)	0.002	0.013	0.050	<0.021	0.11	----	----	----
Molybdenum (Mo)	----	----	----	----	----	----	----	----
Antimony (Sb)	----	0.002	----	----	----	----	----	----
Arsenic total (As(T))	0.0228	0.0002	<0.001	<0.001	<0.001	----	----	----
Arsenite (As(III))	0.0207	<0.0005	----	----	----	----	----	----
Selenium (Se)	----	<0.001	----	----	----	----	----	----
Dissolved organic carbon	----	2.9	n.a.	n.a.	n.a.	----	----	----
δ ¹⁸ O, per mil	-2.8	-3.9	-4.0	-6.5	-7.3	-3.3	-6.8	-4.5
δD, per mil	-111	-112	-106	-115	-119	-118	-116	-118
sum cations, meq/L	17.2	34.2	51.12	26.06	57.90	----	----	----
sum anions, meq/L	15.6	35.0	51.18	24.78	50.81	----	----	----
Charge imbalance, percent	9.3	-2.3	-0.11	5.04	13.1/-21.4	----	----	----

†References for each report/publication are included on the final page of this appendix.

*An explanation of all symbols and abbreviations is included in Appendix I.

Sample #	J7807	J7808	J7809	J7304	J7305	YF467	YF429	YF430
Publication/Report†	96-68	96-68	96-68	75-25	75-25	75-25	75-25	75-25
Date collected	9/29/1978	9/29/1978	9/29/1978	9/22/1973	9/22/1973	9/14/1969	6/22/1968	6/22/1968
Latitude	-?-?-?-	-?-?-?-	-?-?-?-	44°45.972'	44°45.860'	44°45.972'	44°45.886'	44°45.006'
Longitude	110°25.804'	110°25.804'	110°25.804'	110°25.732'	110°25.804'	110°25.732'	110°25.768'	110°25.756'
Temp (°C)	87.0	88.0	88.0	91.0	89.0	-----	86.0	-----
pH - field	4.0	6.5	5.7	8.1	7.9	5.0	-----	-----
pH - lab	3.17	7.75	5.65	8.0	7.69	4.48	-----	-----
S. conductance (µS/cm)	-----	-----	-----	2290	1960	-----	-----	-----
Redox potential, Eh (V)	-----	-----	-----	-----	-----	-----	-----	-----
Constituents (mg/L)*								
Silica (SiO ₂)	266	224	135	247	237	243	-----	-----
Aluminum (Al)	0.50	0.05	0.05	0.20	0.38	3.30	-----	-----
Calcium (Ca)	2.43	2.80	24.0	2.0	2.5	13.6	17.2	-----
Magnesium (Mg)	9.8	1.02	12.7	4.10	0.50	4.33	9.30	-----
Sodium (Na)	16.0	30.0	28.0	9.7	30.0	14.8	27.1	28.6
Potassium (K)	2.0	6.1	5.9	6.5	9.0	7.3	18.7	15.5
Lithium (Li)	0.0	0.1	0.0	0.1	0.1	0.02	0.01	-----
Sulfate (SO ₄)	2860	943	1270	900	712	1260	1950.0	2400
Thiosulfate (S ₂ O ₃)	-----	-----	-----	-----	-----	-----	-----	-----
Polythionate (S ₄ O ₆)	-----	-----	-----	-----	-----	-----	-----	-----
Hydrogen sulfide (H ₂ S)	0.02	0.1	0.01	4.5	7.8	-----	-----	-----
Alkalinity (HCO ₃)	0	122	80	107	140	-----	8.2	-----
Ammonium (NH ₄)	875	400	550	270	210	424	658.0	-----
Barium (Ba)	-----	-----	-----	-----	-----	-----	-----	-----
Strontium (Sr)	-----	<0.10	0.20	-----	-----	-----	-----	-----
Fluoride (F)	0.3	1.3	0.2	0.1	1.8	0.1	0.5	-----
Chloride (Cl)	2.0	24.0	4.0	7.0	2.2	0.1	2.1	0.6
Bromide (Br)	-----	-----	-----	-----	-----	-----	-----	-----
Nitrate (NO ₃)	-----	-----	-----	-----	-----	-----	-----	-----
Nitrite (NO ₂)	-----	-----	-----	-----	-----	-----	-----	-----
Boron (B)	9.4	0.6	0.1	6.60	0.50	6.40	7.84	-----
Rubidium (Rb)	0.1	0.1	0.1	-----	-----	-----	-----	-----
Cesium (Cs)	0.16	0.11	0.12	-----	-----	-----	-----	-----
Phosphate (PO ₄)	-----	-----	-----	-----	-----	-----	-----	-----
Iron total (Fe(T))	-----	-----	-----	0.10	0.20	6.40	-----	-----
Ferrous iron (Fe(II))	-----	-----	-----	-----	-----	-----	-----	-----
Manganese (Mn)	0.17	<0.05	0.13	-----	-----	0.10	-----	-----
Copper (Cu)	-----	-----	-----	-----	-----	-----	-----	-----
Zinc (Zn)	<0.01	<0.01	<0.01	-----	-----	-----	-----	-----
Cadmium (Cd)	-----	-----	-----	-----	-----	-----	-----	-----
Chromium (Cr)	-----	-----	-----	-----	-----	-----	-----	-----
Cobalt (Co)	-----	-----	-----	-----	-----	-----	-----	-----
Mercury (Hg), ng/L	-----	-----	-----	-----	-----	-----	-----	-----
Nickel (Ni)	-----	-----	-----	-----	-----	-----	-----	-----
Lead (Pb)	-----	-----	-----	-----	-----	-----	-----	-----
Beryllium (Be)	-----	-----	-----	-----	-----	-----	-----	-----
Vanadium (V)	-----	-----	-----	-----	-----	-----	-----	-----
Molybdenum (Mo)	-----	-----	-----	-----	-----	-----	-----	-----
Antimony (Sb)	-----	-----	-----	-----	-----	-----	-----	-----
Arsenic total (As(T))	-----	-----	-----	-----	-----	-----	-----	-----
Arsenite (As(III))	-----	-----	-----	-----	-----	-----	-----	-----
Selenium (Se)	-----	-----	-----	-----	-----	-----	-----	-----
Dissolved organic carbon	-----	-----	-----	-----	-----	-----	-----	-----
δ ¹⁸ O, per mil	-6.7	-6.9	-4.4	-----	-----	-----	-----	-----
δD, per mil	-120	-117	-116	-----	-----	-----	-----	-----
sum cations, meq/L	-----	-----	-----	-----	-----	-----	-----	-----
sum anions, meq/L	-----	-----	-----	-----	-----	-----	-----	-----
Charge imbalance, percent	-----	-----	-----	-----	-----	-----	-----	-----

†References for each report/publication are included on the final page of this appendix.

*An explanation of all symbols and abbreviations is included in Appendix I.

Sample #	South area	4th furrow	Western area	Devil's Ink Pot
Publication/Report†	466	466	466	47
Date collected	1925 or 1929	1925 or 1929	1925 or 1929	7/8/1886
Latitude	-----	-----	-----	-----
Longitude	-----	-----	-----	-----
Temp (°C)	79.8 -91.8	79.8 -91.8	79.8 -91.8	92
pH - field	-----	-----	-----	acidic
pH - lab	-----	-----	-----	-----
S. conductance (µS/cm)	-----	-----	-----	-----
Redox potential, Eh (V)	-----	-----	-----	-----
Constituents (mg/L)*				
Silica (SiO ₂)	109	170.0	119	89.7
Aluminum (Al)	-----	2.6	trace	3.7
Calcium (Ca)	41	28.0	5	39.6
Magnesium (Mg)	18	4	2	12.1
Sodium (Na)	31	20	13	24.5
Potassium (K)	20	10	16	8.3
Lithium (Li)	-----	-----	-----	0.4
Sulfate (SO ₄)	1841	1555	2444	2320
Thiosulfate (S ₂ O ₃)	-----	-----	-----	-----
Polythionate (S _n O ₆)	-----	-----	-----	-----
Hydrogen sulfide (H ₂ S)	-----	-----	-----	5.1
Alkalinity (HCO ₃)	57	23	15	-----
Ammonium (NH ₄)	611	532	893	768.7
Barium (Ba)	-----	-----	-----	-----
Strontium (Sr)	-----	-----	-----	-----
Fluoride (F)	-----	-----	-----	-----
Chloride (Cl)	0.5	1.7	-----	5.8
Bromide (Br)	-----	-----	-----	-----
Nitrate (NO ₃)	-----	-----	-----	-----
Nitrite (NO ₂)	-----	-----	-----	-----
Boron (B)	-----	-----	-----	51.8 (B ₂ O ₃)
Rubidium (Rb)	-----	-----	-----	-----
Cesium (Cs)	-----	-----	-----	-----
Phosphate (PO ₄)	-----	-----	-----	-----
Iron total (Fe(T))	-----	5	8	trace
Ferrous iron (Fe(II))	-----	-----	-----	-----
Manganese (Mn)	-----	-----	-----	-----
Copper (Cu)	-----	-----	-----	-----
Zinc (Zn)	-----	-----	-----	-----
Cadmium (Cd)	-----	-----	-----	-----
Chromium (Cr)	-----	-----	-----	-----
Cobalt (Co)	-----	-----	-----	-----
Mercury (Hg), ng/L	-----	-----	-----	-----
Nickel (Ni)	-----	-----	-----	-----
Lead (Pb)	-----	-----	-----	-----
Beryllium (Be)	-----	-----	-----	-----
Vanadium (V)	-----	-----	-----	-----
Molybdenum (Mo)	-----	-----	-----	-----
Antimony (Sb)	-----	-----	-----	-----
Arsenic total (As(T))	-----	-----	-----	-----
Arsenite (As(III))	-----	-----	-----	-----
Selenium (Se)	-----	-----	-----	-----
Dissolved organic carbon	-----	-----	-----	-----
δ ¹⁸ O, per mil	-----	-----	-----	-----
δD, per mil	-----	-----	-----	-----
sum cations, meq/L	-----	-----	-----	-----
sum anions, meq/L	-----	-----	-----	-----
Charge imbalance, percent	-----	-----	-----	-----

†References for each report/publication are included on the final page of this appendix.

*An explanation of all symbols and abbreviations is included in Appendix I.

†References for data in Appendix B. Corresponding report number is in bold.

Allen, E.T., and Day, A.L., 1935, Hot springs of the Yellowstone National Park: Carnegie Institute of Washington Publication **466**, 525 p.

Ball, J.W., McCleskey, R.B., Nordstrom, D.K., and Holloway, J.M., 2007, Water-chemistry data for selected springs, geysers, and streams in Yellowstone National Park, Wyoming, 2003-2005: U.S. Geological Survey Open-File Report **2006-1339**, 183 p.

Ball, J.W., Nordstrom, D.K., Cunningham, K.M., Schoonen, M.A.A., Xu, Y., and DeMonge, J.M., 1998, Water-chemistry and on-site sulfur-speciation data for selected springs in Yellowstone National Park, Wyoming, 1994-1995: U.S. Geological Survey Open-File Report **98-574**, 35 p.

Gooch, F.A., and Whitfield, J.E., 1888, Analyses of waters of the Yellowstone National Park, with an account of the methods of analysis employed: U.S. Geological Survey Bulletin, v. **47**, 84 p.

Kharaka Y.K., Thordsen, J. J., and White L.D., 2002, Isotope and chemical compositions of meteoric and thermal waters and snow from the greater Yellowstone National Park Region: U.S. Geological Survey Open-File Report **02-194**, 75p.

McCleskey, R.B., Ball, J.W., Nordstrom, D.K., Holloway, J.M., and Taylor, H.E., 2005, Water-chemistry data for selected hot Springs, geysers, and streams in Yellowstone National Park, Wyoming, 2001-2002: U.S. Geological Survey Open-File Report **2004-1316**, 94 p.

Thompson, J.M. and DeMonge, J.M., 1996, Chemical analyses of hot springs, pools, and geysers from Yellowstone National Park, Wyoming, and vicinity, 1980-1993: U.S. Geological Survey Open-File Report **96-68**, 66 p.

Thompson, J. M., Presser, T. S., Barnes, R. B., Bird, D. B., 1975, Chemical analysis of the waters of Yellowstone National Park, Wyoming from 1965 to 1973: U.S. Geological Survey Open-File Report **75-25**, 59 p.

**APPENDIX C: Water chemistry data for Inkpot Spring from July 26, 2008 to
August 9, 2008**

Sample #					IKP01	IKP02	IKP03	IKP04
Date collected					7/26/2008	7/29/2008	7/27/2008	7/30/2008
Easting					0545156	0545167	0545153	0545169
Northing					4956751	4956762	4956773	4956774
Temperature °C (average)					82.6	73.2	86.4	76.3
Constituents	Method	MDL*	Units					
aluminum	Al+++	ICP-AES	0.816	mg/L	0.1556	0.0728	0.1136	0.1244
boron	B+++	ICP-AES	0.055	mg/L	15.71	0.7741	4.482	14.66
calcium	Ca++	ICP-AES	0.158	mg/L	29.05	14.36	29.51	40.66
iron	Fe++	ICP-AES	0.192	mg/L	0.0194	0.0395	0.0245	0.0838
potassium	K+	ICP-AES	0.050	mg/L	15.53	7.82	33.47	18.83
magnesium	Mg++	ICP-AES	0.446	mg/L	12.92	6.12	1.453	20.92
sodium	Na+	ICP-AES	1.438	mg/L	34.03	20.45	55.47	29.59
silicon	Si++++	ICP-AES	1.165	mg/L	69.19	57.89	128.9	110.5
silica	SiO ₂	-----	-----	mg/L	148.00	123.83	275.72	236.36
Accuracy								
titanium	Ti++++	ICP-MS	±0.0005	mg/L	0.0144	0.0140	0.0140	0.0128
vanadium	V	ICP-MS	±0.0005	mg/L	0.0180	0.0206	0.0169	0.0170
chromium	Cr	ICP-MS	±0.0005	mg/L	0.0095	0.0094	0.0086	0.0085
manganese	Mn++	ICP-MS	±0.0005	mg/L	0.1205	0.0537	0.0306	0.1430
cobalt	Co	ICP-MS	±0.0005	mg/L	0.0094	0.0094	0.0094	0.0094
nickel	Ni	ICP-MS	±0.0005	mg/L	0.0102	0.0103	0.0102	0.0101
zinc	Zn++	ICP-MS	±0.0005	mg/L	0.0084	0.0190	0.0257	0.0177
rubidium	Rb+	ICP-MS	±0.0005	mg/L	0.0662	0.0288	0.1085	0.0656
strontium	Sr++	ICP-MS	±0.0005	mg/L	0.1947	0.0710	0.1543	0.0869
barium	Ba++	ICP-MS	±0.0005	mg/L	0.0510	0.0334	0.0738	0.0376
lead	Pb	ICP-MS	±0.0005	mg/L	0.0021	0.0022	0.0022	0.0021
copper	Cu	ICP-MS	±0.0005	mg/L	0.0028	0.0021	0.0046	0.0022
galium	Ga+++	ICP-MS	±0.0005	mg/L	0.0011	0.0006	0.0013	0.0006
arsenic	As	ICP-MS	±0.002	mg/L	0.003	0.007	0.002	0.005
molybdenum	Mo	ICP-MS	±0.0005	mg/L	0.0006	0.0007	0.0007	0.0006
tin	Sn++++	ICP-MS	±0.0005	mg/L	0.0001	0.0001	0.0001	0.0001
antimony	Sb	ICP-MS	±0.0005	mg/L	0.0001	0.0003	<0.00005	<0.00005
tungsten	W	ICP-MS	±0.0005	mg/L	0.0007	0.0002	0.0010	0.0001
thallium	Tl++++	ICP-MS	±0.0005	mg/L	0.0001	<0.00005	<0.00005	<0.00005
mercury ‡	Hg (T)	DMA	0.01 ng	mg/L	0.00084	0.00022	0.00029	0.00021
RL								
pH (field average)	pH	Electrode	0.1	pH	6.09	5.96	6.04	4.24
pH (lab)	pH	Titration	-----	pH	7.4	7.4	7.4	4.4
hydroxide alkalinity	OH-	Titration	3.0	mg CaCO ₃ /L	<3	<3	<3	<3
carbonate alkalinity	CO ₃ --	Titration	3.0	mg CaCO ₃ /L	<3	<3	<3	<3
bicarbonate alkalinity	HCO ₃ -	Titration	3.0	mg CaCO ₃ /L	130	170	79	<3
total alkalinity	(HCO ₃ -)	Titration	3.0	mg CaCO ₃ /L	130	170	79	<3
fluoride	F-	IC	0.15	mg/L	NA	NA	1.1	NA
chloride	Cl-	IC	0.20	mg/L	0.53	4.4	0.24	<0.2
nitrite	NO ₂ -	IC	0.050	mg/L	ND	ND	ND	ND
bromide	Br-	IC	0.10	mg/L	ND	ND	ND	ND
nitrate	NO ₃ -	IC	0.050	mg/L	<0.05	0.59	<0.05	ND
o-phosphate	PO ₄ ---	IC	0.10	mg/L	0.31	ND	ND	ND
sulfate	SO ₄ --	IC	0.20	mg/L	1300	2100	1200	2600
ammonia-N	NH ₃	FIA	0.10	mg/L	350	590	300	670
Accuracy								
δ ¹⁸ O	δ ¹⁸ O	GS IR-MS	±0.1	‰	1.402	3.149	-1.496	2.074
δD	δD	TC-EA	±0.1	‰	-109.6	-100.2	-106.9	-100.9

*An explanation of all symbols and abbreviations is included in Appendix I.

‡Mercury analyses of filtered samples with no preservation techniques applied. Complete Hg analyses in Appendix F.

Sample #					IKP06	IKP07	IKP09	IKP10
Date collected					7/30/2008	8/1/2008	8/1/2008	8/2/2008
Easting					0545126	0545155	0545171	0545168
Northing					4956806	4956812	4956785	4956784
Temperature °C (average)					74.7	84.0	88.9	79.3
Constituents	Method	MDL*	Units					
aluminum	Al+++	ICP-AES	0.816	mg/L	0.2649	1.261	0.328	25.94
boron	B+++	ICP-AES	0.055	mg/L	8.087	12.76	59.71	3.138
calcium	Ca++	ICP-AES	0.158	mg/L	32.55	29.37	13.87	7.645
iron	Fe++	ICP-AES	0.192	mg/L	0.0224	0.485	0.3799	6.879
potassium	K+	ICP-AES	0.050	mg/L	14.36	10.64	9.361	13.06
magnesium	Mg++	ICP-AES	0.446	mg/L	16.17	10.8	6.564	3.595
sodium	Na+	ICP-AES	1.438	mg/L	34.69	19.46	24.04	11.31
silcon	Si++++	ICP-AES	1.165	mg/L	69.57	58.11	70.98	127.2
silica	SiO ₂	-----	-----	mg/L	148.81	124.30	151.83	272.08
			<u>Accuracy</u>					
titanium	Ti++++	ICP-MS	±0.0005	mg/L	0.0125	0.0136	0.0122	0.0125
vanadium	V	ICP-MS	±0.0005	mg/L	0.0170	0.0171	0.0169	0.0176
chromium	Cr	ICP-MS	±0.0005	mg/L	0.0082	0.0086	0.0078	0.0094
manganese	Mn++	ICP-MS	±0.0005	mg/L	0.0533	0.0172	0.0157	0.0153
cobalt	Co	ICP-MS	±0.0005	mg/L	0.0094	0.0094	0.0094	0.0094
nickel	Ni	ICP-MS	±0.0005	mg/L	0.0101	0.0104	0.0105	0.0103
zinc	Zn++	ICP-MS	±0.0005	mg/L	0.0118	0.0098	0.0071	0.0158
rubidium	Rb+	ICP-MS	±0.0005	mg/L	0.0393	0.0297	0.0187	0.0249
strontium	Sr++	ICP-MS	±0.0005	mg/L	0.1516	0.1091	0.0811	0.0678
barium	Ba++	ICP-MS	±0.0005	mg/L	0.0611	0.0413	0.0430	0.0450
lead	Pb	ICP-MS	±0.0005	mg/L	0.0023	0.0054	0.0025	0.0211
copper	Cu	ICP-MS	±0.0005	mg/L	0.0028	0.0030	0.0020	0.0013
galium	Ga+++	ICP-MS	±0.0005	mg/L	0.0009	0.0008	0.0007	0.0021
arsenic	As	ICP-MS	±0.002	mg/L	0.002	0.004	0.002	0.005
molybdenum	Mo	ICP-MS	±0.0005	mg/L	0.0006	0.0016	0.0006	0.0006
tin	Sn++++	ICP-MS	±0.0005	mg/L	0.0001	0.0002	0.0001	0.0001
antimony	Sb	ICP-MS	±0.0005	mg/L	<0.00005	0.0001	<0.00005	<0.00005
tungsten	W	ICP-MS	±0.0005	mg/L	0.0006	0.0006	0.0003	<0.00005
thallium	Tl++++	ICP-MS	±0.0005	mg/L	<0.00005	0.0001	<0.00005	0.0002
mercury ‡	Hg (T)	DMA	0.01 ng	mg/L	0.00024	0.00020	0.00019	0.00019
			<u>RL</u>					
pH (field average)	pH	Electrode	0.1	pH	6.06	6.15	6.00	2.94
pH (lab)	pH	Titration	-----	pH	7.4	7.5	7.3	2.2
hydroxide alkalinity	OH-	Titration	3.0	mg CaCO ₃ /L	<3	<3	<3	<3
carbonate alkalinity	CO ₃ --	Titration	3.0	mg CaCO ₃ /L	<3	<3	<3	<3
bicarbonate alkalinity	HCO ₃ -	Titration	3.0	mg CaCO ₃ /L	200	48	37	<3
total alkalinity	(HCO ₃ -)	Titration	3.0	mg CaCO ₃ /L	200	48	37	<3
fluoride	F-	IC	0.15	mg/L	NA	0.59	NA	NA
chloride	Cl-	IC	0.20	mg/L	0.63	0.39	0.86	NA
nitrite	NO ₂ -	IC	0.050	mg/L	ND	ND	ND	NA
bromide	Br-	IC	0.10	mg/L	ND	ND	ND	NA
nitrate	NO ₃ -	IC	0.050	mg/L	ND	ND	<0.05	0.090
o-phosphate	PO ₄ ---	IC	0.10	mg/L	0.26	0.37	ND	<0.1
sulfate	SO ₄ --	IC	0.20	mg/L	1300	1200	900	2500
ammonia-N	NH ₃	FIA	0.10	mg/L	360	320	240	530
			<u>Accuracy</u>					
δ ¹⁸ O	δ ¹⁸ O	GS IR-MS	±0.1	‰	1.976	-2.546	-4.864	-1.916
δD	δD	TC-EA	±0.1	‰	-106.6	-107.6	-107.4	-111.9

*An explanation of all symbols and abbreviations is included in Appendix I.

‡Mercury analyses of filtered samples with no preservation techniques applied. Complete Hg analyses in Appendix F.

Sample #					2IKP01	2IKP02	2IKP03	2IKP04
Date collected					8/3/2008	8/3/2008	8/6/2008	8/3/2008
Easting					0545156	0545167	0545153	0545169
Northing					4956751	4956762	4956773	4956774
Temperature °C (average)					82.6	73.2	86.4	76.3
Constituents	Method	MDL*	Units					
aluminum	Al+++	ICP-AES	0.816	mg/L	0.24	0.0779	0.0799	0.074
boron	B+++	ICP-AES	0.055	mg/L	17.22	0.8052	4.706	15.1
calcium	Ca++	ICP-AES	0.158	mg/L	28.46	12.58	27.28	35.55
iron	Fe++	ICP-AES	0.192	mg/L	0.0087	0.0244	0.0154	0.0092
potassium	K+	ICP-AES	0.050	mg/L	15.27	7.222	32.14	18.79
magnesium	Mg++	ICP-AES	0.446	mg/L	12.62	6.085	1.334	18.52
sodium	Na+	ICP-AES	1.438	mg/L	33.95	14.24	54.56	28.57
silcon	Si++++	ICP-AES	1.165	mg/L	71.24	54.73	131.7	98.54
silica	SiO ₂	-----	-----	mg/L	152.38	117.07	281.71	210.78
Accuracy								
titanium	Ti++++	ICP-MS	±0.0005	mg/L	0.0121	0.0119	0.0120	0.0119
vanadium	V	ICP-MS	±0.0005	mg/L	0.0166	0.0168	0.0165	0.0166
chromium	Cr	ICP-MS	±0.0005	mg/L	0.0077	0.0077	0.0077	0.0076
manganese	Mn++	ICP-MS	±0.0005	mg/L	0.0185	0.0137	0.0098	0.0184
cobalt	Co	ICP-MS	±0.0005	mg/L	0.0093	0.0093	0.0093	0.0093
nickel	Ni	ICP-MS	±0.0005	mg/L	0.0101	0.0101	0.0101	0.0101
zinc	Zn++	ICP-MS	±0.0005	mg/L	0.0070	0.0073	0.0075	0.0070
rubidium	Rb+	ICP-MS	±0.0005	mg/L	0.0360	0.0195	0.0750	0.0415
strontium	Sr++	ICP-MS	±0.0005	mg/L	0.1101	0.0451	0.1077	0.0442
barium	Ba++	ICP-MS	±0.0005	mg/L	0.0683	0.0274	0.0819	0.0356
lead	Pb	ICP-MS	±0.0005	mg/L	0.0025	0.0023	0.0022	0.0022
copper	Cu	ICP-MS	±0.0005	mg/L	0.0029	0.0015	0.0036	0.0019
galium	Ga+++	ICP-MS	±0.0005	mg/L	0.0009	0.0003	0.0010	0.0004
arsenic	As	ICP-MS	±0.002	mg/L	0.002	0.003	0.002	0.007
molybdenum	Mo	ICP-MS	±0.0005	mg/L	0.0006	0.0007	0.0007	0.0007
tin	Sn++++	ICP-MS	±0.0005	mg/L	0.0001	0.0001	0.0001	0.0001
antimony	Sb	ICP-MS	±0.0005	mg/L	<0.00005	0.0001	<0.00005	<0.00005
tungsten	W	ICP-MS	±0.0005	mg/L	0.0006	0.0002	0.0013	0.0001
thallium	Tl++++	ICP-MS	±0.0005	mg/L	<0.00005	<0.00005	<0.00005	<0.00005
mercury ‡	Hg (T)	DMA	0.01 ng	mg/L	0.00025	0.00021	0.00028	0.00023
RL								
pH (field average)	pH	Electrode	0.1	pH	6.09	5.96	6.04	4.24
pH (lab)	pH	Titration	-----	pH	7.3	7.5	7.2	6.5
hydroxide alkalinity	OH-	Titration	3.0	mg CaCO ₃ /L	<3	<3	<3	<3
carbonate alkalinity	CO ₃ --	Titration	3.0	mg CaCO ₃ /L	<3	<3	<3	<3
bicarbonate alkalinity	HCO ₃ -	Titration	3.0	mg CaCO ₃ /L	110	200	76	42
total alkalinity	(HCO ₃ -)	Titration	3.0	mg CaCO ₃ /L	110	200	76	42
fluoride	F-	IC	0.15	mg/L	NA	NA	1.1	NA
chloride	Cl-	IC	0.20	mg/L	0.36	0.22	NA	<0.2
nitrite	NO ₂ -	IC	0.050	mg/L	NA	ND	ND	ND
bromide	Br-	IC	0.10	mg/L	ND	ND	ND	ND
nitrate	NO ₃ -	IC	0.050	mg/L	<0.05	ND	<0.05	<0.05
o-phosphate	PO ₄ ---	IC	0.10	mg/L	0.34	ND	ND	ND
sulfate	SO ₄ --	IC	0.20	mg/L	1300	2100	1100	2600
ammonia-N	NH ₃	FIA	0.10	mg/L	360	620	280	680
Accuracy								
δ ¹⁸ O	δ ¹⁸ O	GS IR-MS	±0.1	‰	1.453	4.231	-4.876	1.798
δD	δD	TC-EA	±0.1	‰	-104.0	-104.4	-103.7	-102.0

*An explanation of all symbols and abbreviations is included in Appendix I.

‡Mercury analyses of filtered samples with no preservation techniques applied. Complete Hg analyses in Appendix F.

Sample #			2IKP06	2IKP07	2IKP09	2IKP10		
Date collected			8/6/2008	8/9/2008	8/8/2008	8/8/2008		
Easting			0545126	0545155	0545171	0545168		
Northing			4956806	4956812	4956785	4956784		
Temperature °C (average)			74.7	84.0	88.9	79.3		
Constituents	Method	MDL*	Units					
aluminum	Al+++	ICP-AES	0.816	mg/L	0.1828	0.1356	0.337	36
boron	B+++	ICP-AES	0.055	mg/L	7.954	11.69	60.7	3.645
calcium	Ca++	ICP-AES	0.158	mg/L	31.89	30.78	19.77	7.02
iron	Fe++	ICP-AES	0.192	mg/L	0.009	0.023	0.0217	13.94
potassium	K+	ICP-AES	0.050	mg/L	14	11.24	13.1	16.9
magnesium	Mg++	ICP-AES	0.446	mg/L	15.68	12.23	11.77	3.737
sodium	Na+	ICP-AES	1.438	mg/L	34.44	18.53	30.27	12.62
silcon	Si++++	ICP-AES	1.165	mg/L	70.37	40.77	69.54	130.7
silica	SiO ₂	-----	-----	mg/L	150.52	87.21	148.75	279.57
				Accuracy				
titanium	Ti++++	ICP-MS	±0.0005	mg/L	0.0119	0.0119	0.0119	0.0121
vanadium	V	ICP-MS	±0.0005	mg/L	0.0166	0.0166	0.0166	0.0169
chromium	Cr	ICP-MS	±0.0005	mg/L	0.0076	0.0077	0.0076	0.0083
manganese	Mn++	ICP-MS	±0.0005	mg/L	0.0137	0.0088	0.0084	0.0085
cobalt	Co	ICP-MS	±0.0005	mg/L	0.0093	0.0093	0.0093	0.0094
nickel	Ni	ICP-MS	±0.0005	mg/L	0.0101	0.0101	0.0101	0.0103
zinc	Zn++	ICP-MS	±0.0005	mg/L	0.0068	0.0065	0.0064	0.0110
rubidium	Rb+	ICP-MS	±0.0005	mg/L	0.0285	0.0255	0.0162	0.0214
strontium	Sr++	ICP-MS	±0.0005	mg/L	0.1088	0.0798	0.0811	0.0631
barium	Ba++	ICP-MS	±0.0005	mg/L	0.0759	0.0735	0.0839	0.0642
lead	Pb	ICP-MS	±0.0005	mg/L	0.0027	0.0024	0.0044	0.0277
copper	Cu	ICP-MS	±0.0005	mg/L	0.0027	0.0013	0.0020	0.0010
galium	Ga+++	ICP-MS	±0.0005	mg/L	0.0009	0.0009	0.0010	0.0040
arsenic	As	ICP-MS	±0.002	mg/L	0.002	0.005	0.003	0.004
molybdenum	Mo	ICP-MS	±0.0005	mg/L	0.0006	0.0019	0.0006	0.0006
tin	Sn++++	ICP-MS	±0.0005	mg/L	0.0001	0.0001	0.0001	0.0001
antimony	Sb	ICP-MS	±0.0005	mg/L	<0.00005	0.0001	0.0001	<0.00005
tungsten	W	ICP-MS	±0.0005	mg/L	0.0008	0.0015	0.0003	<0.00005
thallium	Tl++++	ICP-MS	±0.0005	mg/L	<0.00005	<0.00005	<0.00005	0.0002
mercury ‡	Hg (T)	DMA	0.01 ng	mg/L	0.00022	0.00023	0.00018	0.00019
				RL				
pH (field average)	pH	Electrode	0.1	pH	6.06	6.15	6.00	2.94
pH (lab)	pH	Titration	-----	pH	7.4	6.7	7.2	2.0
hydroxide alkalinity	OH-	Titration	3.0	mg CaCO ₃ /L	<3	<3	<3	<3
carbonate alkalinity	CO ₃ --	Titration	3.0	mg CaCO ₃ /L	<3	<3	<3	<3
bicarbonate alkalinity	HCO ₃ -	Titration	3.0	mg CaCO ₃ /L	210	34	36	<3
total alkalinity	(HCO ₃ -)	Titration	3.0	mg CaCO ₃ /L	210	34	36	<3
fluoride	F-	IC	0.15	mg/L	NA	0.36	NA	NA
chloride	Cl-	IC	0.20	mg/L	0.36	<0.2	0.27	NA
nitrite	NO ₂ -	IC	0.050	mg/L	ND	ND	ND	NA
bromide	Br-	IC	0.10	mg/L	ND	0.12	ND	ND
nitrate	NO ₃ -	IC	0.050	mg/L	ND	<0.05	ND	ND
o-phosphate	PO ₄ ---	IC	0.10	mg/L	0.33	ND	ND	<0.1
sulfate	SO ₄ --	IC	0.20	mg/L	1300	1900	1300	3300
ammonia-N	NH ₃	FIA	0.10	mg/L	360	520	340	640
				Accuracy				
δ ¹⁸ O	δ ¹⁸ O	GS IR-MS	±0.1	‰	2.115	-2.536	-5.341	-2.262
δD	δD	TC-EA	±0.1	‰	-102.6	-110.1	-112.9	-112.3

*An explanation of all symbols and abbreviations is included in Appendix I.

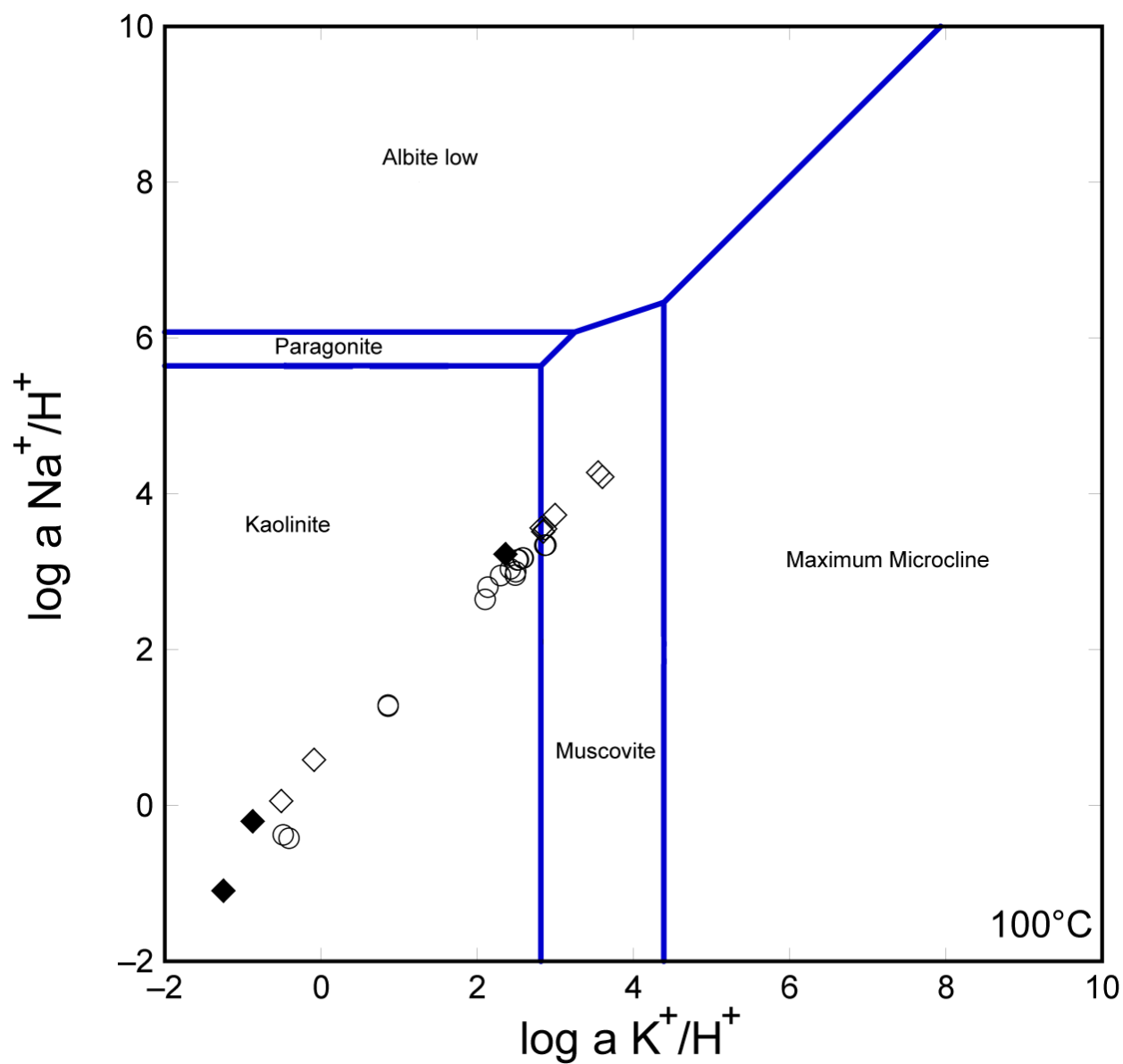
‡Mercury analyses of filtered samples with no preservation techniques applied. Complete Hg analyses in Appendix F.

Sample #					WTS01	WTS02	WTS03
Date collected					7/29/2008	7/29/2008	8/3/2008
Easting					0544430	0544460	0544263
Northing					4956125	4956194	4956501
Temperature °C (average)					38.3	33.8	68.5
Constituents		Method	MDL*	Units			
aluminum	Al+++	ICP-AES	0.816	mg/L	14.17	9.972	0.2083
boron	B+++	ICP-AES	0.055	mg/L	0.0694	0.051	0.0447
calcium	Ca++	ICP-AES	0.158	mg/L	14.7	30.34	44.31
iron	Fe++	ICP-AES	0.192	mg/L	1.733	4.538	0.0475
potassium	K+	ICP-AES	0.050	mg/L	10.37	12.59	11.31
magnesium	Mg++	ICP-AES	0.446	mg/L	9.616	12.93	16.68
sodium	Na+	ICP-AES	1.438	mg/L	8.088	34.13	48.56
silcon	Si++++	ICP-AES	1.165	mg/L	65.84	125.7	96.39
silica	SiO ₂	-----	-----	mg/L	140.83	268.87	206.18
Accuracy							
titanium	Ti++++	ICP-MS	±0.0005	mg/L	0.0119	0.0119	0.0119
vanadium	V	ICP-MS	±0.0005	mg/L	0.0166	0.0168	0.0165
chromium	Cr	ICP-MS	±0.0005	mg/L	0.0079	0.0079	0.0076
manganese	Mn++	ICP-MS	±0.0005	mg/L	0.0138	0.0195	0.0165
cobalt	Co	ICP-MS	±0.0005	mg/L	0.0094	0.0096	0.0093
nickel	Ni	ICP-MS	±0.0005	mg/L	0.0103	0.0107	0.0100
zinc	Zn++	ICP-MS	±0.0005	mg/L	0.0072	0.0078	0.0064
rubidium	Rb+	ICP-MS	±0.0005	mg/L	0.0175	0.0223	0.0216
strontium	Sr++	ICP-MS	±0.0005	mg/L	0.0860	0.1061	0.1791
barium	Ba++	ICP-MS	±0.0005	mg/L	0.0605	0.0600	0.1104
lead	Pb	ICP-MS	±0.0005	mg/L	0.0069	0.0029	0.0021
copper	Cu	ICP-MS	±0.0005	mg/L	0.0008	0.0025	0.0034
galium	Ga+++	ICP-MS	±0.0005	mg/L	0.0032	0.0013	0.0014
arsenic	As	ICP-MS	±0.002	mg/L	0.003	0.007	0.002
molybdenum	Mo	ICP-MS	±0.0005	mg/L	0.0006	0.0007	0.0006
tin	Sn++++	ICP-MS	±0.0005	mg/L	0.0001	0.0001	0.0001
antimony	Sb	ICP-MS	±0.0005	mg/L	<0.00005	0.0001	<0.00005
tungsten	W	ICP-MS	±0.0005	mg/L	<0.00005	<0.00005	0.0001
thallium	Tl++++	ICP-MS	±0.0005	mg/L	0.0001	0.0002	<0.00005
mercury ‡	Hg (T)	DMA	0.01 ng	mg/L	0.00036	0.00023	0.00021
RL							
pH (field average)	pH	Electrode	0.1	pH	2.54	2.73	5.94
pH (lab)	pH	Titration	-----	pH	2.3	2.3	7.6
hydroxide alkalinity	OH-	Titration	3.0	mg CaCO ₃ /L	<3	<3	<3
carbonate alkalinity	CO ₃ --	Titration	3.0	mg CaCO ₃ /L	<3	<3	<3
bicarbonate alkalinity	HCO ₃ -	Titration	3.0	mg CaCO ₃ /L	<3	<3	130
total alkalinity	(HCO ₃ -)	Titration	3.0	mg CaCO ₃ /L	<3	<3	130
fluoride	F-	IC	0.15	mg/L	<0.15	<0.15	<0.15
chloride	Cl-	IC	0.20	mg/L	NA	NA	1.2
nitrite	NO ₂ -	IC	0.050	mg/L	NA	NA	ND
bromide	Br-	IC	0.10	mg/L	ND	ND	ND
nitrate	NO ₃ -	IC	0.050	mg/L	ND	ND	ND
o-phosphate	PO ₄ ---	IC	0.10	mg/L	ND	ND	ND
sulfate	SO ₄ --	IC	0.20	mg/L	490	580	190
ammonia-N	NH ₃	FIA	0.10	mg/L	10	7.2	4.0
Accuracy							
δ ¹⁸ O	δ ¹⁸ O	GS IR-MS	±0.1	‰	-13.704	-15.991	-14.554
δD	δD	TC-EA	±0.1	‰	-126.6	-128.4	-129.5

*An explanation of all symbols and abbreviations is included in Appendix I.

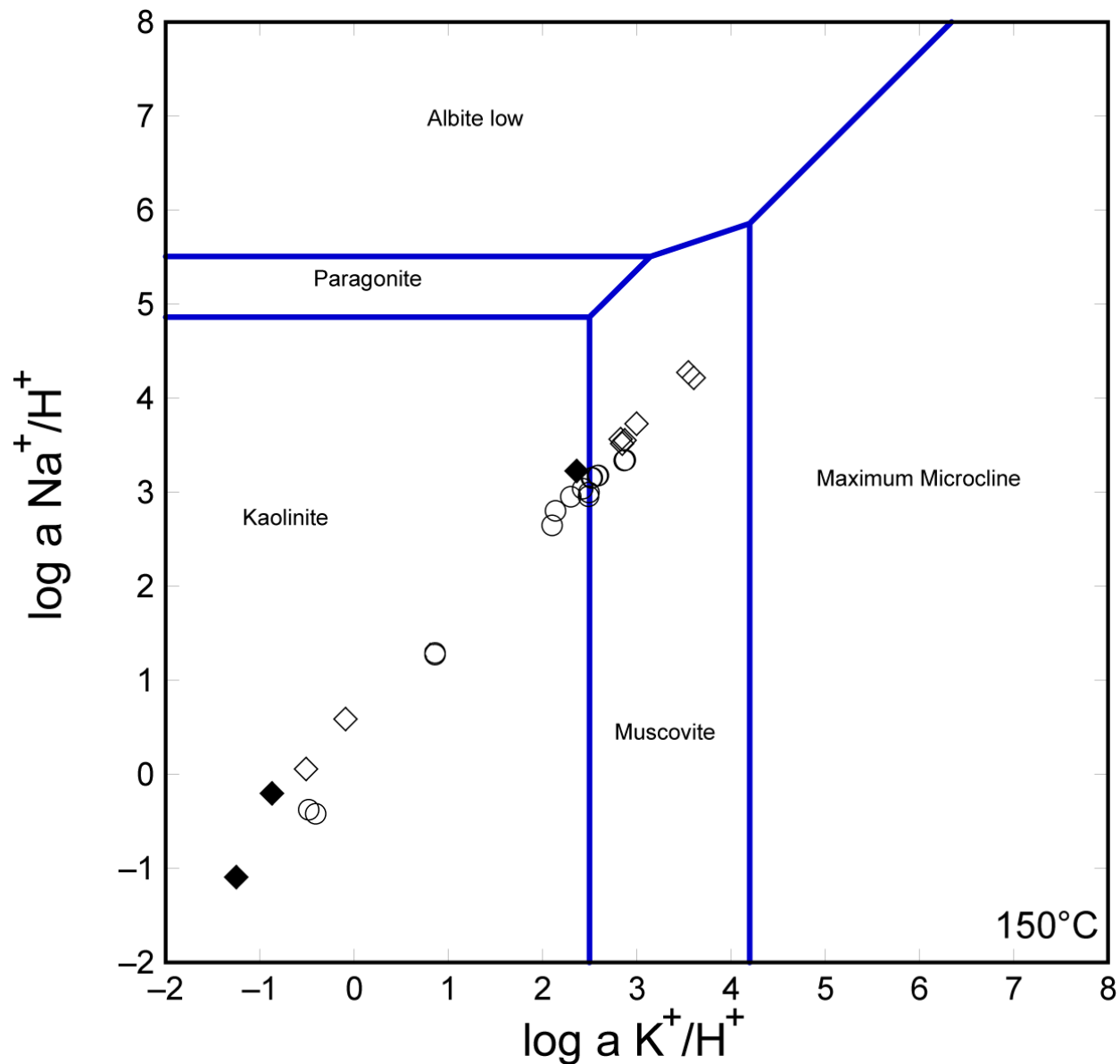
‡Mercury analyses of filtered samples with no preservation techniques applied. Complete Hg analyses in Appendix F.

APPENDIX D: Activity diagrams with Inkpot Spring fluids



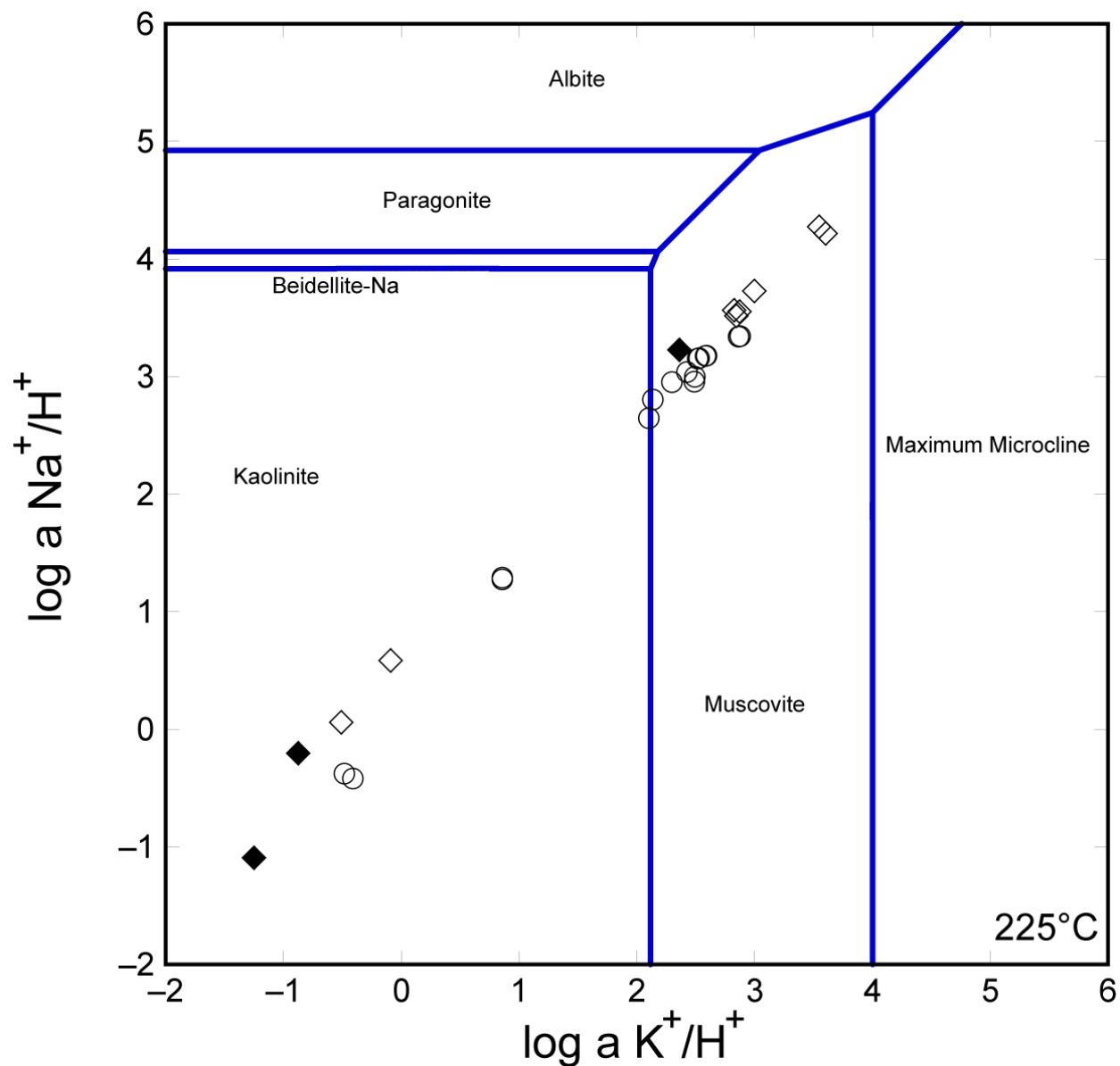
- 2008 Inkpot Spring samples. Data included in Appendix C.
- ◆ 2008 Unnamed thermal spring samples collected SW of Inkpot Spring along Howard Eaton Trail. Data included in Appendix C.
- ◇ 2003 & 2001 Washburn & Inkpot Spring water data from McCleskey et al. (2005) and Ball et al. (2007), included in Appendix B.

Figure D-1. Activity diagram showing the stability of aluminosilicate minerals in the system Na₂O-K₂O-Al₂O₃-H₂O at 100°C as a function of the activity ratios Na⁺/H⁺ and K⁺/H⁺. The diagram is constructed based on Al⁺⁺⁺ conservation. Muscovite is used as a proxy for illite in activity space. Inkpot Spring fluids are in equilibrium with kaolinite and illite.



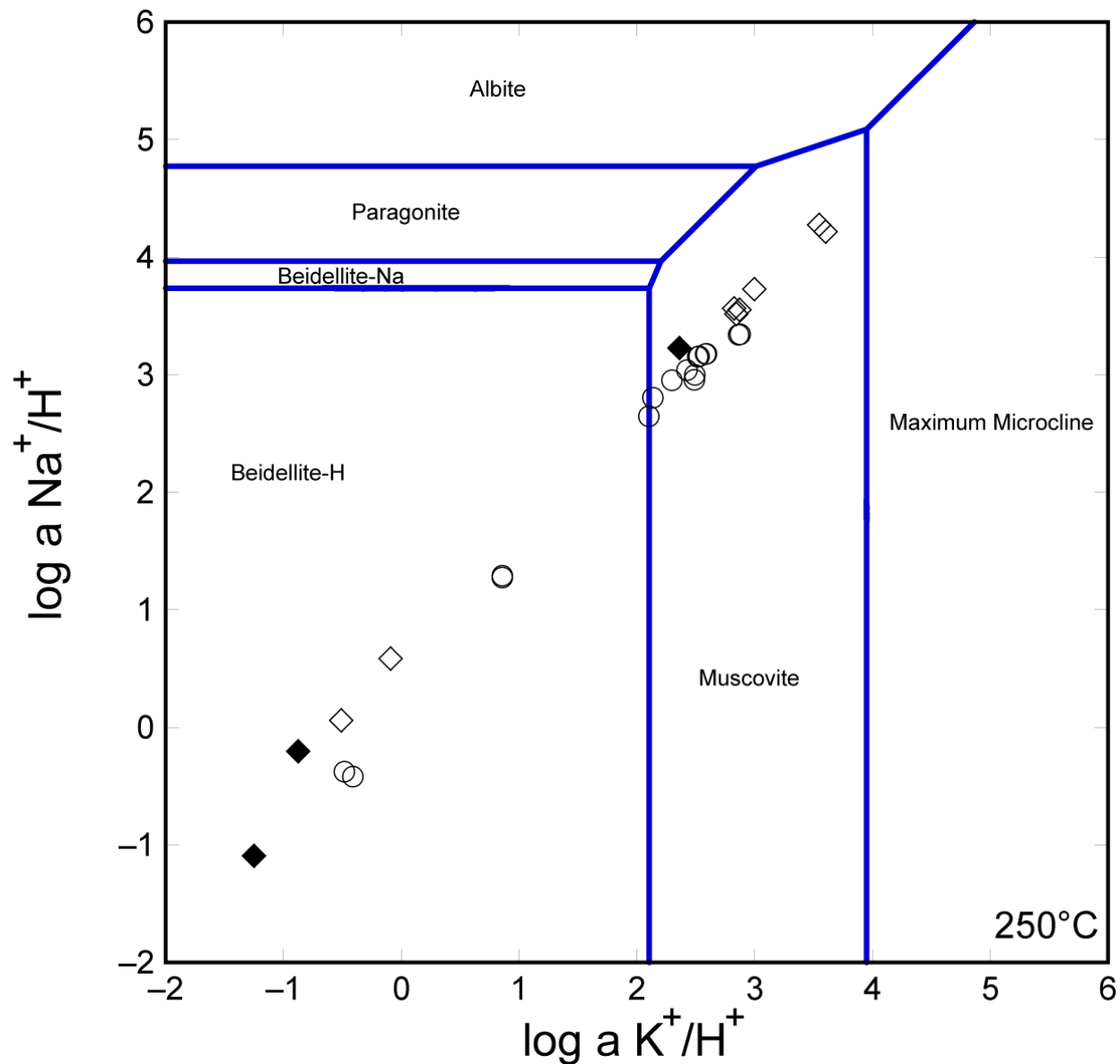
- 2008 Inkpot Spring samples. Data included in Appendix C.
- ◆ 2008 Unnamed thermal spring samples collected SW of Inkpot Spring along Howard Eaton Trail. Data included in Appendix C.
- ◇ 2003 & 2001 Washburn & Inkpot Spring water data from McCleskey et al. (2005) and Ball et al. (2007), included in Appendix B.

Figure D-2. Activity diagram showing the stability of aluminosilicate minerals in the system $\text{Na}_2\text{O}-\text{K}_2\text{O}-\text{Al}_2\text{O}_3-\text{H}_2\text{O}$ at 150°C as a function of the activity ratios Na^+/H^+ and K^+/H^+ . The diagram is constructed based on Al^{+++} conservation. Muscovite is used as a proxy for illite in activity space. Inkpot Spring fluids are in equilibrium with kaolinite and illite.



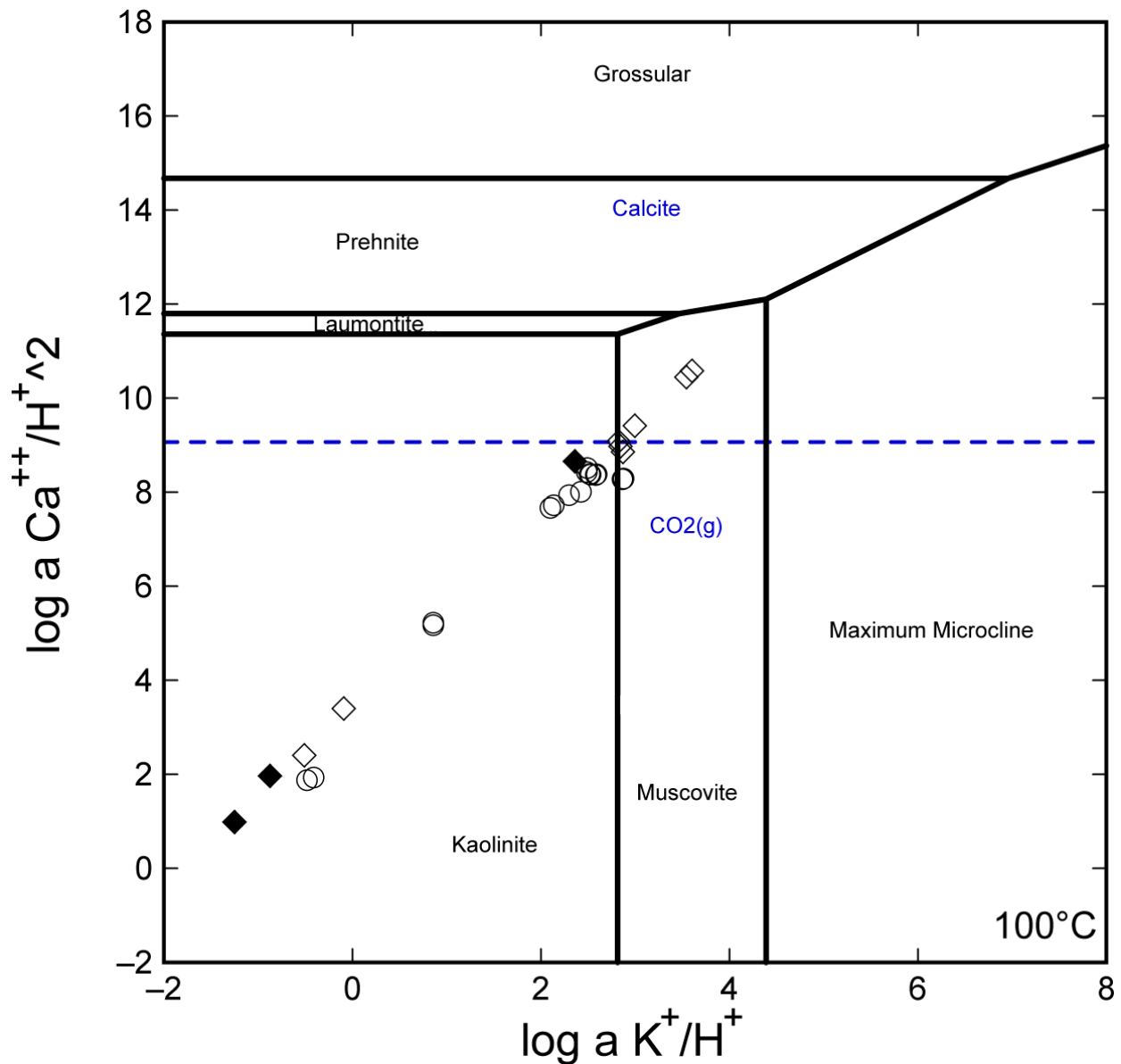
- 2008 Inkpot Spring samples. Data included in Appendix C.
- ◆ 2008 Unnamed thermal spring samples collected SW of Inkpot Spring along Howard Eaton Trail. Data included in Appendix C.
- ◇ 2003 & 2001 Washburn & Inkpot Spring water data from McCleskey et al. (2005) and Ball et al. (2007), included in Appendix B.

Figure D-3. Activity diagram showing the stability of aluminosilicate minerals in the system $\text{Na}_2\text{O}-\text{K}_2\text{O}-\text{Al}_2\text{O}_3-\text{H}_2\text{O}$ at 225°C as a function of the activity ratios Na^+/H^+ and K^+/H^+ . The diagram is constructed based on Al^{+++} conservation. Muscovite is used as a proxy for illite in activity space. Inkpot Spring fluids are in equilibrium with kaolinite and illite.



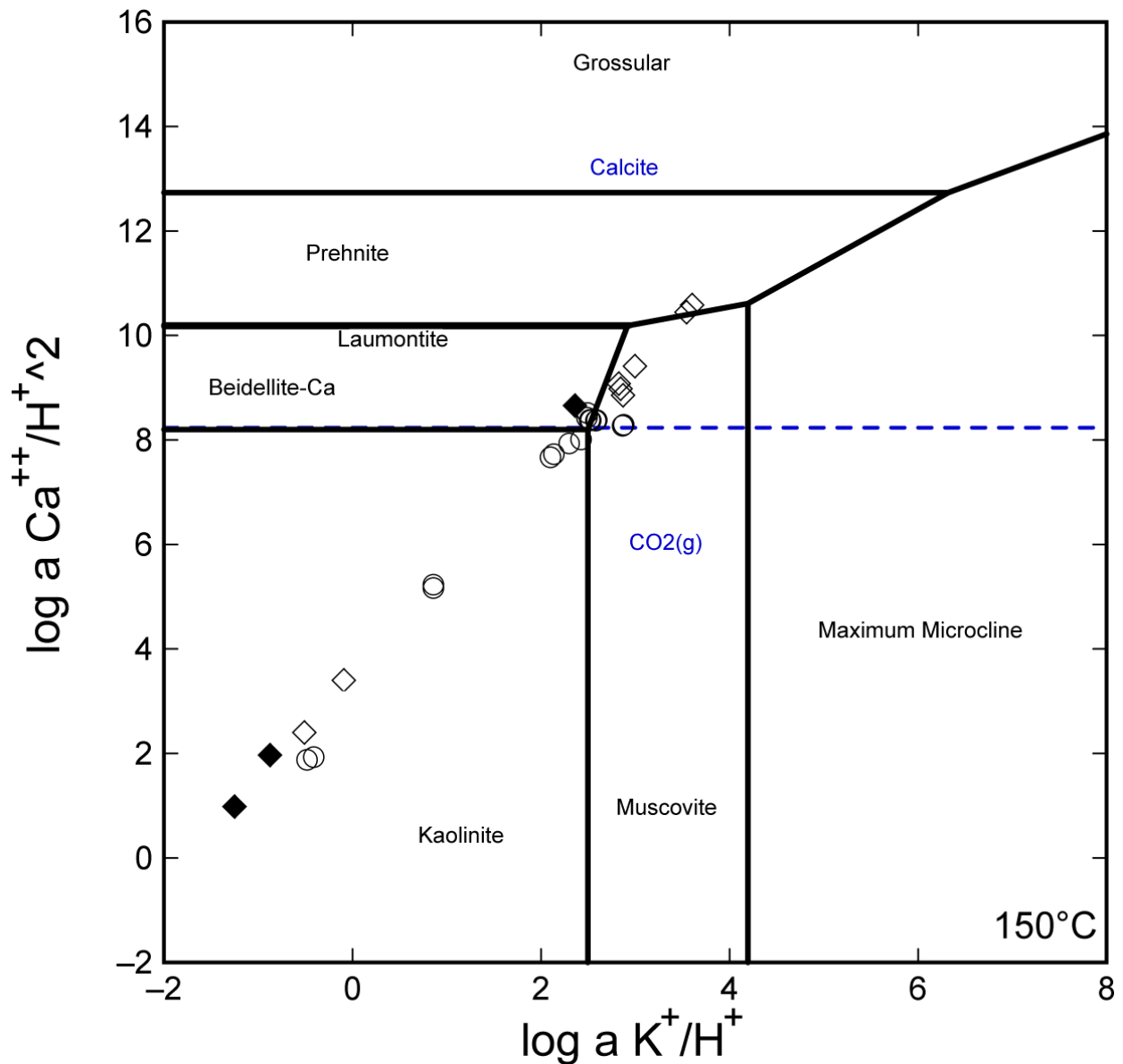
- 2008 Inkpot Spring samples. Data included in Appendix C.
- ◆ 2008 Unnamed thermal spring samples collected SW of Inkpot Spring along Howard Eaton Trail. Data included in Appendix C.
- ◇ 2003 & 2001 Washburn & Inkpot Spring water data from McCleskey et al. (2005) and Ball et al. (2007), included in Appendix B.

Figure D-4. Activity diagram showing the stability of aluminosilicate minerals in the system $\text{Na}_2\text{O}-\text{K}_2\text{O}-\text{Al}_2\text{O}_3-\text{H}_2\text{O}$ at 250°C as a function of the activity ratios Na^+/H^+ and K^+/H^+ . The diagram is constructed based on Al^{+++} conservation. Muscovite is used as a proxy for illite in activity space. Inkpot Spring fluids are in equilibrium with beidellite (montmorillonite) and illite.



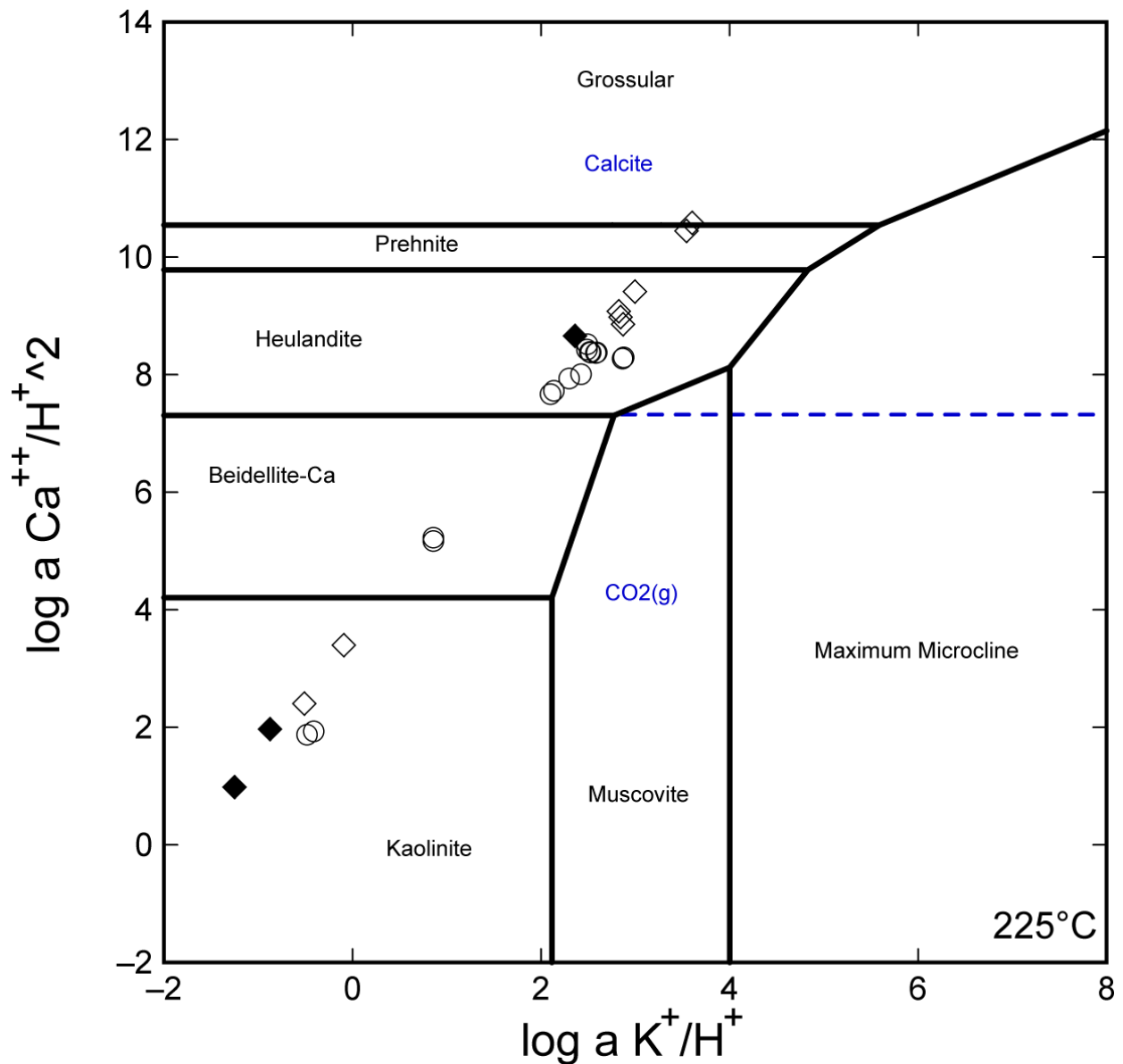
- 2008 Inkpot Spring samples. Data included in Appendix C.
- ◆ 2008 Unnamed thermal spring samples collected SW of Inkpot Spring along Howard Eaton Trail. Data included in Appendix C.
- ◇ 2003 & 2001 Washburn & Inkpot Spring water data from McCleskey et al. (2005) and Ball et al. (2007), included in Appendix B.

Figure D-5. Activity diagram showing the stability of aluminosilicate minerals in the system CaO-Al₂O₃-K₂O-H₂O at 100°C as a function of the activity ratios Ca⁺⁺/H⁺² and K⁺/H⁺. The diagram is constructed based on Al⁺⁺⁺ conservation. Muscovite is used as a proxy for illite in activity space. Inkpot Spring fluids are in equilibrium with kaolinite and illite. Ca⁺⁺ activity may be explained by equilibrium with calcite, gypsum, or anorthitic plagioclase.



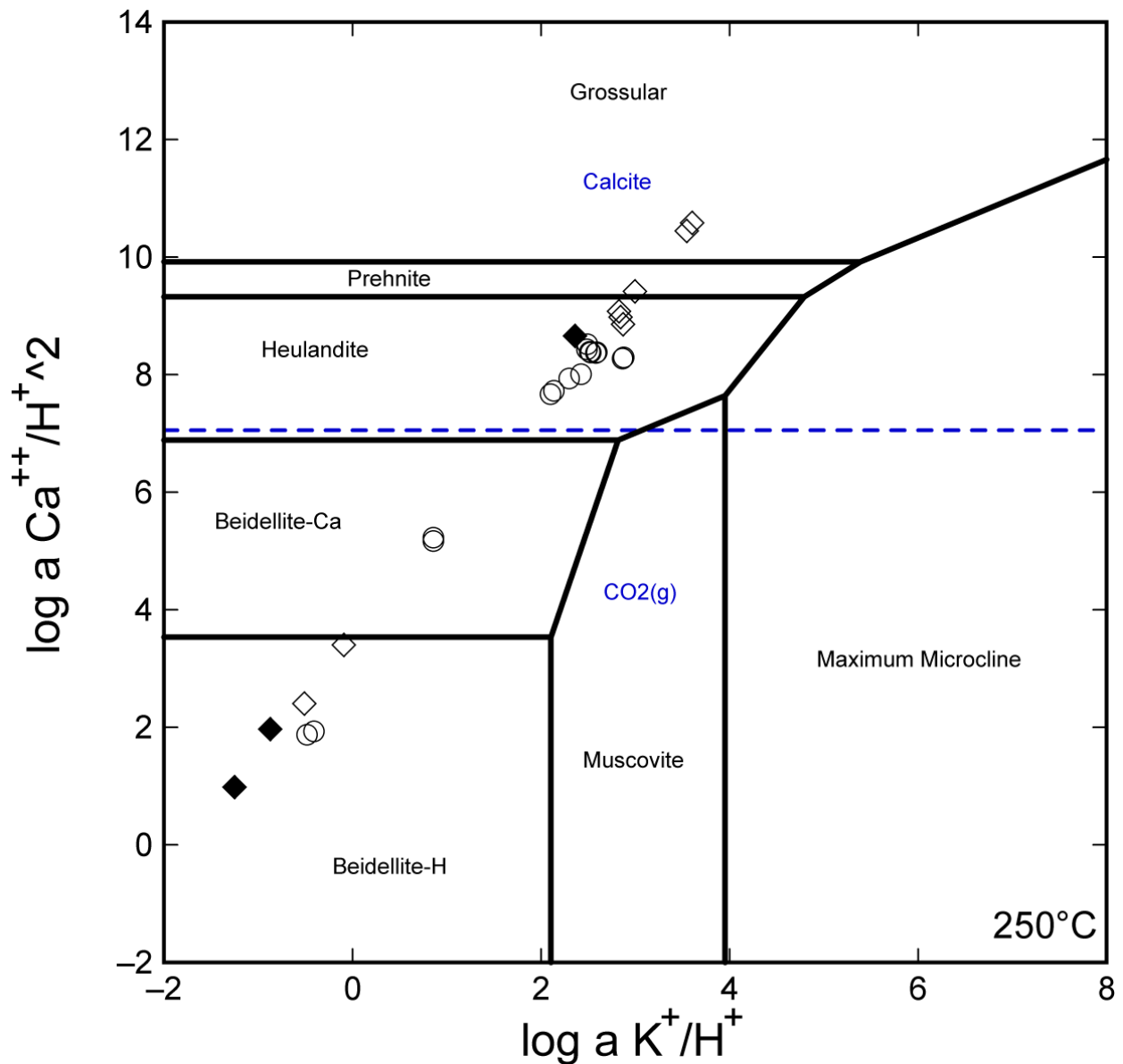
- 2008 Inkpot Spring samples. Data included in Appendix C.
- ◆ 2008 Unnamed thermal spring samples collected SW of Inkpot Spring along Howard Eaton Trail. Data included in Appendix C.
- ◇ 2003 & 2001 Washburn & Inkpot Spring water data from McCleskey et al. (2005) and Ball et al. (2007), included in Appendix B.

Figure D-6. Activity diagram showing the stability of aluminosilicate minerals in the system CaO-Al₂O₃-K₂O-H₂O at 150°C as a function of the activity ratios $\text{Ca}^{++}/\text{H}^{+2}$ and $\text{K}^{+}/\text{H}^{+}$. The diagram is constructed based on Al⁺⁺⁺ conservation. Muscovite is used as a proxy for illite in activity space. Inkpot Spring fluids are in equilibrium with kaolinite, beidellite (Ca-montmorillonite), and illite. Ca⁺⁺ activity may be explained by equilibrium with calcite, gypsum, or anorthitic plagioclase.



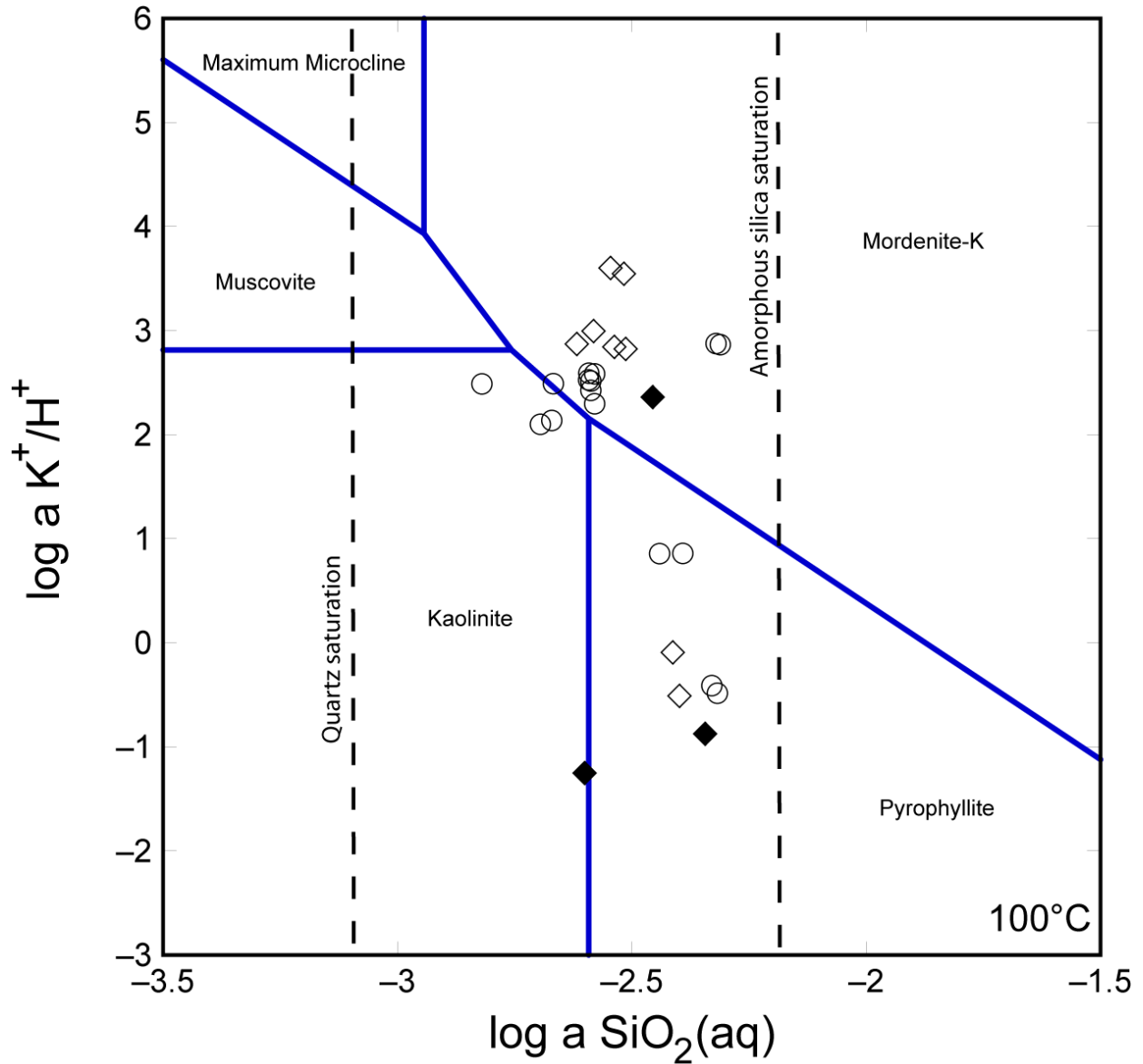
- 2008 Inkpot Spring samples. Data included in Appendix C.
- ◆ 2008 Unnamed thermal spring samples collected SW of Inkpot Spring along Howard Eaton Trail. Data included in Appendix C.
- ◇ 2003 & 2001 Washburn & Inkpot Spring water data from McCleskey et al. (2005) and Ball et al. (2007), included in Appendix B.

Figure D-7. Activity diagram showing the stability of aluminosilicate minerals in the system CaO-Al₂O₃-K₂O-H₂O at 225°C as a function of the activity ratios Ca⁺⁺/H⁺² and K⁺/H⁺. The diagram is constructed based on Al⁺⁺⁺ conservation. Muscovite is used as a proxy for illite in activity space. Inkpot Spring fluids are in equilibrium with kaolinite and beidellite (Ca-montmorillonite) and possibly heulandite. Instead of equilibrium with heulandite, Ca⁺⁺ activity may be better explained by equilibrium with calcite, gypsum, or anorthitic plagioclase.



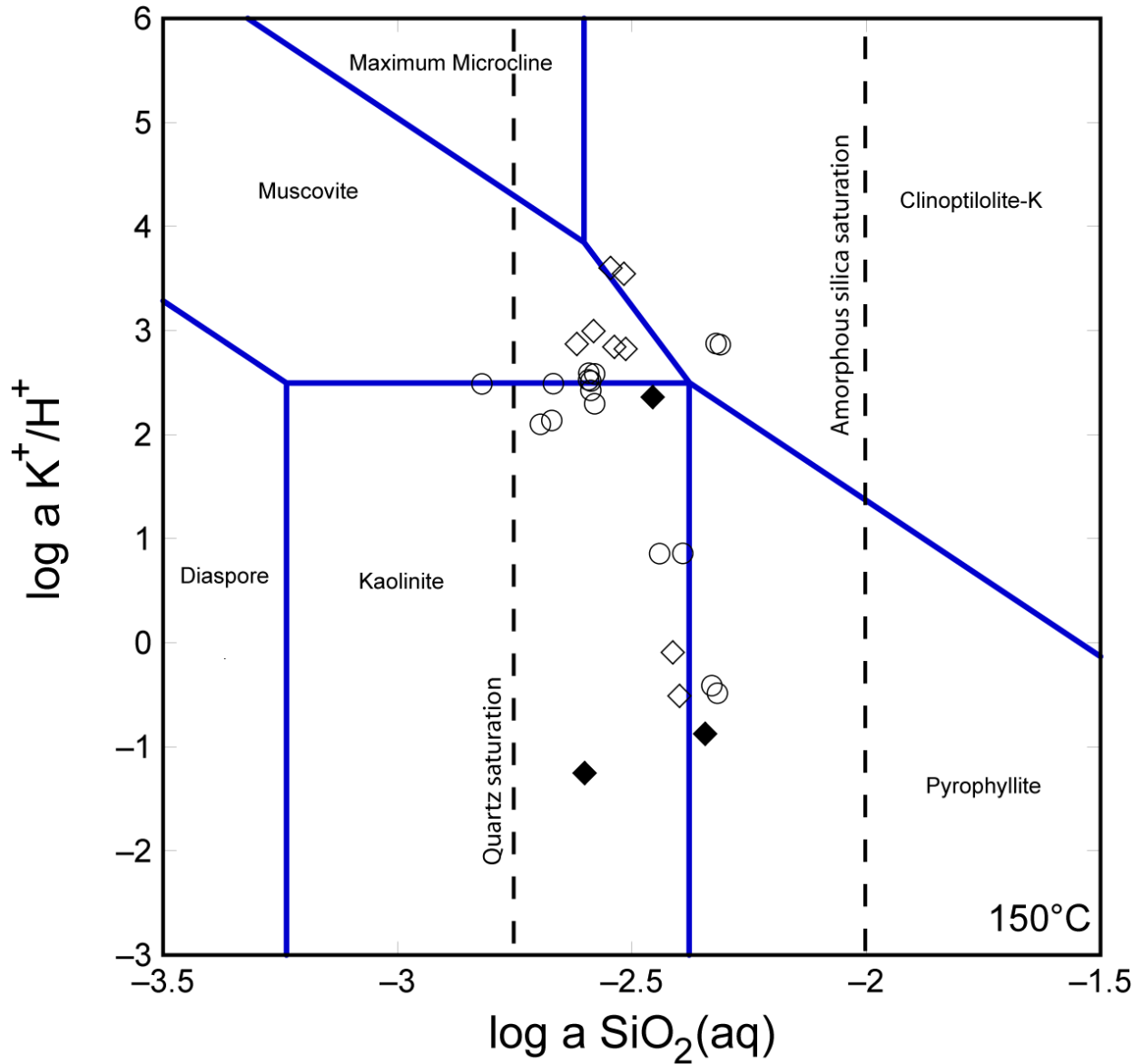
- 2008 Inkpot Spring samples. Data included in Appendix C.
- ◆ 2008 Unnamed thermal spring samples collected SW of Inkpot Spring along Howard Eaton Trail. Data included in Appendix C.
- ◇ 2003 & 2001 Washburn & Inkpot Spring water data from McCleskey et al. (2005) and Ball et al. (2007), included in Appendix B.

Figure D-8. Activity diagram showing the stability of aluminosilicate minerals in the system CaO-Al₂O₃-K₂O-H₂O at 250°C as a function of the activity ratios $\text{Ca}^{++}/\text{H}^{+2}$ and $\text{K}^{+}/\text{H}^{+}$. The diagram is constructed based on Al⁺⁺⁺ conservation. Muscovite is used as a proxy for illite in activity space. Inkpot Spring fluids are in equilibrium with beidellite (montmorillonite) and possibly heulandite. Instead of equilibrium with heulandite, Ca⁺⁺ activity may be better explained by equilibrium with calcite, gypsum, or anorthitic plagioclase.



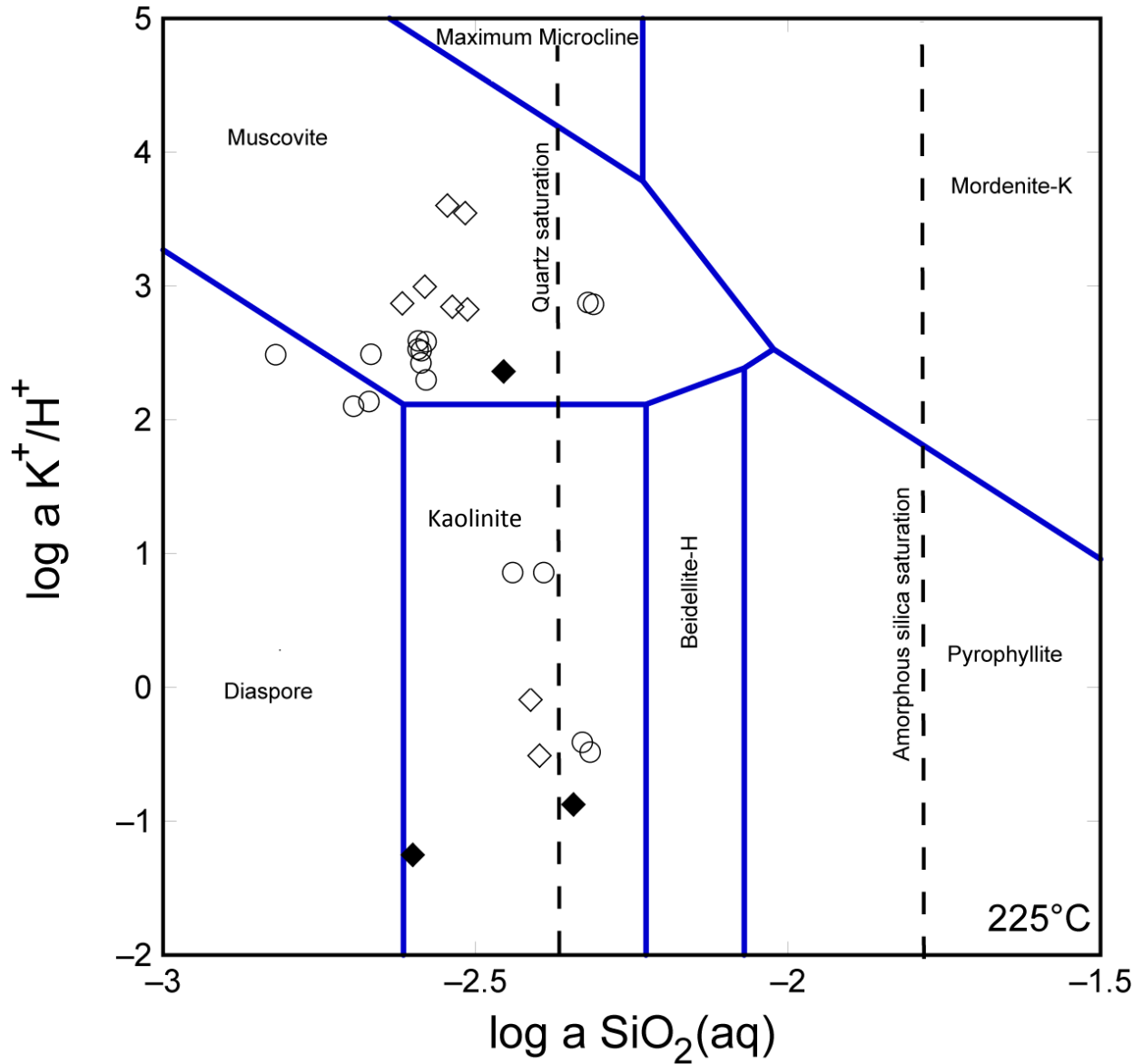
- 2008 Inkpot Spring samples. Data included in Appendix C.
- ◆ 2008 Unnamed thermal spring samples collected SW of Inkpot Spring along Howard Eaton Trail. Data included in Appendix C.
- ◇ 2003 & 2001 Washburn & Inkpot Spring water data from McCleskey et al. (2005) and Ball et al. (2007), included in Appendix B.

Figure D-9. Activity diagram showing the stability of aluminosilicate minerals in the system $\text{Al}_2\text{O}_3\text{-K}_2\text{O-SiO}_2\text{-H}_2\text{O}$ at 100°C as a function of the activity ratio K^+/H^+ and the activity of SiO_2 (aqueous). The diagram is constructed based on Al^{+++} conservation. Muscovite is used as a proxy for illite in activity space. Inkpot Spring fluids are in equilibrium with kaolinite and pyrophyllite and possibly mordenite. At 100°C fluids are saturated with respect to quartz.



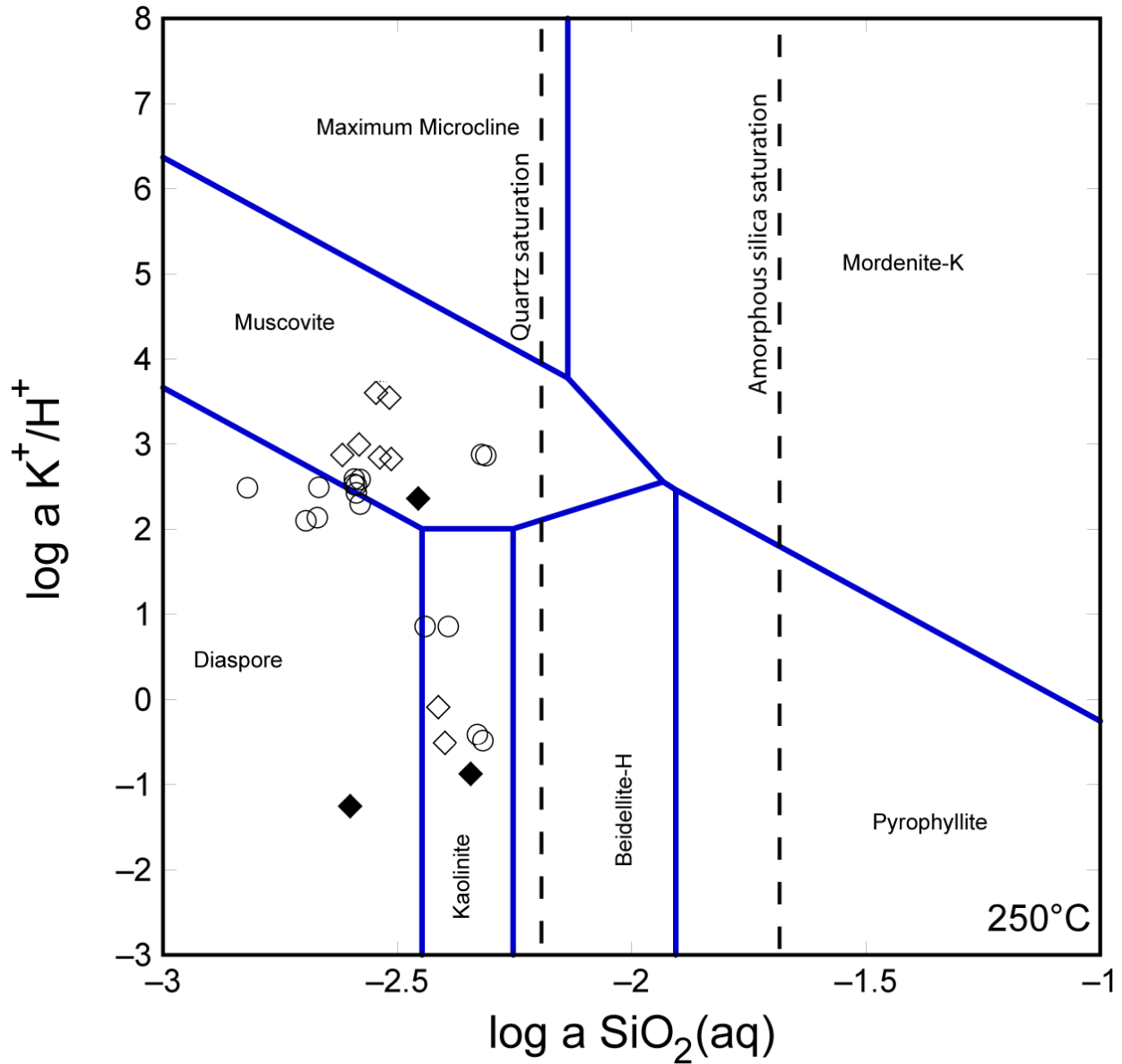
- 2008 Inkpot Spring samples. Data included in Appendix C.
- ◆ 2008 Unnamed thermal spring samples collected SW of Inkpot Spring along Howard Eaton Trail. Data included in Appendix C.
- ◇ 2003 & 2001 Washburn & Inkpot Spring water data from McCleskey et al. (2005) and Ball et al. (2007), included in Appendix B.

Figure D-10. Activity diagram showing the stability of aluminosilicate minerals in the system $\text{Al}_2\text{O}_3\text{-K}_2\text{O-SiO}_2\text{-H}_2\text{O}$ at 150°C as a function of the activity ratio K^+/H^+ and the activity of SiO_2 (aqueous). The diagram is constructed based on Al^{+++} conservation. Muscovite is used as a proxy for illite in activity space. Inkpot Spring fluids are in equilibrium with kaolinite, illite, pyrophyllite, and clinoptilolite. At 150°C fluids are saturated with respect to quartz.



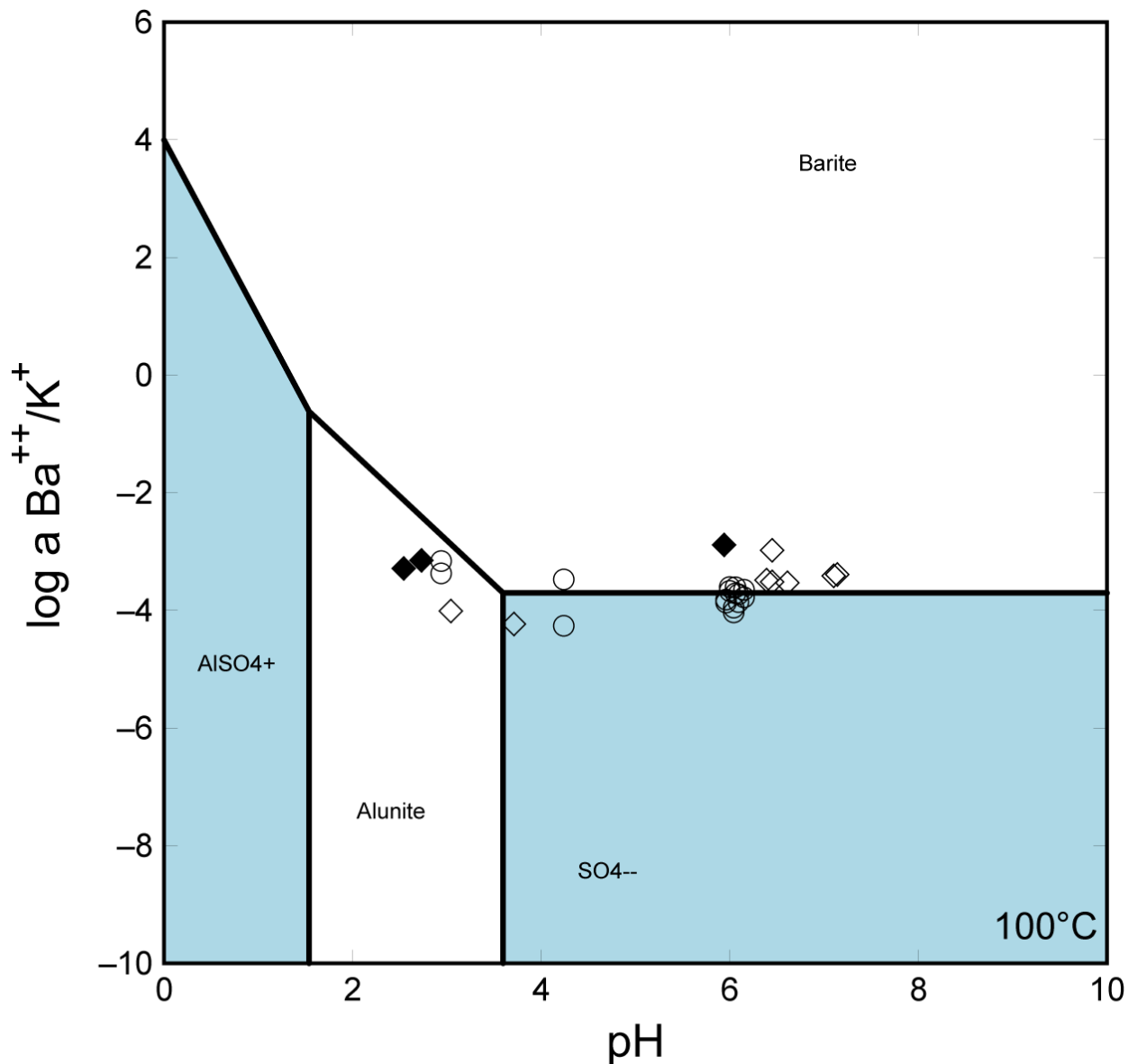
- 2008 Inkpot Spring samples. Data included in Appendix C.
- ◆ 2008 Unnamed thermal spring samples collected SW of Inkpot Spring along Howard Eaton Trail. Data included in Appendix C.
- ◇ 2003 & 2001 Washburn & Inkpot Spring water data from McCleskey et al. (2005) and Ball et al. (2007), included in Appendix B.

Figure D-11. Activity diagram showing the stability of aluminosilicate minerals in the system $\text{Al}_2\text{O}_3\text{-K}_2\text{O-SiO}_2\text{-H}_2\text{O}$ at 225°C as a function of the activity ratio K^+/H^+ and the activity of SiO_2 (aqueous). The diagram is constructed based on Al^{+++} conservation. Muscovite is used as a proxy for illite in activity space. Inkpot Spring fluids are in equilibrium with kaolinite and illite and possibly diaspore. At 225°C fluids are at or slightly below quartz saturation



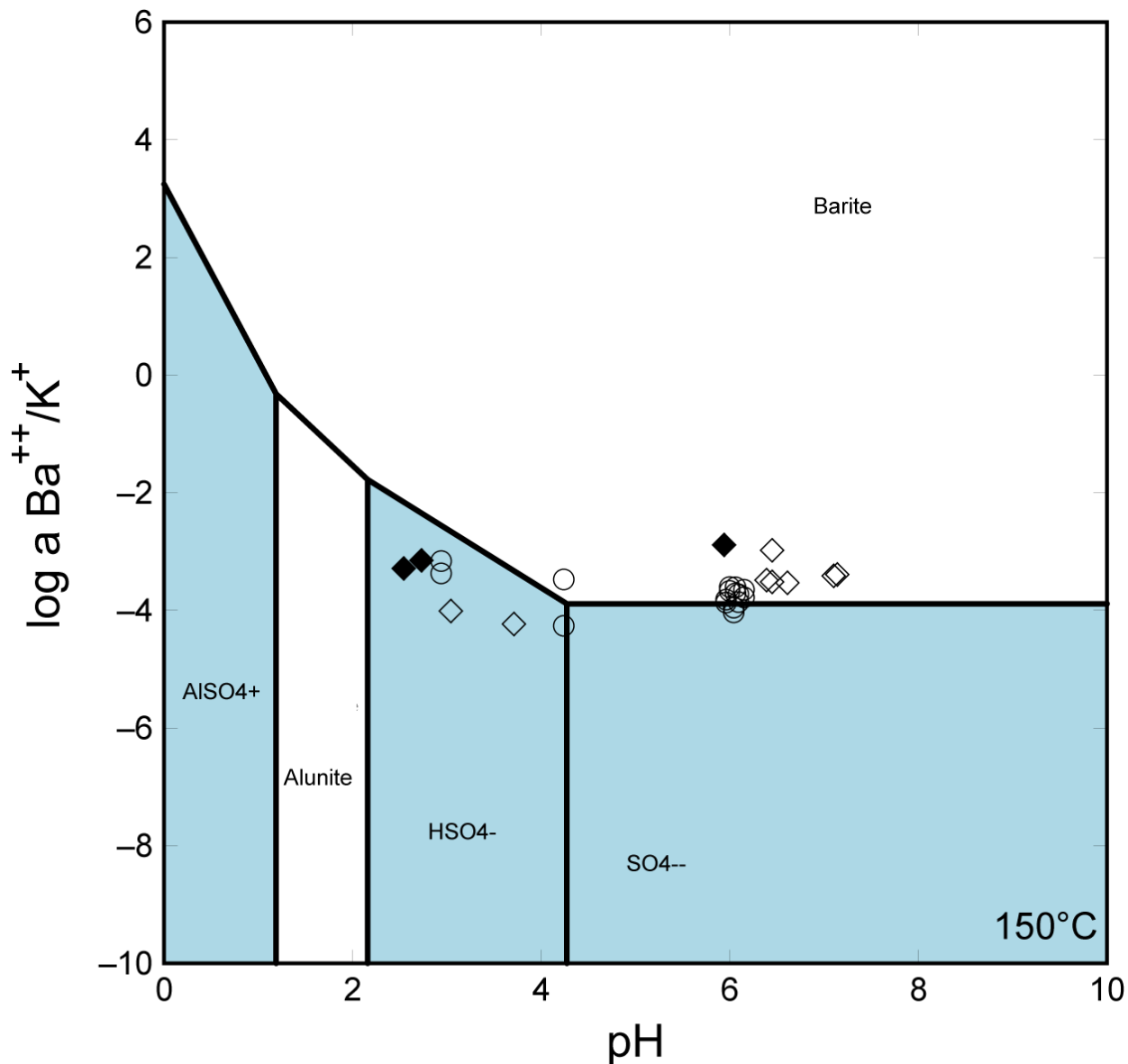
- 2008 Inkpot Spring samples. Data included in Appendix C.
- ◆ 2008 Unnamed thermal spring samples collected SW of Inkpot Spring along Howard Eaton Trail. Data included in Appendix C.
- ◇ 2003 & 2001 Washburn & Inkpot Spring water data from McCleskey et al. (2005) and Ball et al. (2007), included in Appendix B.

Figure D-12. Activity diagram showing the stability of aluminosilicate minerals in the system $\text{Al}_2\text{O}_3\text{-K}_2\text{O-SiO}_2\text{-H}_2\text{O}$ at 250°C as a function of the activity ratio K^+/H^+ and the activity of SiO_2 (aqueous). The diagram is constructed based on Al^{+++} conservation. Muscovite is used as a proxy for illite in activity space. Inkpot Spring fluids are in equilibrium with kaolinite, illite, and diaspore. At 250°C fluids are below quartz saturation.



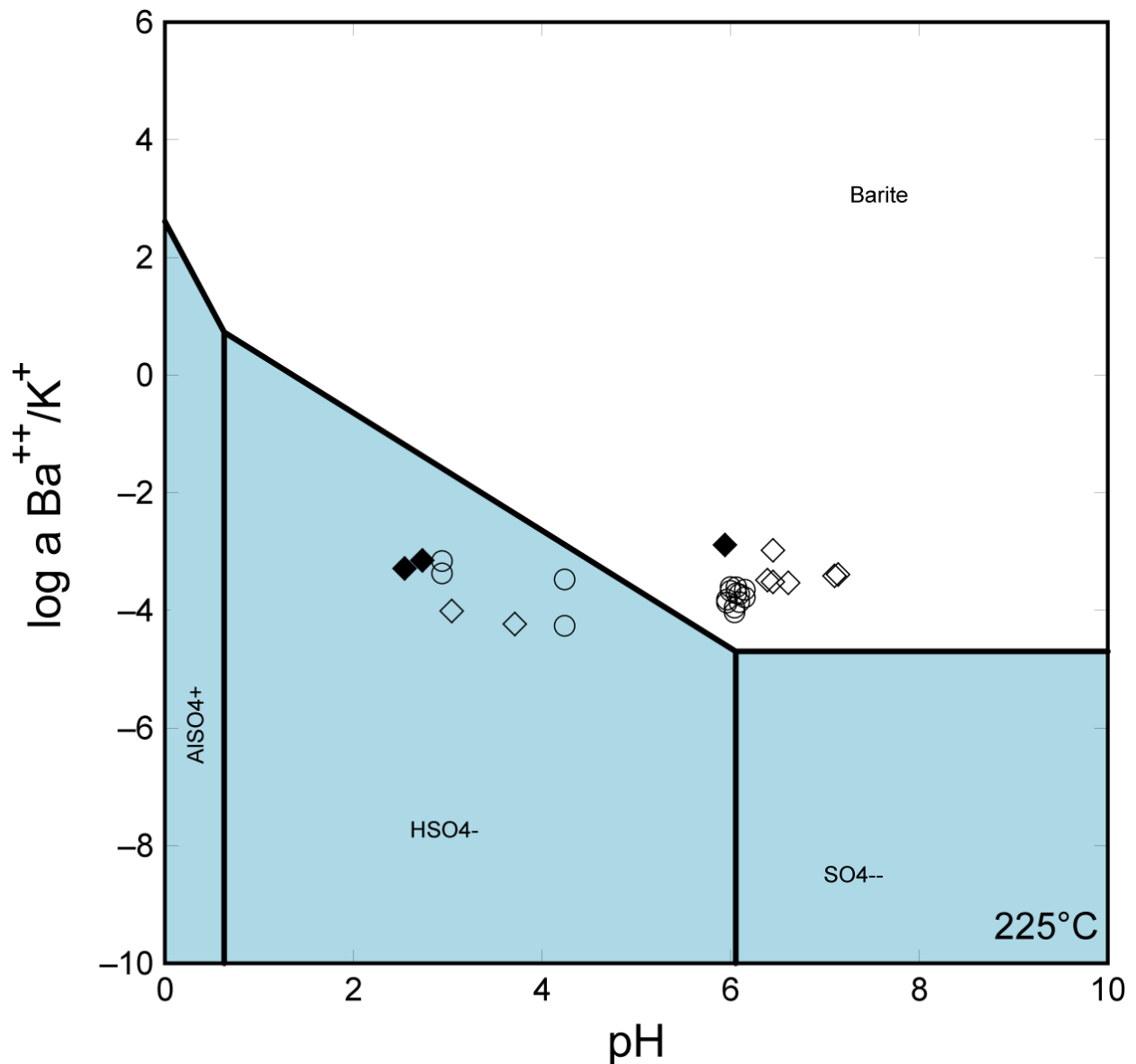
○ 2008 Inkpot Spring samples. Data included in Appendix C.
 ◆ 2008 Unnamed thermal spring samples collected SW of Inkpot Spring along Howard Eaton Trail. Data included in Appendix C.
 ◇ 2003 & 2001 Washburn & Inkpot Spring water data from McCleskey et al. (2005) and Ball et al. (2007), included in Appendix B.

Figure D-13. Activity diagram showing the stability of sulfate species as a function of pH and Ba^{++}/K^+ . Diagram calculated for a temperature of 100°C, with an average $\log SO_4^{2-}$ activity of -2.2483, average $\log K^+$ activity of -3.5562, activity of silica set by cristobalite, and activity of Al^{+++} is fixed by kaolinite. Fields shaded blue are species in solution. Inkpot Spring fluids appear to be at or close to equilibrium with barite and some pools are in equilibrium with alunite. Ba^{++} activity is probably controlled by walthierite and not barite. Walthierite is a Ba-rich sulfate abundant in sediment around the pools. If neutralizing effect of ammonia is ignored, all fluids would plot near alunite/walthierite stability.



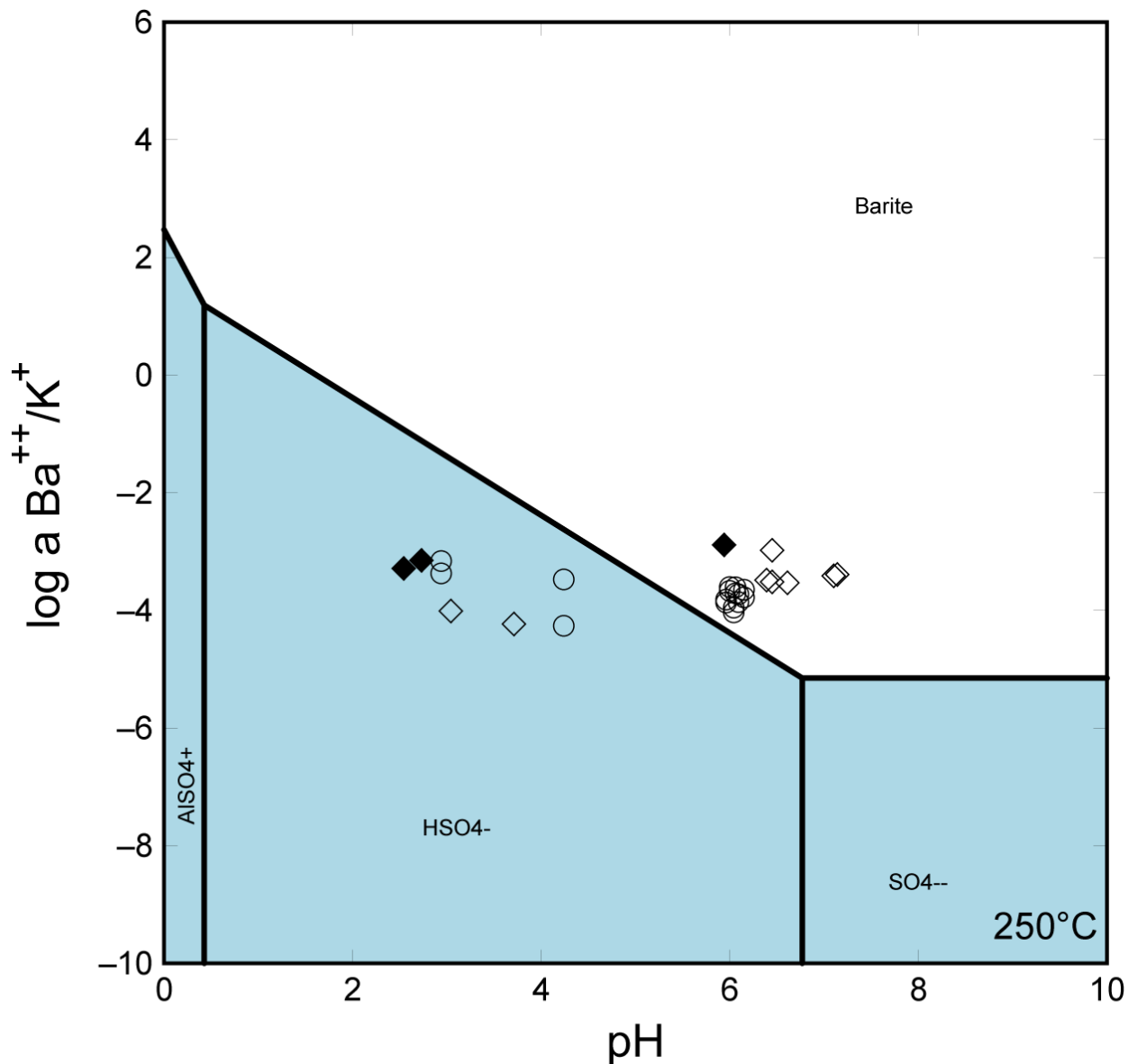
- 2008 Inkpot Spring samples. Data included in Appendix C.
- ◆ 2008 Unnamed thermal spring samples collected SW of Inkpot Spring along Howard Eaton Trail. Data included in Appendix C.
- ◇ 2003 & 2001 Washburn & Inkpot Spring water data from McCleskey et al. (2005) and Ball et al. (2007), included in Appendix B.

Figure D-14. Activity diagram showing the stability of sulfate species as a function of pH and $\text{Ba}^{++}/\text{K}^+$. Diagram calculated for a temperature of 150°C, with an average $\log \text{SO}_4^{2-}$ activity of -2.2483, average $\log \text{K}^+$ activity of -3.5562, activity of silica set by cristobalite, and activity of Al^{+++} is fixed by kaolinite. Fields shaded blue are species in solution. Inkpot Spring fluids appear to be at or close to equilibrium with barite and alunite. Ba^{++} activity is probably controlled by walthierite and not barite. Walthierite is a Ba-rich sulfate abundant in sediment around the pools.



- 2008 Inkpot Spring samples. Data included in Appendix C.
- ◆ 2008 Unnamed thermal spring samples collected SW of Inkpot Spring along Howard Eaton Trail. Data included in Appendix C.
- ◇ 2003 & 2001 Washburn & Inkpot Spring water data from McCleskey et al. (2005) and Ball et al. (2007), included in Appendix B.

Figure D-15. Activity diagram showing the stability of sulfate species as a function of pH and $\text{Ba}^{++}/\text{K}^+$. Diagram calculated for a temperature of 225°C, with an average $\log \text{SO}_4^{2-}$ activity of -2.2483, average $\log \text{K}^+$ activity of -3.5562, activity of silica set by cristobalite, and activity of Al^{+++} is fixed by kaolinite. Fields shaded blue are species in solution. Inkpot Spring fluids appear to be at or close to equilibrium with barite. Ba^{++} activity is probably controlled by walthierite and not barite. Walthierite is a Ba-rich sulfate abundant in sediment around the pools. Alunite is not stable in this system at 225°C.



- 2008 Inkpot Spring samples. Data included in Appendix C.
- ◆ 2008 Unnamed thermal spring samples collected SW of Inkpot Spring along Howard Eaton Trail. Data included in Appendix C.
- ◇ 2003 & 2001 Washburn & Inkpot Spring water data from McCleskey et al. (2005) and Ball et al. (2007), included in Appendix B.

Figure D-16. Activity diagram showing the stability of sulfate species as a function of pH and $\text{Ba}^{++}/\text{K}^+$. Diagram calculated for a temperature of 250°C, with an average $\log \text{SO}_4^{2-}$ activity of -2.2483, average $\log \text{K}^+$ activity of -3.5562, activity of silica set by cristobalite, and activity of Al^{+++} is fixed by kaolinite. Fields shaded blue are species in solution. Inkpot Spring fluids appear to be at or close to equilibrium with barite. Ba^{++} activity is probably controlled by walthierite and not barite. Walthierite is a Ba-rich sulfate abundant in sediment around the pools. Alunite is not stable in this system at 250°C.

**APPENDIX E: Geochemical data from sediment collected around Inkpot Spring
pools from July 26, 2008 to August 9, 2008**

Inkpot Spring, Yellowstone National Park

ELEMENT	METHOD*	UNITS	IKP01	IKP02	IKP03a	IKP03b	IKP04	IKP05	IKP06	IKP07	IKP09	IKP10a	IKP10b	IKP11	YS07AA15 [‡]
Ag	ME-MS41	ppm	0.07	0.09	0.07	0.07	0.09	0.07	0.07	0.04	0.08	0.08	0.04	0.05	0.04
Al	ME-MS41	%	0.85	0.78	0.73	0.45	1.22	1.01	1.22	1.47	0.23	1.6	0.84	0.62	0.73
As	ME-MS41	ppm	3.1	3.4	2.9	5.9	5.6	3.1	3	2.7	2.5	5.6	1.8	2.5	2.5
Au	Au-ICP21	ppm	0.004	0.023	0.004	0.016	0.003	0.005	0.003	0.004	0.002	0.001	0.003	0.003	0.001
Au	ME-MS41	ppm	<0.2	<0.2	<0.2	<0.2	<0.2	<0.2	<0.2	<0.2	<0.2	<0.2	<0.2	<0.2	<0.2
B	ME-MS41	ppm	<10	<10	<10	<10	10	<10	<10	30	<10	10	<10	<10	10
Ba	ME-MS41	ppm	230	280	280	120	20	130	170	70	<10	<10	110	10	290
Be	ME-MS41	ppm	0.32	0.2	0.44	0.27	0.21	0.9	0.36	0.3	0.05	0.97	0.27	0.13	0.23
Bi	ME-MS41	ppm	0.15	0.2	0.23	0.22	0.4	0.15	0.13	0.13	0.22	0.3	0.1	0.1	0.12
Ca	ME-MS41	%	0.04	0.02	0.1	0.04	0.03	0.15	0.06	0.03	0.01	0.07	0.02	0.03	0.03
Cd	ME-MS41	ppm	0.04	0.05	0.04	0.02	0.14	0.07	0.04	0.03	0.06	0.22	0.09	0.12	0.02
Ce	ME-MS41	ppm	40.9	16.8	21.5	27.1	20.2	64.1	42.2	64.1	7.89	40.9	15.6	12.2	33.7
Co	ME-MS41	ppm	3.6	6	0.5	1.9	13.3	5.6	6.1	1.9	4.9	24.3	4.5	12	2.7
Cr	ME-MS41	ppm	25	25	6	11	39	16	36	35	7	30	16	11	20
Cs	ME-MS41	ppm	0.32	0.19	0.61	0.52	0.37	0.48	0.41	0.5	0.09	0.54	0.21	0.07	0.33
Cu	ME-MS41	ppm	13.7	11	6.9	10.9	21	12.3	18.6	12.9	11.3	15.7	6.8	14.2	10.7
Fe	ME-MS41	%	1.1	0.94	0.51	0.87	2.65	1.1	1.29	0.61	0.81	7.54	1.55	3.63	0.73
Ga	ME-MS41	ppm	3.94	2.93	2.53	2.4	4.54	4.42	4.84	5.59	3.26	2.46	2.62	2.49	3.53
Ge	ME-MS41	ppm	0.07	<0.05	0.12	0.11	0.07	0.1	0.07	0.08	<0.05	0.15	<0.05	0.06	0.05
Hf	ME-MS41	ppm	0.57	0.34	0.19	0.25	0.91	0.9	0.45	0.83	2.06	0.38	0.36	0.36	0.3
Hg	ME-MS41	ppm	39.2	61.1	235	122.5	30.3	16.85	38.5	12.3	30.8	16.2	21.7	21.9	32.3
Hg	DMA	ppm	25.44	46.14	>DL	98.56	23.99	13.90	49.52	11.58	34.36	18.26	15.49	17.64	34.39
In	ME-MS41	ppm	0.032	0.026	<0.005	<0.005	0.065	0.054	0.034	0.091	0.037	0.03	0.048	0.036	0.027
K	ME-MS41	%	0.09	0.09	0.11	0.12	0.08	0.09	0.09	0.07	0.05	0.06	0.07	0.05	0.06
La	ME-MS41	ppm	21.2	10.2	11.8	15.2	12	32.4	21.8	31.5	5.2	20	11.3	8.7	17.8
Li	ME-MS41	ppm	5.1	1.8	5.6	5.6	2.3	6.4	8.4	3.6	0.6	7.2	1.8	1.3	6.1
Mg	ME-MS41	%	0.06	0.05	0.02	0.03	0.04	0.13	0.07	0.05	0.01	0.09	0.03	0.02	0.04
Mn	ME-MS41	ppm	73	85	43	64	41	84	73	24	45	91	56	73	31
Mo	ME-MS41	ppm	0.64	0.41	0.8	1.35	0.88	0.56	0.55	0.59	0.9	0.6	0.42	0.99	0.46
Na	ME-MS41	%	0.03	0.02	0.03	0.01	0.02	0.04	0.02	0.02	0.02	0.02	0.02	0.03	0.01
Nb	ME-MS41	ppm	0.87	0.41	0.72	0.85	0.82	0.31	0.68	2.69	0.75	0.35	0.33	0.39	1.42
Ni	ME-MS41	ppm	13	24.7	3.1	6.9	51.5	18.5	19.3	7.1	16.2	91.3	21.1	50.7	8.6
P	ME-MS41	ppm	130	60	40	30	90	100	210	150	30	40	50	50	150
Pb	ME-MS41	ppm	16.5	23.9	14.9	29.6	32.4	18.5	15	15.7	23	20.9	20.4	31	13.1
Rb	ME-MS41	ppm	4.2	4.6	9.3	9.5	4.8	6.7	4.2	4.7	1.9	5.6	3.6	1.6	4.2
Re	ME-MS41	ppm	<0.001	<0.001	<0.001	<0.001	<0.001	<0.001	<0.001	<0.001	<0.001	<0.001	<0.001	<0.001	<0.001
S	ME-MS41	%	1.19	0.98	0.93	1.27	6.53	1.43	1.47	1.51	4.94	9.61	1.81	4.53	0.92
Sb	ME-MS41	ppm	0.19	0.13	0.18	0.26	0.17	0.07	0.13	0.1	0.12	0.11	0.1	0.15	0.09
Sc	ME-MS41	ppm	2.9	2.5	1.7	1.8	2.8	2.9	4.4	6.2	1	4	1.7	1.3	2.8
Se	ME-MS41	ppm	0.7	0.5	0.6	0.4	0.5	0.9	0.8	0.7	0.3	1.2	0.3	0.3	0.6
Sn	ME-MS41	ppm	0.9	0.7	2.8	3	2.1	1.7	0.8	1.6	3.8	0.8	0.8	1.1	0.8
Sr	ME-MS41	ppm	48.9	43.3	31.7	18.6	30.3	36.8	70.6	16	12	39.6	35.8	26.8	38
Ta	ME-MS41	ppm	0.01	<0.01	<0.01	<0.01	<0.01	0.01	<0.01	0.01	<0.01	0.01	<0.01	<0.01	<0.01
Te	ME-MS41	ppm	0.06	0.03	0.01	<0.01	0.04	0.01	0.09	0.01	0.01	0.04	0.01	0.01	0.06
Th	ME-MS41	ppm	5.3	4.2	3.1	3.8	6.3	10.8	5.5	20.2	2.8	4.3	2.7	2.1	5.4
Ti	ME-MS41	%	0.022	0.019	0.007	0.021	0.019	0.012	0.025	0.025	0.02	0.008	0.015	0.024	0.017
Tl	ME-MS41	ppm	0.11	0.13	<0.02	0.03	0.72	0.19	0.14	0.12	0.53	1.85	0.34	0.97	0.11
U	ME-MS41	ppm	0.66	1.29	0.27	0.37	2	1.81	0.68	2.33	1.31	1.23	0.66	0.73	0.58
V	ME-MS41	ppm	17	13	6	8	13	10	24	17	3	19	10	9	13
W	ME-MS41	ppm	0.05	<0.05	0.11	0.11	<0.05	0.05	<0.05	0.14	0.05	<0.05	0.07	0.09	<0.05
Y	ME-MS41	ppm	12.7	3.6	4.61	3.74	10.05	26.9	12.05	22.6	5.32	17.85	4.63	4.21	9.6
Zn	ME-MS41	ppm	33	25	18	18	61	57	32	36	15	126	52	57	20
Zr	ME-MS41	ppm	14.7	10.2	5.8	6.9	27.2	24.2	11.7	20.3	42.6	11.3	9.3	11.3	8.8

*An explanation of all symbols and abbreviations is included in Appendix I.

‡Sample YS07AA15 was analyzed by ICP-MS and XRF at two different labs for quality control purposes.

ELEMENT	METHOD*	UNITS	Inkpot Spring, Yellowstone	Growler/Little Growler Hot Springs,		
			National Park	Lassen Peak, CA [†]		
			YS-07-38PL	07-LP-40	07-LP-41	07-LP-51
Ag	MS-42	ppm	<1	<1	<1	<1
Al	MS-42	%	6.84	8.09	7.67	6.57
As	MS-42	ppm	15	109	1240	1430
Au	FA	ppm	<0.005	0.007	0.027	0.012
B	-----	-----	-----	-----	-----	-----
Ba	MS-42	ppm	937	677	329	323
Be	MS-42	ppm	3.4	2.6	3.5	2.2
Bi	MS-42	ppm	0.17	0.08	0.11	0.09
Ca	MS-42	%	0.55	3.43	2.32	2.43
Cd	MS-42	ppm	0.1	0.1	<0.1	<0.1
Ce	MS-42	ppm	126	29.3	26.4	21.9
Co	MS-42	ppm	6	12.2	10.7	11
Cr	MS-42	ppm	24	38	32	55
Cs	MS-42	ppm	<5	39	274	147
Cu	MS-42	ppm	8.9	21.5	16.9	18.9
Fe	MS-42	%	1.79	3.07	3.2	5.11
Ga	MS-42	ppm	21.7	15.3	16.3	17
Ge	-----	-----	-----	-----	-----	-----
Hf	-----	-----	-----	-----	-----	-----
Hg	CVAA	ppm	13.2	0.94	4.35	8
In	MS-42	ppm	0.09	0.03	0.03	0.03
K	MS-42	%	2.99	1.72	2.36	1
La	MS-42	ppm	65.7	16.2	13.7	11.6
Li	MS-42	ppm	18	36	99	67
Mg	MS-42	%	0.28	1.57	0.77	1.07
Mn	MS-42	ppm	209	590	394	343
Mo	MS-42	ppm	2.41	1.16	1.94	0.08
Na	MS-42	%	1.35	2.82	1.95	1.45
Nb	MS-42	ppm	42.1	6.2	5.6	0.3
Ni	MS-42	ppm	19.1	27.7	20.6	20.1
P	MS-42	ppm	180	550	290	290
Pb	MS-42	ppm	29	183	8.9	4.2
Rb	MS-42	ppm	113	64.5	247	93
Re	-----	-----	-----	-----	-----	-----
S	MS-42	%	2.07	0.27	1.13	4.07
Sb	MS-42	ppm	1.09	107	405	5700
Sc	MS-42	ppm	7.9	12	12.5	14.4
Se	Se Hyd	ppm	<0.2	0.6	0.3	0.4
Sn	MS-42	ppm	4.5	1.2	1.1	0.5
Sr	MS-42	ppm	171	460	957	389
Ta	-----	-----	-----	-----	-----	-----
Te	MS-42	ppm	<0.1	<0.1	<0.1	<0.1
Th	MS-42	ppm	18.7	5.7	6.2	2.6
Ti	MS-42	%	0.23	0.33	0.28	0.29
Tl	MS-42	ppm	1	52.6	105	234
U	MS-42	ppm	4.8	2.2	1.9	1.2
V	MS-42	ppm	31	93	159	67
W	MS-42	ppm	2	2	23.5	0.1
Y	MS-42	ppm	48.3	12.5	10.2	8.9
Zn	MS-42	ppm	70	53	46	32
Zr	-----	-----	-----	-----	-----	-----

*An explanation of all symbols and abbreviations is included in Appendix I.
†Unpublished geochemical data from Growler/Little Growler Hot Springs, Lassen Peak, CA is provided by David John at the USGS, Menlo Park, CA.

Sample #	Tuff of Sulphur Creek-Upper Basin Member- Plateau Rhyolites				Lamar River Formation-Washburn Group-Absaroka Volcanics			Inkpot Spring sediments	
	YS07CP09	YS07CP11	YS07CP12	YS07CP16	YS07AA06	YS07AA10	YS07AA13	YS07AA14	YS07AA15‡
	XRF	XRF	XRF	XRF	XRF	XRF	XRF	XRF	XRF
S03 >=	-----	-----	-----	-----	-----	-----	-----	0.13	0.71
Unnormalized Major Elements (Weight %):									
SiO2	73.33	75.38	72.72	74.99	51.82	53.45	56.58	68.33	67.26
TiO2	0.333	0.311	0.291	0.295	0.711	0.756	0.743	0.872	0.556
Al2O3	12.12	11.86	11.72	9.88	14.71	14.52	14.59	10.95	12.55
FeO*	1.84	0.49	1.32	0.93	6.76	7.03	6.11	2.42	1.74
MnO	0.019	0.010	0.029	0.031	0.122	0.108	0.102	0.021	0.021
MgO	0.04	0.03	0.05	0.04	7.25	6.50	6.41	0.44	0.40
CaO	0.63	0.51	0.53	0.35	6.28	8.01	6.46	0.52	0.50
Na2O	3.28	3.20	2.94	2.36	3.69	2.40	3.20	1.12	1.39
K2O	4.84	4.92	4.92	4.65	1.79	1.27	1.24	2.47	3.14
P2O5	0.032	0.027	0.035	0.021	0.196	0.212	0.157	0.065	0.096
Sum	96.46	96.74	94.57	93.54	93.33	94.26	95.59	87.21	87.66
Normalized Major Elements (Weight %):									
SiO2	76.02	77.92	76.90	80.17	55.53	56.71	59.19	78.36	76.73
TiO2	0.345	0.322	0.308	0.315	0.762	0.802	0.777	1.000	0.635
Al2O3	12.57	12.26	12.40	10.57	15.76	15.40	15.26	12.55	14.32
FeO*	1.90	0.51	1.40	0.99	7.25	7.46	6.39	2.77	1.98
MnO	0.020	0.010	0.031	0.033	0.131	0.115	0.107	0.024	0.024
MgO	0.04	0.03	0.05	0.04	7.77	6.90	6.71	0.51	0.46
CaO	0.66	0.53	0.56	0.37	6.73	8.50	6.76	0.59	0.57
Na2O	3.40	3.31	3.11	2.52	3.95	2.55	3.34	1.29	1.59
K2O	5.02	5.08	5.20	4.97	1.91	1.34	1.30	2.84	3.58
P2O5	0.033	0.028	0.037	0.022	0.210	0.224	0.164	0.074	0.109
Total	100.00	100.00	100.00	100.00	100.00	100.00	100.00	100.00	100.00
Unnormalized Trace Elements (ppm):									
Ni	0	0	0	0	102	85	106	18	5
Cr	2	4	2	2	327	273	360	87	101
Sc	5	4	4	3	22	23	23	8	8
V	3	0	3	0	175	182	148	61	64
Ba	1003	950	882	597	907	968	1323	2052	1269
Rb	172	174	176	170	28	15	16	65	88
Sr	75	64	59	22	739	675	815	314	352
Zr	365	357	329	358	110	111	110	380	224
Y	51	62	64	59	13	14	9	27	30
Nb	48.4	49.3	48.8	48.9	3.0	3.7	4.1	38.1	28.4
Ga	21	19	20	16	17	17	17	19	22
Cu	1	0	0	0	176	33	46	16	11
Zn	66	23	54	47	78	67	65	47	34
Pb	29	29	32	32	11	12	18	44	30
La	61	74	89	66	26	28	26	46	46
Ce	138	147	180	126	46	49	42	78	83
Th	23	26	25	24	3	3	4	17	19
Nd	49	62	67	53	22	20	16	25	29
U	5	7	7	5	2	2	2	5	3
sum trace	2116	2050	2041	1629	2805	2578	3151	3347	2446
in %	0.21	0.21	0.20	0.16	0.28	0.26	0.32	0.33	0.24
sum m+tr	96.68	96.95	94.77	93.71	93.61	94.52	95.91	87.54	87.90
M+Toxides	96.72	96.99	94.81	93.74	93.67	94.57	95.97	87.60	87.95
w/LOI	-----	-----	-----	-----	-----	-----	-----	87.60	87.95
w/SO3	-----	-----	-----	-----	-----	-----	-----	87.73	88.63
Major elements are normalized on a volatile-free basis, with total Fe expressed as FeO.									
NiO	0.0	0.0	0.0	0.0	130.2	108.6	134.8	23.5	6.5
Cr2O3	2.2	5.1	3.4	3.1	477.4	398.7	525.7	127.6	146.9
Sc2O3	8.3	6.4	5.8	5.2	33.7	35.9	34.5	12.4	12.4
V2O3	4.9	0.1	3.7	-0.4	256.9	267.6	217.1	89.3	94.6
BaO	1119.8	1060.8	984.3	667.0	1012.1	1080.4	1477.1	2290.5	1416.5
Rb2O	187.6	190.7	192.5	185.4	30.1	16.1	17.3	70.5	96.3
SrO	88.6	75.3	69.4	25.8	874.1	797.8	964.2	371.7	415.9
ZrO2	498.2	487.1	449.2	488.3	150.2	151.7	150.4	518.8	305.7
Y2O3	65.1	78.7	81.7	75.2	16.8	17.8	11.6	34.4	38.1
Nb2O5	69.2	70.5	69.8	70.0	4.3	5.3	5.9	54.5	40.6
Ga2O3	27.8	25.7	27.3	21.6	23.4	22.6	23.4	25.0	29.8
CuO	0.8	0.3	0.4	-0.1	220.8	41.2	58.1	20.0	13.9
ZnO	82.3	28.2	68.0	59.4	97.3	83.5	81.9	58.7	42.6
PbO	31.1	31.6	34.1	34.7	12.0	12.5	19.7	47.0	32.2
La2O3	71.3	86.3	104.0	77.5	30.0	33.3	30.4	51.1	54.2
CeO2	169.4	180.7	221.0	154.9	56.1	59.7	51.3	96.3	101.5
ThO2	25.7	29.1	27.9	26.5	3.2	2.9	4.9	19.2	20.7
Nd2O3	56.8	71.7	77.6	61.7	25.4	22.9	19.1	29.2	33.9
U2O3	5.9	7.4	7.3	5.6	1.7	2.2	1.9	5.4	3.5
sum trace	2515	2436	2427	1961	3455	3161	3829	3948	2906
in %	0.25	0.24	0.24	0.20	0.35	0.32	0.38	0.39	0.29

‡Sample YS07AA15 was analyzed by ICP-MS and XRF at two different labs for quality control purposes.

**APPENDIX F: Mercury data for Inkpot Spring fluids and sediments from
July 26, 2008 to August 9, 2008**

FLUID SAMPLES			Filtered, no preservation		Filtered, 1% (v/v) HNO ₃ added		Unfiltered, no preservation (sediment slurry)	
Sample #	Method*	DL	Hg (ng)	Hg (mg/L)	Hg (ng)	Hg (mg/L)	Hg (ng)	Hg (mg/L)
IKP01	DMA	0.005 ng	0.83911	0.000839	0.41483	0.000413	1.62505	0.032963
IKP02	DMA	0.005 ng	0.22137	0.000223	0.23725	0.000235	444.10266	8.690854
IKP03	DMA	0.005 ng	0.29041	0.000289	0.44754	0.000445	0.45165	0.009180
IKP04	DMA	0.005 ng	0.20756	0.000207	0.24660	0.000246	6.16634	0.126101
IKP06	DMA	0.005 ng	0.24438	0.000244	0.16248	0.000162	1.99578	0.040647
IKP07	DMA	0.005 ng	0.20295	0.000202	0.15781	0.000158	0.08287	0.001705
IKP09	DMA	0.005 ng	0.18914	0.000189	0.16248	0.000167	0.04928	0.000998
IKP10	DMA	0.005 ng	0.18914	0.000189	2.56623	0.002590	0.48917	0.009842
2IKP01	DMA	0.005 ng	0.24610	0.000245				
2IKP02	DMA	0.005 ng	0.21216	0.000211				
2IKP03	DMA	0.005 ng	0.27660	0.000276				
2IKP04	DMA	0.005 ng	0.23517	0.000235				
2IKP06	DMA	0.005 ng	0.22137	0.000222				
2IKP07	DMA	0.005 ng	0.22597	0.000226				
2IKP09	DMA	0.005 ng	0.17533	0.000175				
2IKP10	DMA	0.005 ng	0.19375	0.000193				
WTS01	DMA	0.005 ng	0.36106	0.000360				
WTS02	DMA	0.005 ng	0.23057	0.000230				
WTS03	DMA	0.005 ng	0.21216	0.000212				

SEDIMENT AND PRECIPITATE SAMPLES					
Sample #	Method*	ppm	Method	Hg (ng)	ppm
IKP01	ME-MS41	39.2	DMA	768.27	25.44
IKP02	ME-MS41	61.1	DMA	687.53	46.14
IKP03a	ME-MS41	235	DMA	>DL	>DL
IKP03b	ME-MS41	122.5	DMA	611.08	98.56
IKP04	ME-MS41	30.3	DMA	729.30	23.99
IKP05	ME-MS41	16.85	DMA	232.13	13.90
IKP06	ME-MS41	38.5	DMA	524.87	49.52
IKP07	ME-MS41	12.3	DMA	221.20	11.58
IKP09	ME-MS41	30.8	DMA	391.65	34.36
IKP10a	ME-MS41	16.2	DMA	388.97	18.26
IKP10b	ME-MS41	21.7	DMA	207.58	15.49
IKP11	ME-MS41	21.9	DMA	372.22	17.64
YS07AA15	ME-MS41	32.3	DMA	422.95	34.39
SSAA08 (sulfur)	ME-MS41	-----	DMA	>DL	>DL

*An explanation of all symbols and abbreviations is included in Appendix I.

**APPENDIX G: Previous organic and inorganic gas chemistry data from
Washburn-Inkpot Spring geothermal area**

Constituents	Sample #	YGS03-24		YGS03-25		YGS03-26		90		91	
		Burnett (2004)		Burnett (2004)		Gunter & Musgrave (1966)		Gunter & Musgrave (1966)		Allen & Day (1935)	
	Units*										
pH	°C										
temp											
Xg	mmol/mol	4.95	6.94					6.7	81.5	7.0	
xCO ₂	mmol/mol	856	805			13.6				82.0	
xS _t	mmol/mol	13.2	17.1			909					
xSO ₂	mmol/mol	1.14	1.83			16.7					811.5
xH ₂ S	mmol/mol	12.0	15.3			2.02					
xHCl	mmol/mol	17.0	12.6			14.7				0.4	
xNH ₃	mmol/mol	2.99	6.70			4.15					
xHe	mmol/mol	8.82E-03	<0.001			0.49					
xAr	mmol/mol	0.107	0.206			8.61E-03					
xH ₂	mmol/mol	35.57	47.06			0.116					
xO ₂	mmol/mol	0.082	<0.01			14.79		12.3		12.1	2.5
xN ₂	mmol/mol	9.21	23.8			0.054		0.7		0.4	0.0
xCH ₄	mmol/mol	66.32	87.00			32.9		23.2		13.1	37.0
xCO	mmol/mol	<3E-04	<3E-04			21.27		122.8		162.5	132.0
δ ¹⁵ N	‰	4.56 ± 1.12	5.21 ± 1.27			<1E-04					
C ₂ H ₆	mmol/mol					1.89 ± 0.17					
C ₂ H ₆	ppm	521	1400								1.15
C ₃ H ₈	ppm	175	255			1820					
C ₄ H ₁₀	ppm	26.3	104			365					
C ₄ H ₁₀	ppm	34.0	69.6			122					
C ₅ H ₁₂	ppm	7.43	15.5			69.9					
C ₅ H ₁₂	ppm	5.81	6.49			26.7					
(CH ₃) ₂ CHCH(CH ₃) ₂	ppm	0.415	2.11			12.4					
C ₆ H ₁₄	ppm	1.57				1.46					
C ₆ H ₁₄	ppm	2.15	0.728			2.90					
C ₆ H ₆	ppm	22.5	13.1			4.13					
C ₇ H ₈ or C ₆ H ₅ CH ₃	ppm					13.9					
						0.121					
		Burnett (2004)									
		δ ¹³ C-CO ₂									
										-4.0 ‰	
		δ ¹³ C-CH ₄									
										-24.2 ‰	

* An explanation of all symbols and abbreviations is included in Appendix I.

**APPENDIX H: Organic and inorganic gas chemistry data from Inkpot Spring
measured on August 5, 2008**

AMMONIA (ppm) (background=0.5 ppm)												
Pool		INKP01				INKP04		INKP06		INKP07	INKP10	
		<u>Location A</u>		<u>Location B</u>								
Height measured from		1 m	0.5 m	1 m	0.5 m	1 m	0.5 m	1 m	0.5 m	2 m	1 m	0.5 m
		1.4	2.4	0.8	0.6	8.6	9.0	0.5	0.7	0.2	11.3	12.2
		1.9	2.5	0.4	0.8	8.5	9.1	1.2	0.7	0.9	11.5	11.9
		2.2	2.8	0.6	1.1	8.6	9.1	0.6	0.8	0.3	11.6	11.9
				0.6	0.9	8.5	9.1	0.5	1.1	0.3	11.7	12.0
					1.5	8.7	8.9	0.5	0.9	0.4	11.9	13.3
							8.9		1.3	0.7		13.3
							9.8		1.1	0.9		13.2
							9.0		1.3	0.5		
									0.9			
									0.9			
NH ₃ Averages		1.8	2.6	0.6	1.0	8.6	9.1	0.7	1.0	0.5	11.6	12.5

METHANE (ppm) (background=0.0-0.5 ppm)													
Pool		INKP01				INKP04		INKP06			INKP07	INKP10	
		<u>Location A</u>		<u>Location B</u>									
Height measured from		1 m	0.5 m	1 m	0.5 m	1 m	0.5 m	1 m	0.5 m	0.25 m	2 m	1 m	0.5 m
		2.7	6.1	9.1	19.3	7.7	3.7	6.1	10.1	11.1	5.9	11.5	8.4
		10.4	7.9	9.1	48.1	6.5	4.3	12.1	5.4	13.9	17.8	11.7	15.3
		5.9	7.9	2.5		5.6	4.3	11.1	5.4	8.7	36.9	11.9	22.4
		6.9	9.5	4.0		3.9	7.7	11.1	7.5	6.5	42.6	21.2	9.1
		5.4	9.4	6.5		3.0	10.5	7.4		7.0		11.5	10.2
		11.2	11.4			7.1	19.3	8.5		14.3			17.7
		8.3	11.3			7.1	19.3						
						9.0	15.5						
							7.4						
							4.7						
							4.4						
CH ₄ Averages		7.3	9.1	6.2	33.7	6.2	9.2	9.4	7.1	10.3	25.8	13.6	13.9

ETHANE (ppm) (background=0.0 ppm)												
Pool		INKP01				INKP04		INKP06		INKP07	INKP10	
		<u>Location A</u>		<u>Location B</u>								
Height measured from		1 m	0.5 m	1 m	0.5 m	1 m	0.5 m	1 m	0.5 m	2 m	1 m	
		1.0	1.0	0.0	4.0	2.0	2.0	6.0	2.0	2.0	1.0	
		0.0	2.0	1.0	4.0	1.0	2.0	5.0	4.0	4.0	7.0	
		0.0	2.0	2.0	4.0	1.0	1.0	5.0	4.0	4.0	6.0	
			1.0	0.0	7.0		1.0	2.0	2.0	3.0	1.0	
			1.0	0.0	5.0		2.0		3.0	4.0	1.0	
			0.0	3.0			6.0			4.0	2.0	
							5.0			5.0	3.0	
										2.0		
C ₂ H ₆ Averages		0.3	1.2	1.0	4.8	1.3	2.7	4.5	3.0	3.5	3.0	

CARBON DIOXIDE (ppm) (background=10.0 ppm)												
Pool		INKP01				INKP04		INKP06		INKP07	INKP10	
Height measured from		<u>Location A</u>		<u>Location B</u>		1 m	0.5 m	1 m	0.5 m	2 m	1 m	
		11	50	21	231	66	165	86	112	199	166	
		36	157	137	155	87	109	85	154	214	180	
		36	249	147	320	115	109	85	69	224	595	
		117	112	56	403	117	174	75	61	229	456	
		102	115	59	128				135		201	
		72	212	514	90				137		278	
		72		392					152		403	
		50							151		265	
											207	
CO ₂ Averages		62	149	189	221	96	139	83	121	217	306	

SULFUR DIOXIDE (ppm) (background=0.92 ppm)												
Pool		INKP01				INKP04		INKP06			INKP10	
Height measured from		<u>Location A</u>		<u>Location B</u>		1 m	0.5 m	1 m	0.5 m		1 m	0.5 m
		2.38	4.58	1.47	1.61	3.96	4.98	5.31	6.98		3.36	3.87
		2.78	6.71	1.16	1.81	5.42	4.89	6.11	6.98		4.09	0.55
		6.67	3.16	2.15	1.53	6.78	5.53	6.25	3.91		6.01	1.61
		4.85	2.62	2.31	0.42	2.33	5.54	6.23	6.60		1.77	3.23
		3.80	7.69	3.52	4.64	4.35	5.30	6.45	5.41		6.25	5.96
		4.32				4.39			5.52			
						4.68						
SO ₂ Averages		4.13	4.95	2.12	2.00	4.56	5.25	6.07	5.90		4.30	3.04

APPENDIX I: Explanation of symbols and abbreviations

*Explanation of symbols and abbreviations	
- - - - -	not analyzed, measured, or calculated
±	plus or minus
<	less than
%	percent
‰	per mil
°C	degrees Celsius
Au-ICP21	ALS Chemex method including fire assay fusion and ICP-AES
CVAA	cold vapor atomic absorption
DMA	direct mercury analysis
Eh	redox potential
FA	fire assay
FIA	flow injection analysis
GS IR-MS	gas source isotope ratio mass spectrometer
IC	ion chromatography
ICP-AES	inductively coupled plasma atomic emission spectrometry
ICP-MS	inductively coupled plasma mass spectrometry
LOI	loss on ignition
MDL	mean detection limit
ME-MS41	ALS Chemex method including ICP-MS and ICP-AES
meq/L	milliequivalents per liter
mg CaCO ₃ /L	milligrams calcium carbonate per liter
mg/L	milligrams per liter
mM	millimoles per liter
mmol/mol	millimoles per mole
mg/L	milligrams per liter
MS-42	ALS Chemex method including ICP-MS
µS/cm	microsiemens per centimeter
n	number of analyses
NA	not applicable
ND	not detected
ng	nanograms
ng/L	nanograms per liter
ppm	parts per million
RL	reporting limit
TC-EA	temperature conversion elemental analysis
V	volts
v/v	volume per volume
XRF	X-ray fluorescence